

CERN-Proceedings-2014-001

February 2014

**"Cosmology and Particle Physics beyond Standard Models"**  
**- Ten Years of the SEENET-MTP Network -**

Editors:

Luis Álvarez-Gaumé,

Goran S. Djordjević,

Dejan Stojković

CERN  
GENEVA  
2014

CERN–Proceedings–2014–001

ISBN 978-92-9083-398-7

Copyright © The Authors, 2014. Published by CERN

Available online at <https://cds.cern.ch/>

This volume should be cited as:

Cosmology and Particle Physics beyond Standard Models. Ten Years of the SEENET-MTP Network, edited by Luis Álvarez-Gaumé, Goran S. Djordjević, Dejan Stojković, CERN–Proceedings–2014–001 (CERN, Geneva, 2014)

A contribution in this volume should be cited as:

[Author name(s)], in Cosmology and Particle Physics beyond Standard Models. Ten Years of the SEENET-MTP Network, edited by Luis Álvarez-Gaumé, Goran S. Djordjević, Dejan Stojković, CERN–Proceedings–2014–001, pp. [first page] – [lastpage]

## Abstract

This publication - "Cosmology and Particle Physics beyond Standard Models" - is dedicated to the celebration of the tenth anniversary of the Southeastern European Network in Mathematical and Theoretical Physics (SEENET-MTP). As a Theme Collection, rather than a Monograph or Proceedings, this volume presents a number of reports and overviews, a few research papers and a short note. However, some of them are excellent examples of a nowadays increasingly deep interplay between particle physics and cosmology. Contributions span a wide range of topics in cosmology, particle physics, but also gravity, including the interface of these fields. The presented work is of both theoretical and experimental/observational nature. The contributions represent recent progress in their respective fields: inflation, dark matter, neutrino physics, supersymmetry, collider physics, string theory, quantum gravity, black hole physics and massive gravity



## Preface

### Cosmology and Particle Physics Beyond Standard Models

Dear reader(s),

This publication is dedicated to the celebration of the tenth anniversary of the Southeastern European Network in Mathematical and Theoretical Physics (SEENET-MTP)<sup>1</sup> and initiated by a number of high level reports on particle physics and cosmology presented at the BW2013 Workshop held in Vrnjacka Banja, Serbia.

The origins of the Southeastern European Network in Mathematical and Theoretical Physics (SEENET-MTP) are closely linked to Julius Wess and his initiative: Wissenschaftler in globaler Verantwortung (WIGV) "Scientists in global responsibility" launched in 1999. The establishing of SEENET-MTP, which also took place in Vrnjacka Banja at the kick-off Workshop BW2003 in August 2003, was a natural continuation of WIGV, in a broader framework than the former Yugoslavia.

A large number of participants and numerous high level scientific meetings, joint publications and continuous exchange of researchers and students in the Balkans, strengthened the existing regional and rather global collaborations with many institutions, groups and individuals - mostly from Europe, but also from USA, Brazil, India and other countries.

The main purpose of the SEENET-MTP and its meetings and actions remains to foster communication and collaboration among researchers in the Balkan region, as well as between them and their international colleagues. This initiative created the opportunity for researchers working in the general area of high energy physics, cosmology and related fields at different institutions in the Balkan countries to present their work and results. This issue is motivated by the recent breakthrough in particle physics, the discovering of the Higgs boson, and continuous discoveries in cosmology - always followed by new puzzles and challenges, for instance dark matter and dark energy.

From about 20 invited authors, long term members or supporters of the SEENET-MTP, we are pleased to announce 13 full term papers and one summary. As a Theme Collection, rather than a Monograph, this Volume presents a number of reports and overviews, a few research papers and a short note. However, some of them are excellent examples of increasingly deep interplay between particle physics and cosmology.

Contributions span a wide range of topics in cosmology, particle physics, gravity, including the interface of these fields. The presented work is of both theoretical and experimental/observational nature. The contributions represent recent progress in their respective fields from inflation, dark matter, neutrino physics, supersymmetry, collider physics, string theory, quantum gravity, black hole physics and massive gravity.

After the final editing of the Volume, the editors gave up on the separation of the Volume in two parts: Particle Physics and Cosmology and decided to submit the whole manuscript in the present form. The papers are listed in alphabetical order of the first authors. All papers have been peer-reviewed, at least by one referee and the editor. We express our gratitude to the referees whose suggestions improved the scientific quality of the papers.

We would like to thank Milan Milosević from the University of Nis, Serbia for his great help in the preparation of this Volume. We would also like to thank Dragoljub Dimitrijević, from the same institution, for his help in communication with the authors, and both of them, as many others, for enabling the SEENET-MTP to be a sustainable mission.

---

<sup>1</sup>Web: [www.seenet-mtp.info](http://www.seenet-mtp.info)

Among many institutions which supported the SEENET-MTP and its workshops and research-training-exchange program during the previous decade, we acknowledge here with a great pleasure:

- UNESCO Office in Venice, Italy, and UNESCO (the IBSP program, Paris, France)
- ICTP (The Abdus Salam International Centre for Theoretical Physics, Trieste, Italy)
- SMES (Serbian Ministry of Education and Science)
- DAAD (Deutscher Akademischer Austauschdienst, Germany and its Office in Belgrade, Serbia)
- EPS (European Physical Society)
- CERN-TH, Geneva, Swiss Confederation
- CEI (Central European Initiative Trieste, Italy)
- Faculty of Science and Mathematics, University of Nis, Serbia.

Geneva, Nis, Buffalo  
February, 2014

Luis Alvarez-Gaume, Goran S. Djordjević, Dejan Stojković

## Contents

|   |     |
|---|-----|
| Preface   |     |
| <i>Luis Alvarez-Gaume, Goran S. Djordjević, Dejan Stojković</i> .....                                 | v   |
| Initial conditions for inflation and the energy scale of SUSY-breaking from the (nearly) gaussian sky |     |
| <i>Luis Álvarez-Gaumé, César Gómez and Raul Jimenez</i> .....   | 1   |
| Mass hierarchy and string phenomenology in the LHC era  |     |
| <i>Ignatios Antoniadis</i> .....  | 11  |
| Scalar potentials, propagators and global symmetries in AdS/CFT                                       |     |
| <i>Borut Bajc and Adrián R. Lugo</i> .....  | 25  |
| A Minimal Supersymmetric Model of Particle Physics and the Early Universe                             |     |
| <i>W. Buchmüller, V. Domcke, K. Kamada and K. Schmitz</i> .....                                       | 47  |
| Black Hole Macro-Quantumness  |     |
| <i>Gia Dvali and Cesar Gomez</i> .....  | 79  |
| Massive spin-2 theories   |     |
| <i>Sarah Folkerts, Cristiano Germani and Nico Wintergerst</i> .....                                   | 87  |
| Higgs, Top, and Bottom Mass Predictions in Finite Unified Theories                                    |     |
| <i>Sven Heinemeyer, Myriam Mondragón and George Zoupanos</i> .....                                    | 99  |
| Beyond the Standard Model of Physics with Astronomical Observations                                   |     |
| <i>Raul Jimenez</i> .....   | 111 |
| Neutrinos and Physics Beyond Electroweak and Cosmological Standard Models                             |     |
| <i>Daniela Kirilova</i> .....   | 131 |
| Is there a fundamental cosmological dipole?   |     |
| <i>Leandros Perivolaropoulos</i> .....  | 139 |
| Can we push the fundamental Planck scale above $10^{19}$ GeV?   |     |
| <i>Dejan Stojkovic</i> .....  | 159 |
| REM - the Shape of Potentials for f(R) Theories in Cosmology and Tachyons                             |     |
| <i>Dumitru N. Vulcanov, Goran S. Djordjevic and Ciprian A. Sporea</i> .....                           | 165 |
| Fermi Large Area Telescope as a dark matter search tool   |     |
| <i>Gabrijela Zaharijas, Aldo Morselli and Eric Nuss</i> .....   | 171 |
| <b>Summary Reports</b> .....  | 177 |
| AdS braneworld with Backreaction  |     |
| <i>Neven Bilić and Gary B. Tupper</i> .....   | 179 |



# Initial conditions for inflation and the energy scale of SUSY-breaking from the (nearly) gaussian sky

Luis Álvarez-Gaumé<sup>a,\*</sup>, César Gómez<sup>b,c,†</sup> and Raul Jimenez<sup>d,a,‡</sup>

<sup>a</sup> Theory Group, Physics Department, CERN, CH-1211, Geneva 23, Switzerland

<sup>b</sup> Arnold Sommerfeld Center for Theoretical Physics, Department für Physik, Ludwig-Maximilians-Universität München Theresienstr. 37, 80333 München, Germany

<sup>c</sup> Physics Department and Instituto de Física Teórica UAM/CSIC, 28049 Cantoblanco, Madrid, Spain

<sup>d</sup> ICREA & ICC, University of Barcelona (IEEC-UB), Martí i Franques 1, Barcelona 08028, Spain

## Abstract

We show how general initial conditions for small field inflation can be obtained in multi-field models. This is provided by non-linear angular friction terms in the inflaton that provide a phase of non-slow-roll inflation before the slow-roll inflation phase. This in turn provides a natural mechanism to start small-field slow-roll at nearly zero velocity for arbitrary initial conditions. We also show that there is a relation between the scale of SUSY breaking ( $\sqrt{f}$ ) and the amount of non-gaussian fluctuations generated by the inflaton. In particular, we show that in the local non-gaussian shape there exists the relation  $\sqrt{f} = 10^{13} \text{GeV} \sqrt{f_{\text{NL}}}$ . With current observational limits from Planck, and adopting the minimum amount of non-gaussian fluctuations allowed by single-field inflation, this provides a very tight constraint for the SUSY breaking energy scale  $\sqrt{f} = 3 - 7 \times 10^{13} \text{ GeV}$  at 95% confidence. Further limits, or detection, from next year's Planck polarisation data will further tighten this constraint by a factor of two. We highlight that the key to our approach is to identify the inflaton with the scalar component of the goldstino superfield. This superfield is universal and implements the dynamics of SUSY breaking as well as superconformal breaking.

## 1 Introduction

Recent constraints on inflation by the Planck satellite [1,2] have provided new insight on the properties of the inflaton. We know that the generation of non-gaussian fluctuations has been restricted significantly, with no detection by Planck and only upper limits reported (for the local case Planck reports  $f_{\text{NL}} < 14$  at 95% confidence). Further, constraints on the non-detection of the tensor-to-scalar ratio ( $r < 0.1$ ) have served to eliminate many candidates for the inflaton. In fact, the above "non-detections" already point toward a model for the inflaton in which perturbations were nearly Gaussian and most likely generated by a single-field slow-roll scalar with canonical kinetic energy; further, it seems likely the field is in the so-called "small-field" class with displacement of  $\sim M$  (hereafter  $M$  is the Planck mass scale) to produce the required e-folds to explain flatness. An excellent review on this class of models can be found in Ref. [3,4].

One very interesting question to be answered after the Planck results is how to set-up sufficiently general initial conditions for the inflaton in the "small-field" class, in other words: how can we have inflation to start with nearly zero velocity at the time it will start slow-rolling in a flat potential? Here we present a general mechanism, inspired by SUSY, to do so.

---

\*E-mail: luis.alvarez-gaume@cern.ch

†E-mail: cesar.gomez@uam.es

‡E-mail: raul.jimenez@icc.ub.edu

Unless one has a single-field slow-roll inflaton with canonical kinetic energy, nearly all other models produce measurable amounts of non-gaussianity [5–14] with values of the parameter that measures non-gaussianity  $f_{\text{NL}} \gg O(1)$ . Even the single-field slow-roll inflaton will produce values of non-gaussianity at the level of the tilt ( $\sim n_s - 1$ ) which might be detected in futuristic 21cm experiments that measure all modes in the current horizon. The nice feature of being able to measure non-gaussian fluctuations is that it provides all the correlators of the inflaton, thus one could construct, from observations, the effective lagrangian of the inflaton itself, very much in the fashion that is done in high-energy physics at accelerators like the LHC for the standard model of particles and beyond.

In the minimal-inflation [15–17] scenario the field  $X$  that drives the exponential expansion of the Universe can often be represented at low energies by a Goldstino composite  $GG$ . Our main motivation to propose to identify the inflaton field with the order parameter of supersymmetry breaking is guided by the fact that, independently of the particular microscopic mechanism driving supersymmetry breaking (in what follows we will restrict ourselves to  $F$ -breaking) we can define a superfield  $X$  whose  $\theta$  component at large distances becomes the “Goldstino” (see [18, 19]). In the UV the scalar component  $x$  of  $X$  is well defined as a fundamental field while in the IR, once supersymmetry is spontaneously broken, this scalar field may be expressed as a two Goldstino state. The explicit realisation of  $x$  as a fermion bilinear depends on the low-energy details of the model. In models of low-energy supersymmetry the realization of  $x$  as  $GG$  can be implemented by imposing a non linear constraint in the IR for the  $X$  field of the type  $X^2 = 0$ . In our approach to inflation we use one real component of the UV  $x$  field as the inflaton. We assume the existence of a  $F$ -breaking effective superpotential for the  $X$ -superfield and we induce a potential for  $x$  from gravitational corrections to the Kähler potential.

In this paper we show that for generic trajectories of the minimal inflation model there is a level of generated non-gaussian fluctuations that depends directly on the scale of SUSY breaking. Therefore the further the value of non-gaussianity in the sky is constraint by current CMB experiments like Planck, the better we can constraint the SUSY energy scale and therefore make predictions for the feasibility of discovering SUSY at the LHC.

As a final observation we would like to make several remarks to highlight the similarities and differences between our approach and other attempts to identify the inflaton as well as the underlying dynamics of inflation. The key to our approach is to identify the inflaton with the scalar component of the goldstino superfield. This superfield is universal and implements the dynamics of SUSY breaking as well as superconformal breaking. In our approach SUSY breaking is unavoidably linked to inflation and the constraints we get for the SUSY breaking scale are partially dictated by requiring a SUGRA vacuum with zero cosmological constant. Finally our approach can be understood as similar to Higgs inflation with the important difference of using what could be understood as the Higgs of the SUSY breaking.

## 2 Setup

In order to study under what conditions the inflaton in our model will produce general initial conditions for small-field slow-roll inflation, we generate randomly 1000 trajectories for different starting points in the inflation potential (see Fig. I).

Let us briefly recall the form of the inflation potential and how inflationary trajectories are found.

In our minimal inflationary scenario [15, 16] we use only the Ferrara-Zumino (FZ) multiplet to drive inflation. The scalar potential in the Einstein frame is given by:

$$V_E = e^{\frac{K}{M^2}} \left( -\frac{3}{M^2} W \bar{W} + G^{X\bar{X}} D_X W D_{\bar{X}} \bar{W} \right), \quad (1)$$

where the Kähler metric and the Kähler covariant derivatives are given by:

$$G_{X\bar{X}} = \partial_X \bar{\partial}_{\bar{X}} K(X, \bar{X}) \quad D W(X) = \partial_X W(X) + \frac{1}{M^2} \partial_X K W(X). \quad (2)$$

In our approach we make an explicit, but reasonably generic choice for  $K$  and  $W$ .

For us the inflaton superfield is the FZ-chiral superfield  $X = z + \sqrt{2} \theta \psi + \theta^2 F$ , the order parameter of supersymmetry breaking. We will consider the simplest superpotential implementing F-breaking of supersymmetry. More elaborate superpotentials often reduce to this one once heavy fields are integrated out.

$$W = fX + f_0 M \quad (3)$$

with  $f_0$  some constant to be fixed later by imposing the existence of a global minimum with vanishing cosmological constant and with  $f$  the supersymmetry breaking scale  $f = \mu_{susy}^2$ .

We are interested in sub-planckian inflation, and not in the ultraviolet complete theory that should underlie the scenario. Hence we simply parametrize the subplanckian theory in terms of the previous superpotential, and a general Kähler potential whose coefficient will be taken of order one. We try to use our ignorance of the ultraviolet theory to our advantage. The Kähler potential  $K$  we consider is:

$$K = X\bar{X} + \frac{a}{2M}(X^2\bar{X} + c.c.) - \frac{b}{6M^2}(X\bar{X})^2 - \frac{c}{9M^2}(X^3\bar{X} + c.c.) + \dots - 2M^2 \log\left(1 + \frac{X + \bar{X}}{M}\right) \quad (4)$$

Which can be understood as a Taylor series expansion of all terms up-to  $1/M^2$  plus a term (the log) that breaks R-symmetry. In our case, the scalar fields form a complex scalar field, the partner of the goldstino field. Our complex field can be written as  $z = M(\alpha + i\beta)/\sqrt{2}$ . The potential is  $V(z, \bar{z}) = f^2 V(\alpha, \beta)$ , since we only include for simplicity two scales, the Planck scale  $M$  and the supersymmetry breaking scale  $f^{1/2}$ . In supergravity models, the gravitino mass is up to simple numerical factors given by  $m_{3/2} \sim f/M$ . It is convenient to write down dimensionless equations of motion such that time is counted in units of  $f^{-1/2}$ .

The system of differential equations for the trajectory becomes:

$$\begin{aligned} \alpha'' + 3\frac{a'}{a}\alpha' + \frac{1}{2}\partial_\alpha \log g(\alpha'^2 - \beta'^2) + \partial_\beta \log g\alpha'\beta' + g^{-1}V'_\alpha &= 0 \\ \beta'' + 3\frac{a'}{a}\beta' + \frac{1}{2}\partial_\beta \log g(\beta'^2 - \alpha'^2) + \partial_\alpha \log g\alpha'\beta' + g^{-1}V'_\beta &= 0 \\ \frac{a'}{a} = \frac{H}{m_{3/2}} = \frac{1}{\sqrt{3}} \left( \frac{1}{2}g(\alpha'^2 + \beta'^2) + V(\alpha, \beta) \right)^{1/2} & \quad (5) \end{aligned}$$

The coefficients  $f_0, a, b, c$  will be chosen appropriately so that we obtain flat directions. For our purposes it is convenient to chose  $a = 0$ , as this guarantees the existence of a global minimum.  $f_0$  will be adjusted such that the global minimum is at a vanishing value of the potential. So the model only has  $b, c$  as free parameters, which we try to keep of order one to avoid fine-tuning in the potential.

From the collection of potentials considered, not all will show flat directions where it is possible to inflate during enough e-foldings ( $> 55$ ) for any choice of the microscopic parameters  $f_0, a, b, c$ . We will restrict to cases where the potential has a global minimum with vanishing cosmological constant and thus we fix the value of the minimum at 0 tuning the value of  $f_0$ .

We can now compute trajectories and attractors in more detail using the equations above. An example of the potential is shown in Fig. 1 for values of the parameters  $a = 0, b = 1, c = -1.5$ . Note that there is a flat direction where slow-roll takes place. We elaborate on this in the next section.

### 3 General initial conditions for small-field inflation

There are a number of important properties of the system of equations 5 and its solutions that are shared by large classes of supersymmetric theories. In our approach, the inflaton is always the scalar component of the goldstino superfield, and the Kähler potential and the superpotential completely determine its dynamics. For a multifield inflationary theory, with a non-canonical kinetic term, the dynamical equations

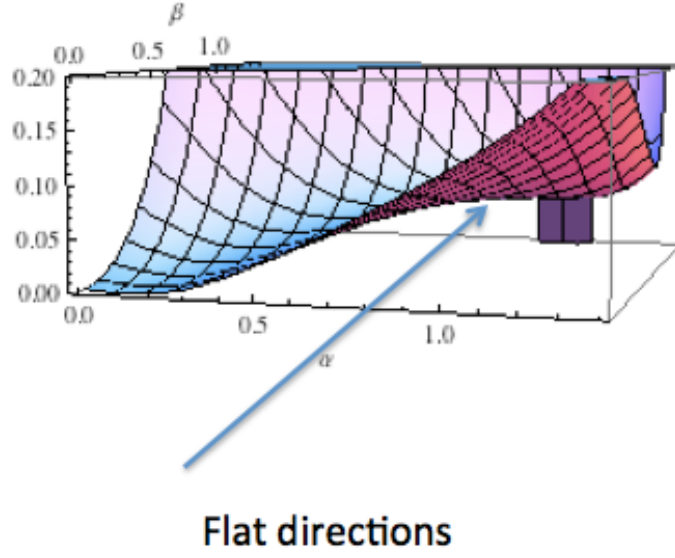


**Fig. I:** The potential (shown in units of  $V/f^2$ ) as a function of the real fields  $(\alpha, \beta)$  for the case with parameters  $(a = 0, b = 1, c = -1.4, f_0 \sim -f)$ , note that this creates a very flat "bottom-valley" region, where slow-roll conditions are fulfilled.

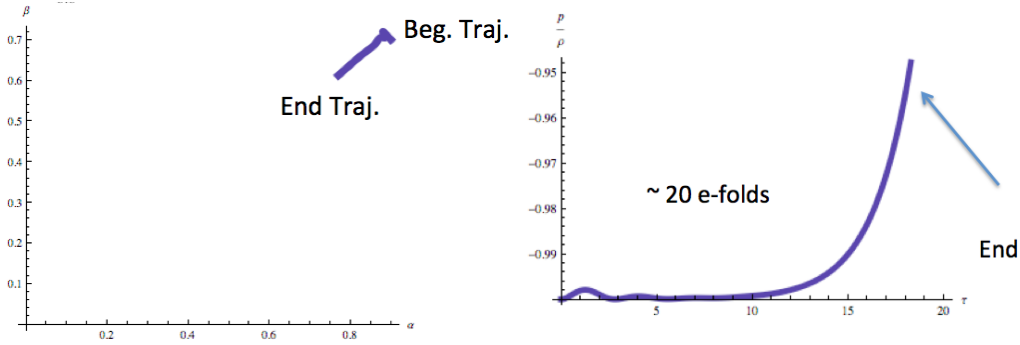


**Fig. II:** Left panel: a trajectory in the plane  $\alpha, \beta$  for zero velocity initial conditions. Right panel: the equation of state as a function of e-folds. Note that trajectory stays always in the slow-roll regime for nearly 20 e-folds.

of motion take the form:

$$H^2 = \frac{8\pi G}{3} \left( \frac{1}{2} G_{ij} \dot{X}^i \dot{X}^j + V(X) \right)$$

$$\frac{D\dot{X}^i}{dt} + 3H\dot{X}^i + G^{ij} \partial_j V = 0, \quad (6)$$

where  $D/dt$  is the covariant derivative with respect to the metric  $G$  in field space. We can define the energy functional for a given trajectory as:

$$E[X] = \frac{1}{2} G_{ij} \dot{X}^i \dot{X}^j + V(X). \quad (7)$$

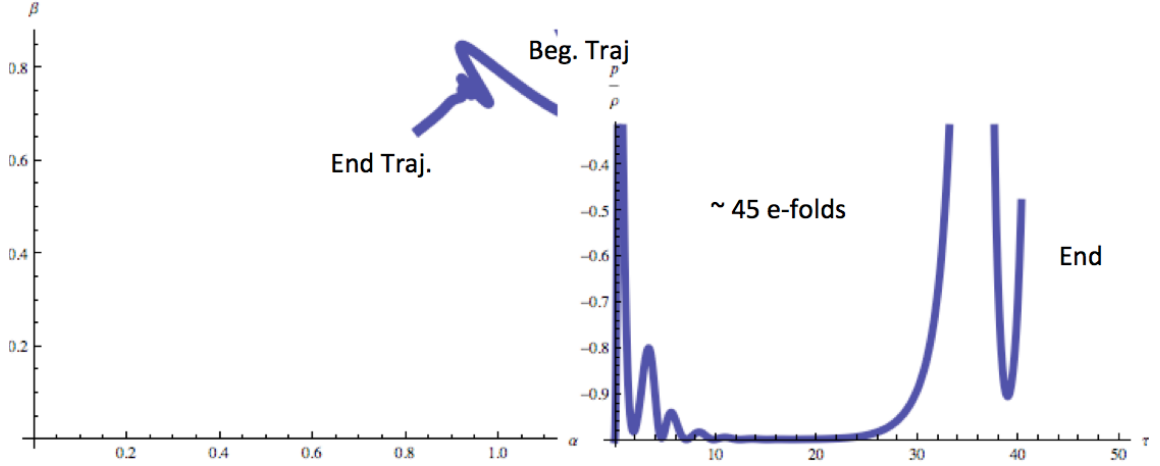


**Fig. III:** An example of a trajectory for the potential shown in Fig. I. The left panel shows the trajectory in the plane  $\alpha, \beta$ . Note that we start the trajectory at an arbitrary position with random velocities in the steep part of the potential. Because of the non-linear friction in our equations of motion, every time the inflaton turns, there will be significant friction and therefore will be slowed down. This happens until it reaches the valley where it slow-rolls as a single field inflaton. The right panel shows the equation of state ( $p/\rho$ ) as a function of number of e-folds ( $\tau$ ). Recall that  $p/\rho \sim (\epsilon - 1)$ , where  $\epsilon$  is the first slow-roll parameter, so that traditional slow-roll happens when  $p/\rho = -1$ . The trajectory generates non-gaussianity both at the largest scales (at the current horizon scale) and the smallest (below the dwarf galaxies). It is in these scales that non-gaussianity could be generated depending on the SUSY scale.

It is easy to see that in an expanding universe it is a monotonically decreasing function of time:

$$\frac{dE[X]}{dt} = -3H G_{ij} \dot{X}^i \dot{X}^j \quad (8)$$

When we use the scalar component of the goldstino superfield, the trajectories are always plane curves in the plane  $(\alpha, \beta)$  whose metric is always of Gaussian form:

$$ds^2 = 2G(\alpha, \beta) (d\alpha^2 + d\beta^2), \quad (9)$$

and the first two equations in 5 can be succinctly written as:

$$\ddot{z} + \partial_z \log G \dot{z}^2 + 3H \dot{z} + G^{-1} \partial_{\bar{z}} V = 0.$$

The slow roll equations are simply:

$$3H \dot{z} + G^{-1} \partial_{\bar{z}} V = 0.$$

It is clarifying to analyse these equations (the first and second order sets) in terms of polar coordinates. In the models we consider we start inflation close but below the Planck scale. In polar coordinates, the change of the energy of the system is given by:

$$\frac{dE[X]}{dt} = -3H G(\rho, \theta) (\dot{\rho}^2 + \rho^2 \dot{\theta}^2), \quad z = \rho e^{i\theta}$$

The initial value for  $\rho$  will be close to one in Planck units, hence if we choose some generic initial conditions with an arbitrary direction for the speed of the field, it is clear that for high values of  $\theta$  the slashing of the angular component will rapidly damp the energy and the field will join any of the

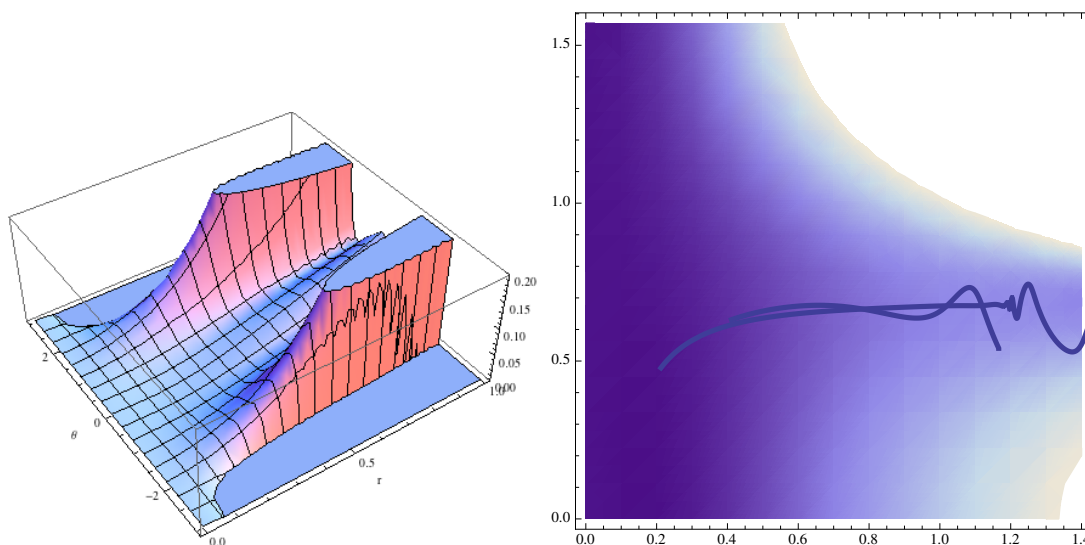


**Fig. IV:** Left panel: polar plot of the potential used to compute inflationary trajectories. Right panel: contour plot version of the left panel ( $\theta$  (y-axis) range from 0 to  $\pi/2$ ) with some inflationary trajectories over-plotted.

trajectories determined by the extrema of the potential with respect to the angular variable  $\partial_\theta V = 0$ . From the angular part of the slow roll equations one sees easily that those constant  $\theta = \theta_0$  satisfying the extremum condition are exact solutions to the slow roll equations. Each of those values is a potential attractor. General trajectories will join one of this attractors and then the  $\rho$  will roll to the origin as in single field inflation theories. The number of e-folding generated will depend, of course, on the initial conditions and the parameters of the model, but it is important to remark that in most models in this approach it is typical to obtain a number of order ten e-foldings. The number of effective attractor trajectories depends on the potential and the metric.

If we analyse the full set of second order equations, hence without the slow roll conditions, the conclusions are rather similar. The attractor-like trajectories, i.e. exact solutions with  $\theta = \theta_0$  constant are also characterised by the extremal point of the potential with respect to the angle. Some examples can be found in the figures below. For some values of the parameters of our model, we plot the potential in polar coordinates. It is easy to see attractor trajectories in the three dimensional plot in Fig. I, and also the corresponding valleys of attraction in Fig. IV, which portrays the same potential but in a contour plot.

In the next section we explore some explicit examples and trajectories with reasonable number of e-foldings. The general remarks just presented of course apply to the cases studied below.

#### 4 Examples

As explained before, we always need to set  $a = 0$ , so we concentrate on the values of  $b$  and  $c$ . From a Monte-Carlo simulation that samples more than 1000 values for  $b$  and  $c$  we have found that the most favourable values to produce enough e-folds is when  $b \sim -c$ , so from now on we focus on this case. This is the case already depicted in Fig. I. Note the main features of the potential: a very steep part at values of the field  $\sim M$ , a flat part at  $< M$  and finally a global minimum. Let us start with a trajectory where the field starts near the flat part. This is shown in Fig. II. the left panels shows the trajectory in the plane  $\alpha, \beta$  while the right panel shows the value of the equation of state  $p/\rho$ , recall that slow-roll implies  $p/\rho \sim -1 \sim (\epsilon - 1)$  where  $\epsilon$  is the first slow-roll parameter, as a function of the number of e-folds ( $\tau$ ). First, the trajectory is very flat (note the small values of  $p/\rho$  on the y-axis) but last only for about 20

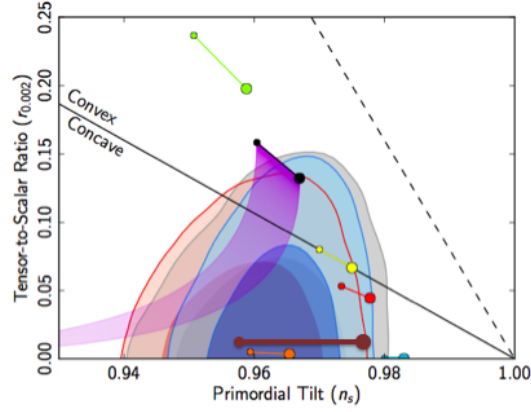


**Fig. V:** Dark-red thick line shows the prediction for our model in the plane  $r - n_s$  (plot adapted from Planck team release).

e-fold, enough to explain the observed universe but not its flatness.

So we now explore the case when the field starts from the steeper part at positions of the field  $\sim M$  and with arbitrary position in velocity and direction. An example is shown in Fig. III. First, note that despite the initial steepness of the potential and arbitrary velocity, the field is slowed-down by the non-linear friction terms at the turns. This period is “slashing” ends into the field reaching nearly zero velocity at the beginning of the flat part of the potential. From the right panel we observe that this early phase provides a few e-folds before entering the slow-roll phase that last for about 25 e-folds. The field then exits slow-roll and enters a final phase of no slow-roll adding and extra 10 e-folds. In total we obtain the required 45 e-folds to explain flatness and the required slow roll phase to explain the observed slope of the primordial power spectrum  $n_s = 0.96 \pm 0.007$ .

This is typical of what we found in the Monte-Carlo simulation for arbitrary trajectories starting at positions of the field  $\geq M$ . Note that because we do not have control on how the potential behaves beyond values of the field of  $M$ , it is important that even for very steep values the non-linear friction is efficient at slowing down the inflaton and providing initial conditions for slow-roll.

Thus general trajectories in our model look very much like the one in Fig. III. Note that obtaining order 50 e-folds is not difficult with values of  $b, c$  order one (as in Fig. I). More e-folds can be obtained if the values of  $b, c$  are tune in one part in 100, although this does not seem to be necessary. We note that further fine-tuning of the parameters will not lead to any improvement of the model.

We show the general prediction of our model for the ratio of tensor-to-scalar perturbations in Fig. V. As expected [20], because of the small displacement of the field ( $\Delta\alpha, \beta \sim 0.2 - 0.3M$ ),  $r$  is small  $\sim 0.001$ .

## 5 Non-gaussianities

We now answer the following question: will non-gaussian fluctuations be generated by our model? We first note that the kinetic term is always non-canonical, but weakly so for  $\alpha, \beta < 1$  as can be seen from the choice of the Kahler potential. So although our inflaton is a “pion” we will not generate any non-gaussianity from this source. The only place where one could generate measurable non-gaussianity is from those situations in which the inflaton turns.

We can estimate the value of the non-gaussian fluctuations following [21]. The overall level of

non-gaussianity is given by their Eq. 17, which reads

$$f_{\text{NL}}^{\text{int}} = \alpha(\nu) \frac{1}{P_{\xi}^{1/2}} \left( \frac{-V'''}{H} \right) \left( \frac{\dot{\theta}}{H} \right)^3 \quad (10)$$

where  $V'''$  is the third derivative of the potential at the turn,  $\dot{\theta}$  is the angular velocity of the inflaton as it turns,  $P_{\xi}$  is the power spectrum of the fluctuations and  $\alpha(\nu)$  is a numerical factor (which we compute using [22]).

In order to estimate the different terms in the above equation in our models we proceed as follows: we generate 1000 random trajectories for different values of our potential, but limited to the case where  $c = -g \times b$ , where  $g$  is a number between 1 – 2, as we know by previous experience that this is the case when the potential can harbour trajectories with  $O(40 - 50)$  e-folds; we also limit  $b, c$  to have the freedom to vary only in the first decimal place as to not produce fine tuning of the potential. Finally, the trajectory are all started with random values for both position and velocity at different values of the two real fields  $\alpha, \beta$ . A typical trajectory is shown in Fig. III. Note that the interesting part of the trajectory where non-gaussianities can be generated are at very large scales, comparable to the horizon scale today and at scales smaller than dwarf galaxies, i.e. very small scale perturbations. This behaviour is typical of our model for most trajectories.

From this set of trajectories we compute the distribution of  $\dot{\theta}$  and  $V'''$ . This is shown in Fig. VI. We can now evaluate Eq. 10 noting that  $\alpha(\nu) \sim 10$ ,  $\frac{\dot{\theta}}{H} \sim 10$ ,  $P_{\xi}^{1/2} = 6 \times 10^{-9}$  and  $\frac{-V'''}{H} \sim 5(f/M^2)$ , thus the relation between the SUSY breaking scale and the level of non-gaussianity reads

$$\sqrt{f} = \frac{\sqrt{f_{\text{NL}}}}{10^5} M \quad (11)$$

Using current observational limits from Planck [2] ( $f_{\text{NL}} < 14$ ), and adopting the minimum amount of non-gaussian fluctuations allowed by single-field inflation [23], provides a very tight constraint for the SUSY breaking energy scale  $\sqrt{f} = 3 - 7 \times 10^{13}$  GeV at 95% confidence.

In passing we note that the turns will generate isocurvature fluctuations at a level similar to the one needed to explain the observed power asymmetry at large scales [24, 25]; we will elaborate on this subject in a future publication.

## 6 Conclusions

We have presented in this article some more quantitative phenomenological findings for our proposal to identify the inflaton with the order parameter of SUSY breaking. We are motivated by finding a physical candidate for the inflaton, which seems to be the paradigm supported by current cosmological observations [1] to explain the origin, size, flatness and perturbations of the Universe. The model is successful at answering questions about the fundamental physics behind inflation. In particular:

1. Why does the inflaton start the slow-roll phase with nearly zero velocity? Because the non-linear friction term (loss of angular momentum) provided by the fact that we have broken R-symmetry; this produces a "slashing" phase.
2. Why does the universe inflate  $\sim 50$  e-folds? Because the inflaton rolls for about one Planck mass.
3. Why is the value of the CMB fluctuations the observed one? Due to the fact that in this model the fluctuations are proportional to the SUSY breaking scale, so thus the value of the fluctuations on the sky are linked to the energy chosen by nature to break SUSY.
4. Why does inflation end? At low energies the inflaton "integrates itself out" and manifests as a fermi gas of goldstinos, thus not behaving anymore as a scalar field.

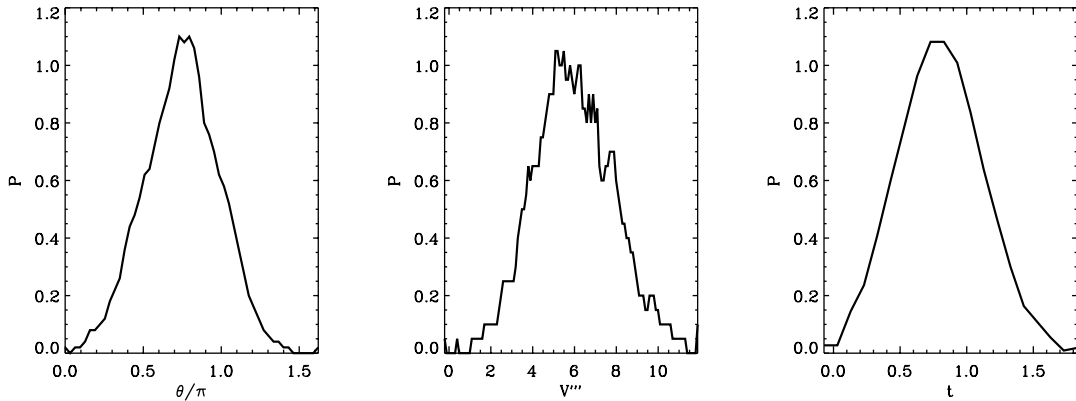


**Fig. VI:** The probability distribution for the values of  $\theta$  (angle of the turn),  $V'''$  (third derivative of the potential) and  $t$  (time it takes to turn) as derived from 1000 random trajectories generated for different initial conditions and values of the potential that generate at least 45 e-folds. These values are used to compute the amount of non-gaussianity generated in the trajectories.

Our model makes a very precise prediction: that the scale of SUSY breaking has to be at  $\sim 10^{13}$  GeV. This can be tested in the next LHC run starting in 2015. This relatively high energy scale implies that the possibility of observing SUSY at the LHC is slim but not completely excluded. The details will depend on the explicit parameters chosen to make contact with the low energy world ( $\sim 10$  TeV).

## References

- [1] Planck Collaboration, Ade, P. A. R., Aghanim, N., et al. 2013, arXiv:1303.5084
- [2] Planck Collaboration, Ade, P. A. R., Aghanim, N., et al. 2013, arXiv:1303.5082
- [3] V. Mukhanov, arXiv:1303.3925 [astro-ph.CO].
- [4] Martin, J., Ringeval, C., & Vennin, V. 2013, arXiv:1303.3787
- [5] Allen, T. J., Grinstein, B., & Wise, M. B. 1987, Physics Letters B, 197, 66
- [6] Salopek, D. S., & Bond, J. R. 1990, PRD, 42, 3936
- [7] Falk, T., Rangarajan, R., & Srednicki, M. 1993, ApJL, 403, L1
- [8] Gangui, A., Lucchin, F., Matarrese, S., & Mollerach, S. 1994, ApJ, 430, 447
- [9] L. Verde, L. -M. Wang, A. Heavens and M. Kamionkowski, Mon. Not. Roy. Astron. Soc. **313** (2000) L141
- [10] Wang, L., & Kamionkowski, M. 2000, PRD, 61, 063504
- [11] E. Komatsu and D. N. Spergel, Phys. Rev. D **63** (2001) 063002 [astro-ph/0005036].
- [12] V. Acquaviva, N. Bartolo, S. Matarrese and A. Riotto, Nucl. Phys. B **667** (2003) 119 [astro-ph/0209156].
- [13] J. M. Maldacena, JHEP **0305** (2003) 013 [astro-ph/0210603].
- [14] N. Bartolo, E. Komatsu, S. Matarrese and A. Riotto, Phys. Rept. **402** (2004) 103 [astro-ph/0406398].
- [15] L. Álvarez-Gaumé, C. Gómez, R. Jimenez, Phys. Lett. **B690**, 68-72 (2010). [arXiv:1001.0010] [hep-th]]
- [16] L. Alvarez-Gaume, C. Gomez, R. Jimenez, JCAP **1103** (2011) 027. [arXiv:1101.4948 [hep-th]].

- [17] L. Alvarez-Gaume, C. Gomez and R. Jimenez, JCAP **1203** (2012) 017 [arXiv:1110.3984 [astro-ph.CO]].
- [18] D. V. Volkov and V. P. Akulov, Phys. Lett. B **46**, 109 (1973).
- [19] Z. Komargodski and N. Seiberg, JHEP **0909**, 066 (2009) [arXiv:0907.2441 [hep-th]].
- [20] L. Verde, H. Peiris and R. Jimenez, JCAP **0601** (2006) 019 [astro-ph/0506036].
- [21] X. Chen and Y. Wang, Phys. Rev. D **81** (2010) 063511 [arXiv:0909.0496 [astro-ph.CO]].
- [22] X. Chen and Y. Wang, JCAP **1004** (2010) 027 [arXiv:0911.3380 [hep-th]].
- [23] L. Verde and S. Matarrese, Astrophys. J. **706** (2009) L91 [arXiv:0909.3224 [astro-ph.CO]].
- [24] L. Dai, D. Jeong, M. Kamionkowski and J. Chluba, arXiv:1303.6949 [astro-ph.CO].
- [25] P. A. R. Ade *et al.* [Planck Collaboration], arXiv:1303.5083 [astro-ph.CO].

# Mass hierarchy and string phenomenology in the LHC era

Ignatios Antoniadis<sup>\*,†</sup>

Department of Physics, CERN - Theory Unit, 1211 Geneva 23, Switzerland

## Abstract

I will discuss the status of the mass hierarchy problem and prospects for beyond the Standard Model physics in the light of the Higgs scalar discovery at the LHC and the experimental searches for new physics. In particular, I will discuss in this context low energy supersymmetry, living with the fine tuning and strings at the TeV scale.

## 1 Introduction

During the last few decades, physics beyond the Standard Model (SM) was guided from the problem of mass hierarchy. This can be formulated as the question of why gravity appears to us so weak compared to the other three known fundamental interactions corresponding to the electromagnetic, weak and strong nuclear forces. Indeed, gravitational interactions are suppressed by a very high energy scale, the Planck mass  $M_P \sim 10^{19}$  GeV, associated to a length  $l_P \sim 10^{-35}$  m, where they are expected to become important. In a quantum theory, the hierarchy implies a severe fine tuning of the fundamental parameters in more than 30 decimal places in order to keep the masses of elementary particles at their observed values. The reason is that quantum radiative corrections to all masses generated by the Higgs vacuum expectation value (VEV) are proportional to the ultraviolet cutoff which in the presence of gravity is fixed by the Planck mass. As a result, all masses are "attracted" to about  $10^{16}$  times heavier than their observed values.

Besides compositeness, there are two main theories that have been proposed and studied extensively during the last years, corresponding to different approaches of dealing with the mass hierarchy problem. (1) Low energy supersymmetry with all superparticle masses in the TeV region. Indeed, in the limit of exact supersymmetry, quadratically divergent corrections to the Higgs self-energy are exactly cancelled, while in the softly broken case, they are cutoff by the supersymmetry breaking mass splittings. (2) TeV scale strings, in which quadratic divergences are cutoff by the string scale and low energy supersymmetry is not needed. Both ideas are experimentally testable at high-energy particle colliders and in particular at LHC. Another option is to live with the hierarchy, addressing differently questions such as gauge coupling unification, dark matter candidate and electroweak (EW) vacuum stability. Split supersymmetry is an interesting example of such a possibility. All these ideas are experimentally testable at high-energy particle colliders and in particular at the LHC.

On the other hand, the recent major discovery of the Higgs boson at the LHC with a mass around 126 GeV is so far compatible with the Standard Model within  $2\sigma$  and its precision tests. It is also compatible with low energy supersymmetry, although with some degree of fine-tuning in its minimal version. Indeed, in the minimal supersymmetric Standard Model (MSSM), the lightest Higgs scalar mass  $m_h$  satisfies the following inequality:

$$m_h^2 \lesssim m_Z^2 \cos^2 2\beta + \frac{3}{(4\pi)^2} \frac{m_t^4}{v^2} \left[ \ln \frac{m_{\tilde{t}}^2}{m_t^2} + \frac{A_t^2}{m_{\tilde{t}}^2} \left( 1 - \frac{A_t^2}{12m_{\tilde{t}}^2} \right) \right] \lesssim (130 \text{ GeV})^2, \quad (1)$$

where the first term in the r.h.s. corresponds to the tree-level prediction and the second term includes the one loop corrections due to the top and stop loops. Here,  $m_Z$ ,  $m_t$ ,  $m_{\tilde{t}}$  are the  $Z$ -boson, the top and stop

---

<sup>†</sup> On leave from CPHT (UMR CNRS 7644) Ecole Polytechnique, F-91128 Palaiseau.

\*E-mail: ignatios.antoniadis@cern.ch

quark masses, respectively,  $v = \sqrt{v_1^2 + v_2^2}$  with  $v_i$  the VEVs of the two higgses,  $\tan \beta = v_2/v_1$ , and  $A_t$  the trilinear stop scalar coupling. Thus, a Higgs mass around 126 GeV requires a heavy stop  $m_{\tilde{t}} \simeq 3$  TeV for vanishing  $A_t$ , or  $A_t \simeq 3m_{\tilde{t}} \simeq 1.5$  TeV in the ‘best’ case. These values are obviously consistent with the present LHC bounds on supersymmetry searches, but they will certainly be probed in the next run at double energy. Theoretically, they imply a fine-tuning of the EW scale at the percent to per mille level. This fine-tuning can be alleviated in supersymmetric models beyond the MSSM, as discussed in the next session.

## 2 MSSM Higgs sector with dimension-five and dimension-six operators

Although extremely successful, the Standard Model or its supersymmetric version (MSSM) is not a fundamental theory, and this motivated the theoretical efforts to understand the nature of new physics beyond it. This search can be done using an effective field theory approach, in which the “new physics” is parametrised by effective operators. The power of this approach resides in arranging these operators in powers of  $1/M_*$  where  $M_*$  is the scale of new physics that generated them. To improve the predictive power, one considers additional organising principles, such as: **(i)** symmetry constraints that these operators should respect, often inspired by phenomenology (for example: R-parity, lepton or baryon number conservation, etc). **(ii)** a truncation of the series of operators to a given order in the power of the inverse scale  $1/M_*$ . The effective low-energy Lagrangian then takes the form

$$\mathcal{L} = \mathcal{L}_0 + \sum_{i,n} \frac{c_{n,i}}{M_*^n} \mathcal{O}_{n,i} \quad (2)$$

where  $\mathcal{L}_0$  is the SM or the MSSM Lagrangian;  $\mathcal{O}_{n,i}$  is an operator of dimension  $d = n + 4$  with the index  $i$  running over the set of operators of a given dimension;  $c_{n,i}$  are some coefficients of order  $\mathcal{O}(1)$ . This description is appropriate for scales  $E$  which satisfy  $E \ll M_*$ . Constraints from phenomenology can then be used to set bounds on the scale of new physics  $M_*$ .

Regarding the origin of operators  $\mathcal{O}_{n,i}$ , they can be generated classically or at the quantum level. At the classical level, this can happen by integration of some new massive states, via the equations of motion and one then generates an infinite series. This can happen even in 4D renormalisable theories; indeed, even though the low energy interaction looks nonrenormalisable, it may actually point to a renormalisable theory valid up to a much higher scale (a familiar example is the Fermi interaction). Such effective operators are also generated at the quantum level, for example following compactification of a higher dimensional theory, by the radiative corrections associated with momentum and winding modes of the compactification [1–5].

The effects of these operators on the low energy observables can be comparable to the radiative effects of light states in the SM/MSSM [6] and this shows the importance of their study. In the following we shall study these effects to the case of the MSSM Higgs sector with additional operators of dimensions  $d = 5$  and  $d = 6$ . In particular we show that the mass of lightest SM-like Higgs can easily be increased close to the observed value by new physics in the region of few TeV. We then discuss the nature of the “new physics” behind the effective operators.

### 2.1 MSSM with d=5 operators.

As an application, consider the MSSM extended by all possible  $d = 5$  operators that respect R-parity, baryon and lepton number symmetry. The Lagrangian is  $\mathcal{L} = \mathcal{L}_0 + \mathcal{L}^{(5)}$  where

$$\begin{aligned} \mathcal{L}_0 &= \int d^4\theta \sum_{i=1,2} Z_i(S, S^\dagger) H_i^\dagger e^{V_i} H_i + \left\{ \int d^2\theta \mu_0 (1 + B_0 S) H_1 \cdot H_2 + h.c. \right\} + \dots \\ &+ \int d^2\theta \left[ Q \lambda_U(S) U^c H_2 - Q \lambda_D(S) D^c H_1 - L \lambda_E(S) E^c H_1 \right] + h.c. \end{aligned} \quad (3)$$

The dots stand for Higgs-independent terms and  $Z_i(S, S^\dagger) = 1 - c_i S^\dagger S$ ,  $c_i \sim \mathcal{O}(1)$ . Further

$$\begin{aligned} \mathcal{L}^{(5)} = & \frac{1}{M_*} \int d^4\theta \left[ H_1^\dagger e^{V_1} Q Y_U U^c + H_2^\dagger e^{V_2} Q Y_D D^c + H_2^\dagger e^{V_2} L Y_E E^c \right. \\ & \left. + a D^\alpha [b H_2 e^{-V_1}] D_\alpha [c e^{V_1} H_1] + \delta(\bar{\theta}^2) [QU^c T_Q QD^c + QU^c T_L LE^c + \lambda_H (H_1 H_2)^2] + h.c. \right] \end{aligned} \quad (4)$$

with a standard notation. We introduced here some spurion dependent functions:  $a, b, c, Z_{1,2}, Y_F, F = U, D, E$ , which are general functions of  $(S, S^\dagger)$  while  $T_Q, T_L, \lambda_H$ , are holomorphic functions of  $S$ . Here  $S = m_0 \theta^2$  is the spurion superfield and  $m_0$  the supersymmetry breaking scale, with  $m_0 = \langle F_{hidden} \rangle / M_P$ , so supersymmetry breaking is transmitted via gravitational interaction. Any supersymmetry breaking associated with the presence of the above interactions is included using the spurion field technique. Not all operators in (4) are independent [6]. To remove the redundant operators we use field re-definitions:

$$\begin{aligned} H_1 & \rightarrow H_1 - \frac{1}{M_*} \bar{D}^2 \left[ \Delta_1 H_2^\dagger e^{V_2} (i\sigma_2) \right]^T + \frac{1}{M_*} Q \rho_U U^c \\ H_2 & \rightarrow H_2 + \frac{1}{M_*} \bar{D}^2 \left[ \Delta_2 H_1^\dagger e^{V_1} (i\sigma_2) \right]^T + \frac{1}{M_*} Q \rho_D D^c + \frac{1}{M_*} L \rho_E E^c \end{aligned} \quad (5)$$

where  $\rho_F = \rho_F(S)$ ,  $F = U, D, E$ ,  $\Delta_i = \Delta_i(S, S^\dagger)$ ,  $i = 1, 2$ , can be chosen arbitrarily. To avoid the presence of flavour changing neutral currents, the following simple ansatz can be made:

$$\begin{aligned} T_Q(S) & = c_Q(S) \lambda_U(0) \otimes \lambda_D(0), & T_L(S) & = c_L(S) \lambda_U(0) \otimes \lambda_E(0), \\ \rho_F(S) & = c_F(S) \lambda_F(0), & Y_F(S, S^\dagger) & = y_F(S, S^\dagger) \lambda_F(0), \quad F = U, D, E. \end{aligned} \quad (6)$$

and, as usual  $\lambda_F(S) = \lambda_F(0) (1 + A_F S)$ . Using a suitable choice for the (otherwise arbitrary) coefficients of the spurion entering in  $\Delta_{1,2}$ , one can set  $T_Q = T_L = 0$  also  $a = b = c = 0$  and  $Y_F \rightarrow y_F(S^\dagger) \lambda_F(0)$ . Then one finds [6]

$$\begin{aligned} \mathcal{L}^{(5)} = & \frac{1}{M_*} \int d^4\theta \left[ H_1^\dagger e^{V_1} Q Y'_U(S^\dagger) U^c + H_2^\dagger e^{V_2} Q Y'_D(S^\dagger) D^c + H_2^\dagger e^{V_2} L Y'_E(S^\dagger) E^c + h.c. \right] \\ & + \frac{1}{M_*} \int d^2\theta \lambda'_H(S) (H_1 H_2)^2 + h.c. \end{aligned} \quad (7)$$

Detailed calculations show [6] that the new Yukawa couplings  $Y'_F(S^\dagger)$  now depend on  $S^\dagger$  only,  $Y'_F(S^\dagger) = \lambda_F(0) (x_0^F + x_2^F S^\dagger)$ . After (5), the couplings of  $\mathcal{L}_0$  also acquired, at tree level, threshold corrections which depend on  $M_*$  [6]. The new form of  $\mathcal{L}^{(5)}$  in (7) gives the minimal irreducible set of R-parity, B, L conserving  $d=5$  operators that can be present beyond MSSM.

A consequence of this analysis is the generation of new couplings, beyond those in the MSSM at the tree level. For example there is a ‘‘wrong’’-Higgs Yukawa coupling, that exchanges the holomorphic dependence on one Higgs by that on the hermitian conjugate of the other [8, 9]. Such couplings do arise in the MSSM at one-loop, after integrating out massive squarks and are suppressed by  $m_0^2/M_*^2 \times (\text{loop-factor})$ . Here they are suppressed by  $m_0/M_*$  only, as seen below:

$$\frac{M_s}{M_*} \left[ x_2^U [\lambda_U(0)]_{ij} (h_1^\dagger q_{L i}) u_{R j}^c + x_2^D [\lambda_D(0)]_{ij} (h_2^\dagger q_{L i}) d_{R j}^c + x_2^E [\lambda_E(0)]_{ij} (h_2^\dagger l_{L i}) e_{R j}^c + h.c. \right] \quad (8)$$

These couplings bring a  $\tan \beta$  enhancement of a prediction for a physical observable, such as the bottom quark mass, relative to bottom quark Yukawa coupling:

$$m_b = (1/\sqrt{2}) v \cos \beta (\lambda_b + \delta \lambda_b + \Delta \lambda_b \tan \beta) \quad (9)$$

Here  $\lambda_b$  is the usual bottom quark Yukawa coupling,  $\delta \lambda_b$  is its one-loop correction in MSSM and  $\Delta \lambda_b$  is a ‘‘wrong’’-Higgs coupling’ corrections, obtained after integrating out at one-loop massive squarks in MSSM; in our case  $\Delta \lambda_b$  receives an extra correction from (8), which can actually be larger than its one-loop-generated MSSM counterpart [8, 10–12]. This can bring a  $\tan \beta$  enhancement of the Higgs decay rate into bottom quarks pairs (for further details see [6]).

## 2.2 MSSM Higgs sector with $d=5$ and $d=6$ operators

We can extend the previous discussion by including all effective operators of both dimension  $d = 5$  and  $d = 6$  that can exist beyond the MSSM Higgs sector. This can be motivated in various ways. The MSSM Higgs sector is a minimal construction and extension of that of the SM. It does not take into account possible non-perturbative effects [13] or additional massive states that can couple to the Higgs sector and generate, when integrated out, new contributions. The fine tuning [14, 15] needed to have the SM-like Higgs mass well above the LEP bound [16] can also be a problem and it may indicate the existence of new physics beyond the Higgs sector. Such problems may be addressed by using a model-independent approach, using the effective operators. In the leading order, new physics beyond the MSSM Higgs sector can manifest itself as operators of either  $d = 5$  [6, 17–19] or  $d = 6$  [7, 20] or both. If generated by the same new physics, by comparing  $\mathcal{O}(1/M^*)$  and  $\mathcal{O}(1/M_*^2)$  terms one can estimate when the series expansion in  $1/M_*$  breaks down. The operators in the Higgs sector of dimension  $d = 5$  were:

$$\begin{aligned}\mathcal{L}_1 &= \frac{1}{M_*} \int d^2\theta \lambda'_H(S) (H_2 \cdot H_1)^2 + h.c. = 2\zeta_{10} (h_2 \cdot h_1)(h_2 \cdot F_1 + F_2 \cdot h_1) + \zeta_{11} m_0 (h_2 \cdot h_1)^2 + h.c., \\ \mathcal{L}_2 &= \frac{1}{M_*} \int d^4\theta \left\{ a(S, S^\dagger) D^\alpha \left[ b(S, S^\dagger) H_2 e^{-V_1} \right] D_\alpha \left[ c(S, S^\dagger) e^{V_1} H_1 \right] + h.c. \right\}\end{aligned}\quad (10)$$

where

$$\lambda'_H(S)/M_* = \zeta_{10} + \zeta_{11} m_0 \theta\theta, \quad \zeta_{10}, \zeta_{11} \sim 1/M_*, \quad (11)$$

$\mathcal{L}_1$  can be generated by integrating out a massive gauge singlet or  $SU(2)$  triplet. Indeed, in the MSSM with a massive gauge singlet, with an F-term of type  $M_* \Sigma^2 + \Sigma H_1 \cdot H_2$ , when integrating out  $\Sigma$  generates  $\mathcal{L}_1$ .  $\mathcal{L}_2$  can be generated in various ways (see Appendix A, B in [6]) but perhaps the simplest way is via an additional pair of massive Higgs doublets of mass of order  $M_*$ . As already discussed,  $\mathcal{L}_2$  can be removed by general spurion-dependent field redefinitions, up to soft terms and  $\mu$  term renormalisation and  $\mathcal{O}(1/M_*^2)$  corrections [6].

We assume that  $m_0 \ll M_*$ , so that the effective approach is reliable. If this is not respected and the “new physics” is represented by “light” states (like the MSSM states), the  $1/M_*$  expansion is not reliable and one should work in a setup where these are not integrated out.

The list of  $d = 6$  operators is longer [21]:

$$\begin{aligned}\mathcal{O}_1 &= \frac{1}{M_*^2} \int d^4\theta \mathcal{Z}_1 (H_1^\dagger e^{V_1} H_1)^2, & \mathcal{O}_5 &= \frac{1}{M_*^2} \int d^4\theta \mathcal{Z}_5 (H_1^\dagger e^{V_1} H_1) H_2 \cdot H_1 + h.c. \\ \mathcal{O}_2 &= \frac{1}{M_*^2} \int d^4\theta \mathcal{Z}_2 (H_2^\dagger e^{V_2} H_2)^2, & \mathcal{O}_6 &= \frac{1}{M_*^2} \int d^4\theta \mathcal{Z}_6 (H_2^\dagger e^{V_2} H_2) H_2 \cdot H_1 + h.c. \\ \mathcal{O}_3 &= \frac{1}{M_*^2} \int d^4\theta \mathcal{Z}_3 (H_1^\dagger e^{V_1} H_1) (H_2^\dagger e^{V_2} H_2), & \mathcal{O}_7 &= \frac{1}{M_*^2} \int d^2\theta \mathcal{Z}_7 \text{Tr} W^\alpha W_\alpha (H_2 H_1) + h.c. \\ \mathcal{O}_4 &= \frac{1}{M_*^2} \int d^4\theta \mathcal{Z}_4 (H_2 \cdot H_1) (H_2 \cdot H_1)^\dagger, & \mathcal{O}_8 &= \frac{1}{M_*^2} \int d^4\theta \mathcal{Z}_8 (H_2 H_1)^2 + h.c.\end{aligned}\quad (12)$$

where  $W^\alpha = (-1/4) \overline{D}^2 e^{-V} D^\alpha e^V$  is the chiral field strength of  $SU(2)_L$  or  $U(1)_Y$  vector superfields  $V_w$  and  $V_Y$  respectively. Also  $V_{1,2} = V_w^\alpha (\sigma^\alpha/2) + (\mp 1/2) V_Y$  with the upper (minus) sign for  $V_1$ . The remaining  $d = 6$  operators involve extra space-time derivatives:

$$\begin{aligned}\mathcal{O}_9 &= \frac{1}{M_*^2} \int d^4\theta \mathcal{Z}_9 H_1^\dagger \overline{\nabla}^2 e^{V_1} \nabla^2 H_1 & \mathcal{O}_{12} &= \frac{1}{M_*^2} \int d^4\theta \mathcal{Z}_{12} H_2^\dagger e^{V_2} \nabla^\alpha W_\alpha^{(2)} H_2 \\ \mathcal{O}_{10} &= \frac{1}{M_*^2} \int d^4\theta \mathcal{Z}_{10} H_2^\dagger \overline{\nabla}^2 e^{V_2} \nabla^2 H_2 & \mathcal{O}_{13} &= \frac{1}{M_*^2} \int d^4\theta \mathcal{Z}_{13} H_1^\dagger e^{V_1} W_\alpha^{(1)} \nabla^\alpha H_1\end{aligned}$$

$$\mathcal{O}_{11} = \frac{1}{M_*^2} \int d^4\theta \mathcal{Z}_{11} H_1^\dagger e^{V_1} \nabla^\alpha W_\alpha^{(1)} H_1 \quad \mathcal{O}_{14} = \frac{1}{M_*^2} \int d^4\theta \mathcal{Z}_{14} H_2^\dagger e^{V_2} W_\alpha^{(2)} \nabla^\alpha H_2 \quad (13)$$

Also  $\nabla_\alpha H_i = e^{-V_i} D_\alpha e^{V_i} H_i$  and  $W_\alpha^i$  is the field strength of  $V_i$ . To be general, in the above operators one should include spurion ( $S$ ) dependence under any  $\nabla_\alpha$ , of arbitrary coefficients, to account for supersymmetry breaking effects associated to them. Finally, the wavefunction coefficients are spurion dependent and have the structure

$$(1/M_*^2) \mathcal{Z}_i(S, S^\dagger) = \alpha_{i0} + \alpha_{i1} m_0 \theta\theta + \alpha_{i1}^* m_0 \bar{\theta}\bar{\theta} + \alpha_{i2} m_0^2 \theta\theta\bar{\theta}\bar{\theta}, \quad \alpha_{ij} \sim 1/M_*^2. \quad (14)$$

Regarding the origin of these operators:  $\mathcal{O}_{1,2,3}$  can be generated in the MSSM by an additional, massive  $U(1)'$  gauge boson or  $SU(2)$  triplets, when integrated out [17].  $\mathcal{O}_4$  can be generated by a massive gauge singlet or  $SU(2)$  triplet, while  $\mathcal{O}_{5,6}$  can be generated by a combination of  $SU(2)$  doublets and massive gauge singlet.  $\mathcal{O}_7$  is essentially a threshold correction to the gauge coupling, with a moduli field replaced by the Higgs.  $\mathcal{O}_8$  exists only in non-susy case, but is generated when removing the  $d = 5$  derivative operator  $\mathcal{L}_2$  by field redefinitions [6], so we keep it.

It can be shown that operators  $\mathcal{O}_{9,\dots,14}$ , can be eliminated along the lines discussed in the previous sections. For example, in the absence of gauge interactions,  $\mathcal{O}_9$  is similar to the operator in eq.(7) and only brings a wavefunction renormalisation,  $\mathcal{O}_9 \sim |\mu|^2/M_*^2 \int d^4\theta H_1^\dagger H_1$ , and similar for  $\mathcal{O}_{10}$ . Regarding  $\mathcal{O}_{11,12}$ , in the supersymmetric case they vanish, following the definition of  $\nabla^\alpha$  and an integration by parts. Further,  $\mathcal{O}_{13,14}$  are similar to  $\mathcal{O}_{9,10}$ , which can be seen by using the definition of  $W_\alpha^{(i)}$  and the relation between  $\nabla^2, (\bar{\nabla}^2)$  and  $D^2, (\bar{D}^2)$ . In the presence of supersymmetry breaking, elimination of these operators and their supersymmetry breaking contribution is still possible, up to a renormalisation of the soft terms and  $\mu$  term [6].

### 2.3 Higgs mass corrections from $d = 5$ and $d = 6$ operators.

With the remaining set of independent, effective operators  $\mathcal{L}_1, \mathcal{O}_{1,\dots,8}$  of dimensions  $d = 5$  and  $d = 6$ , one finds the scalar potential  $V$  and its EW minimum; this is perturbed by  $\mathcal{O}(1/M_*^2)$  corrections from that of the MSSM. The expression of  $V$  is long and it is not given here (see [7] for its form). From  $V$  one computes the mass of CP-odd/even Higgs fields. One has:

$$m_A^2 = (m_A^2)_{\text{MSSM}} - \frac{2\zeta_{10}\mu_0 v^2}{\sin 2\beta} + 2m_0\zeta_{11}v^2 + \delta m_A^2, \quad \delta m_A^2 = \mathcal{O}(1/M_*^2) \quad (15)$$

for the pseudoscalar Higgs, with  $(m_A^2)_{\text{MSSM}}$  the MSSM value, with  $\delta m_A^2$  due to  $\mathcal{O}(1/M_*^2)$  corrections from  $d = 5$  and  $d = 6$  operators. For the CP-even Higgs one has [6, 17, 19]

$$\begin{aligned} m_{h,H}^2 &= (m_{h,H}^2)_{\text{MSSM}} \\ &+ (2\zeta_{10}\mu_0)v^2 \sin 2\beta \left[ 1 \pm \frac{m_A^2 + m_Z^2}{\sqrt{\tilde{w}}} \right] + \frac{(-2\zeta_{11}m_0)v^2}{2} \left[ 1 \mp \frac{(m_A^2 - m_Z^2) \cos^2 2\beta}{\sqrt{\tilde{w}}} \right] \\ &+ \delta m_{h,H}^2, \quad \text{where} \quad \delta m_{h,H}^2 = \mathcal{O}(1/M_*^2) \end{aligned} \quad (16)$$

The upper (lower) signs correspond to  $h$  ( $H$ ), and  $\tilde{w} \equiv (m_A^2 + m_Z^2)^2 - 4m_A^2 m_Z^2 \cos^2 2\beta$ . With this result one can show that the mass  $m_h$  can be increased near the observed value, also with the help of quantum corrections [6, 17–19].

Regarding the  $\mathcal{O}(1/M_*^2)$  corrections of  $\delta m_{h,H}^2, \delta m_A^2$  and  $\delta m_{h,H}^2$  of (15), (16), in the general case of including all operators and their associated supersymmetry breaking, they have a complicated form.

Exact expressions can be found in [7, 20]. For most purposes, an expansion of these in  $1/\tan\beta$  is accurate enough. At large  $\tan\beta$ ,  $d = 6$  operators bring corrections comparable to those of  $d = 5$  operators. The relative  $\tan\beta$  enhancement of  $\mathcal{O}(1/M_*^2)$  corrections compensates for the extra suppression that these have relative to  $\mathcal{O}(1/M_*)$  operators (which involve both  $h_1, h_2$  and are not enhanced in this limit). Note however that in some models only  $d = 6$  operators may be present, depending on the details of the “new physics” generating the effective operators.

Let us present the correction  $\mathcal{O}(1/M^2)$  to  $m_{h,H}^2$  for the case  $m_A$  is kept fixed to an appropriate value. The result is, assuming  $m_A > m_Z$ , (otherwise  $\delta m_h^2$  and  $\delta m_H^2$  are exchanged):

$$\begin{aligned} \delta m_h^2 = & -2v^2 \left[ \alpha_{22} m_0^2 + (\alpha_{30} + \alpha_{40}) \mu_0^2 + 2\alpha_{61} m_0 \mu_0 - \alpha_{20} m_Z^2 \right] - (2\zeta_{10} \mu_0)^2 v^4 (m_A^2 - m_Z^2)^{-1} \\ & + v^2 \cot\beta \left[ (m_A^2 - m_Z^2)^{-1} \left( 4m_A^2 \left( (2\alpha_{21} + \alpha_{31} + \alpha_{41} + 2\alpha_{81}) m_0 \mu_0 + (2\alpha_{50} + \alpha_{60}) \mu_0^2 + \alpha_{62} m_0^2 \right) \right. \right. \\ & \left. \left. - (2\alpha_{60} - 3\alpha_{70}) m_A^2 m_Z^2 - (2\alpha_{60} + \alpha_{70}) m_Z^4 \right) + 8(m_A^2 + m_Z^2) (\mu_0 m_0 \zeta_{10} \zeta_{11}) v^2 / (m_A^2 - m_Z^2)^2 \right] \\ & + \mathcal{O}(1/\tan^2\beta) \end{aligned} \quad (17)$$

A similar formula exists for the correction to  $m_H$ :

$$\begin{aligned} \delta m_H^2 = & \left[ -2(m_0 \mu_0 (\alpha_{51} + \alpha_{61}) + \alpha_{82}), m_0^2 \right] v^2 + (2\zeta_{10} \mu_0)^2 v^4 (m_A^2 - m_Z^2)^{-1} \\ & + v^2 \cot\beta \left[ (m_A^2 - m_Z^2)^{-1} \left( 2m_A^2 \left( 2(\alpha_{11} - \alpha_{21}) m_0 \mu_0 + (\alpha_{60} - \alpha_{50}) \mu_0^2 + (\alpha_{52} - \alpha_{62}) m_0^2 - \alpha_{60} m_A^2 \right) \right. \right. \\ & \left. \left. - \left[ 4(\alpha_{11} + \alpha_{21} + \alpha_{31} + \alpha_{41} + 2\alpha_{81}) m_0 \mu_0 + 6(\alpha_{50} + \alpha_{60}) \mu_0^2 + 2(\alpha_{52} + \alpha_{62}) m_0^2 \right. \right. \right. \\ & \left. \left. \left. - (\alpha_{50} + 5\alpha_{60} - 2\alpha_{70}) m_A^2 m_Z^2 - (\alpha_{50} - \alpha_{60}) m_Z^4 \right) - 8(m_A^2 + m_Z^2) (\mu_0 m_0 \zeta_{10} \zeta_{11}) v^2 / (m_A^2 - m_Z^2)^2 \right] \\ & + \mathcal{O}(1/\tan^2\beta) \end{aligned} \quad (18)$$

The mass corrections in (17), (18) must be added to the rhs of eqs.(16) to obtain the full value of  $m_{h,H}^2$ . Together with (12), (14), these corrections identify the operators of  $d = 6$  with the largest contributions, which is important for model building beyond the MSSM Higgs sector. These operators are  $\mathcal{O}_{2,3,4}$  in the absence of supersymmetry breaking and  $\mathcal{O}_{2,6}$  when this is broken. It is preferable, however, to increase  $m_h^2$  by supersymmetric rather than supersymmetry-breaking effects of the effective operators, because the latter are less under control in the effective approach; also, one would favour a supersymmetric solution to the fine-tuning problem associated with increasing the MSSM Higgs mass. Therefore  $\mathcal{O}_{2,3,4}$  are the leading operators, with the remark that  $\mathcal{O}_2$  has a smaller effect, of order  $(m_Z/\mu_0)^2$  relative to  $\mathcal{O}_{3,4}$  (for similar  $\alpha_{j0}$ ,  $j = 2, 3, 4$ ). At smaller  $\tan\beta$ ,  $\mathcal{O}_{5,6}$  can also give significant contributions, while  $\mathcal{O}_7$  has a relative suppression factor  $(m_Z/\mu_0)^2$ . Note that we kept all operators  $\mathcal{O}_i$  independent. By doing so, one can easily single out the individual contribution of each operator, which helps in model building, since not all operators are present in a specific model.

One limit to consider is that where the operators of  $d = 6$  have coefficients such that their contributions add up to maximise  $\delta m_h^2$ . Since  $\alpha_{ij}$  are not known, one can choose:

$$-\alpha_{22} = -\alpha_{61} = -\alpha_{30} = -\alpha_{40} = \alpha_{20} > 0 \quad (19)$$

In this case, at large  $\tan\beta$ :

$$\delta m_h^2 \approx 2v^2 \alpha_{20} [m_0^2 + 2m_0 \mu_0 + 2\mu_0^2 + m_Z^2] \quad (20)$$

A simple numerical example is illustrative. For  $m_0 = 1$  TeV,  $\mu_0 = 350$  GeV, and with  $v \approx 246$  GeV, one has  $\delta m_h^2 \approx 2.36 \alpha_{20} \times 10^{11} (\text{GeV})^2$ . Assuming  $M_* = 10$  TeV and ignoring  $d = 5$  operators,

with  $\alpha_{20} \sim 1/M_*^2$  and the MSSM value of  $m_h$  taken to be its upper classical limit  $m_Z$  (reached for large  $\tan \beta$ ), we obtain an increase of  $m_h$  from  $d = 6$  operators alone of about  $\Delta m_h = 12.15$  GeV to  $m_h \approx 103$  GeV. An increase of  $\alpha_{20}$  by a factor of 2.5 to  $\alpha_{20} \sim 2.5/M_*^2$  would give  $\Delta m_h \approx 28$  GeV to  $m_h \approx 119.2$  GeV, which is already above the LEP bound. Note that this increase is realised even for a scale  $M_*$  of “new physics” beyond the LHC reach.

The above choice of  $M_* = 10$  TeV was partly motivated by the fine-tuning results [18] (for  $d = 5$  operators) and on convergence grounds: the expansion parameter of our effective analysis is  $m_q/M_*$  where  $m_q$  is any scale of the theory, in particular it can be  $m_0$ . For a susy breaking scale  $m_0 \sim \mathcal{O}(1)$  TeV (say  $m_0 = 3$  TeV) and  $c_{1,2}$  or  $\alpha_{ij}$  of  $\mathcal{Z}_i(S, S^\dagger)$  of order unity (say  $c_{1,2} = 2.5$ ) one has for  $M_* = 10$  TeV that  $c_{1,2} m_0/M_* = 0.75$  which is already close to unity, and at the limit of validity of the effective expansion in powers of  $1/M_*$ . To conclude, even for a scale of “new physics” above the LHC reach, one can still classically increase  $m_h$  to near the LHC measured value.

## 2.4 Final remarks

The final step is to identify the nature of “new physics” that generated the operators with the largest correction to  $m_h$ , ideally from a renormalisable model. At the level of dimension  $d = 5$  operators, this is clear from previous discussion: a massive gauge singlet can generate operator  $\mathcal{L}_1$  of (10) and the needed increase of  $m_h$ , for a scale  $M_* \sim 5 - 10$  TeV [18]; this can provide a solution to the little hierarchy problem, provided that one can fix dynamically the scale  $M_*$ .

For dimension-six operators, from the above discussion one finds that to increase  $m_h$  it is needed that one or more of the following conditions are satisfied:

$$\alpha_{20} > 0, \alpha_{30} < 0, \alpha_{40} < 0 \quad (21)$$

First recall that  $\mathcal{O}_{1,2,3}$  can be most easily generated by integrating out a massive gauge boson  $U(1)'$  or  $SU(2)$  triplets [17], while  $\mathcal{O}_4$  can be generated by a massive gauge singlet or  $SU(2)$  triplets. Let us discuss the signs of the operators when they are generated as above:

- (a):** Integrating out a massive vector superfield  $U(1)'$  under which Higgs fields have opposite charges (to avoid a Fayet-Iliopoulos term), one finds  $\alpha_{20} < 0$  and  $\alpha_{30} > 0$  (also  $\alpha_{10} < 0$ ) [17], which is opposite to what we need. This can be changed, if for example there are additional pairs of massive Higgs doublets also charged under new  $U(1)'$ ; then  $\mathcal{O}_3$  could be generated with  $\alpha_{30} < 0$ .
- (b):** Integrating massive  $SU(2)$  triplets that couple to the MSSM Higgs sector would bring  $\alpha_{20} > 0$ ,  $\alpha_{40} < 0$ ,  $\alpha_{30} > 0$ , so the first two relations agree with what we need.
- (c):** Integrating a massive gauge singlet would bring  $\alpha_{40} > 0$ , which would instead decrease  $m_h$ .

Finally, at large  $\tan \beta$ , due to additional corrections that effective operators bring to the  $\rho$  parameter [22], it turns out that  $\alpha_{40}$  and  $\alpha_{30}$  can have the largest correction to  $m_h^2$ , while avoiding  $\rho$ -parameter constraints. The case of a massive gauge singlet or additional  $U(1)'$  vector superfield (giving  $\mathcal{O}_{3,4}$ ) have the advantage of preserving gauge couplings unification at one-loop. Following the above information, one can proceed to construct explicit models with additional states that can generate these effective operators.

Let us mention that the method provided here to reduce the fine tuning in the MSSM for  $m_h$ , relies on introducing an additional scale in the visible sector, due to “new physics” in this sector. Other solutions to this problem may exist, which essentially rely on a low scale in the hidden sector of supersymmetry breaking [23]. In this case the quartic coupling and the mass of the SM-like Higgs are increased by a factor proportional to  $(\mu^2/f)^2$ , where  $f$  is the hidden sector supersymmetry breaking scale. While not without problems, the advantage of this latter method is that it does not pay the “cost” of an additional parameter (scale) in the visible sector, as models with effective operators do.

### 3 Strings and extra dimensions

The appropriate and most convenient framework for low energy supersymmetry and grand unification is the perturbative heterotic string. Indeed, in this theory, gravity and gauge interactions have the same origin, as massless modes of the closed heterotic string, and they are unified at the string scale  $M_s$ . As a result, the Planck mass is predicted to be proportional to  $M_s$ :

$$M_P = M_s/g, \quad (22)$$

where  $g$  is the gauge coupling. In the simplest constructions all gauge couplings are the same at the string scale, given by the four-dimensional (4d) string coupling, and thus no grand unified group is needed for unification. In our conventions  $\alpha_{\text{GUT}} = g^2 \simeq 0.04$ , leading to a discrepancy between the string and grand unification scale  $M_{\text{GUT}}$  by almost two orders of magnitude. Explaining this gap introduces in general new parameters or a new scale, and the predictive power is essentially lost. This is the main defect of this framework, which remains though an open and interesting possibility.

The other other perturbative framework that has been studied extensively in the more recent years is type I string theory with D-branes. Unlike in the heterotic string, gauge and gravitational interactions have now different origin. The latter are described again by closed strings, while the former emerge as excitations of open strings with endpoints confined on D-branes [24]. This leads to a braneworld description of our universe, which should be localized on a hypersurface, i.e. a membrane extended in  $p$  spatial dimensions, called  $p$ -brane (see Fig. 1). Closed strings propagate in all nine dimensions of string theory: in those extended along the  $p$ -brane, called parallel, as well as in the transverse ones. On the contrary, open strings are attached on the  $p$ -brane. Obviously, our  $p$ -brane world must have at least the

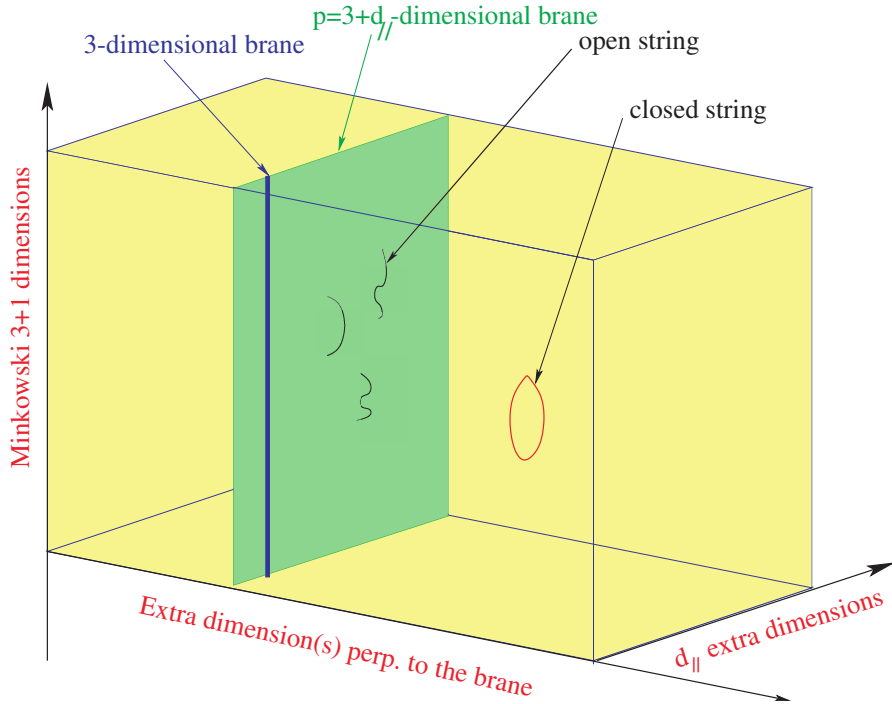


**Fig. 1:** D-brane world universe in type I string framework.

three known dimensions of space. But it may contain more: the extra  $d_{||} = p-3$  parallel dimensions must have a finite size, in order to be unobservable at present energies, and can be as large as  $\text{TeV}^{-1} \sim 10^{-18}$

m [25]. On the other hand, transverse dimensions interact with us only gravitationally and experimental bounds are much weaker: their size should be less than about 0.1 mm [26]. In the following, I review the main properties and experimental signatures of low string scale models [27].

### 3.1 Framework of low scale strings

In type I theory, the different origin of gauge and gravitational interactions implies that the relation between the Planck and string scales is not linear as (22) of the heterotic string. The requirement that string theory should be weakly coupled, constrain the size of all parallel dimensions to be of order of the string length, while transverse dimensions remain unrestricted. Assuming an isotropic transverse space of  $n = 9 - p$  compact dimensions of common radius  $R_\perp$ , one finds:

$$M_P^2 = \frac{1}{g_s^2} M_s^{2+n} R_\perp^n, \quad g_s \simeq g^2. \quad (23)$$

where  $g_s$  is the string coupling. It follows that the type I string scale can be chosen hierarchically smaller than the Planck mass [27, 28] at the expense of introducing extra large transverse dimensions felt only by gravity, while keeping the string coupling small [27]. The weakness of 4d gravity compared to gauge interactions (ratio  $M_W/M_P$ ) is then attributed to the largeness of the transverse space  $R_\perp$  compared to the string length  $l_s = M_s^{-1}$ .

An important property of these models is that gravity becomes effectively  $(4 + n)$ -dimensional with a strength comparable to those of gauge interactions at the string scale. The first relation of Eq. (23) can be understood as a consequence of the  $(4 + n)$ -dimensional Gauss law for gravity, with  $M_*^{(4+n)} = M_s^{2+n}/g^4$  the effective scale of gravity in  $4 + n$  dimensions. Taking  $M_s \simeq 1$  TeV, one finds a size for the extra dimensions  $R_\perp$  varying from  $10^8$  km, .1 mm, down to a Fermi for  $n = 1, 2$ , or 6 large dimensions, respectively. This shows that while  $n = 1$  is excluded,  $n \geq 2$  is allowed by present experimental bounds on gravitational forces [26, 29]. Thus, in these models, gravity appears to us very weak at macroscopic scales because its intensity is spread in the ‘‘hidden’’ extra dimensions. At distances shorter than  $R_\perp$ , it should deviate from Newton’s law, which may be possible to explore in laboratory experiments.

### 3.2 Large number of species

Here, we open a parenthesis to describe that low scale gravity with large extra dimensions is actually a particular case of a more general framework, where the ultraviolet (UV) cutoff is lower than the Planck scale due to the existence of a large number of particle species coupled to gravity [30]. Indeed, it was shown that the effective UV cutoff  $M_*$  is given by

$$M_*^2 = M_P^2/N, \quad (24)$$

where the counting of independent species  $N$  takes into account all particles which are not broad resonances, having a width less than their mass. The derivation is based on black hole evaporation but here we present a shorter argument using quantum information storage [31]. Consider a pixel of size  $L$  containing  $N$  species storing information. The energy required to localize  $N$  wave functions is then given by  $N/L$ , associated to a Schwarzschild radius  $R_s = N/LM_P^2$ . The latter must be less than the pixel size in order to avoid the collapse of such a system to a black hole,  $R_s \leq L$ , implying a minimum size  $L \geq L_{min}$  with  $L_{min} = \sqrt{N}/M_P$  associated precisely to the effective UV cutoff  $M_* = L_{min}$  given in eq. (24). Imposing  $M_* \simeq 1$  TeV, one should then have  $N \sim 10^{32}$  particle species below about the TeV scale!

In the string theory context, there are two ways of realizing such a large number a particle species by lowering the string scale at a TeV:

1. In large volume compactifications with the SM localized on D-brane stacks, as described in the previous section. The particle species are then the Kaluza-Klein (KK) excitations of the graviton

(and other possible bulk modes) associated to the large extra dimensions, given by  $N = R_{\perp}^n l_s^n$ , up to energies of order  $M_* \simeq M_s$ .

2. By introducing an infinitesimal string coupling  $g_s \simeq 10^{-16}$  with the SM localized on Neveu-Schwarz NS5-branes in the framework of little strings [32]. In this case, the particle species are the effective number of string modes that contribute to the black hole bound [33]:  $N = 1/g_s^2$  and gravity does not become strong at  $M_s \sim \mathcal{O}(\text{TeV})$ .

Note the both TeV string realizations above are compatible with the general expression (23), but in the second case there is no relation between the string and gauge couplings.

### 3.3 Experimental implications in accelerators

We now turn to the experimental predictions of TeV scale strings. Their main implications in particle accelerators are of four types, in correspondence with the four different sectors that are generally present:

1. New compactified parallel dimensions; In this case  $RM_s \gtrsim 1$ , and the associated compactification scale  $R_{\parallel}^{-1}$  would be the first scale of new physics that should be found increasing the beam energy [25, 34]. The main consequence is the existence of KK excitations for all SM particles that propagate along the extra parallel dimensions. These can be produced on-shell at LHC as new resonances [35].
2. New extra large transverse dimensions and low scale quantum gravity,. The main experimental signal is gravitational radiation in the bulk from any physical process on the world-brane [36].
3. Genuine string and quantum gravity effects. Direct production of string resonances in hadron colliders leads generically to a universal deviation from Standard Model in jet distribution [37]. In particular, the first Regge excitation of the gluon has spin 2 and a width an order of magnitude lower than the string scale, leading to a characteristic peak in dijet production; similarly, the first excitations of quarks have spin 3/2.
4. Extra  $U(1)$ 's arising generically in D-brane models as part of unitary gauge group factors. They obtain in general masses due to four- or higher-dimensional anomalies, via the so-called Green-Schwarz anomaly cancellation mechanism involving axionic fields from the closed string sector. The resulting masses are therefore suppressed by a loop factor compared to the string scale. From the low energy point of view, they gauge global symmetries of the Standard Model, such as the baryon and lepton number. An important property of the anomaly cancellation mechanism is that the anomalous  $U(1)$  gauge bosons acquire masses leaving behind the corresponding global symmetries unbroken in perturbation theory. Thus, this is a way to guarantee proton stability (from unbroken baryon number) and avoid large Majorana neutrino masses (from unbroken lepton number) due to dimension-5 operators involving two higgses and two leptons that are suppressed only by the TeV string scale. Such extra  $U(1)$ s have interesting properties and distinct experimental signatures [38–40].
5. Concerning possible micro-black hole production, note that a string size black hole has a horizon radius  $r_H \sim 1$  in string units, while the Newton's constant behaves as  $G_N \sim g_s^2$ . It follows that the mass of a  $d$ -dimensional black hole is [41]:  $M_{\text{BH}} \sim r_H^{d/2-1}/G_N \simeq 1/g_s^2$ . Using the value of the SM gauge couplings  $g_s \simeq g^2 \sim 0.1$ , one finds that the energy threshold  $M_{\text{BH}}$  of micro-black hole production is about four orders of magnitude higher than the string scale, implying that one would produce  $10^4$  string states before reaching  $M_{\text{BH}}$ .

### 3.4 Electroweak symmetry breaking

Non-supersymmetric TeV strings offer also a framework to realize gauge symmetry breaking radiatively. Indeed, from the effective field theory point of view, one expects quadratically divergent one-loop con-

tributions to the masses of scalar fields. The divergences are cut off by  $M_s$  and if the corrections are negative, they can induce electroweak symmetry breaking and explain the mild hierarchy between the weak and a string scale at a few TeV, in terms of a loop factor [42]. More precisely, in the minimal case of one Higgs doublet  $H$ , the scalar potential is:

$$V = \lambda(H^\dagger H)^2 + \mu^2(H^\dagger H), \quad (25)$$

where  $\lambda$  arises at tree-level. Moreover, in any model where the Higgs field comes from an open string with both ends fixed on the same brane stack, it is given by an appropriate truncation of a supersymmetric theory. Within the minimal spectrum of the SM,  $\lambda = (g_2^2 + g'^2)/8$ , with  $g_2$  and  $g'$  the  $SU(2)$  and  $U(1)_Y$  gauge couplings. On the other hand,  $\mu^2$  is generated at one loop:

$$\mu^2 = -\varepsilon^2 g^2 M_s^2, \quad (26)$$

where  $\varepsilon$  is a loop factor that can be estimated from a toy model computation and varies in the region  $\varepsilon \sim 10^{-1} - 10^{-3}$ .

Indeed, consider for illustration a simple case where the whole one-loop effective potential of a scalar field can be computed. We assume for instance one extra dimension compactified on a circle of radius  $R > 1$  (in string units). An interesting situation is provided by a class of models where a non-vanishing VEV for a scalar (Higgs) field  $\phi$  results in shifting the mass of each KK excitation by a constant  $a(\phi)$ :

$$M_m^2 = \left( \frac{m + a(\phi)}{R} \right)^2, \quad (27)$$

with  $m$  the KK integer momentum number. Such mass shifts arise for instance in the presence of a Wilson line,  $a = q \oint \frac{dy}{2\pi} gA$ , where  $A$  is the internal component of a gauge field with gauge coupling  $g$ , and  $q$  is the charge of a given state under the corresponding generator. A straightforward computation shows that the  $\phi$ -dependent part of the one-loop effective potential is given by [43]:

$$V_{eff} = -Tr(-)^F \frac{R}{32\pi^{3/2}} \sum_n e^{2\pi i n a} \int_0^\infty dl l^{3/2} f_s(l) e^{-\pi^2 n^2 R^2 l} \quad (28)$$

where  $F = 0, 1$  for bosons and fermions, respectively. We have included a regulating function  $f_s(l)$  which contains for example the effects of string oscillators. To understand its role we will consider the two limits  $R \gg 1$  and  $R \ll 1$ . In the first case only the  $l \rightarrow 0$  region contributes to the integral. This means that the effective potential receives sizable contributions only from the infrared (field theory) degrees of freedom. In this limit we would have  $f_s(l) \rightarrow 1$ . For example, in the string model considered in [42]:

$$f_s(l) = \left[ \frac{1}{4l} \frac{\theta_2}{\eta^3} \left( il + \frac{1}{2} \right) \right]^4 \rightarrow 1 \quad \text{for} \quad l \rightarrow 0, \quad (29)$$

and the field theory result is finite and can be explicitly computed. As a result of the Taylor expansion around  $a = 0$ , we are able to extract the one-loop contribution to the coefficient of the term of the potential quadratic in the Higgs field. It is given by a loop factor times the compactification scale [43]. One thus obtains  $\mu^2 \sim g^2/R^2$  up to a proportionality constant which is calculable in the effective field theory. On the other hand, if we consider  $R \rightarrow 0$ , which by  $T$ -duality corresponds to taking the extra dimension as transverse and very large, the one-loop effective potential receives contributions from the whole tower of string oscillators as appearing in  $f_s(l)$ , leading to squared masses given by a loop factor times  $M_s^2$ , according to eq. (26).

More precisely, from the expression (28), one finds:

$$\varepsilon^2(R) = \frac{1}{2\pi^2} \int_0^\infty \frac{dl}{(2l)^{5/2}} \frac{\theta_2^4}{4\eta^{12}} \left( il + \frac{1}{2} \right) R^3 \sum_n n^2 e^{-2\pi n^2 R^2 l}, \quad (30)$$

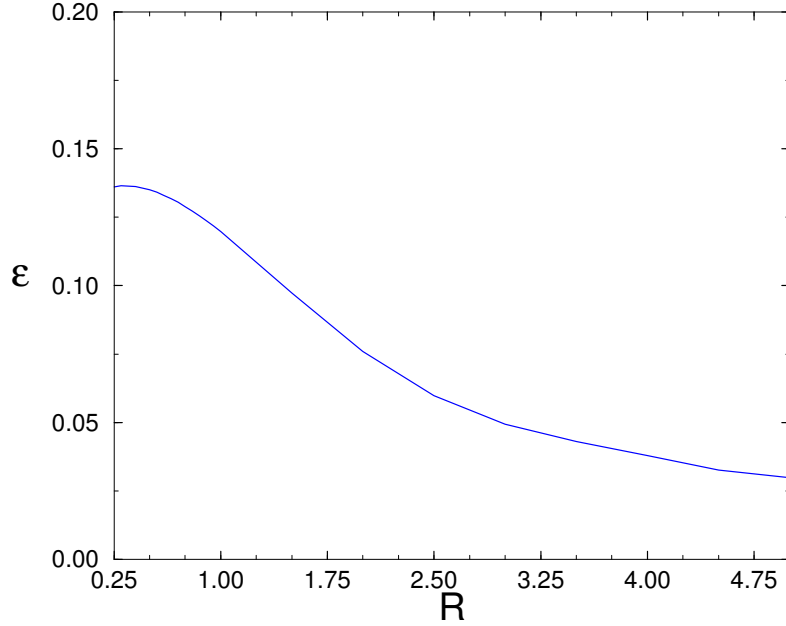


**Fig. 2:** The coefficient  $\varepsilon$  of the one loop Higgs mass (26).

which is plotted in Fig. 2. For the asymptotic value  $R \rightarrow 0$  (corresponding upon T-duality to a large transverse dimension of radius  $1/R$ ),  $\varepsilon(0) \simeq 0.14$ , and the effective cut-off for the mass term is  $M_s$ , as can be seen from Eq. (26). At large  $R$ ,  $\mu^2(R)$  falls off as  $1/R^2$ , which is the effective cut-off in the limit  $R \rightarrow \infty$ , as we argued above, in agreement with field theory results in the presence of a compactified extra dimension [44, 45]. In fact, in the limit  $R \rightarrow \infty$ , an analytic approximation to  $\varepsilon(R)$  gives:

$$\varepsilon(R) \simeq \frac{\varepsilon_\infty}{M_s R}, \quad \varepsilon_\infty^2 = \frac{3\zeta(5)}{4\pi^4} \simeq 0.008. \quad (31)$$

The potential (25) has the usual minimum, given by the VEV of the neutral component of the Higgs doublet  $v = \sqrt{-\mu^2/\lambda}$ . Using the relation of  $v$  with the  $Z$  gauge boson mass,  $M_Z^2 = (g_2^2 + g'^2)v^2/4$ , and the expression of the quartic coupling  $\lambda$ , one obtains for the Higgs mass a prediction which is the Minimal Supersymmetric Standard Model (MSSM) value for  $\tan\beta \rightarrow \infty$  and  $m_A \rightarrow \infty$ :  $m_H = M_Z$ . The tree level Higgs mass is known to receive important radiative corrections from the top-quark sector and rises to values around 120 GeV. Furthermore, from (26), one can compute  $M_s$  in terms of the Higgs mass  $m_H^2 = -2\mu^2$ :

$$M_s = \frac{m_H}{\sqrt{2}g\varepsilon}, \quad (32)$$

yielding naturally values in the TeV range.

### Acknowledgments

Work supported in part by the European Commission under the ERC Advanced Grant 226371 and the contract PITN-GA-2009-237920.

## References

- [1] D. M. Ghilencea and H. M. Lee, *JHEP* **0509** (2005) 024.
- [2] D. M. Ghilencea, *Phys. Rev. D* **70** (2004) 045018.
- [3] S. Groot Nibbelink, M. Hillenbach, *Phys. Lett. B* **616** (2005) 125.
- [4] S. Groot Nibbelink, M. Hillenbach, *Nucl. Phys. B* **748** (2006) 60.
- [5] J. F. Oliver, J. Papavassiliou and A. Santamaria, *Phys. Rev. D* **67** (2003) 125004.
- [6] I. Antoniadis, E. Dudas, D. Ghilencea, P. Tziveloglou, *Nucl. Phys. B* **808** (2009) 155.
- [7] I. Antoniadis, E. Dudas, D. Ghilencea, P. Tziveloglou, *Nucl. Phys. B* **831** (2010) 133.
- [8] H. E. Haber, J. D. Mason, *Phys. Rev. D* **77** 115011 (2008).
- [9] S. P. Martin, *Phys. Rev. D* **61** 035004 (2000).
- [10] M. S. Carena, H. E. Haber, H. E. Logan, S. Mrenna, *Phys. Rev. D* **65** 055005 (2002).
- [11] D. M. Pierce, J. A. Bagger, K. T. Matchev, R. J. Zhang, *Nucl. Phys. B* **491** 3-67 (1997).
- [12] L. J. Hall, R. Rattazzi and U. Sarid, *Phys. Rev. D* **50** 7048-7065 (1994).
- [13] G. F. Giudice, C. Grojean, A. Pomarol and R. Rattazzi, *JHEP* **0706** (2007) 045.
- [14] S. Cassel, D. M. Ghilencea, G. G. Ross, *Nucl. Phys. B* **835** (2010) 110.
- [15] S. Cassel, D. M. Ghilencea and G. G. Ross, *Phys. Lett. B* **687** (2010) 214.
- [16] R. Barate *et al.* [LEP Working Group for Higgs boson searches and ALEPH, DELPHI, L3, OPAL Collaborations, *Phys. Lett. B* **565** (2003) 61; S. Schael *et al.* ALEPH, DELPHI, L3, OPAL and LEP Working Group for Higgs Boson Searches, *Eur. Phys. J. C* **47**(2006)547
- [17] M. Dine, N. Seiberg, S. Thomas, *Phys. Rev. D* **76** (2007) 095004.
- [18] S. Cassel, D. Ghilencea, G. G. Ross, *Nucl. Phys. B* **825** (2010) 203.
- [19] K. Blum, C. Delaunay and Y. Hochberg, arXiv:0905.1701 [hep-ph].
- [20] M. Carena, K. Kong, E. Ponton and J. Zurita, arXiv:0909.5434 [hep-ph].  
M. Carena, E. Ponton and J. Zurita, arXiv:1005.4887 [hep-ph].
- [21] D. Piriz and J. Wudka, *Phys. Rev. D* **56** (1997) 4170.
- [22] A. Brignole, J. A. Casas, J. R. Espinosa and I. Navarro, *Nucl. Phys. B* **666** (2003) 105.
- [23] I. Antoniadis, E. Dudas, D. M. Ghilencea and P. Tziveloglou, arXiv:1006.1662 [hep-ph].
- [24] C. Angelantonj and A. Sagnotti, *Phys. Rept.* **371** (2002) 1 [Erratum-ibid. **376** (2003) 339] [arXiv:hep-th/0204089].
- [25] I. Antoniadis, *Phys. Lett. B* **246** (1990) 377.
- [26] D. J. Kapner, T. S. Cook, E. G. Adelberger, J. H. Gundlach, B. R. Heckel, C. D. Hoyle and H. E. Swanson, *Phys. Rev. Lett.* **98** (2007) 021101.
- [27] N. Arkani-Hamed, S. Dimopoulos and G. R. Dvali, *Phys. Lett. B* **429** (1998) 263 [arXiv:hep-ph/9803315]; I. Antoniadis, N. Arkani-Hamed, S. Dimopoulos and G. R. Dvali, *Phys. Lett. B* **436** (1998) 257 [arXiv:hep-ph/9804398].
- [28] J. D. Lykken, *Phys. Rev. D* **54** (1996) 3693 [arXiv:hep-th/9603133].
- [29] J.C. Long and J.C. Price, *Comptes Rendus Physique* **4** (2003) 337; R.S. Decca, D. Lopez, H.B. Chan, E. Fischbach, D.E. Krause and C.R. Jamell, *Phys. Rev. Lett.* **94** (2005) 240401; R.S. Decca et al., arXiv:0706.3283 [hep-ph]; S.J. Smullin, A.A. Geraci, D.M. Weld, J. Chiaverini, S. Holmes and A. Kapitulnik, arXiv:hep-ph/0508204; H. Abele, S. Haeßler and A. Westphal, in 271th WE-Heraeus-Seminar, Bad Honnef (2002).
- [30] G. Dvali, arXiv:0706.2050 [hep-th]; *Int. J. Mod. Phys. A* **25** (2010) 602 [arXiv:0806.3801 [hep-th]]; G. Dvali and M. Redi, *Phys. Rev. D* **77** (2008) 045027 [arXiv:0710.4344 [hep-th]]; R. Brustein, G. Dvali and G. Veneziano, *JHEP* **0910** (2009) 085 [arXiv:0907.5516 [hep-th]].
- [31] G. Dvali and C. Gomez, *Phys. Lett. B* **674** (2009) 303.

- [32] I. Antoniadis and B. Pioline, *Nucl. Phys. B* **550** (1999) 41; I. Antoniadis, S. Dimopoulos and A. Giveon, *JHEP* **0105** (2001) 055 [arXiv:hep-th/0103033]; I. Antoniadis, A. Arvanitaki, S. Dimopoulos and A. Giveon, arXiv:1102.4043.
- [33] G. Dvali and D. Lust, arXiv:0912.3167 [hep-th]; G. Dvali and C. Gomez, arXiv:1004.3744 [hep-th].
- [34] I. Antoniadis and K. Benakli, *Phys. Lett. B* **326** (1994) 69.
- [35] I. Antoniadis, K. Benakli and M. Quirós, *Phys. Lett. B* **331** (1994) 313 and *Phys. Lett. B* **460** (1999) 176; P. Nath, Y. Yamada and M. Yamaguchi, *Phys. Lett. B* **466** (1999) 100 T. G. Rizzo and J. D. Wells, *Phys. Rev. D* **61** (2000) 016007; T. G. Rizzo, *Phys. Rev. D* **61** (2000) 055005; A. De Rujula, A. Donini, M. B. Gavela and S. Rigolin, *Phys. Lett. B* **482** (2000) 195.
- [36] G.F. Giudice, R. Rattazzi and J.D. Wells, *Nucl. Phys. B* **544** (1999) 3; E.A. Mirabelli, M. Perelstein and M.E. Peskin, *Phys. Rev. Lett.* **82** (1999) 2236; T. Han, J.D. Lykken and R. Zhang, *Phys. Rev. D* **59** (1999) 105006; K. Cheung, W.-Y. Keung, *Phys. Rev. D* **60** (1999) 112003; C. Balázs *et al.*, *Phys. Rev. Lett.* **83** (1999) 2112; J.L. Hewett, *Phys. Rev. Lett.* **82** (1999) 4765.
- [37] L.A. Anchordoqui, H. Goldberg, D. Lust, S. Nawata, S. Stieberger and T.R. Taylor, *Phys. Rev. Lett.* **101** (2008) 241803 [arXiv:0808.0497 [hep-ph]].
- [38] I. Antoniadis, E. Kiritsis and T. N. Tomaras, *Phys. Lett. B* **486**, 186 (2000) [arXiv:hep-ph/0004214]; I. Antoniadis, E. Kiritsis and J. Rizos, *Nucl. Phys. B* **637**, 92 (2002) [arXiv:hep-th/0204153]; I. Antoniadis, E. Kiritsis, J. Rizos and T. N. Tomaras, *Nucl. Phys. B* **660**, 81 (2003) [arXiv:hep-th/0210263].
- [39] G. Shiu and S.-H. H. Tye, *Phys. Rev. D* **58** (1998) 106007; Z. Kakushadze and S.-H. H. Tye, *Nucl. Phys. B* **548** (1999) 180; L. E. Ibáñez, C. Muñoz and S. Rigolin, *Nucl. Phys. B* **553** (1999) 43.
- [40] L. A. Anchordoqui, I. Antoniadis, H. Goldberg, X. Huang, D. Lust and T. R. Taylor, *Phys. Rev. D* **85** (2012) 086003 [arXiv:1107.4309 [hep-ph]].
- [41] G.T. Horowitz and J. Polchinski, *Phys. Rev. D* **55** (1997) 6189.
- [42] I. Antoniadis, K. Benakli and M. Quirós, *Nucl. Phys. B* **583** (2000) 35.
- [43] I. Antoniadis, K. Benakli and M. Quirós, *New Jour. Phys.* **3** (2001) 20.
- [44] I. Antoniadis, C. Muñoz and M. Quirós, *Nucl. Phys. B* **397** (1993) 515; I. Antoniadis and M. Quirós, *Phys. Lett. B* **392** (1997) 61; A. Pomarol and M. Quirós, *Phys. Lett. B* **438** (1998) 225; I. Antoniadis, S. Dimopoulos, A. Pomarol and M. Quirós, *Nucl. Phys. B* **544** (1999) 503; A. Delgado, A. Pomarol and M. Quirós, *Phys. Rev. D* **60** (1999) 095008; R. Barbieri, L. J. Hall and Y. Nomura, *Phys. Rev. D* **63** (2001) 105007.
- [45] I. Antoniadis, S. Dimopoulos and G. Dvali, *Nucl. Phys. B* **516** (1998) 70; S. Ferrara, C. Kounnas and F. Zwirner, *Nucl. Phys. B* **429** (1994) 589.

# Scalar potentials, propagators and global symmetries in AdS/CFT

Borut Bajc<sup>a, b, \*</sup> and Adrián R. Lugo<sup>a, c, †</sup>

<sup>a</sup> J. Stefan Institute, 1000 Ljubljana, Slovenia

<sup>b</sup> Department of Physics, University of Ljubljana, 1000 Ljubljana, Slovenia

<sup>c</sup> Instituto de Física de La Plata-CONICET and Departamento de Física; Facultad de Ciencias Exactas, Universidad Nacional de La Plata, Argentina<sup>‡</sup>

## Abstract

We study the transition of a scalar field in a fixed  $AdS_{d+1}$  background between an extremum and a minimum of a potential. We first prove that two conditions must be met for the solution to exist. First, the potential involved cannot be generic, i.e. a fine-tuning of their parameters is mandatory. Second, at least in some region its second derivative must have a negative upper limit which depends only on the dimensionality  $d$ . We then calculate the boundary propagator for small momenta in two different ways: first in a WKB approximation, and second with the usual matching method, generalizing the known calculation to arbitrary order. Finally, we study a system with spontaneously broken non-Abelian global symmetry, and show in the holographic language why the Goldstone modes appear.

## 1 Introduction

The simplest example of AdS-CFT correspondence [1–3] is gravity plus a real scalar field system in asymptotic anti-de-Sitter (AdS) space (for a partial list see [4–10]).

Apart from some special cases (see for example [11]) it is expected that the even simplified version of such systems, i.e. the no-back-reaction limit where the gravitational coupling  $\kappa \rightarrow 0$ , would give the relevant information (for some reviews on this subject see for example [12–15]). Recently this has been done in [16], where the potential of the real scalar field has been approximated by a piece-wise quadratic potential in order to allow analytic treatment. It has been then shown that: a) in order for the solution between the UV extremum and the IR minimum to exist, there must be some non-trivial constraint among parameters in the potential; b) at least one region needs  $V'' < -d^2/4$ , where  $d$  is the dimension of the boundary; c) a solution of such a system has vanishing action and d) the propagator in the boundary theory exhibits a simple  $1/q^2$  pole as predicted by the Goldstone theorem applied to the spontaneously broken dilatation invariance [17].

The last two points has been considered in more detail in [18] (see also [19] and [20]) following an inspiring paper [21], where it was explicitly shown that even such a simplified system has a BPS type solution which exhibits the Goldstone theorem for a spontaneously broken conformal invariance in subtle way, i.e. mixing the normalizable and non-normalizable modes in the bulk at the next-to-leading order of the matching method.

The purpose of this contribution is twofold. First, we would like to shed more light on the first two issues, i.e. on the constraints the potential must satisfy for allowing a solution. Second, we would like to see the  $1/q^2$  propagator of the Goldstone in a different way, generalize the matching method at all orders, and present few examples of its use.

---

<sup>‡</sup>Permanent address

\*E-mail: borut.bajc@ijs.si

<sup>†</sup>E-mail: lugo@fisica.unlp.edu.ar

The plan of the paper is the following. After setting the notation and main formulae in Section 2, we summarize in Section 3 the wall solution found in [16]. In Section 4 we then explain the reason for a fine-tuning of the potential parameters and explicitly show how one can find BPS-type solutions to the first order equation of motion even in this no-backreaction limit, i.e. generalize the usual  $\kappa \neq 0$  expression of the potential through the superpotential to the  $\kappa \rightarrow 0$  limit. With it we can prove in Section 5 in complete generality that for the solution to exist, the second derivative of the scalar potential must be smaller than  $-d^2/4$  in at least some region. In section 6 we find the same  $1/q^2$  propagator in the  $q \rightarrow 0$  limit of the dilaton using then WKB approximation, while a long Section 7 is devoted to a detailed analysis of the matching method to all orders. This is then used in Section 8 to show in an explicit example what exactly makes the Goldstone boson of a global symmetry massless in the holographic language. We conclude in section 9 with a brief summary of the results.

## 2 The no back-reaction limit ( $\kappa \rightarrow 0$ )

We will consider in most of this paper a real scalar field  $t$  in  $d+1$  dimensions with bulk euclidean action

$$S^{(bulk)}[t] = \int d^{d+1}x \sqrt{\det g_{ab}} \left( \frac{1}{2} g^{ab} \partial_a t \partial_b t + V(t) \right) \quad (1)$$

in a non-dynamical  $AdS_{d+1}$  background

$$g = \frac{1}{z^2} (dz^2 + \delta_{\mu\nu} dx^\mu dx^\nu) \quad (2)$$

where  $(x^\mu)$  are the QFT coordinates with  $x^d \equiv i x^0$  the euclidean time and the AdS scale has been set to 1. The boundary is located at  $z = 0$  (UV region) while the horizon is at  $z = \infty$  (IR region).

The dimensionless field variable  $t$  is normalized to have extrema of the potential at  $t = 0, 1$ . More precisely, we will consider potentials (throughout the paper we will indicate with a dot the derivative w.r.t. the bulk coordinate  $z$  and with a prime a field derivative)

$$V(0) = 0 \quad , \quad V'(0) = 0 \quad ; \quad V(1) < 0 \quad , \quad V'(1) = 0 \quad , \quad V''(1) > 0 \quad (3)$$

i.e.  $t = 1$  will be the true minimum, while at the origin the potential can have a minimum (being a false vacuum thus) or even a maximum, provided that it is in the Breitenlohner-Freedman conformal window  $-d^2/4 < V''(0) < 0$ .

We will be interested in regular, Poincarè invariant solutions  $t = t(z)$  that interpolate between the UV (extremum at  $t = 0$ ) and IR (true minimum at  $t = 1$ ) regions. They obey the equation of motion

$$z^2 \ddot{t}(z) - (d-1) z \dot{t}(z) = V'(t) \quad (4)$$

and necessary behave in the UV and IR as

$$t(z) \xrightarrow{z \rightarrow 0} a_{UV} z^{\Delta^{UV}} \quad ; \quad t(z) \xrightarrow{z \rightarrow \infty} 1 + a_{IR} z^{d-\Delta^{IR}} \quad (5)$$

respectively, where

$$\Delta^{UV/IR} \equiv \frac{d}{2} + \nu_{UV/IR} \quad ; \quad \nu_{UV/IR} \equiv \sqrt{\frac{d^2}{4} + m_{UV/IR}^2} \quad (6)$$

with  $m_{UV}^2 \equiv V''(0)$  and  $m_{IR}^2 \equiv V''(1) > 0$  ( $t = 1$  is a minimum according to (3))<sup>1</sup>.

We recall as a last remark that the symmetries of AdS space translate in the scale invariance of equation (4), i.e. if  $t(z)$  is a solution so it is  $t(\lambda z)$ , a fact of great relevance.

<sup>1</sup>In the window  $-\frac{d^2}{4} < V''(0) < 0$  the term  $z^{d-\Delta^{UV}}$  could also be present in the small  $z$  power expansion of  $t(z)$ . From the AdS/CFT point of view this term is interpreted as a source that breaks explicitly the scale invariance of the boundary QFT; then we should not expect a Goldstone mode to appear, situation we are not interested in. These domain walls are interpreted as dual to renormalization group flows generated by deformation of the UV CFT by a relevant operator, i.e. one of dimension less than  $d$  [15].

### 3 Analytic solutions for approximated bulk potentials

In this section we shortly summarize the results presented in [16].

The interesting region for  $t$  is between the local minimum at 0 and the global minimum at 1. We will divide this region into a number of sections, and in each of them the potential can be locally approximated by a quadratic form:

$$V(t) = \frac{A}{2} t^2 + B t + C \quad (7)$$

The minimum number of such sections is three: (1)  $0 < t < t_1$ , (2)  $t_1 < t < t_2$ , (3)  $t_2 < t < 1$ . The coefficients in (7) are parameterized in each region as

$$A = \begin{cases} A_1 > 0 \\ A_2 < 0 \\ A_3 > 0 \end{cases} ; \quad B = \begin{cases} 0 \\ -A_2 t_M \\ -A_3 \end{cases} ;$$

$$C = \begin{cases} 0 \\ (A_1 - A_2) t_1^2/2 + A_2 t_M t_1 \\ (A_2 - A_3) t_2^2/2 + A_3 t_2 - A_2 t_M t_2 + (A_1 - A_2) t_1^2/2 + A_2 t_M t_1 \end{cases} \quad (8)$$

respectively. The strange choice of  $C$ 's is required by the continuity of the potential. Furthermore, we will require the continuity of the first derivatives of the potential which yields to

$$t_1 = \frac{-A_2 t_M}{A_1 - A_2} ; \quad t_2 = \frac{A_3 - A_2 t_M}{A_3 - A_2} \quad (9)$$

relations that automatically satisfy  $0 < t_1 < t_M < t_2 < 1$  for any  $0 < t_M < 1$ . In this way we remain with four relevant parameters, the  $A_i$ 's and  $t_M$ .

Similarly as in (6) we introduce

$$\Delta_i^\pm = d/2 \pm \nu_i ; \quad \nu_i^2 \equiv \frac{d^2}{4} + A_i \quad (10)$$

We will consider the case of real  $\nu_{1,3} > \frac{1}{2} (A_{1,3} > 0)$  and pure imaginary  $\nu_2 \equiv i \bar{\nu}_2 (A_2 < -\frac{d^2}{4})$  with  $\bar{\nu}_2 > 0$ .

The solution to (4) with the piece-wise quadratic potential (7) is known

$$t_b(z) = \begin{cases} t_1 (z/z_1)^{\Delta_1^+} & , \quad 0 < z < z_1 \\ t_M + D_+ (z/z_2)^{\Delta_2^+} + D_- (z/z_2)^{\Delta_2^-} & , \quad z_1 < z < z_2 \\ 1 - (1 - t_2) (z/z_2)^{\Delta_3^-} & , \quad z_2 < z < \infty \end{cases} \quad (11)$$

Continuity of the solution and its derivative at  $z_{1,2}$  requires

$$D_+ = \frac{(1 - t_M) \Delta_2^- \Delta_3^- (\nu_3 - i \bar{\nu}_2)}{2i \bar{\nu}_2 (A_3 - A_2)} , \quad D_- = D_+^* \quad (12)$$

$$t_M = \left( 1 - \frac{\Delta_1^+}{\Delta_3^-} \left( \frac{\nu_3^2 + \bar{\nu}_2^2}{\nu_1^2 + \bar{\nu}_2^2} \right)^{1/2} \left( \frac{z_2}{z_1} \right)^{d/2} \right)^{-1} \quad (13)$$

$$\bar{\nu}_2 \log(z_2/z_1) = (2k + 1)\pi - \alpha_1 - \alpha_3 \quad (14)$$

with

$$\alpha_i \equiv \arctan(\bar{\nu}_2/\nu_i) , \quad i = 1, 3 \quad (15)$$

Notice here two things:

- there is one relation (fine-tuning) among the potential parameters  $A_i, t_M$ , see eqs. (13) and (14),
- $\nu_2$  needs to be purely imaginary.

The whole procedure can be repeated with more intervals, but these two conclusions still remain: A non-trivial fine-tuning among parameters is needed, and at least in one interval  $\nu^2 = d^2/4 + V''$  needs to be negative. In the next two sections we will try to understand better these two issues.

#### 4 Why the potential cannot be generic

Eqs. (13) and (14) represent the quantization condition on the potential for the solution to exist at all. As it has been noted in [16] and remarked before, this follows from the invariance of the equation of motion under dilatations  $z \rightarrow \lambda z$  for any positive real  $\lambda$ . There is thus an infinite family of solutions: the location of the domain wall is not determined. In our previous example this is seen explicitly by the fact that the coordinates  $z_1$  and  $z_2$  cannot be determined both, but due to dilatation invariance of the original equation of motion only their ratio. The four equations (functions and derivatives at  $z_{1,2}$ ) cannot be satisfied by only three parameters  $D_{+,-}, z_2/z_1$ , so a non-trivial relation among potential parameters follow. This simple counting can be easily generalized to an arbitrary number of intervals.

What happens if a fine-tuned potential changes a bit, i.e. if we relax the constraint among the potential parameters? The numerical output will make  $t(z)$  diverge, so that for  $z \rightarrow \infty$  limit it will not reach the unit value. In other words, the transition is not from the extremum in the origin to the minimum at  $t = 1$ , but it escapes to infinity. In order to make the field land to the minimum, one needs a constrained value for the model parameters.

There are two simple ways to see why there must be some constraint among the model parameters, if we are looking for a solution of (4).

First of all, we have a second order differential equation. In the limit  $z \rightarrow 0$  this non-linear equation can be linearized, call the two independent solutions of this linearized version  $t_+(z)$  and  $t_-(z)$ . Let them be defined so that for  $z \rightarrow 0$ ,  $t_+(z) \propto z^{\Delta^{UV}}$  with  $\Delta^{UV}$  given in (6) and  $t_-(z) \propto z^{d-\Delta^{UV}}$ . This second  $t_-(z)$  is interpreted in the AdS-CFT dictionary as a source. All solutions to the original full non-linear equations have to evolve only towards  $t_+(z)$  for  $z \rightarrow 0$  in order for the source to vanish. There is however no guarantee that these solutions are finite for  $z \rightarrow \infty$ . In general it will not be the case, only solutions which evolve to some linear combination  $a t_+(z) + b t_-(z)$  for  $z \rightarrow 0$  will be finite in the opposite limit at  $z \rightarrow \infty$ . We can enforce  $b = 0$  and thus have a  $t(z)$  sourceless at  $z \rightarrow 0$  and finite at  $z \rightarrow \infty$  only by carefully choosing the parameters of the original Lagrangian, i.e. the potential. From here the fine-tuning among parameters.

Another way perhaps more familiar of setting the problem is through the linearized perturbation equation around the assumed solution  $t(z)$ . If we write the perturbation as  $\xi(z; q) e^{iq \cdot \frac{x}{L}}$ , such equation results (82). We can rewrite this linearized equation for perturbations in a Schrödinger-like form. Taking  $\xi(z; q) = z^{\frac{d-1}{2}} f(z; q)$  we get,

$$\ddot{f}(z; q) - \left[ q^2 + \frac{1}{z^2} \left( \frac{d^2 - 1}{4} + V''(t(z)) \right) \right] f(z; q) = 0 \quad (16)$$

Now, well-known symmetry arguments (in this case related to dilatation invariance) show that  $\xi(z; 0) \sim z \dot{t}(z)$  solves equation (82) with  $q^2 = 0$ . But (16) is a second order linear differential equation with two independent solutions and then standard quantum mechanics arguments work. By definition, necessary  $f(z; 0) \sim z^{\frac{1}{2}-\nu_{IR}}$  for  $z \rightarrow \infty$  and the solution that goes as  $z^{\frac{1}{2}+\nu_{IR}}$  must be discarded. Similarly,  $f(z; 0) \sim z^{\frac{1}{2}+\nu_{UV}}$  for  $z \rightarrow 0$  and the solution that goes as  $z^{\frac{1}{2}-\nu_{UV}}$  must be discarded too. The only way for this solution of (16) to exist is that in both cases we remain with the same function. As the “energy” is zero it cannot be quantized as it is usually the case in QM, so  $z \dot{t}(z)$  can exist only when a fine-tuned relation among parameters in the potential holds, and so also the solution  $t(z)$  of (4) exists only in this case.

#### 4.1 Fine-tuning the cosmological constant on the boundary

As it has been explained in [24] the fine-tuning needed for the potential parameters is nothing else than the requirement for a vanishing cosmological constant on the boundary. To see it more explicitly we have of course to reintroduce gravity, i.e. a non-zero  $\kappa$ .

Let us thus consider the gravity-scalar system defined by the action,

$$S = \int d^{d+1}x \sqrt{|g|} \left( \frac{1}{2\kappa^2} (R + d(d-1)) - \frac{1}{2} D^M t D_{Mt} - V(t) \right) \quad (17)$$

The following equations of motion follow,

$$\begin{aligned} R_{MN} &= -d g_{MN} + \kappa^2 \left( T_{MN} - \frac{T^P_P}{d-1} g_{MN} \right) \\ D^K D_{Kt} &= V'(t) \end{aligned} \quad (18)$$

where the energy momentum-tensor for the scalar field is,

$$T_{MN} = D_{Mt} D_{Nt} - \left( \frac{1}{2} D^K t D_{Kt} + V(t) \right) g_{MN} \quad (19)$$

We are going to consider the ansatz,

$$\begin{aligned} g &= d\rho^2 + A^2(\rho) \hat{g} \\ t &= t(\rho) \end{aligned} \quad (20)$$

where  $\hat{g} \equiv \eta_{mn} \hat{\omega}^m \hat{\omega}^n$  is the metric ( $\{\hat{\omega}^m\}$  is a vielbein) on a  $d$ -dimensional space-time with generic coordinates  $\Omega$ . In the obvious local basis,

$$\omega^m \equiv A(\rho) \hat{\omega}^m \quad , \quad m = 0, 1, \dots, d-1 \quad ; \quad \omega^d \equiv d\rho \quad (21)$$

the connections are,

$$\omega^m_n = \hat{\omega}^m_n \quad ; \quad \omega^m_d = \frac{A'(\rho)}{A(\rho)} \omega^m \quad (22)$$

where only in this subsection a prime means  $d/d\rho$ .

The two-forms defining the curvature tensor result,

$$\mathcal{R}_{mn} = \hat{\mathcal{R}}_{mn} - \frac{A'(\rho)^2}{A(\rho)^2} \omega_m \wedge \omega_n \quad ; \quad \mathcal{R}_{md} = -\frac{A''(\rho)}{A(\rho)} \omega_m \wedge \omega^d \quad (23)$$

Finally the Ricci tensor components are,

$$\begin{aligned} R_{mn} &= \frac{1}{A(\rho)^2} \hat{R}_{mn} - \left( \frac{A''(\rho)}{A(\rho)} + (d-1) \frac{A'(\rho)^2}{A(\rho)^2} \right) \eta_{mn} \\ R_{dd} &= -d \frac{A''(\rho)}{A(\rho)} \\ R_{md} &= 0 \end{aligned} \quad (24)$$

and the Ricci scalar,

$$R = \frac{1}{A(\rho)^2} \hat{R} - 2d \frac{A''(\rho)}{A(\rho)} - d(d-1) \frac{A'(\rho)^2}{A(\rho)^2} \quad (25)$$

With (20) and (24) the equations (18) become,

$$\hat{R}_{mn} - A^2 \left( \frac{A''(\rho)}{A(\rho)} + (d-1) \frac{A'(\rho)^2}{A(\rho)^2} - d + \frac{2\kappa^2}{d-1} V(t) \right) \eta_{mn} = 0$$

$$\begin{aligned} \frac{A''(\rho)}{A(\rho)} - 1 + \frac{\kappa^2}{d} \left( t'(\rho)^2 + \frac{2}{d-1} V(t) \right) &= 0 \\ t''(\rho) + d \frac{A'(\rho)}{A(\rho)} t'(\rho) - \frac{dV}{dt}(t) &= 0 \end{aligned} \quad (26)$$

We have now two possible cases.

#### Case I: Vacuum solutions

Let us consider  $t(\rho) = t_v$  an extremum of the potential,  $V'(t_v) = 0$ , and let us take  $V(t_v) = 0$ . Then there exist three non equivalent, exact solutions to the gravity equations in (26),

$$\begin{aligned} g &= d\rho^2 + e^{2\rho} \hat{g} & ; & \quad \hat{R}_{mn} = 0 \\ g &= d\rho^2 + \cosh^2(\rho) \hat{g} & ; & \quad \hat{R}_{mn} = -(d-1) \eta_{mn} \\ g &= d\rho^2 + \sinh^2(\rho) \hat{g} & ; & \quad \hat{R}_{mn} = +(d-1) \eta_{mn} \end{aligned} \quad (27)$$

We recognize the first case as plane  $AdS_{1,d}$  if  $\hat{g}$  is identified with the flat Minkowski metric, the maximally symmetric case. On the other hand, the second/third solutions correspond to Einstein space-times of negative/positive curvature, being the most symmetric choices for  $\hat{g}$  the spaces  $AdS_{1,d-1}/dS_{1,d-1}$  with scale  $L = 1$ . However from (18) we see that in any case the equation for the bulk metric  $g$  is just  $R_{MN} = -d g_{MN}$ ; so the maximally symmetric choices should lead to the same space, i.e. the three cases in (27) must correspond to  $AdS_{1,d}$  sliced differently.<sup>2</sup> An observation:  $z \equiv e^{-\rho}$  is the usual coordinate with  $z = 0$  the boundary and  $z = \infty$  the horizon iff the  $\rho$ -coordinate is the one defined in the patch of the first solution, i.e.  $\rho$  represents different coordinates in each line of (27).

#### Case II: Domain wall solutions

In this case the profile of the scalar must be non trivial; in particular we are interested in interpolating solutions like the ones considered in the papers. We can however always take the weak gravity, decoupling limit  $\kappa \rightarrow 0$ , and we must solve the scalar equation in the background (27). Now, if we consider the flat slicing, we found the need of fine-tuning the potential in order to get a solution. The question is: if we interpret the other two slicings as leading to  $AdS$  and  $dS$  space-time geometries of the boundary theory instead of Minkowski, is it necessary to fine-tuning the potential to get a domain wall solution also in these cases?

With the new variable  $z = e^{-\rho}$  (and for simplicity keeping the same notation for  $t = t(z)$ ) the equation to solve is,

$$z^2 \ddot{t}(z) - \frac{(d-1) + k(d+1)z^2}{1 - kz^2} z \dot{t}(z) - \frac{dV}{dt}(t) = 0 \quad (28)$$

where  $k = +1, 0, -1$  in the  $dS$ , Minkowski,  $AdS$  slicing. There is no dilatation symmetry anymore, so no need for fine-tuning. In the language of the piece-wise-quadratic potential, all the coordinates of different intervals can be determined, and not only ratios. No relations among parameters is needed for the solution to exist. It is now clear the physical meaning of it: it is just the fine-tuning of the boundary cosmological constant.

## 4.2 The BPS solutions

A solution that spontaneously breaks conformal invariance makes the on-shell action vanish (see for example [23]). This is a hint that the solution may be of the BPS type, i.e. it solves a first order equation [16]. Instead of proving this statement, we will show how one can define the superpotential that

<sup>2</sup>In fact the third form can be found in equation (3.1) of [25].

allows a smooth  $\kappa \rightarrow 0$  limit. Let's go back to (17). We will search for solutions to the equations of motion of the form

$$\begin{aligned} g &= \frac{1}{z^2} \left( d\vec{x}^2 + L^2 \frac{dz^2}{F(z)} \right) \\ t &= t(z) \end{aligned} \quad (29)$$

The b.c. at the boundary  $z = 0$  are,

$$t(z) \rightarrow 0 \quad ; \quad F(z) \rightarrow 1 \quad (30)$$

where,

$$V(0) = 0 \quad ; \quad V'(t)|_{t=0} = 0 \quad (31)$$

This assures for the solution to be asymptotically AdS with fixed radius  $L = 1$ .

At the horizon  $z = \infty$  we impose,

$$t(\infty) < \infty \quad ; \quad F(z) = F_h + \mathcal{O}\left(\frac{1}{z}\right) \quad (32)$$

The equations of motion result

$$\begin{aligned} z F'(z) &= \kappa^2 z^2 F(z) \dot{t}^2(z) \\ z^{d+1} F^{\frac{1}{2}}(z) \frac{d}{dz} \left( \frac{F^{\frac{1}{2}}(z)}{z^{d-1}} \frac{dt}{dz}(z) \right) &= V'(t) \end{aligned} \quad (33)$$

With no back-reaction ( $\kappa = 0$ ),  $F(z) = 1$  and it is the second equation to solve, just the scalar fields in the AdS background. When back-reaction is taken into account ( $\kappa > 0$ ) we can use the superpotential trick. The usual choice is consider potentials which can be written as

$$V(t) = \frac{1}{2} W'^2(t) - \frac{d\kappa^2}{4} W^2(t) + \frac{d}{\kappa^2} \quad (34)$$

Then it is possible to show that a solution of,

$$\begin{aligned} F(z) &= \frac{\kappa^4}{4} W^2(t)|_{t=t(z)} \\ t'(z) &= \frac{2}{\kappa^2 z} \frac{W'(t)}{W(t)} \Big|_{t=t(z)} \end{aligned} \quad (35)$$

solves (33).

This ansatz implicitly assume that  $\kappa \neq 0$ . On the other side, if we want eventually to get the no-backreaction limit  $\kappa \rightarrow 0$ , we choose a potential of the form

$$V(t) = \frac{1}{2} W'^2(t) - dW(t) - \frac{\kappa^2 d}{4} W^2(t) \quad (36)$$

It is then possible to show that a solution of,

$$\begin{aligned} F(z) &= H^2(W(t)) \Big|_{t=t(z)} \\ z \dot{t}(z) &= \frac{W'(t)}{H(W(t))} \Big|_{t=t(z)} \end{aligned} \quad (37)$$

where

$$H(W) \equiv 1 + \frac{\kappa^2}{2} W \quad (38)$$

is a solution of (33). The  $\kappa \rightarrow 0$  limit is now small and points toward the potential

$$V(t) = \frac{1}{2} W'^2(t) - dW(t) \quad (39)$$

and the following BPS like equation,

$$z \dot{t}(z) = W'(t(z)) \quad (40)$$

whose solutions satisfy also the full second order equation of motion (4) and for which the action (17) vanishes.

At least for polynomial superpotentials and potentials the fine-tuning for vanishing boundary cosmological constant is simply the special form (39). With this we mean that all coefficients of the polynomial in the potential are not independent and thus the potential itself is not generic.

Before ending this section, let us see some examples of superpotentials  $W(t)$  (in [18] we already showed another choice).

#### 4.2.1 The $Z_2$ symmetric case

An interesting case consists of the sixth order potential with the  $Z_2$  symmetry  $t \rightarrow -t$ . The ansatz for the superpotential

$$W(t) = \Delta \left( \frac{1}{2} t^2 - \frac{1}{4} t^4 \right) \quad (41)$$

leads to the solution,

$$t(z) = \frac{z^\Delta}{(1 + z^{2\Delta})^{1/2}} \quad (42)$$

From here we see that

$$\Delta^{UV} = \Delta \quad , \quad \Delta^{IR} = d + 2\Delta \quad (43)$$

#### 4.2.2 A case with $\Delta^{UV}$ and $\Delta^{IR}$ independent

In the examples of [18] and above a correlation between the UV and IR  $\Delta$ 's was present. This is however not a generic feature of the system. In fact, choosing for example

$$W(t) = -\frac{1}{4} (\Delta^{IR} - (d + \Delta^{UV})) t^4 + \frac{1}{3} (\Delta^{IR} - (d + \Delta^{UV}) - \Delta^{UV}) t^3 + \frac{\Delta^{UV}}{2} t^2 \quad (44)$$

we get the solution

$$z(t) = \left[ \frac{\Delta^{UV} + (\Delta^{IR} - (d + \Delta^{UV})) t}{1 - t} \right]^{\frac{1}{\Delta^{IR} - d}} \left[ \frac{t}{\Delta^{UV} + (\Delta^{IR} - (d + \Delta^{UV})) t} \right]^{\frac{1}{\Delta^{UV}}} \quad (45)$$

which has the limits (5) with

$$a_{UV} = (\Delta^{UV})^{\frac{\Delta^{IR} - (d + \Delta^{UV})}{\Delta^{IR} - d}} \quad ; \quad a_{IR} = -(\Delta^{IR} - d)^{-\frac{\Delta^{IR} - (d + \Delta^{UV})}{\Delta^{UV}}} \quad (46)$$

The parameters  $\Delta^{UV} > d/2$  (corresponding to the maximum or minimum in the UV) and  $\Delta^{IR} > d + \Delta^{UV}$  (minimum in the IR) can be otherwise arbitrary.

## 5 $V''(t) < -d^2/4$

As we said before, in a piece-wise quadratic potential at least in some interval the second derivative of the potential must be smaller than  $-d^2/4$  for the solution to exist. Let us here show this statement for a general potential  $V(t)$  characterized by (39). Let us define

$$F \equiv \int d\mu W'(t)^2 \left( V''(t) + \frac{d^2}{4} \right) \Big|_{t=t(z)} \quad (47)$$

where  $t(z)$  is the solution of the BPS equation (40) and to simplify the notation we will use in this subsection the abbreviation

$$\int d\mu \dots \equiv \int_0^\infty dz z^{-d-1} \dots \quad (48)$$

and omit the field dependence. Our aim is to show that the quantity  $F$  is non-positive, so that  $V'' < -d^2/4$  at least in some region.

First we rewrite (47) using (39)

$$F = \int d\mu \left( W'^2 W''^2 + W'^3 W''' - d W'^2 W'' + \frac{d^2}{4} W'^2 \right) \quad (49)$$

Now we use (assuming vanishing boundary terms, which is easily verified)

$$\int d\mu W'^2 = \frac{2}{d} \int d\mu W'^2 W'' \quad (50)$$

$$\int d\mu W'^3 W''' = \int d\mu (d W'^2 W'' - 2 W'^2 W''^2) \quad (51)$$

to rewrite (49) as

$$F = \frac{d}{2} \int d\mu W'^2 W'' - \int d\mu W'^2 W''^2 \quad (52)$$

Finally we use the Schwartz inequality

$$\int d\mu f g \leq \left( \int d\mu f^2 \right)^{\frac{1}{2}} \left( \int d\mu g^2 \right)^{\frac{1}{2}} \quad (53)$$

to derive from (50)

$$\int d\mu W'^2 \leq \frac{4}{d^2} \int d\mu W'^2 W''^2 \quad (54)$$

Using then (53) we get first

$$\int d\mu W'^2 W'' \leq \left( \int d\mu W'^2 \right)^{\frac{1}{2}} \left( \int d\mu W'^2 W''^2 \right)^{\frac{1}{2}} \quad (55)$$

from which finally it follows

$$F \leq 0 \quad (56)$$

This proves our statement: the inequality  $V'' < -d^2/4$  is valid at least in some region of  $z$  for any potential  $V$  of the form (39).

Notice that since at the horizon ( $z \rightarrow \infty$ ) the potential has a minimum and at the boundary ( $z = 0$ ) a minimum or a maximum in the conformal window (i.e.  $V'' + d^2/4 > 0$ ), there are always an even number of times that  $V''$  crosses the particular value  $-d^2/4$ .

## 6 The WKB approximation method

Here we shall try to apply the WKB method in order to compute the two-point correlation function of operators dual through the AdS/CFT correspondence to a bulk scalar field. The recipe to get it is to consider the solution to the perturbation equation (82), and identify the propagator by looking at the behavior near the boundary  $z \rightarrow 0$ ,

$$\xi(z; q) \sim z^{d-\Delta^{UV}} + G_2(q) z^{\Delta^{UV}} \quad (57)$$

The straightest way of doing it is to consider the Schrödinger-type equation (16) with “potential”

$$Q(z; q) \equiv q^2 + \frac{1}{z^2} \left( \frac{d^2 - 1}{4} + V''(t(z)) \right) \quad (58)$$

where we remember that  $t(z)$  is the solution of (4). For simplicity we consider the case  $V''(0) \equiv m_{UV}^2 > 0$ , although it is not necessary for the argument.

The WKB approximation results a good one if the slowly varying “Compton length” condition holds,

$$\left| \frac{d|Q(z; q)|^{-\frac{1}{2}}}{dz} \right| = \left| \frac{\dot{Q}(z; q)}{2|Q(z; q)|^{\frac{3}{2}}} \right| \ll 1 \quad (59)$$

This condition applied to (58) reads,

$$\frac{\left| \frac{d^2-1}{4} + V''(t(z)) - \frac{1}{2} V'''(t(z)) z \dot{t}(z) \right|}{\left| \frac{d^2-1}{4} + V''(t(z)) + q^2 z^2 \right|^{\frac{3}{2}}} \ll 1 \quad (60)$$

From here is straightforward to see that the WKB solution is trustable for any  $q^2$  around  $z = 0$  and  $z = \infty$  if,

$$\nu_{UV} \gg \frac{1}{2} \quad ; \quad \nu_{IR} \gg \frac{1}{2} \quad (61)$$

respectively, with  $\nu_{UV/IR}$  as in (6). Furthermore,  $Q(z; q)$  is positive near  $z = 0$  (and diverges quadratically there), but it is also positive for large  $z$  (going to  $q^2$  from above). What happens in the middle? From section 5 we know that for  $q$  small enough  $Q(z; q)$  must become negative; then for some  $z_M$  where  $t(z_M) = t_M$  it should have a local minimum. Then there must exist  $z_i = z_i(q)$ ,  $z_1(q) < z_M < z_2(q)$  such that,

$$z_i^2 Q(z_i; q) = \frac{d^2 - 1}{4} + V''(t(z_i)) + q^2 z_i^2 = 0 \quad ; \quad i = 1, 2 \quad (62)$$

Near these zeroes of  $Q(z; q)$  the WKB approximation breaks down.

If we admit that  $V''(t_M)$  is large enough then it is seen from (60) that in the region near  $z_M$  the WKB solution is trustable too. Therefore, calling *I*, *II*, *III* the regions near  $z = 0$ ,  $z_M$  and  $z \gg 1$  respectively, we can write the approximate WKB solution in each region as,

$$\xi_I(z; q) = C_I^+ z^{\frac{d}{2}} \frac{\exp\left(\int_{z_1}^z \frac{dz}{z} \sqrt{z^2 Q(z; q)}\right)}{(z^2 Q(z; q))^{\frac{1}{4}}} + C_I^- z^{\frac{d}{2}} \frac{\exp\left(-\int_{z_1}^z \frac{dz}{z} \sqrt{z^2 Q(z; q)}\right)}{(z^2 Q(z; q))^{\frac{1}{4}}} \quad (63)$$

$$\xi_{II}(z; q) = C_{II} z^{\frac{d}{2}} \frac{\exp\left(i \int_{z_1}^z \frac{dz}{z} \sqrt{-z^2 Q(z; q)}\right)}{(-z^2 Q(z; q))^{\frac{1}{4}}} + C_{II}^* z^{\frac{d}{2}} \frac{\exp\left(-i \int_{z_1}^z \frac{dz}{z} \sqrt{-z^2 Q(z; q)}\right)}{(-z^2 Q(z; q))^{\frac{1}{4}}} \quad (64)$$

$$\xi_{III}(z; q) = C_{III}^+ z^{\frac{d}{2}} \frac{\exp\left(\int_{z_2}^z \frac{dz}{z} \sqrt{z^2 Q(z; q)}\right)}{(z^2 Q(z; q))^{\frac{1}{4}}} + C_{III}^- z^{\frac{d}{2}} \frac{\exp\left(-\int_{z_2}^z \frac{dz}{z} \sqrt{z^2 Q(z; q)}\right)}{(z^2 Q(z; q))^{\frac{1}{4}}} \quad (65)$$

where the coefficients are related by,

$$C_I^\pm = \frac{1 \pm 3}{2} \text{Im}\left(C_{II} e^{\pm i\frac{\pi}{4}}\right) \leftrightarrow C_{II} = \frac{1}{2} e^{+i\frac{\pi}{4}} C_I^+ + e^{-i\frac{\pi}{4}} C_I^- = (C_{II}^*)^* \quad (66)$$

$$C_{III}^\pm = \frac{3 \pm 1}{2} \text{Im}\left(C_{II} e^{i(\varphi(q) \mp \frac{\pi}{4})}\right) \leftrightarrow$$

$$C_{II} = e^{-i\varphi(q)} \left(-\frac{1}{2} e^{-i\frac{\pi}{4}} C_{III}^+ + e^{+i\frac{\pi}{4}} C_{III}^-\right) = (C_{II}^*)^* \quad (67)$$

and,

$$\varphi(q) \equiv \int_{z_1(q)}^{z_2(q)} \frac{dz}{z} \sqrt{-z^2 Q(z; q)} \quad (68)$$

Now, imposing finiteness when  $z \rightarrow \infty$  implies  $C_{III}^+ = 0$ . By using the relations (66) and (67) we get all the constants in terms of  $C_{III}^-$ ; in particular for the solution near  $z = 0$  we get,

$$\xi_I(z; q) = C_{III}^- \left( 2 \cos \varphi(q) z^{\frac{d}{2}} \frac{\exp\left(\int_{z_1(q)}^z \frac{dz}{z} \sqrt{z^2 Q(z; q)}\right)}{(z^2 Q(z; q))^{\frac{1}{4}}} \right. \\ \left. + \sin \varphi(q) z^{\frac{d}{2}} \frac{\exp\left(-\int_{z_1(q)}^z \frac{dz}{z} \sqrt{z^2 Q(z; q)}\right)}{(z^2 Q(z; q))^{\frac{1}{4}}} \right) \quad (69)$$

From here we should be able to extract the propagator as a function of  $q^2$ , at least for  $q$  not so large. But we know from section 4 that for  $q = 0$  (69) must be equal to  $z t'(z)$  and thus going only as  $z^{\Delta_{UV}}$  for  $z \rightarrow 0$ . We will show now that this implies the constraint  $\varphi(0) = k \pi$  with  $k$  an integer. First we rewrite

$$\exp\left(\pm \int_{z_1(q)}^z \frac{dz}{z} \sqrt{z^2 Q(z; q)}\right) = \left(\frac{z}{z_1(q)}\right)^{\pm \sqrt{\nu_{UV}^2 - 1/4}} \\ \times \exp\left(\pm \int_{z_1(q)}^z \frac{dz}{z} \left(\sqrt{z^2 Q(z; q)} - \sqrt{\nu_{UV}^2 - 1/4}\right)\right) \quad (70)$$

Since we are interested only in  $\nu_{UV} \gg 1/2$  and leading behavior at  $z \rightarrow 0$ , we can see with the help of (70) that the first term on the r.h.s. of (69) goes like  $z^{\Delta_{UV}}$ , while the second goes like  $z^{d-\Delta_{UV}}$ . Since this last one should not be present in the solution  $z t'(z)$  of the  $q = 0$  perturbation, we have to impose (otherwise no solution with the right asymptotic behavior exists)

$$\varphi(0) \equiv \int_{z_1(0)}^{z_2(0)} \frac{dz}{z} \sqrt{-z^2 Q(z; 0)} = k \pi \quad (71)$$

This means that only potentials which satisfy this constraint are acceptable. This is the WKB analog of the fine-tuning mentioned before.

This simple conclusion is the reason for the  $1/q^2$  behavior of the boundary propagator. In fact, it is easy to derive the form of the propagator in the WKB approximation; from (57) we get:

$$G_2(q) = \frac{2 \exp\left(-2 \int_0^{z_1(q)} \frac{dz}{z} \left(\sqrt{z^2 Q(z; q)} - \sqrt{\nu_{UV}^2 - 1/4}\right)\right)}{(z_1(q))^2 \sqrt{\nu_{UV}^2 - 1/4} \tan \varphi(q)} \quad (72)$$

Clearly, due to (71), we get for  $q \rightarrow 0$  the usual Goldstone pole

$$G_2(q) \approx \frac{2 \exp\left(-2 \int_0^{z_1(0)} \frac{dz}{z} \left(\sqrt{z^2 Q(z; 0)} - \sqrt{\nu_{UV}^2 - 1/4}\right)\right)}{(z_1(0))^2 \sqrt{\nu_{UV}^2 - 1/4} (d\varphi(q)/dq^2)_{q^2=0}} \times \frac{1}{q^2} \quad (73)$$

where

$$\left. \frac{d\varphi(q)}{dq^2} \right|_{q^2=0} = -\frac{1}{2} \int_{z_1(0)}^{z_2(0)} dz \frac{z}{\sqrt{-z^2 Q(z; 0)}} \quad (74)$$

Although the denominator vanishes at the integration boundaries, the integral itself is finite.

## 7 The matching method to all orders

Let  $t(z)$  be the solution of the equation of motion (4) that behaves for  $z \rightarrow 0$  (UV) and  $z \rightarrow \infty$  (IR) as,

$$t(z) \xrightarrow{z \rightarrow 0} a_{UV} z^{\Delta_+^{UV}} (1 + b_{UV} z^{\alpha_{UV}} + \dots) \quad ; \quad t(z) \xrightarrow{z \rightarrow \infty} 1 + a_{IR} z^{\Delta_-^{IR}} (1 + b_{IR} z^{\alpha_{IR}} + \dots) \quad (75)$$

respectively. Here  $\alpha_{UV} > 0$  and  $\alpha_{IR} < 0$ , while that

$$\Delta_{\pm}^{UV/IR} \equiv \frac{d}{2} \pm \nu_{UV/IR} \quad ; \quad \nu_{UV/IR} \equiv \sqrt{\frac{d^2}{4} + m_{UV/IR}^2} \quad (76)$$

with  $m_{UV}^2 \equiv V''(0)$  and  $m_{IR}^2 \equiv V''(1) > 0$ . Note that in order for  $t(z)$  to be finite in the asymptotic expansions (75) neither  $\Delta_-^{UV}$  appears in the UV nor  $\Delta_+^{IR}$  in the IR.

Let us introduce for further use the following expansions of the functions  $\xi_{\pm}(z)$

$$\xi_{\pm}(z) = a_{\pm}^{UV/IR} z^{\Delta_{\pm/\mp}^{UV/IR}} \bar{\xi}_{\pm}^{UV/IR}(z) \quad ; \quad \bar{\xi}_{\pm}^{UV/IR}(z) \xrightarrow{z \rightarrow 0/\infty} 1 \quad (77)$$

that follow by plugging (75) in the definitions

$$\xi_+(z) \equiv z \dot{t}(z) \quad (78)$$

$$\xi_-(z) \equiv \xi_+(z) \left( \int_{z_i}^z dy \frac{y^{d-1}}{\xi_+^2(y)} + \frac{\xi_-(z_i)}{\xi_+(z_i)} \right) \quad (79)$$

where  $z_i$  and  $\xi_-(z_i)$  are integration constants. We find

$$a_+^{UV/IR} \equiv a_{UV/IR} \Delta_{+/-}^{UV/IR} \quad ; \quad a_-^{UV/IR} \equiv \left( a_+^{UV/IR} (d - 2 \Delta_{+/-}^{UV/IR}) \right)^{-1} \quad (80)$$

Clearly the UV/IR expansion of  $\xi_+(z)$  can not contain the  $z^{\Delta_{-/+}^{UV/IR}}$ -power, but  $\xi_-(z)$  could contain the  $z^{\Delta_{+/-}^{UV/IR}}$ -power.

Our aim is to solve the equation for perturbations around the solution  $t(z)$ , i.e. if we write (for a general treatment see for example the appendix of [16])

$$t(z; q) \equiv t(z) + \xi(z; q) e^{iq \frac{x}{L}} \quad (81)$$

then the second equation in (18) gives to first order in  $\xi(z; q)$

$$z^2 \ddot{\xi}(z; q) - (d-1) z \dot{\xi}(z; q) - (q^2 z^2 + V''(t(z))) \xi(z; q) = 0 \quad (82)$$

We will do it in two different approximations.

### 7.1 The large $z$ expansion.

We write (82) as

$$z^2 \ddot{\xi}(z; q) - (d-1) z \dot{\xi}(z; q) - (q^2 z^2 + m_{IR}^2) \xi(z; q) = \delta(z) \xi(z; q) \quad (83)$$

and consider  $\delta(z) \equiv V''(t(z)) - V''(1)$  small in the sense,

$$|\delta(z)| = |V''(t(z)) - V''(1)| \ll V''(1) \quad \longrightarrow \quad z > z_\infty \equiv \left| \frac{V''(1)}{V'''(1) a_{IR}} \right|^{\frac{1}{\Delta_{IR}}} \quad (84)$$

independently of the value of  $q$ . Then the solution for  $z > z_\infty$  can be hopefully expanded in orders of  $\delta(z)$ ,

$$\delta(z) = V'''(1) a_{IR} z^{\Delta_{IR}} (1 + b_{IR} z^{\alpha_{IR}} + \dots) \quad (85)$$

The order zero term is the solution to the l.h.s. of (83) equal to zero, which is given by,

$$\xi_\infty(z; q) \equiv \frac{2}{\Gamma(\nu_{IR})} \left(\frac{q}{2}\right)^{\nu_{IR}} z^{\frac{d}{2}} K_{\nu_{IR}}(qz) \quad (86)$$

where we have dropped the solution that diverges in the IR and fixed the normalization in such a way that  $\xi_\infty(z; 0) = z^{\Delta_{IR}^-}$ . It is not difficult to see that the expansion for large  $z > z_\infty$  is of the form,

$$\xi(z; q) = \xi_\infty(z; q) \left(1 + \frac{f_0(qz)}{z^{-\Delta_{IR}^-}} + \dots\right) \quad (87)$$

where for completeness we quote the first correction,

$$f_0(u) = V'''(1) a_{IR} x^{-\Delta_{IR}^-} \int_\infty^u \frac{dx}{x K_{\nu_{IR}}^2(x)} \int_\infty^x \frac{dy}{y^{1-\Delta_{IR}^-}} K_{\nu_{IR}}^2(y) \quad (88)$$

However corrections to the leading term of  $\xi(z; q)$  in negative powers of  $z$  will not be relevant in the matching procedure, at least not to compute the leading order behavior of the two-point function.

### 7.2 The small $q$ expansion.

This time we write (82) as

$$z^{d-1} \frac{d}{dz} \left( z^{1-d} \frac{d\xi(z; q)}{dz} \right) - \frac{V''(t(z))}{z^2} \xi(z; q) = q^2 \xi(z; q) \quad (89)$$

and consider  $q$  small in the sense,

$$q \ll \frac{|V''(t(z))|^{\frac{1}{2}}}{z} \quad (90)$$

This condition certainly holds in the UV region near  $z = 0$ , but also in the IR region if

$$q^2 z^2 \ll |V''(t(z))| \sim m_{IR}^2 \quad \longrightarrow \quad qz \ll m_{IR} \quad (91)$$

that is, when  $z$  is large and  $q$  small but  $qz$  fixed and small enough.

Under this condition we can try a solution for small  $q$  as a power series in  $q^2$ ,

$$\xi(z; q) = \sum_{m \geq 0} q^{2m} \xi^{(m)}(z; q) \quad (92)$$

Plugging this expansion in (89) we get,

$$z^{d-1} \frac{d}{dz} \left( z^{1-d} \frac{d\xi^{(0)}(z; q)}{dz} \right) - \frac{V''(t(z))}{z^2} \xi^{(0)}(z; q) = 0 \quad (93)$$

$$z^{d-1} \frac{d}{dz} \left( z^{1-d} \frac{d\xi^{(m)}(z; q)}{dz} \right) - \frac{V''(t(z))}{z^2} \xi^{(m)}(z; q) = \xi^{(m-1)}(z; q) \quad ; \quad m = 1, 2, \dots \quad (94)$$

The solution to lowest order is,

$$\xi^{(0)}(z; q) = C_+^{(0)}(q) \xi_+(z) + C_-^{(0)}(q) \xi_-(z) \quad (95)$$

where  $C_{\pm}^{(0)}(q)$  are integration constants. With  $\xi^{(0)}(z; q)$  we can determine  $\xi^{(1)}(z; q)$  from (94), and so on.

This iterative procedure yields the solution in the following form. First we introduce the set of functions,

$$\begin{aligned} f_{ij}^{(k)}(z) &\equiv \int_{z_i}^z \frac{dw}{w^{d-1}} \xi_i(w) \xi_j^{(k)}(w) \quad ; \quad i, j = +, - \quad , \quad k = 0, 1, \dots \\ \xi_{\pm}^{(0)}(z) &\equiv \xi_{\pm}(z) \end{aligned} \quad (96)$$

where

$$\xi_{\pm}^{(k)}(z) \equiv -f_{-\pm}^{(k-1)}(z) \xi_+(z) + f_{+\pm}^{(k-1)}(z) \xi_-(z) \quad , \quad k = 1, 2, \dots \quad (97)$$

All of them are obtained iteratively: first, from (96) with  $k = 0$  we get  $f_{ij}^{(0)}(z)$ , then we go to (97) with  $k = 1$  and get  $\xi_{\pm}^{(1)}(z)$ , then we come back to (96) with  $k = 1$  and get  $f_{ij}^{(1)}(z)$  and so on. The functions  $\xi_m(z; q)$  can be expressed in terms of the  $\xi_{\pm}^{(k)}(z)$ 's yielding the full expansion (92) in the form,

$$\xi(z; q) = \sum_{m \geq 0} q^{2m} \sum_{k=0}^m \left( C_+^{(m-k)}(q) \xi_+^{(k)}(z) + C_-^{(m-k)}(q) \xi_-^{(k)}(z) \right) \quad (98)$$

where the  $C_{\pm}^{(k)}$ 's are, as in (95), the integration constants of the homogeneous solution in (94). After some rearrangement, we can write (98) as,

$$\xi(z; q) = C_+(q) \sum_{m \geq 0} q^{2m} \xi_+^{(m)}(z) + C_-(q) \sum_{m \geq 0} q^{2m} \xi_-^{(m)}(z) \quad (99)$$

where we have redefined the coefficients

$$C_{\pm}(q) \equiv \sum_{k \geq 0} C_{\pm}^{(k)}(q) q^{2k} \quad (100)$$

We should not be surprised of this expression; after all (89) is a second order linear differential equation and both sums in (99) are linearly independent solutions of it as it can be quickly checked. Note furthermore that they are holomorphic in  $q^2$ ; the reason behind this fact can be traced directly to the assumption (92).

### 7.3 The two-point function.

For  $qz \ll m_{IR}$  expansion (99) hopefully holds, and it can be used to compute the two-point correlation function at low momenta as follows. After adjusting the constant of integration in (75) to get rid of the  $z^{\Delta_{+}^{UV}}$  term in  $\xi_-(z)$ , we parametrize the  $z \rightarrow 0$  behavior as

$$\begin{aligned} \xi(z; q) &\rightarrow \left[ (1 - q^2 \epsilon_{-+}^{UV}(q)) C_+(q) - q^2 \epsilon_{--}^{UV}(q) C_-(q) \right] a_+^{UV} z^{\Delta_+^{UV}} + \dots \\ &+ \left[ (1 + q^2 \epsilon_{+-}^{UV}(q)) C_-(q) + q^2 \epsilon_{++}^{UV}(q) C_+(q) \right] a_-^{UV} z^{\Delta_-^{UV}} + \dots \end{aligned} \quad (101)$$

where

$$\epsilon_{+\pm}^{UV}(q) = - \sum_{m \geq 0} q^{2m} \int_0^{z_i} dw w^{1-d} \xi_+(w) \xi_{\pm}^{(m)}(w) \quad (102)$$

while we were unable to find a closed expression for  $\epsilon_{-\pm}^{UV}$  without specifying the potential.

Applying the holographic recipe (57) the two-point function results,

$$G_2(q) \xrightarrow{q \rightarrow 0} \frac{a_+^{UV}/a_-^{UV}}{\left(q^2 \epsilon_{++}^{UV}(q) + \frac{C_-(q)}{C_+(q)}\right)_{q \rightarrow 0}} \quad (103)$$

The knowledge of the leading order behavior of the quotient  $C_-(q)/C_+(q)$  for  $q \rightarrow 0$  will allow to compute the leading power in  $q$  of  $G_2(q)$ . The  $z_i$ -dependence of the coefficients  $\epsilon_{++}^{UV}$  (and the  $z_i$ -independence of the physics) gives a hint that this power is  $-2$ , as we will confirm below.

#### 7.4 The infrared expansion

Here we define the functions  $\bar{F}_{ij}^{(m)}(z)$  and the constants  $\bar{\varphi}_{ij}^{(m)}$  by means of the integrals,

$$\begin{aligned} & a_i^{IR} a_j^{IR} \sigma_j^{(m)} \int_{z_i}^z dw w^{1+2m+\Delta_{(i)}+\Delta_{(j)}-d} \bar{\xi}_i^{(0)}(w) \bar{\xi}_j^{(m)}(w) \\ \equiv & \bar{\varphi}_{ij}^{(m)} + \frac{a_i^{IR} a_j^{IR} \sigma_j^{(m)} z^{2+2m+\Delta_{(i)}+\Delta_{(j)}-d}}{2+2m+\Delta_{(i)}+\Delta_{(j)}-d} \bar{F}_{ij}^{(m)}(z) \quad ; \quad m = 0, 1, \dots \end{aligned} \quad (104)$$

where  $\bar{\varphi}_{ij}^{(m)}$  is defined to be the only  $z$ -independent part in the large  $z$  expansion, and

$$\sigma_{\pm}^{(m)} \equiv \frac{\Gamma(1 \mp \nu_{IR})}{2^{2m} m! \Gamma(1 \mp \nu_{IR} + m)} \quad ; \quad m = 0, 1, \dots \quad (105)$$

With them we can calculate ( $m = 1, 2, \dots$ ),

$$\varphi_{ij}^{(m)} \equiv \bar{\varphi}_{ij}^{(m)} + \sum_{k=0}^{m-1} \left( \bar{\varphi}_{i-}^{(k)} \varphi_{+j}^{(m-1-k)} - \bar{\varphi}_{i+}^{(k)} \varphi_{-j}^{(m-1-k)} \right) \quad (106)$$

$$\bar{\xi}_{\pm}^{(m)}(z) \equiv \frac{1}{\nu_{IR}} \left( (\nu_{IR} \mp m) \bar{F}_{\mp\pm}^{(m-1)}(z) \bar{\xi}_{\pm}^{(0)}(z) \pm m \bar{F}_{\pm\pm}^{(m-1)}(z) \bar{\xi}_{\mp}^{(0)}(z) \right) \quad (107)$$

The general form of  $\xi_{\pm}^{(m)}(z)$  for  $m = 1, 2, \dots$ , results,

$$\begin{aligned} \xi_{\pm}^{(m)}(z) &= a_{\pm}^{IR} \sigma_{\pm}^{(m)} z^{\Delta_{\mp}^{IR}+2m} \bar{\xi}_{\pm}^{(m)}(z) \\ &+ \sum_{k=0}^{m-1} \left( -a_+^{IR} \sigma_+^{(k)} \varphi_{-\pm}^{(m-1-k)} z^{\Delta_-^{IR}+2k} \bar{\xi}_+^{(k)}(z) + a_-^{IR} \sigma_-^{(k)} \varphi_{+\pm}^{(m-1-k)} z^{\Delta_+^{IR}+2k} \bar{\xi}_-^{(k)}(z) \right) \end{aligned} \quad (108)$$

where the ingredients to construct it are iteratively computed as described above.

#### 7.5 The matching procedure.

According to (84) and (91), in the region

$$z > z_{\infty} \quad ; \quad x \equiv qz \ll m_{IR} \quad (109)$$

both expansions (87) and (99) hold and therefore they should coincide *exactly*, i.e.

$$\xi_{\infty}(z; q) \left( 1 + \frac{f_0(qz)}{z^{-\Delta_-^{IR}}} + \dots \right) = C_+(q) \sum_{m \geq 0} q^{2m} \xi_+^{(m)}(z) + C_-(q) \sum_{m \geq 0} q^{2m} \xi_-^{(m)}(z) \quad (110)$$

This equation must be used to compute the unknown coefficients  $C^\pm(q)$ . As we will see shortly, this is not an easy task in general; fortunately the leading order behavior necessary to compute (103) is relatively simple to get. To proceed we need the IR behavior of the  $\xi_\pm^{(m)}(z)$ 's. By plugging (108) in (99) we get,

$$\begin{aligned} z^{-\Delta_-^{IR}} \xi(z; q) &= z^{-\Delta_-^{IR}} r.h.s. \quad (110) \\ &= \left( (1 - q^2 \epsilon_{-+}^{IR}(q)) C_+(q) - q^2 \epsilon_{--}^{IR}(q) C_-(q) \right) a_+^{IR} \sum_{m \geq 0} \sigma_+^{(m)} x^{2m} \bar{\xi}_+^{(m)} \left( \frac{x}{q} \right) \\ &+ \left( (1 + q^2 \epsilon_{+-}^{IR}(q)) C_-(q) + q^2 \epsilon_{++}^{IR}(q) C_+(q) \right) \frac{a_-^{IR}}{q^{2\nu_{IR}}} \sum_{m \geq 0} \sigma_-^{(m)} x^{2m+2\nu_{IR}} \bar{\xi}_-^{(m)} \left( \frac{x}{q} \right) \end{aligned} \quad (111)$$

where we have introduced the holomorphic functions,

$$\epsilon_{ij}^{IR}(q) \equiv \sum_{m \geq 0} \varphi_{ij}^{(m)} q^{2m} \quad (112)$$

On the other hand, by using the series expansion of  $\xi_\infty \left( \frac{x}{q}; q \right)$  valid for  $x < 1$  we have,

$$z^{-\Delta_-^{IR}} \xi_\infty(z; q) = \sum_{m \geq 0} \left( \sigma_+^{(m)} x^{2m} + \gamma \sigma_-^{(m)} x^{2m+2\nu_{IR}} \right) \quad ; \quad \gamma \equiv \frac{\Gamma(-\nu_{IR})}{2^{2\nu_{IR}} \Gamma(\nu_{IR})} \quad (113)$$

Now from (110) we have that at fixed  $x < \text{minimum}(m_{IR}, 1)$ , in the limit  $q \rightarrow 0$  equations (111) and (113) should coincide. More specifically, if we introduce  $\delta C_\pm(q)$  by,

$$\begin{aligned} C_+(q) &\equiv \frac{1}{D(q)} \left( \frac{1}{a_+^{IR}} (1 + q^2 \epsilon_{+-}^{IR}(q)) + \frac{\gamma}{a_-^{IR}} q^{2+2\nu_{IR}} \epsilon_{--}^{IR}(q) \right) + \delta C_+(q) \\ C_-(q) &\equiv \frac{1}{D(q)} \left( -\frac{1}{a_+^{IR}} q^2 \epsilon_{++}^{IR}(q) + \frac{\gamma}{a_-^{IR}} q^{2\nu_{IR}} (1 - q^2 \epsilon_{-+}^{IR}(q)) \right) + \delta C_-(q) \end{aligned} \quad (114)$$

where,

$$D(q) = 1 + q^2 (\epsilon_{+-}^{IR}(q) - \epsilon_{-+}^{IR}(q)) + q^4 (\epsilon_{++}^{IR}(q) \epsilon_{--}^{IR}(q) - \epsilon_{+-}^{IR}(q) \epsilon_{-+}^{IR}(q)) \quad (115)$$

then we should get,

$$\begin{aligned} &\lim_{q \rightarrow 0} \left\{ \sum_{m \geq 0} \sigma_+^{(m)} x^{2m} \left( \bar{\xi}_+^{(m)} \left( \frac{x}{q} \right) - 1 \right) + \gamma \sum_{m \geq 0} \sigma_-^{(m)} x^{2m+2\nu_{IR}} \left( \bar{\xi}_-^{(m)} \left( \frac{x}{q} \right) - 1 \right) \right. \\ &+ \left( (1 - q^2 \epsilon_{-+}^{IR}(q)) \delta C_+(q) - q^2 \epsilon_{--}^{IR}(q) \delta C_-(q) \right) a_+^{IR} \sum_{m \geq 0} \sigma_+^{(m)} x^{2m} \bar{\xi}_+^{(m)} \left( \frac{x}{q} \right) \\ &\left. + \left( (1 + q^2 \epsilon_{+-}^{IR}(q)) \delta C_-(q) + q^2 \epsilon_{++}^{IR}(q) \delta C_+(q) \right) \frac{a_-^{IR}}{q^{2\nu_{IR}}} \sum_{m \geq 0} \sigma_-^{(m)} x^{2m+2\nu_{IR}} \bar{\xi}_-^{(m)} \left( \frac{x}{q} \right) \right\} = 0 \end{aligned} \quad (116)$$

While the first line is automatically zero, the second and third lines should be zero separately because they present different power series<sup>3</sup>. From the third line we get,

$$\delta C_-(q) \xrightarrow{q \rightarrow 0} -\varphi_{++}^{(0)} q^2 \delta C_+(q) + q^{2\nu_{IR}} A(q) \quad (117)$$

<sup>3</sup>A subtlety (not present in the case considered in the text) arises if  $\bar{\xi}_-^{(m)}(z)$  contains powers of the form  $z^{-2\nu_{IR}-2n}$  with  $n \in \mathbb{N}$ ; in that case it can be easily showed that the effect is that the coefficients of  $\delta C^\pm(q)$  on the second line of (116) get modified by holomorphic functions; this fact does not modify the subsequent arguments.

where  $A(q) \xrightarrow{q \rightarrow 0} 0$ . Then the second line of (116) yields,

$$\delta C_+(q) \xrightarrow{q \rightarrow 0} \varphi_{--}^{(0)} q^{2\nu_{IR}+2} A(q) \Rightarrow \delta C_-(q) \xrightarrow{q \rightarrow 0} q^{2\nu_{IR}} A(q) \quad (118)$$

Going to (114) with (118) we get the leading behaviors,

$$C_+(0) = \frac{1}{a_+^{IR}} \quad ; \quad C_-(q)|_{q \rightarrow 0} = -\frac{\bar{\varphi}_{++}^{(0)}}{a_+^{IR}} q^2 \quad (119)$$

This yields for the two-point function (103) the Goldstone pole,

$$G_2(q) \xrightarrow{q \rightarrow 0} \frac{\alpha}{q^2} \quad (120)$$

where by using (102) and (104), i.e.

$$\bar{\varphi}_{++}^{(0)} = \int_{z_i}^{\infty} dw w^{1-d} \xi_+(w)^2 \quad (121)$$

we get for the residue,

$$\alpha = \frac{2\nu_{UV} (a_+^{UV})^2}{\int_0^{\infty} dw w^{1-d} \xi_+(w)^2} \quad (122)$$

The result is reassuring in the sense that both contributions in the denominator of (103) add to yield a  $z_i$ -independent result.

## 8 Global symmetries and AdS/CFT

Let us now use all this machinery for a simple  $d$ -dimensional strongly coupled system with a spontaneously broken global symmetry. We would like to see explicitly what makes Nambu-Goldstone bosons massless in the AdS/CFT picture: it is the square integrability of the solution  $\xi_+(z)$  of the perturbation equation. In other words, a normalizable perturbation is massless.

In general let the original symmetry group be  $G$ , spontaneously broken to  $H$ . The simplest example seems to be  $SU(3) \rightarrow SU(2) \times U(1)$ , i.e.  $G = SU(3)$  and  $H = SU(2) \times U(1)$ . A physically more appealing case could be the case of the unification group  $SU(5) \rightarrow SU(3) \times SU(2) \times U(1)$ , which will not consider here though. The hope is that eventually one could then weakly couple the system to gauge bosons, i.e. gauge it. Let's consider a real adjoint transforming under  $SU(3)$  as  $\Sigma \rightarrow U\Sigma U^\dagger$ , which we parametrize as

$$\Sigma = \frac{1}{\sqrt{2}} \begin{pmatrix} t/\sqrt{3} + t_3 & t_1 - it_2 & w_1 - iw_2 \\ t_1 + it_2 & t/\sqrt{3} - t_3 & w_3 - iw_4 \\ w_1 + iw_2 & w_3 + iw_4 & -2t/\sqrt{3} \end{pmatrix} \quad (123)$$

and a complex fundamental (under  $SU(3)$ ,  $F \rightarrow UF$ ):

$$F^T = (T_1 \quad T_2 \quad H)^T \quad (124)$$

The  $SU(2) \times U(1)$  final symmetry will be preserved by  $\langle \Sigma \rangle = t\lambda_8$  (with  $\lambda_8$  the Gell-Mann matrix) and  $\langle F \rangle = 0$ . To get it let the  $SU(3)$  invariant superpotential be

$$W = \Delta \left( \frac{1}{2} Tr \Sigma^2 + \frac{\sqrt{6}}{3} Tr \Sigma^3 \right) + F^\dagger (m - \sqrt{6}\alpha \Sigma) F \quad (125)$$

The strange relation between the  $\Sigma^2$  and  $\Sigma^3$  coefficients are chosen so that the straightforward generalization of the potential (39)

$$V = \frac{1}{2} \left( \frac{\partial W}{\partial t} \right)^2 + \frac{1}{2} \sum_{i=1}^3 \left( \frac{\partial W}{\partial t_i} \right)^2 + \frac{1}{2} \sum_{a=1}^4 \left( \frac{\partial W}{\partial w_a} \right)^2 + \sum_{i=1}^2 \left( \frac{\partial W}{\partial T_i} \right) \left( \frac{\partial W}{\partial T_i^*} \right) + \left( \frac{\partial W}{\partial H} \right) \left( \frac{\partial W}{\partial H^*} \right) - d W \quad (126)$$

has an extremum at  $t = 0$  and a minimum at  $t = 1$  with all other fields vanishing, and the potential for  $t$  is the same as in [18]:

$$W(t) = \Delta \left( \frac{t^2}{2} - \frac{t^3}{3} \right) \quad (127)$$

$$\begin{aligned} V(t) &= \frac{1}{2} W'^2(t) - d W(t) \\ &= \Delta(\Delta - d) \frac{t^2}{2} - \Delta(3\Delta - d) \frac{t^3}{3} + 2\Delta^2 \frac{t^4}{4} \end{aligned} \quad (128)$$

The solution to the e.o.m. is

$$t(z) = \frac{z^\Delta}{1 + z^\Delta}, \quad t_i, w_a = 0 \quad (129)$$

One can calculate the mass matrix

$$\frac{\partial V}{\partial t^2} \equiv m^2(t) = \Delta(\Delta - d) - 2\Delta(3\Delta - d)t + 6\Delta^2 t^2 \quad (130)$$

$$\frac{\partial V}{\partial w_a \partial w_b} \equiv m_w^2(t) \delta^{ab} = (\Delta(\Delta - d) - \Delta(3\Delta - d)t + 2\Delta^2 t^2) \delta^{ab} \quad (131)$$

$$\frac{\partial V}{\partial t_i \partial t_j} \equiv m_t^2(t) \delta^{ij} = (\Delta(\Delta - d) + 2\Delta(3\Delta - d)t + 2\Delta^2 t^2) \delta^{ij} \quad (132)$$

$$\frac{\partial V}{\partial T_\alpha^* \partial T_\beta} \equiv m_T^2(t) \delta^{\alpha\beta} = (m(m - d) - \alpha(2m + \Delta - d)t + \alpha(\alpha + \Delta)t^2) \delta^{\alpha\beta} \quad (133)$$

$$\frac{\partial V}{\partial H^* \partial H} \equiv m_H^2(t) = m(m - d) + 2\alpha(m + \Delta - d)t + 2\alpha(2\alpha - \Delta)t^2 \quad (134)$$

with all other elements vanishing.

This means that it is easy to solve the perturbation equation since the different modes decouple. In an obvious notation:

$$z^2 \ddot{\xi}(z; q) - (d - 1) z \dot{\xi}(z; q) - (q^2 z^2 + m^2(t(z))) \xi(z; q) = 0 \quad (135)$$

$$z^2 \ddot{\xi}^w(z; q) - (d - 1) z \dot{\xi}^w(z; q) - (q^2 z^2 + m_w^2(t(z))) \xi^w(z; q) = 0 \quad (136)$$

$$z^2 \ddot{\xi}^t(z; q) - (d - 1) z \dot{\xi}^t(z; q) - (q^2 z^2 + m_t^2(t(z))) \xi^t(z; q) = 0 \quad (137)$$

$$z^2 \ddot{\xi}^T(z; q) - (d - 1) z \dot{\xi}^T(z; q) - (q^2 z^2 + m_T^2(t(z))) \xi^T(z; q) = 0 \quad (138)$$

$$z^2 \ddot{\xi}^H(z; q) - (d - 1) z \dot{\xi}^H(z; q) - (q^2 z^2 + m_H^2(t(z))) \xi^H(z; q) = 0 \quad (139)$$

The first equation (135) has a well known solution at  $q^2 = 0$  (corresponding to the dilaton)

$$\xi_+(z) = z \dot{t}(z) \quad (140)$$

The second one (136) is for the Goldstone-bosons of the global symmetry. Since

$$m_w^2(t) = \frac{1}{t} V'(t) \quad (141)$$

the well-behaved solution at  $q^2 = 0$  is simply

$$\xi_+^w(z) = t(z) \quad (142)$$

This is why it has a pole at  $q^2 = 0$ . We just need to do the usual expansion derived in general in the previous section, see also [18], with the result for the propagator

$$G_2^w(q) = \frac{\alpha}{q^2} \quad (143)$$

with the general expression

$$\alpha = \frac{2\nu_{UV} (a_+^{UV})^2}{(\int_0^\infty dx x^{1-d} (\xi_+^w(x))^2)} \quad (144)$$

In our specific case (136) we have

$$a_+^{UV} = 1 \quad (145)$$

with the integral in the denominator finite.

Then, what about the third equation (137), i.e. for  $\xi^t$ ? One can easily find the solution for  $q = 0$ :

$$\xi^t(z) = C_1 z^\Delta (1 + z^\Delta)^2 + C_2 \frac{z^{d-\Delta}}{1 + z^\Delta} {}_2F_1(1, -5 + d/\Delta, -1 + d/\Delta, -z^\Delta) \quad (146)$$

For  $z \rightarrow \infty$  we get

$$\xi^t(z) \rightarrow C_1 z^\Delta (1 + z^\Delta)^2 + C_2 \frac{z^{d-\Delta}}{1 + z^\Delta} z^{5\Delta-d} \frac{\Gamma(6 - d/\Delta)\Gamma(-1 + d/\Delta)(1 + z^\Delta)^3}{2z^{3\Delta}} \quad (147)$$

and so

$$C_1 = -\frac{C_2}{2} \Gamma(6 - d/\Delta)\Gamma(-1 + d/\Delta) \quad (148)$$

In the opposite limit  $z \rightarrow 0$  (137) becomes

$$\xi^t(z) \rightarrow C_1 (z^\Delta + \dots) + C_2 (z^{d-\Delta} + \dots) \quad (149)$$

so that due to (148) we get in the IR limit  $q \rightarrow 0$

$$G_2^t(0) = \frac{C_1}{C_2} = -\frac{1}{2} \Gamma(6 - d/\Delta)\Gamma(1 - d/\Delta) \quad (150)$$

Obviously there is no pole here at  $q = 0$ , a pole is expected at finite  $q$ . The reason for no pole at  $q = 0$  is thus due to the fact that there is no solution finite in the whole positive  $z$ -axis. This was true

for  $\xi(z) = z \dot{t}(z)$  and  $\xi^w(z) = t(z)$ , and this is why the next order in  $q$  was needed there. In other words, if the integral in (122) is finite, the propagator obeys (120), if it is not, then the leading term in this expansion is a constant.

Equations (138) and (139) for  $\xi^T$  and  $\xi^H$  seem to point to the same conclusion as for  $\xi^t$ : no pole, i.e. no light degree of freedom. So if we would like one of the two to be light, i.e. for example  $\xi^H$  (the analog of the light SM doublet in SU(5)), we would need to further fine-tune the system, similarly as one obtains the usual doublet-triplet splitting in a SU(5) grand unified theory.

## 9 Summary of results

We have studied some simple examples of the AdS/CFT correspondence, i.e. the domain wall solution in the AdS bulk of a scalar field in the limit of no gravity back-reaction. To obtain analytical results we rewrote the bulk scalar potential in terms of an appropriate superpotential. The correspondence between the two is a bit unusual, i.e. it is the one that survives the infinite Planck scale limit. Since the superpotential was written as a simple polynomial of the scalar field, the potential itself is obviously tuned, i.e. it is not the most general one of given order. We showed explicitly that such tuning of the parameters is necessary for the solution to exist at all, and that it is just a consequence of a vanishing boundary cosmological constant, in accord with a known result from the literature. We proved another general requirement for the existence of such domain walls: the second field derivative of the potential must be smaller than  $-d^2/4$  at least in some interval of the bulk coordinate, where  $d$  is the boundary space-time dimension. We then found the solution of the perturbation equation for the dilaton mode by the WKB approximation and by the matching method to all orders. We generalized in this way the known result of a massless mode corresponding to the spontaneously broken Nambu-Goldstone excitation (dilaton) due to the spontaneously broken translational symmetry in AdS. The existence of a massless mode is essentially due to the existence of a normalizable mode at  $q^2 = 0$ : this interpretation is confirmed in the case of spontaneously broken internal global symmetries. We gave an explicit example in terms of a SU(3) theory spontaneously broken by an adjoint vev to SU(2)→U(1).

## Acknowledgments

We would like to thank Mirjam Cvetič, Fidel Schaposnik and Guillermo Silva for discussions, and Mirjam Cvetič, Carlos Hoyos, Uri Kol, Cobi Sonnenschein and Shimon Yankielowicz for correspondence. This work has been supported in part by the Slovenian Research Agency, and by the Argentinian-Slovenian programme BI-AR/12-14-004 // MINCYT-MHEST SLO/11/04.

## References

- [1] J. M. Maldacena, “The Large  $N$  Limit of Superconformal Field Theories and Supergravity,” *Adv. Theor. Math. Phys.* **2** (1998) 231 [hep-th/9711200].
- [2] S. S. Gubser, I. R. Klebanov, A. M. Polyakov and , “Gauge Theory Correlators from Noncritical String Theory,” *Phys. Lett. B* **428** (1998) 105 [hep-th/9802109].
- [3] E. Witten, “Anti-de Sitter Space and Holography,” *Adv. Theor. Math. Phys.* **2** (1998) 253 [hep-th/9802150].
- [4] L. Girardello, M. Petrini, M. Porrati, A. Zaffaroni, “Novel Local CFT and Exact Results on Perturbations of  $\mathcal{N} = 4$  Super Yang Mills from AdS Dynamics,” *JHEP* **9812** (1998) 022 [hep-th/9810126].
- [5] D. Z. Freedman, S. S. Gubser, K. Pilch, N. P. Warner, “Continuous Distributions of D3-Branes and Gauged Supergravity,” *JHEP* **0007** (2000) 038 [hep-th/9906194].
- [6] G. Arutyunov, S. Frolov, S. Theisen, “A Note on Gravity Scalar Fluctuations in Holographic RG Flow Geometries,” *Phys. Lett. B* **484** (2000) 295 [hep-th/0003116].

- [7] W. Mück, “Correlation Functions in Holographic Renormalization Group Flows,” Nucl. Phys. B **620** (2002) 477 [hep-th/0105270].
- [8] D. Martelli, A. Miemiec, “CFT / CFT Interpolating RG Flows and the Holographic C Function,” JHEP **0204** (2002) 027 [hep-th/0112150].
- [9] M. Berg, H. Samtleben, “Holographic Correlators in a Flow to a Fixed Point,” JHEP **0212** (2002) 070 [hep-th/0209191].
- [10] D. Z. Freedman, C. Nunez, M. Schnabl, K. Skenderis, “Fake Supergravity and Domain Wall Stability,” Phys. Rev. D **69** (2004) 104027 [hep-th/0312055].
- [11] M. Cvetič, S. Griffies, S. -J. Rey, “Static Domain Walls in  $\mathcal{N} = 1$  Supergravity,” Nucl. Phys. B **381** (1992) 301 [hep-th/9201007].
- [12] O. Aharony, S. S. Gubser, J. M. Maldacena, H. Ooguri, Y. Oz, “Large  $N$  Field Theories, String Theory and Gravity,” Phys. Rept. **323** (2000) 183 [hep-th/9905111].
- [13] O. DeWolfe, D. Z. Freedman, “Notes on Fluctuations and Correlation Functions in Holographic Renormalization Group Flows,” hep-th/0002226.
- [14] E. D’Hoker, D. Z. Freedman, “Supersymmetric Gauge Theories and the AdS / CFT Correspondence,” hep-th/0201253.
- [15] K. Skenderis, “Lecture Notes on Holographic Renormalization,” Class. Quant. Grav. **19** (2002) 5849 [hep-th/0209067].
- [16] B. Bajc, A. R. Lugo and M. B. Sturla, “Spontaneous Breaking of a Discrete Symmetry and Holography,” JHEP **1204** (2012) 119 [arXiv:1203.2636 [hep-th]].
- [17] M. Bianchi, D. Z. Freedman, K. Skenderis, “How to Go with an RG Flow,” JHEP **0108** (2001) 041 [hep-th/0105276].
- [18] B. Bajc and A. R. Lugo, “On the Matching Method and the Goldstone Theorem in Holography,” JHEP **1307** (2013) 056 [arXiv:1304.3051 [hep-th]].
- [19] C. Hoyos, U. Kol, J. Sonnenschein and S. Yankielowicz, “The Holographic Dilaton,” arXiv:1307.2572 [hep-th].
- [20] U. Kol, “On the Dual Flow of Slow-Roll Inflation,” arXiv:1309.7344 [hep-th].
- [21] C. Hoyos, U. Kol, J. Sonnenschein and S. Yankielowicz, “The A-Theorem and Conformal Symmetry Breaking in Holographic RG Flows,” arXiv:1207.0006 [hep-th].
- [22] S. A. Hartnoll, “Lectures on holographic methods for condensed matter physics,” Class. Quant. Grav. **26**, 224002 (2009) [arXiv:0903.3246 [hep-th]].
- [23] D. S. Berman and E. Rabinovici, hep-th/0210044.
- [24] F. Coradeschi, P. Lodone, D. Pappadopulo, R. Rattazzi and L. Vitale, “A Naturally Light Dilaton,” arXiv:1306.4601 [hep-th].
- [25] J. Maldacena, “Vacuum Decay into Anti De Sitter Space,” arXiv:1012.0274 [hep-th].



# A Minimal Supersymmetric Model of Particle Physics and the Early Universe

*W. Buchmüller<sup>a,\*</sup>, V. Domcke<sup>a,†</sup>, K. Kamada<sup>a,‡</sup> and K. Schmitz<sup>b,§</sup>*

<sup>a</sup> Deutsches Elektronen-Synchrotron DESY, 22607 Hamburg, Germany

<sup>b</sup> Kavli IPMU, TODIAS, University of Tokyo, Kashiwa 277-8583, Japan

## Abstract

We consider a minimal supersymmetric extension of the Standard Model, with right-handed neutrinos and local  $B-L$ , the difference between baryon and lepton number, a symmetry which is spontaneously broken at the scale of grand unification. To a large extent, the parameters of the model are determined by gauge and Yukawa couplings of quarks and leptons. We show that this minimal model can successfully account for the earliest phases of the cosmological evolution: Inflation is driven by the energy density of a false vacuum of unbroken  $B-L$  symmetry, which ends in tachyonic preheating, i.e. the decay of the false vacuum, followed by a matter dominated phase with heavy  $B-L$  Higgs bosons. Nonthermal and thermal processes produce an abundance of heavy neutrinos whose decays generate primordial entropy, baryon asymmetry via leptogenesis and dark matter consisting of gravitinos or nonthermal WIMPs. The model predicts relations between neutrino and superparticle masses and a characteristic spectrum of gravitational waves.

## 1 Introduction

Today we have the Standard Model of particle physics as well as the  $\Lambda$ CDM model of cosmology, which describe a wealth of experimental and observational data with an accuracy far beyond expectation [1]. On the other hand, despite this success, it is obvious that both standard models do not represent a final theory. The symmetry structure of the Standard Model, the smallness of neutrino masses and the discovery of a Higgs boson [2, 3] with a mass in between the vacuum stability and the triviality bound point towards grand unification as the next step beyond the Standard Model. Similarly, the parameters of the  $\Lambda$ CDM model, the abundance of matter and dark matter, the apparent cosmological constant and the temperature anisotropies of the cosmic microwave background ask for an explanation, which requires physics beyond the Standard Model.

Supersymmetry is an attractive framework to extrapolate the Standard Model of particle physics to the energy scale of grand unification,  $\Lambda_{\text{GUT}} \sim 10^{16}\text{GeV}$ . It also introduces natural dark matter candidates [4–6] and scalar fields which can realize inflation, thereby providing an important link between particle physics and cosmology. Moreover, neutrino masses require right-handed neutrinos whose large Majorana masses can account for the tiny masses of the known neutrinos via the seesaw mechanism. These Majorana masses break the symmetry  $B-L$ , the difference between baryon and lepton number, and their decays can generate a baryon asymmetry via leptogenesis [7]. Extrapolating the feature of the Standard Model that all masses are generated by spontaneous symmetry breaking, suggests that also  $B-L$  is a spontaneously broken local symmetry.

---

\*E-mail: buchmuwi@desy.de

†E-mail: valerie.domcke@desy.de

‡E-mail: kohei.kamada@desy.de

§E-mail: kai.schmitz@ipmu.jp

Following these arguments we arrive at a minimal supersymmetric extension of the Standard Model, which is described by the superpotential

$$W = \sqrt{\lambda} \Phi \left( \frac{v_{B-L}^2}{2} - S_1 S_2 \right) + \frac{1}{\sqrt{2}} h_i^n n_i^c n_i^c S_1 + h_{ij}^\nu \mathbf{5}_i^* n_j^c H_u + W_{\text{MSSM}}, \quad (1)$$

where  $S_1$  and  $S_2$  are the chiral superfields containing the Higgs field responsible for breaking  $B-L$ , and  $n_i^c$  denote the superfields containing the charge conjugates of the right-handed neutrinos. The symmetry-breaking sector of Eq. (1), involving the superfields  $S_1$ ,  $S_2$  and  $\Phi$ , is precisely the superpotential of F-term hybrid inflation, with  $\Phi$  being a singlet whose scalar component  $\phi$  acts as the inflaton [8, 9].  $v_{B-L}$  is the scale at which  $B-L$  is broken. The  $B-L$  charges are  $q_S \equiv q_{S_2} = -q_{S_1} = 2$ ,  $q_\Phi = 0$ , and  $q_{n_i^c} = 1$ .  $h$  and  $\lambda$  denote coupling constants, and  $W_{\text{MSSM}}$  represents the MSSM superpotential,

$$W_{\text{MSSM}} = h_{ij}^u \mathbf{10}_i \mathbf{10}_j H_u + h_{ij}^d \mathbf{5}_i^* \mathbf{10}_j H_d. \quad (2)$$

For convenience, all superfields have been arranged in  $SU(5)$  multiplets,  $\mathbf{10} = (q, u^c, e^c)$  and  $\mathbf{5}^* = (d^c, l)$ , and  $i, j = 1, 2, 3$  are flavour indices. We assume that the colour triplet partners of the electroweak Higgs doublets  $H_u$  and  $H_d$  have been projected out. The vacuum expectation values  $v_u = \langle H_u \rangle$  and  $v_d = \langle H_d \rangle$  break the electroweak symmetry. In the following we will assume large  $\tan \beta = v_u/v_d$ , implying  $v_d \ll v_u \simeq v_{\text{EW}} = \sqrt{v_u^2 + v_d^2}$ . We will restrict our analysis to the case of a hierarchical heavy (s)neutrino mass spectrum,  $M_1 \ll M_2, M_3$ , where  $M_i = h_i^n v_{B-L}$ . Furthermore we assume the heavier (s)neutrino masses to be of the same order of magnitude as the common mass  $m_S$  of the particles in the symmetry-breaking sector, for definiteness we set  $M_2 = M_3 = m_S$ . Key parameters of the analysis are then the  $B-L$  breaking scale  $v_{B-L}$ , the mass of the lightest of the heavy (s)neutrinos  $M_1$ , and the effective light neutrino mass parameter  $\tilde{m}_1$  (cf. [10]),

$$v_{B-L} \simeq \frac{v_{\text{EW}}^2}{\bar{m}_\nu}, \quad M_1 \ll v_{B-L}, \quad \tilde{m}_1 \equiv \frac{(h^{\nu\dagger} h^\nu)_{11} v_{\text{EW}}^2}{M_1}. \quad (3)$$

Here,  $\bar{m}_\nu = \sqrt{m_2 m_3} \sim 3 \times 10^{-2} \text{eV}$  is the geometric mean of the two light neutrino mass eigenvalues  $m_2$  and  $m_3$ , and characterizes the light neutrino mass scale. In addition to the chiral superfields, the model also contains a vector supermultiplet  $V$  ensuring invariance under local  $B-L$  transformations and the gravity supermultiplet consisting of the graviton  $G$  and the gravitino  $\tilde{G}$ .

In the following sections we shall show that this Minimal Supersymmetric Model (MSM), whose parameters are largely fixed by low energy experiments, provides a consistent description of the transition from an inflationary phase to the hot early universe. During this ‘pre- and reheating’ process the matter-antimatter asymmetry and the dark matter abundance are generated. Most of our discussion will be based on Refs. [10–12].

Our work is closely related to previous studies of thermal leptogenesis [13, 14] and nonthermal leptogenesis via inflaton decay [15–18], where the inflaton lifetime determines the reheating temperature. In supersymmetric models with global  $B-L$  symmetry the scalar superpartner  $\tilde{N}_1$  of the lightest heavy Majorana neutrino  $N_1$  can play the role of the inflaton in chaotic [19, 20] or hybrid [21, 22] inflation models. Local  $B-L$  breaking in connection with hybrid, shifted hybrid and smooth hybrid inflation has been considered in Ref. [23]. One of the main motivations for nonthermal leptogenesis has been that the ‘gravitino problem’ for heavy unstable gravitinos [24–28] can be avoided by means of a low reheating temperature. In the following we shall assume that the gravitino is either the lightest superparticle (LSP) or very heavy,  $m_{3/2} \gtrsim 10 \text{TeV}$ . In the first case, gravitinos, thermally produced at a reheating temperature compatible with leptogenesis, can explain the observed dark matter abundance [29]. For very heavy gravitinos, thermal production and subsequent decay into a wino or higgsino LSP can yield nonthermal WIMP dark matter [30–32].

The MSM, defined in Eq. (1), postdicts the earliest phases of the cosmological evolution. The energy density of a false vacuum with unbroken  $B-L$  symmetry drives inflation. Consistency with the measured amplitude of the temperature anisotropies of the cosmic microwave background fixes  $v_{B-L}$ , the scale of  $B-L$  symmetry breaking, to be the GUT scale. Inflation ends by tachyonic preheating [33], i.e. the decay of the false vacuum, which sets the stage for a phase dominated by nonrelativistic matter in the form of heavy  $B-L$  Higgs bosons. The further development is described by Boltzmann equations. Nonthermal and thermal processes produce an abundance of heavy neutrinos whose decays generate primordial entropy, baryon asymmetry via leptogenesis and gravitino dark matter from scatterings in the thermal bath. This whole pre- and reheating process is imprinted on the spectrum of primordial gravitational waves [34]. It is remarkable that the initial conditions of the radiation dominated phase are not free parameters of a cosmological model. Instead, they are determined by the parameters of a Lagrangian, which in principle can be measured by particle physics experiments and astrophysical observations. The consistency of hybrid inflation, leptogenesis and dark matter entails interesting relations between the lightest neutrino mass  $m_1$ , the gravitino mass and possibly wino or higgsino masses.

The paper is organized as follows. In Section 2 we discuss F-term hybrid inflation. Corrections from supersymmetry breaking lead to a two-field model which can account for all results deduced from the recently released Planck data. Section 3 deals with tachyonic preheating and the important topic of cosmic string formation, with emphasis on the current theoretical uncertainties. The description of the reheating process by means of Boltzmann equations and the resulting relations between neutrino masses and superparticle masses are the subject of Section 4. The predictions of the gravitational wave spectrum due to inflation, cosmic strings, pre- and reheating are reviewed in Section 5. Finally, observational prospects are addressed in Section 6.

## 2 Inflation

The superpotential of the MSM, cf. Eq. (1), allows for a phase of F-term hybrid inflation. For  $|\phi| \gg v_{B-L}$ , the  $B-L$  Higgs fields are fixed at zero,  $B-L$  is unbroken and the energy density of the universe is dominated by the false vacuum energy,  $\rho_0 \simeq (\lambda/4) v_{B-L}^4 \equiv V_0$ , generated by the non-vanishing vacuum expectation value (vev) of the auxiliary field  $F_\phi$  and inducing spontaneous supersymmetry breaking. Here, we briefly review the dynamics and predictions of this inflation model, with particular focus on the status of F-term hybrid inflation in the light of the recent Planck results [35].

### The scalar potential

At the high energy scales involved in inflation, supergravity corrections to the Lagrangian become important, resulting in a tree-level scalar F- and D-term potential given by

$$V_{\text{SUGRA}}^F = e^{K/M_P^2} \left[ \sum_{\alpha\bar{\beta}} K^{\alpha\bar{\beta}} \mathcal{D}_\alpha W \mathcal{D}_{\bar{\beta}} W^* - 3 \frac{|W|^2}{M_P^2} \right], \quad V_{\text{SUGRA}}^D = \frac{1}{2} g^2 \left( \sum_\alpha q_\alpha K_\alpha z_\alpha \right)^2, \quad (4)$$

where  $\mathcal{D}_\alpha W = W_\alpha + K_\alpha W/M_P^2$ ; the subscript  $\alpha$  ( $\bar{\alpha}$ ) denotes the derivative with respect to the (complex conjugate of the) scalar component  $z_\alpha$  of the superfield  $\Phi_\alpha$  carrying the  $U(1)$  gauge charge  $q_\alpha$ ,  $K^{\alpha\bar{\beta}}$  is the inverse Kähler metric and  $M_P = 2.4 \times 10^{18}$  GeV is the reduced Planck mass. For a canonical Kähler potential,

$$K = \sum_\alpha |z_\alpha|^2, \quad (5)$$

the D-term scalar potential reduces to the expression familiar from global supersymmetry, but an important supergravity contribution arises from the F-term potential,  $V_{\text{SUGRA}}^F \supset |z_\alpha|^2 \rho_0/M_P^2$ . This yields large contributions to the masses of the scalar fields  $z_\alpha$  of the theory. For the superpotential (1), this stabilizes the singlet sneutrinos and the MSSM scalars at a vanishing field value. The  $B-L$  Higgs boson masses also obtain various supergravity contributions. However, these are suppressed by factors of

$(v_{B-L}/M_P)^2$  or  $(\phi/M_P)^2$  compared to the leading order terms, which match the result found in global supersymmetry,

$$(m_{\pm}^S)^2 = \lambda(|\phi|^2 \pm \frac{1}{2}v_{B-L}^2), \quad (m_f^S)^2 = \lambda|\phi|^2. \quad (6)$$

The F-term supergravity contribution discussed above does not give a mass-term to the inflaton  $\phi$  because after expanding  $e^{K/M_P^2}$  in Eq. (4), the term in question is cancelled by the corresponding term in  $D_{\phi}W D_{\bar{\phi}}W^*$ . The leading order supergravity contribution to the inflaton mass thus stems from the term proportional to  $|\phi|^4 v_{B-L}^4/M_P^4$  in the scalar potential [36]. In addition, since supersymmetry is broken during inflation, we need to take the one-loop Coleman-Weinberg (CW) potential for the inflaton field into account, obtained by integrating out the heavy  $B-L$  Higgs bosons,

$$V_{1l} = \frac{1}{64\pi^2} \text{STr} \left[ M^4 \left( \ln \left( \frac{M^2}{Q^2} \right) - \frac{1}{2} \right) \right] \simeq \frac{\lambda^2 v_{B-L}^4}{64\pi^2} \left[ \ln \left( \frac{2|\phi|^2}{v_{B-L}^2} \right) + \mathcal{O} \left( \frac{v_{B-L}^4}{4|\phi|^4} \right) \right], \quad (7)$$

Here STr denotes the supertrace running over all degrees of freedom of  $S_1$  and  $S_2$ .  $M$  is the corresponding mass matrix, cf. Eq. (6), and  $Q$  an appropriate renormalization scale, which we have set to  $Q^2 = \lambda v_{B-L}^2/2$ .

From the resulting scalar potential,  $V = V_{\text{SUGRA}}^{F+D} + V_{1l}$ , we find the following picture: For  $|\phi| > v_{B-L}/\sqrt{2}$ , the Higgs fields  $s_{1,2}$  are fixed at zero and the inflaton slowly rolls towards the origin. At  $|\phi| = v_{B-L}/\sqrt{2}$ ,  $(m_{\pm}^S)^2$  becomes negative, triggering a tachyonic instability. The Higgs fields acquire a vev and  $B-L$  is broken. Both the Higgs (which, now that  $B-L$  is broken, is best parametrized in unitary gauge as a radial degree of freedom dubbed  $\sigma'$  in Ref. [10], see also Ref. [37] for the explicit relation between  $\sigma'$  and the symmetry-breaking Higgs mass eigenstate in arbitrary gauge) and the inflaton field then quickly fall into their true vacuum,  $|\phi| \rightarrow 0$  and  $\sigma' \rightarrow \sqrt{2} v_{B-L}$ , eliminating the vacuum energy contributions of the scalar potential and ending inflation.

### Slow-roll inflation

In the slow-roll approximation, the dynamics of the homogeneous inflaton field is governed by  $3H\dot{\phi} = -\partial V/\partial\phi^*$ , where  $H$  denotes the Hubble parameter. For a scalar potential only depending on the absolute value of  $\phi$ , cf. Eq. (7), we can rewrite this in terms of the radial and angular component of  $\phi = \frac{1}{\sqrt{2}}\varphi e^{-i\theta}$ ,

$$3H\dot{\varphi} = -V'(\varphi), \quad \dot{\theta} = 0. \quad (8)$$

Turning to the quantum fluctuations of the inflaton field which are visible today in the CMB, we now evaluate the scalar potential and its derivatives at  $\varphi = \varphi_*$ , the value of  $\varphi$  at  $N_* \approx 55$  e-folds before the end of inflation, when the reference scale commonly used to describe the CMB fluctuations left the horizon. With  $\varphi_f$  denoting the value of the inflaton at the end of inflation,<sup>1</sup>  $\varphi_*$  is given by

$$\varphi_*^2 \approx \varphi_f^2 + \frac{\lambda}{4\pi^2} M_P^2 N_* \quad (9)$$

Of particular interest in the following will be the predictions from F-term hybrid inflation for the amplitude of the scalar fluctuations  $A_s$ , the scalar spectral index  $n_s$  and the tensor-to-scalar ratio  $r$ :

$$\begin{aligned} A_s &= \frac{H^2}{8\pi^2\epsilon M_P^2} \Big|_{\varphi_*} \approx \frac{1}{3} \left( \frac{v_{B-L}}{M_P} \right)^4 N_*, \\ n_s &= 1 - 6\epsilon + 2\eta \Big|_{\varphi_*} \approx 1 - \frac{1}{N_*}, \\ r &= \frac{A_t}{A_s} = 16\epsilon \Big|_{\varphi_*} \approx \frac{\lambda}{2\pi^2} \frac{1}{N_*}, \end{aligned} \quad (10)$$

<sup>1</sup>Here,  $\varphi_f$  is determined by either  $m_{\pm}^S(\varphi_c) = 0$ , cf. Eq. (6), or by the violation of the slow-roll condition, i.e.  $|\eta(\varphi_f)| = 1$ , cf. Eq. (11), whatever occurs earlier:  $\varphi_f \approx \max\{v_{B-L}, \sqrt{\lambda}M_P/(\sqrt{8\pi})\}$ .

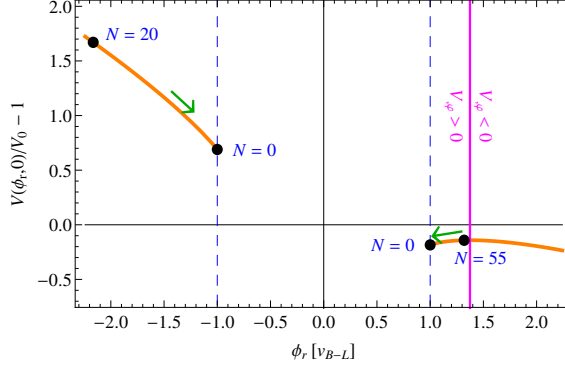


**Fig. 1:** Scalar potential for inflation along the real axis in the complex  $\phi$  field space after adding a constant term  $W_0$  to the superpotential. Slow-roll inflation is possible both for  $\theta = 0$  and  $\theta = \pi$ . Here  $\lambda = 4.5 \times 10^{-6}$ ,  $v_{B-L} = 2.9 \times 10^{15}$  GeV and  $m_{\tilde{G}} = 47.5$  TeV.

where  $A_t = 2H^2/(\pi^2 M_P^2)|_{\phi^*}$  denotes the amplitude of the tensor fluctuations, and  $\epsilon$  and  $\eta$  are the so-called slow-roll parameters,

$$\epsilon = \frac{M_P^2}{2} \left( \frac{V'}{V} \right)^2, \quad \eta = M_P^2 \frac{V''}{V}. \quad (11)$$

Moreover, in Eq. (10) we have employed the approximation<sup>2</sup>  $\varphi_*^2 \gg \varphi_f^2$ .

### F-term hybrid inflation in the light of Planck

Comparing these results with the recently published Planck data [35,38],

$$A_s = (2.18 \pm 0.05) \times 10^9, \quad n_s = 0.963 \pm 0.0007, \quad r < 0.26, \quad (12)$$

we find that the  $B-L$  breaking scale is fixed to  $v_{B-L} \approx 8 \times 10^{15}$  GeV by requiring the correct normalization of  $A_s$ , the spectral index  $n_s \approx 0.98$  is rather large and the tensor-to-scalar ratio is easily below the current bound. In particular the large value for  $n_s$  has raised the question whether F-term hybrid inflation is still viable in view of the Planck results. To answer this question, we must go beyond the approximations leading to Eq. (10). First, we will drop the approximation  $\varphi_*^2 \gg \varphi_f^2$ , leading to corrections of the predictions listed in Eq. (10). Second, taking into account soft supersymmetry breaking, the superpotential receives a constant term  $W_0 = m_{\tilde{G}} M_P^2$  proportional to the gravitino mass [39], leading to an additional contribution to the scalar potential, studied e.g. in Refs [40,41],

$$V_{m_{\tilde{G}}} = -2\sqrt{\lambda} v_{B-L}^2 m_{\tilde{G}} |\phi| \cos \theta. \quad (13)$$

This term breaks the degeneracy appearing in Eq. (7), which only depends on the absolute value  $|\phi|$  of the inflaton field but not on its phase  $\theta$ . As a result, the inflationary predictions found in Ref. [40] assuming  $\theta = \pi$  differ from those in Ref. [41], which uses  $\theta = 0$ .<sup>3</sup> In particular, for sufficiently large  $V_{m_{\tilde{G}}}$ , we find a hill-top potential for  $\theta = 0$ , while for  $\theta = \pi$ , one still finds a monotonously decreasing potential along the inflationary trajectory (along the arrows in Fig. 2), cf. Fig. 1.

Indeed, these are only two extreme cases for possible inflationary trajectories in the full two-field inflation model resulting from Eqs. (7) and (13). In the two-field model, the ending point of inflation  $\phi_f$  becomes a ‘critical line’ in the complex  $\phi$  plane, with each point on this line representing a possible

<sup>2</sup>Note that for small values of  $\lambda$ , the two terms in Eq. (9) can be of similar importance, leading to a slight deviation from the results listed in Eq. (10).

<sup>3</sup>Note that Refs. [40,41] use a different sign convention in the superpotential, implying  $\theta \rightarrow \theta + \pi$ .

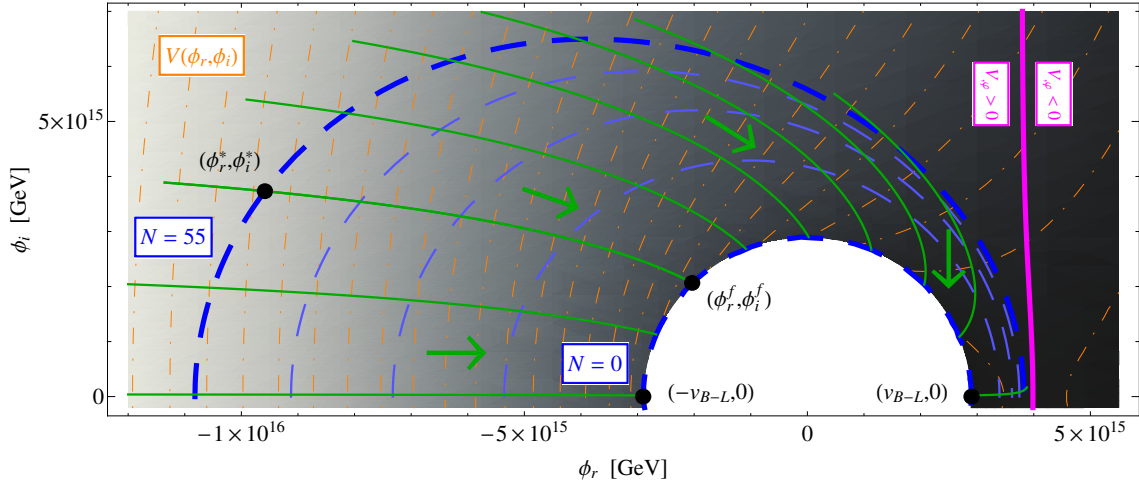


**Fig. 2:** Inflationary trajectories in the full two-field inflation model. Selection of possible trajectories (solid green lines) in the scalar potential  $V(\phi_r, \phi_i)$  depicted by the dot-dashed orange contour lines and the shading. Lines of constant  $N$  are marked by the dashed blue contours, with the beginning and end of inflation ( $N = N_*$  and  $N = 0$ , respectively) marked by thicker contours.

ending point for inflation. Hence as opposed to the single-field case there is an additional degree of freedom, i.e. the choice of the inflationary trajectory labeled by  $\theta_f$ . This is visualized in Fig. 2 which shows a selection of possible inflationary trajectories (in green) in the scalar potential (dot-dashed orange contour lines and shading). Contour lines denoting constant numbers of e-folds  $N$  are shown as dashed blue lines, with the ‘critical line’,  $N = 0$ , and the onset of the last  $N_*$  e-folds,  $N = N_{55}$  emphasized. To demonstrate the dependence of the model predictions on the choice of the trajectory, Fig. 3 shows the predictions for the amplitude  $A_s$  and the spectral index  $n_s$  as functions of the final phase  $\theta_f$  for  $\lambda = 4.5 \times 10^{-6}$ ,  $v_{B-L} = 2.9 \times 10^{15}$  GeV and  $m_{\tilde{G}} = 47.5$  TeV. For this parameter example, we see that  $\theta_f \simeq 16^\circ$  reproduces the correct amplitude, cf. Eq. (12), while simultaneously yielding a value for the spectral index of  $n_s = 0.965$  in very good agreement with the data.

A third possibility of manipulating Eq. (10) is by resorting to a non-minimal Kähler potential [42]. This in particular introduces a term quadratic in  $\phi$  in the scalar potential. Tuning the expansion coefficients of such a Kähler potential, the spectral index can be tuned to lower values, achieving accordance with the Planck data even for  $\theta = \pi$ . However, the quadratic term then comes with a negative sign, implying, together with the positive  $|\phi|^4$  term the existence of a hill-top potential and a local minimum at  $|\phi| \neq 0$  where the inflaton can get trapped. Avoiding this requires some fine-tuning in the initial conditions for  $|\phi|$  [40].

On top of that, there are also further constraints which must be taken into account in a realistic model. First, the superpotential Eq. (1) will lead to the production of cosmic strings at the end of inflation, due to the spontaneous breaking of  $U(1)_{B-L}$ . We will come back to this point in Sec. (3.2). Moreover, the abundance of nonthermally produced gravitinos, controlled by the symmetry-breaking scale, the common mass of the inflaton and  $B-L$  Higgs in the true vacuum, and the reheating temperature [43,44],

$$Y_{3/2} \propto \frac{v_{B-L}^2 m_S^2}{T_{RH}}, \quad (14)$$

must be sufficiently low, so that the sum of nonthermal and thermal (cf. section 4) gravitino abundance does not produce a gravitino problem [24–28, 45–47]. Note, however, that the nonthermal gravitino abundance can be suppressed compared to the estimate in Eq. (14), if the massive particle governing the universe during the reheating phase decays sufficiently fast.

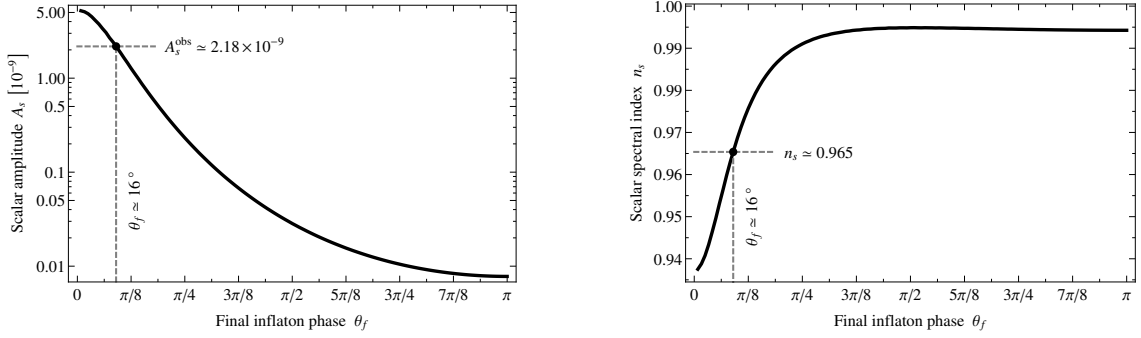


**Fig. 3:** Amplitude and spectral index of the scalar primordial fluctuations for  $\lambda = 4.5 \times 10^{-6}$ ,  $v_{B-L} = 2.9 \times 10^{15}$  GeV and  $m_{\tilde{G}} = 47.5$  TeV. The phase of the endpoint of inflation,  $\theta_f$ , labels different inflationary trajectories.

Taking all of this together, we find that F-term hybrid inflation is indeed still viable in light of the Planck data, however some tuning is required. Accepting a non-minimal Kähler potential with some tuning in its coefficients as well as in the initial conditions for  $|\phi|$ , accordance with the Planck data can be achieved for  $\theta_f \sim \pi$ . Staying with a minimal Kähler potential one has two options to reproduce the experimental data. Either, one tunes the amplitude of the linear term (13) against the CW term (7) in the potential, leading to the situation shown in Fig. 2. In this case small values for  $n_s$  can be achieved for  $\theta_f \sim 0$ , but again tuning of the initial condition for the radial degree  $|\phi|$  is necessary to prevent the inflaton from being trapped on the wrong side of the hill-top potential.<sup>4</sup> The second possibility is to allow the linear term to dominate over the CW term, however then the initial phase of  $\phi$  must be tuned because otherwise one lands on a trajectory where inflation does not end, because it ‘misses’ the minimum generated by the CW term at small  $|\phi|$ , such that  $|\phi|$  always remains larger than the critical value. For a more detailed analysis of the full two-field inflation model, see Ref. [48].

In summary, successful inflation can be achieved but it imposes constraints on the  $B-L$  breaking scale and on the coupling  $\lambda$ . In the context of the Froggatt-Nielsen flavour model used to parametrize the Yukawa couplings in Ref. [10], this then constrains the mass of the heaviest of the right-handed neutrinos  $M_1$ . In the following, we will thus consider the restricted parameter space

$$\begin{aligned} v_{B-L} &= 5 \times 10^{15} \text{ GeV}, \\ 10^9 \text{ GeV} &\leq M_1 \leq 3 \times 10^{12} \text{ GeV}, \\ 10^{-5} \text{ eV} &\leq \tilde{m}_1 \leq 1 \text{ eV}, \end{aligned} \tag{15}$$

where the variation of the effective light neutrino mass parameter  $\tilde{m}_1$  accounts for the uncertainties of the Froggatt-Nielsen model. The values of  $v_{B-L}$  and  $\lambda$  quoted here correspond to the option of choosing  $\theta_f = \pi$  and using a non-minimal Kähler potential, cf. Ref. [40]. For a discussion of cosmological  $B-L$  breaking involving smaller values for  $v_{B-L}$ , cf. Ref. [12].

### 3 Tachyonic Preheating and Cosmic Strings

The end of hybrid inflation induces a negative squared mass term for the  $B-L$  Higgs field  $\sigma'$  in the false vacuum, triggering the  $U(1)_{B-L}$  breaking phase transition. The cosmological realization of this phase transition is accompanied by two important nonperturbative processes, tachyonic preheating [33] and the formation of cosmic strings [49].

<sup>4</sup>Note that nevertheless, an arbitrary amount of e-folds of inflation can be realized in this setup.

### 3.1 Tachyonic preheating

#### The phase transition

Tachyonic preheating is a fast and nonperturbative process triggered by the tachyonic instability in the scalar potential in the direction of the Higgs field. As the inflaton field passes a critical point  $\phi_c$ , the Higgs field  $\sigma'$  acquires a negative effective mass squared  $-m_\sigma^2$ , with  $m_\sigma^2 = \sqrt{2}\lambda v_{B-L}|\dot{\phi}_c|t$  in the linearized equation of motion for  $\sigma'$  close to the instability point  $\phi_c$ . This causes a faster than exponential growth of the quantum fluctuations of the Higgs field  $\sigma'_k$  with wave numbers  $|\vec{k}| < m_\sigma$  [50], while the average value of the Higgs field remains zero. Once the amplitude of these fluctuations,  $v(t) = \frac{1}{\sqrt{2}}\langle\sigma'^2\rangle = \frac{1}{\sqrt{2}}\langle\sigma'^2(t, \mathbf{x})\rangle_{\mathbf{x}}^{1/2}$ ,<sup>5</sup> reaches  $\langle\sigma'^2(t_*)\rangle = \mathcal{O}(v_{B-L}^2)$ , the curvature of the potential for the homogeneous background field  $\sigma'$  becomes positive and the usual oscillating behaviour of the modes is re-established [33] while  $v(t)$  approaches  $v_{B-L}$ . A direct consequence of the early phase of exponential growth are high occupation numbers in the low-momentum Higgs modes and hence a semi-classical situation with a large abundance of non-relativistic  $B-L$  Higgs bosons.

A further result of this nonperturbative process is the formation of ‘bubble’-like inhomogeneities which randomly feature different phases of the complex Higgs field [50, 51]. Their initial size is given by the smallest scale amplified during tachyonic preheating, referred to as  $k_*^{-1}$ . These bubbles expand at the speed of light, thereby colliding with each other. This phase of the preheating process is an important source of gravitational waves (GWs), cf. [53], a point to which we will return in Sec. 5. After this very turbulent phase the true Higgs vev is reached in almost the entire volume, with the regimes of false vacuum reduced to topologically stable cosmic strings, cf. Sec. 3.2, separated by the characteristic length scale  $k_*^{-1} \approx (\sqrt{2}\lambda v_{B-L}|\dot{\phi}_c|)^{-1/3}$ .

#### Secondary Particle production

The mode equations for the particles coupled to the  $B-L$  Higgs field, i.e. for the gauge, Higgs, inflaton and neutrino supermultiplets, feature masses proportional to  $v(t)$ . The growth of  $\langle\sigma'^2\rangle$  during tachyonic preheating thus induces a rapid change of their effective masses. The resulting particle production was studied in Ref. [52], with the results depicted in Fig. 4. Here, for simplicity, an abrupt transition of the inflaton vev to zero is assumed, introducing the parameter  $m = m_\sigma(\phi_c t \rightarrow \phi_c)$ .<sup>6</sup> The left panel shows the evolution of  $\langle\sigma'^2\rangle$  normalized to the symmetry-breaking scale  $v_{B-L}$ , calculated using a lattice simulation (green curve). For comparison, the red curve shows an analytical approximation,  $v(t) = \frac{v_{B-L}}{2} \left(1 + \tanh \frac{m(t-t_*)}{2}\right)$ . The pink and blue curves depict the number densities of bosonic particles coupled to the Higgs, again calculated using a lattice calculation and an analytical approximation, respectively. The right panel examines the momentum distribution of these bosons (and also of fermions coupled to the Higgs) showing the spectrum of occupation numbers. Again both the numerical and analytical results are shown. We see that just like the Higgs bosons themselves, the particles coupled to it are produced with very low momentum, i.e. non-relativistically.

Based on these results, the energy and number densities for bosons and fermions coupled to the Higgs boson after tachyonic preheating have been estimated as [52]<sup>7</sup>

$$\begin{aligned} \rho_B/\rho_0 &\simeq 2 \times 10^{-3} g_\sigma \lambda f(x_1, 1.3), & n_B(x_1) &\simeq 1 \times 10^{-3} g_\sigma m_S^3 f(x_1, 1.3)/x_1, \\ \rho_F/\rho_0 &\simeq 1.5 \times 10^{-3} g_\sigma \lambda f(x_1, 0.8), & n_F(x_1) &\simeq 3.6 \times 10^{-4} g_\sigma m_S^3 f(x_1, 0.8)/x_1, \end{aligned} \quad (16)$$

with  $f(x_1, x_2) = (x_1^2 + x_2^2)^{1/2} - x_2$  and  $x_1 = m_i/m_S$ , where  $m_i$  denotes the mass of the respective particle in the true vacuum and  $g_\sigma$  counts its spin and internal degrees of freedom.

<sup>5</sup>Here, bold letters indicate 3-vectors.

<sup>6</sup>The effect of the inflaton dynamics on this nonperturbative particle production requires further investigation.

<sup>7</sup>Note that particle production can be significantly enhanced by quantum effects [54], which require further investigation.

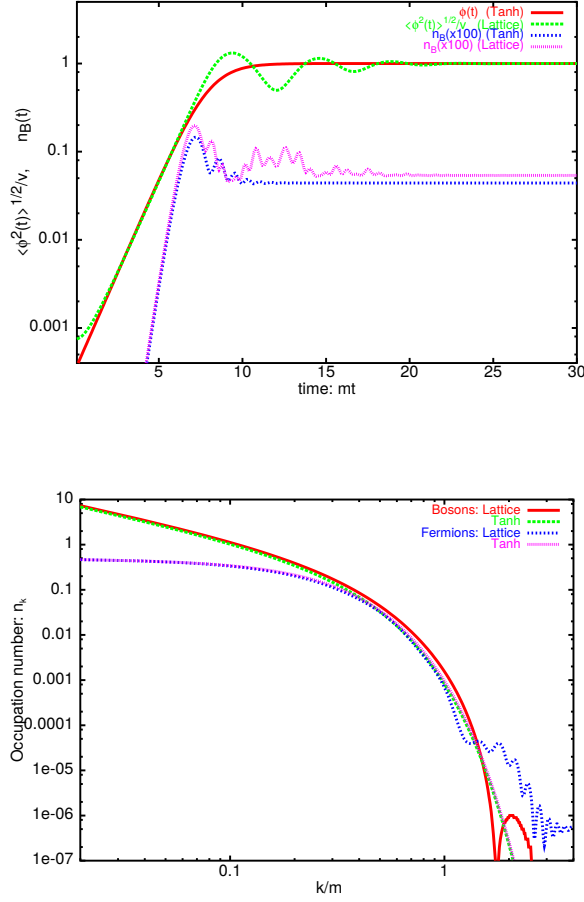


**Fig. 4:** Numerical and analytical results for particle production during tachyonic preheating, taken from Ref. [52]. **Left panel:** Evolution of the quantum fluctuations of the Higgs field  $\phi(t) \equiv \sigma'(t)/\sqrt{2}$ , normalized to the symmetry-breaking scale  $v \equiv v_{B-L}$ , as well as the number density  $n_B$  of bosonic particles coupled to it. **Right panel:** Spectrum of occupation numbers for bosonic and fermionic particles coupled to the Higgs.

### 3.2 Cosmic strings

Due to the non-trivial topology of its vacuum manifold, the Abelian Higgs model underlying the  $B-L$  phase transition gives rise to solitonic field configurations, so-called cosmic strings (for a review, see e.g. [55–57]). These cosmic strings are formed during the process of tachyonic preheating and are topologically stable. The evolution of the resulting network is governed by the intersection of the infinite strings, which leads to the formation of closed loops separated from the infinite string, as well as by the energy loss due to the emission of GWs, Higgs and gauge particles. After a relaxation time the network reaches the scaling regime, i.e. the typical length scale of the cosmic string network remains constant relative to the size of the horizon. This implies that a constant fraction of the total energy density is stored in cosmic strings throughout the further evolution of the universe and that there are  $\mathcal{O}(1)$  cosmic strings per Hubble volume.

In the scaling regime, the cosmic string network is characterized by the energy per unit length  $\mu$ . In the Abelian Higgs model, which is based on a field theory featuring a spontaneously broken local

$U(1)$  symmetry,  $\mu$  is given by [58]

$$\mu = 2\pi B(\beta)v_{B-L}^2, \quad (17)$$

where  $\beta = (m_S/m_G)^2 = \lambda/(8g^2)$  is the ratio of the masses of the symmetry-breaking Higgs boson and the gauge boson in the true vacuum, and  $B(\beta)$  is a slowly varying function parametrizing the deviation from the Bogomol'nyi bound,

$$B(\beta) \simeq \begin{cases} 1.04 \beta^{0.195}, & \text{if } 10^{-2} < \beta \ll 1 \\ 2.4 (\ln \frac{2}{\beta})^{-1}, & \text{if } \beta < 10^{-2} \end{cases}. \quad (18)$$

For the special case of  $\beta = 1$  the Bogomol'nyi bound is saturated and  $B(1) = 1$  [59].

Further important quantities describing the string network are the cosmic string width, given by  $m_G^{-1}$  in the Abelian Higgs model, and the length scale  $\xi$  separating two strings. From Sec. 3.1, we know that the characteristic length separating two strings at the time of their formation is

$$\xi = k_*^{-1} = (\sqrt{2}\lambda v_{B-L} |\dot{\phi}_c|)^{-1/3}. \quad (19)$$

This also determines the relaxation time of the cosmic string network,  $\tau_{\text{string}} \sim \xi$  [50,60]. Note that in the Nambu-Goto model, an alternative to the Abelian Higgs cosmic string model which assumes infinitely thin cosmic strings, the energy scale  $\mu$  is an input parameter.

### **Observational prospects**

So far, no experimental evidence for the existence of cosmic strings has been found. However, current and upcoming experiments are starting to seriously probe the cosmologically interesting regions of the parameter space. First, cosmic strings give rise to anisotropies in the CMB temperature map. They distort the surface of last scattering of the CMB photons, leaving an imprint on the spectrum observable today. Since the CMB photons observable today stem from roughly  $10^5$  Hubble patches during recombination, these observations are mainly sensitive to the effect of long (Hubble-sized) strings at recombination and not to small cosmic string loops. In contrast to the perturbations due to inflation, these anisotropies are not phase correlated across distant Hubble patches and hence the resulting multipole spectrum of the two-point correlation function is suppressed at large scales and moreover does not show the oscillations characteristic to inflation. Moreover, whereas the primordial power spectrum due to inflation is (nearly) scale-invariant, the anisotropies on the last scattering surface due to cosmic strings are governed by a characteristic scale. The resulting spectrum thus features a single broad peak associated with this scale. Due to the re-scattering of a fraction of the CMB photons at reionisation, the CMB spectrum is, to a lesser extent, also sensitive to the long cosmic strings present at reionisation. This leads to a second, smaller peak in the spectrum, in particular visible in the power spectrum of the B-mode polarization, see e.g. [61] for a recent analysis. The fraction of the amplitude of the scalar power spectrum due to a possible cosmic string contribution to the CMB temperature anisotropies is conventionally measured at the multipole  $l = 10$  and is referred to as  $f_{10}$ . The Planck data implies that  $f_{10}$  can at most be a few percent,  $f_{10} < 2.8\%$  [38].

Second, the gravitational field of cosmic strings gives rise to weak and strong lensing effects of (CMB) photons on their way from the surface of last scattering or from an astrophysical source to us. The non-observation of such effects puts a bound on the string tension  $\mu$ . Again, this effect is mainly sensitive to long (Hubble-sized) strings.

Third, the energy emitted by cosmic strings in the scaling regime is at least partly emitted in form of GWs. Due to their extremely weak coupling, these can then propagate freely through the universe and are therefore in principle detectable today. We will come back to the resulting GW background and the discovery potential of current and upcoming GW experiments in detail in Sec. 5.

Finally, the Abelian Higgs cosmic string model entails the emission of massive radiation from cosmic strings, i.e. the emission of the Higgs and gauge particles whose field configurations form the

string. If this mechanism is still active at late times it could yield ultra-high-energetic cosmic rays and GeV-scale  $\gamma$ -rays, which have not been observed. This too, can be translated into a (model-dependent) bound on  $\mu$  [62–66].

Currently the most stringent and model-independent bound on the cosmic string tension comes from CMB observations,  $G\mu < 3.2 \times 10^{-7}$  [38], and we shall mainly employ this in the following.

### Numerical simulations and theoretical uncertainties

A quantitative understanding of the formation of cosmic strings, the dynamics of the cosmic string network and the energy loss mechanism during the scaling regime requires lattice simulations. Performing these is extremely challenging due to the huge range of scales involved in the problem [56]: the width of the string remains constant while the scales of the network are blown up as the universe expands. Or, in comoving coordinates, the comoving width of the string shrinks, until it becomes comparable with the lattice spacing and the simulation loses its validity. There have been different approaches to tackle this problem. Simulations based on solving the field equations for the Abelian Higgs (AH) model set the comoving width to a finite constant before it comes too close to the lattice spacing [60, 67, 68]. Simulations based on the Nambu-Goto (NG) string model assume cosmic strings to be infinitely thin, i.e. strictly one-dimensional objects, throughout the simulation [69–72]. The outcome of simulations based on these two models is dramatically different. The AH simulations show the formation of large, Hubble-sized structures which lose their energy predominantly by emitting massive radiation, i.e. particles of the Higgs and gauge fields forming the string configuration. The NG simulations on the other hand display the formation of small loops, which lose their energy into GWs. The size of these loops is thought to be controlled by gravitational backreaction, but is as yet undetermined [56]. Concerning the network of long strings, both simulations, however, yield a similar result [56]. Which of these two simulation methods is closer to reality is currently an open question.

In the following, we will adopt the following hypothesis: For early times, while the comoving cosmic string width is large compared to the lattice spacing, the AH simulation describes the  $U(1)$  phase transition very well. We will thus use the results from these simulations when discussing the formation and early evolution of cosmic strings. For late times, the AH simulations become questionable and the NG approximations of infinitely thin strings appears reasonable. Hence for late times, in particular when discussing possible GW signatures from cosmic strings, cf. Sec. 5, we shall discuss both the AH as well as the NG results.

## 4 Reheating

Tachyonic preheating nonperturbatively generates a large abundance of non-relativistic  $B-L$  Higgs bosons as well as, to a much lesser extent, non-relativistic abundances of the particles coupled to the Higgs boson, cf. Sec. 3.1. Among these are the particles of the  $B-L$  gauge supermultiplet, which decay quickly due to their comparatively strong gauge interactions. This sets the initial conditions for the following slow, perturbative reheating process, depicted by the solid arrows in the left panel of Fig. 5: The particles from the symmetry-breaking sector decay into particles of the  $N_1$  supermultiplet. These (s)neutrinos, just as the (s)neutrinos produced through gauge particle decays and tachyonic preheating as well as thermally produced (s)neutrinos, decay into MSSM particles, thereby generating the entropy of the thermal bath as well as a lepton asymmetry [73]. Finally, the thermal bath produces a thermal gravitino abundance, which will turn out to be in the right ballpark to yield the observed dark matter abundance.

The main tool to obtain a time-resolved description of this reheating process are Boltzmann equations, which describe the evolution of the phase space densities of the various particles species due to decay and scattering processes in an expanding universe. After briefly introducing the formalism of Boltzmann equations in Sec. 4.1, we will turn to the implications for leptogenesis and dark matter production in Sec. 4.2. The results presented here are based on the analyses of Refs. [10–12].

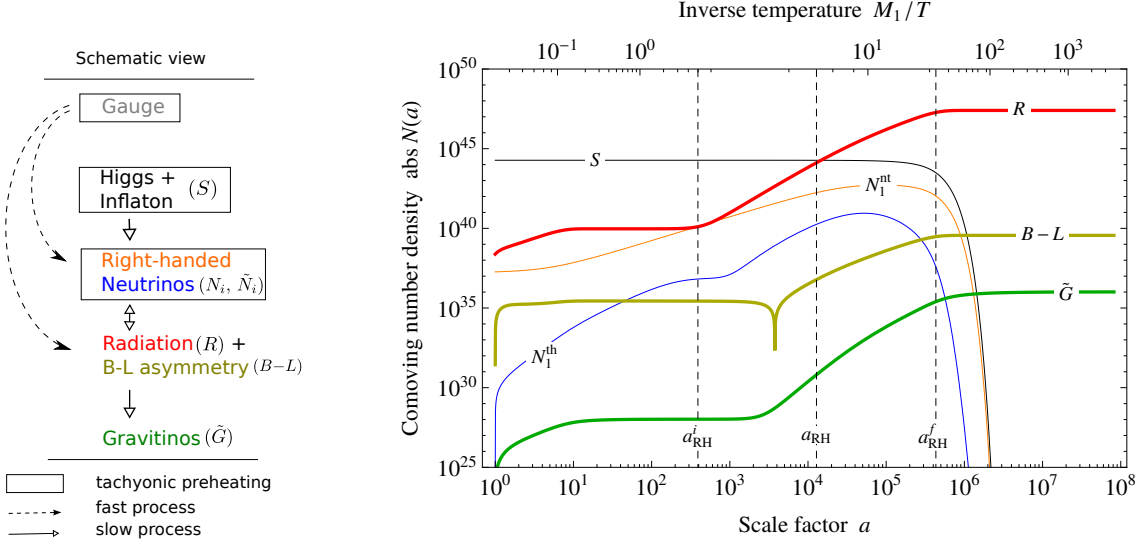


**Fig. 5:** Evolution of the comoving number densities during the reheating process. **Left panel:** schematic overview, distinguishing production via tachyonic preheating, fast decay processes of the  $B-L$  gauge sector and slow processes described by Boltzmann equations. **Right panel:** Comoving number densities of the particles of the  $B-L$  Higgs sector ( $S$ ), the thermal and nonthermal (s)neutrinos ( $N_1^{\text{th}}$ ,  $N_1^{\text{nt}}$ ), the MSSM radiation ( $R$ ), the gravitinos ( $\tilde{G}$ ) and the  $B-L$  asymmetry ( $B-L$ ). Obtained by solving the Boltzmann equations for  $v_{B-L} = 5 \times 10^{15}$  GeV,  $M_1 = 5.4 \times 10^{10}$  GeV,  $\tilde{m}_1 = 4.0 \times 10^{-2}$  eV,  $m_{\tilde{G}} = 100$  GeV and  $m_{\tilde{g}} = 1$  TeV. From Ref. [10].

#### 4.1 Boltzmann equations

The evolution of the phase space density  $f_X(t, p)$  of a particle species  $X$  is determined by a coupled set of Boltzmann equations,

$$E \left( \frac{\partial}{\partial t} - H p \frac{\partial}{\partial p} \right) f_X(t, p) = \sum_{i'j'..} \sum_{ij..} C_X(Xi'j'.. \leftrightarrow ij..), \quad (20)$$

augmented by the Friedmann equation, which governs the evolution of the scale factor. The left-hand side of Eq. (20) describes the evolution of the phase space density in an expanding Friedman-Robertson-Walker (FRW) universe whereas the collision operators  $C_X$  on the right-hand side account for all relevant scattering, decay and inverse decay processes involving the particle  $X$ . The set of Boltzmann equations we have to solve here is determined by the allowed interactions of the underlying particle physics model, cf. solid blue arrows in the left panel of Fig. 5.

From the phase space density  $f_X(t, p)$  one directly obtains the comoving number density  $N_X(t)$ , i.e. the number of  $X$  particles in a volume  $(a/\text{GeV})^3$ , and the energy density  $\rho_X(t)$  by integrating over momentum space,

$$\begin{aligned} N_X(t) &= \left( \frac{a(t)}{\text{GeV}} \right)^3 n_X = \left( \frac{a(t)}{\text{GeV}} \right)^3 g_X \int \frac{d^3p}{(2\pi)^3} f_X(t, p), \\ \rho_X(t) &= g_X \int \frac{d^3p}{(2\pi)^3} E_X(p) f_X(t, p), \end{aligned} \quad (21)$$

with  $a$  denoting the scale factor. A rescaling of  $a$  leaves the physical number density  $n_X$  invariant. For convenience, we will thus set  $a_{\text{PH}} \equiv 1$  at the end of preheating. In the following, decay rates  $\Gamma$ , comoving number densities  $N$  and energy densities  $\rho$  will sometimes appear with upper and lower indices. In this case, the lower index refers to the particle species under consideration, while the upper index refers to its origin, e.g. its parent particle or ‘PH’ for preheating.

## 4.2 Outcome of the reheating process

Solving the Boltzmann equations with the initial conditions given by tachyonic preheating and the successive decay of the  $B-L$  gauge bosons yields a time-resolved picture of the evolution of all particle species. In the right panel of Fig. 5, we show an overview of the resulting comoving number densities for a representative parameter point.

### A two-stage reheating process

After the end of preheating, the lion's share of the energy is stored in non-relativistic  $B-L$  Higgs bosons. Assuming a hierarchical spectrum of heavy Majorana neutrinos, these decay exclusively into heavy, typically relativistic (s)neutrinos of the first generation, thereby forming the main part of the right-handed (s)neutrino population. The decay of these (s)neutrinos then generates a thermal bath of MSSM particles. The process of reheating is hence governed by the interplay of two time-scales, the vacuum decay rate of the non-relativistic Higgs bosons  $\Gamma_S^0$  and the effective decay rate of the neutrinos produced in the Higgs boson decays  $\Gamma_{N_1}^S$ . The latter differs from the zero-temperature decay rate  $\Gamma_{N_1}^0$  due to the time-dilation of the relativistic neutrinos,

$$\Gamma_S^0 = \frac{1}{32\pi} \left( \frac{M_1}{v_{B-L}} \right)^2 m_S \left( 1 - 4 \frac{M_1^2}{m_S^2} \right)^{1/2}, \quad (22)$$

$$\Gamma_{N_1}^S := \Gamma_{N_1}^S(a_{\text{RH}}) = \gamma^{-1}(a_{\text{RH}}) \Gamma_{N_1}^0 \quad \text{with} \quad \gamma^{-1}(a) = \left\langle \frac{M_1}{E_{N_1}} \right\rangle_a^{(S)}, \quad \Gamma_{N_1}^0 = \frac{1}{4\pi} \frac{\tilde{m}_1 M_1^2}{v_{\text{EW}}^2}.$$

In most of the viable parameter space, we find  $\Gamma_S^0 < \Gamma_{N_1}^S$ . In this case,  $\Gamma_S^0$  determines the overall time-scale of the reheating process. On the contrary  $a_{\text{RH}}$ , defined by  $H(a_{\text{RH}}) = \Gamma_{N_1}^S(a_{\text{RH}})$ , marks a characteristic point in the middle of the reheating process, which will be in particular relevant for determining the reheating temperature. Once the Higgs bosons decay into neutrinos, these decay nearly instantaneously into MSSM particles, so that the era of Higgs domination is directly followed by the radiation dominated epoch. On the other hand, if  $\Gamma_S^0 > \Gamma_{N_1}^S$ , the effective neutrino decay rate governs the time-scale of reheating. The energy density is then successively governed by non-relativistic Higgs bosons, relativistic nonthermal neutrinos and finally relativistic thermal MSSM particles.

Solving the Boltzmann equations allows us to determine the temperature of the thermal bath throughout the reheating process. As a consequence, the ‘reheating temperature’ is no longer a cosmological input parameter, but is rather determined by the parameters of the  $B-L$  Higgs and neutrino sector. In Fig. 6 we show the resulting evolution of the temperature. A remarkable feature is the epoch of nearly constant temperature during the main part of the reheating process, which arises because the entropy production from the neutrino decays just compensates the expansion of the universe. A typical value for this plateau is given by  $T_{\text{RH}}^N \equiv T(a_{\text{RH}})$ , with  $a_{\text{RH}}$  as defined above. The dashed vertical lines labeled  $a_{\text{RH}}^i$  and  $a_{\text{RH}}^f$  in Figs. 5 and 6 mark the beginning and the end of the reheating process, defined as the period when the effective production rate of MSSM particles exceeds the Hubble rate.

### Thermal and nonthermal leptogenesis

The decays of the thermally and nonthermally produced neutrinos give rise to a thermal and a nonthermal  $B-L$  asymmetry, as depicted in Fig. 7. The nonthermal lepton asymmetry receives a first contribution from the decay of the heavy (s)neutrinos of the second and third generation. To clearly distinguish this contribution from the main contribution arising due to the decay of the first-generation (s)neutrinos, we have assigned opposite signs to the parameters  $\epsilon_{2,3}$  and  $\epsilon_1$  quantifying the  $CP$  asymmetry in decays of the respective neutrino generations. This entails the change of sign visible at  $a \simeq 4.6 \times 10^3$  in Fig. 7, when the decay of  $N_1^S$  neutrinos becomes efficient and the main part of the nonthermal asymmetry is produced. Wash-out effects are negligibly small throughout this process and hence, once the production of the nonthermal asymmetry becomes inefficient, the asymmetry freezes out.

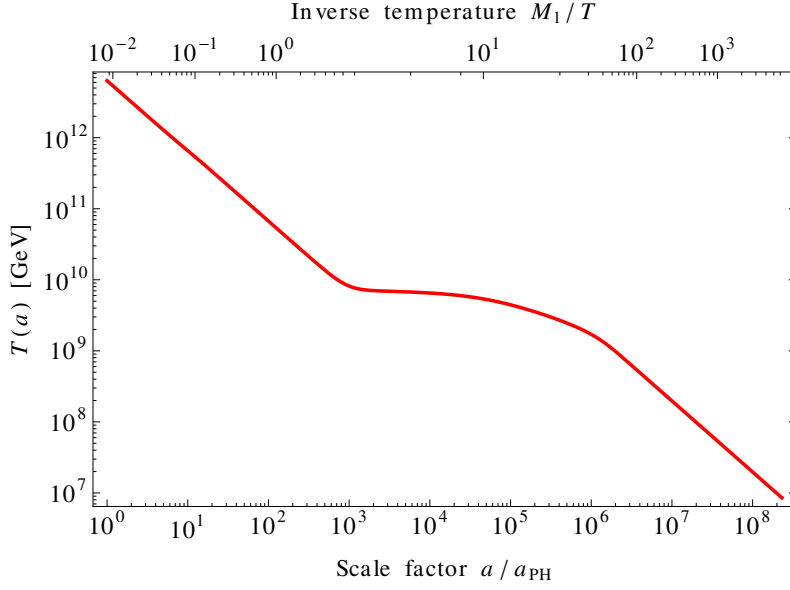


**Fig. 6:** Temperature of the thermal bath for the same parameter values as in Fig. 5. From Ref. [10].

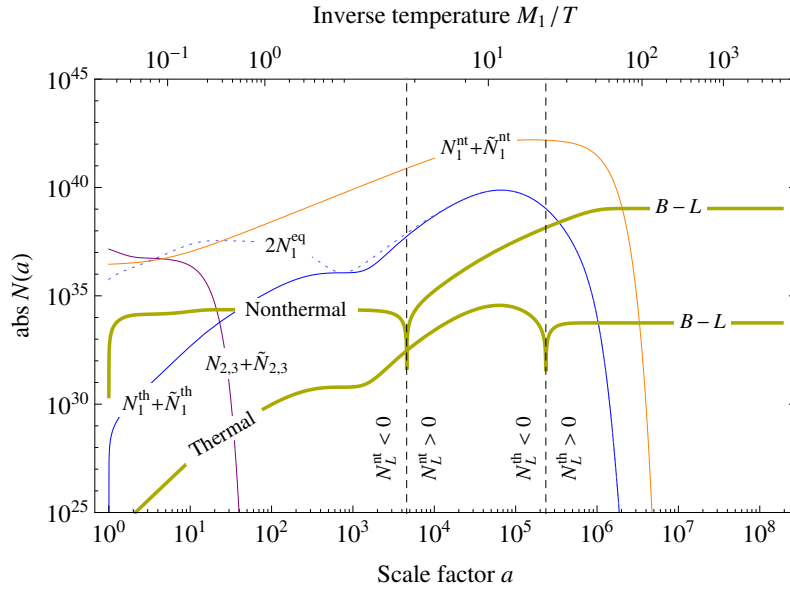


**Fig. 7:** Comoving number densities for the nonthermal ( $N_L^{\text{nt}}$ ) and thermal ( $N_L^{\text{th}}$ ) contributions to the total lepton asymmetry as well as all (s)neutrino species ( $N_1^{\text{nt}} + \tilde{N}_1^{\text{nt}}$ ,  $N_1^{\text{th}} + \tilde{N}_1^{\text{th}}$ ,  $2N_1^{\text{eq}}$  for comparison and  $N_{2,3} + \tilde{N}_{2,3}$ ) as functions of the scale factor  $a$ . The vertical lines mark the changes in the signs of the two components of the lepton asymmetry. From Ref. [10].

The production of the thermal asymmetry is driven by the deviation of the thermal (s)neutrino abundance from the equilibrium value. This leads to an initially negative asymmetry with a rapidly increasing absolute value. This increase slows down as the thermal (s)neutrino abundance approaches the equilibrium value. At around  $a \simeq 6.3 \times 10^4$  wash-out processes start to play a role, leading to a decrease of the asymmetry. The situation rapidly changes when the thermal (s)neutrino abundance overshoots the equilibrium abundance towards the end of the reheating process. This generates an asymmetry with an opposite sign, which overcompensates the asymmetry generated so far. Shortly after, both the wash-out rate and production rate drop significantly below the Hubble rate and the asymmetry freezes out.

The final values of thermal and nonthermal asymmetry as depicted in Fig. 7 allow us to infer the present baryon asymmetry  $\eta_B$  as well as its composition in terms of a nonthermal ( $\eta_B^{\text{nt}}$ ) and a thermal ( $\eta_B^{\text{th}}$ ) contribution,

$$\eta_B = \frac{n_B^0}{n_\gamma^0} = \eta_B^{\text{nt}} + \eta_B^{\text{th}}, \quad \eta_B^{\text{nt,th}} = C_{\text{sph}} \frac{g_{*,s}^{\text{RH}}}{g_{*,s}^0} \frac{N_L^{\text{nt,th}}}{N_\gamma} \Big|_{a_f}. \quad (23)$$

Here,  $C_{\text{sph}} = 8/23$  denotes the sphaleron conversion factor,  $g_{*,s}^{\text{RH}} = 915/4$  and  $g_{*,s}^0 = 43/11$  are the effective numbers of relativistic degrees of freedom in the MSSM that enter the entropy density  $s$  of the thermal bath in the high- and low-temperature regime, respectively,  $N_L^{\text{nt,th}}$  refers to the comoving number density for the nonthermal and thermal contribution to the lepton asymmetry and  $N_\gamma = g_\gamma/g_{*,n} N_r$  is the comoving number density of photons. For our parameter example we find

$$\eta_B \simeq 3.7 \times 10^{-9}, \quad \eta_B^{\text{nt}} \simeq 3.7 \times 10^{-9}, \quad \eta_B^{\text{th}} \simeq 1.9 \times 10^{-14}. \quad (24)$$

Note that to obtain these values, we have set the  $CP$ -violation parameter in the first generation neutrino decays  $\epsilon_1$  to the maximally allowed value, see Ref. [10]. Hence  $\eta_B$  in Eq. (24) yields an upper bound on the baryon asymmetry produced in this setup and is thus perfectly compatible with the observed value,  $\eta_B^{\text{obs}} \simeq 6.2 \times 10^{-10}$  [74]. In fact, the Froggatt-Nielsen model typically predicts a value for  $\epsilon_1$  that is smaller than the maximal possible value by roughly a factor of  $\mathcal{O}(10)$ , cf. Ref. [75], implying excellent agreement between prediction and observation for this parameter example,  $\eta_B \simeq \eta_B^{\text{obs}}$ .

### Gravitino or neutralino dark matter

The thermal bath produced in the decays of the heavy neutrinos gives rise to a thermal gravitino abundance, which can, depending on the underlying low-energy supersymmetry mass spectrum, be either directly or via its decay products linked to today's dark matter abundance. In the former case, we assume the gravitino to be the lightest supersymmetric particle (LSP), as arises for instance in gaugino-mediated supersymmetry breaking. In this case, we can deduce today's gravitino dark matter abundance  $\Omega_{\tilde{G}} h^2$  from the final value of the comoving gravitino abundance  $N_{\tilde{G}}$ :

$$\Omega_{\tilde{G}} h^2 = \frac{\rho_{\tilde{G}}^0}{\rho_c/h^2} = \frac{m_{\tilde{G}} n_\gamma^0 g_{*,s}^0}{\rho_c/h^2 g_{*,s}^{\text{RH}}} \frac{N_{\tilde{G}}}{N_\gamma} \Big|_{a_f}, \quad (25)$$

where  $\rho_c = 3H^2/(8\pi G) = 1.05 \times 10^{-5} h^2 \text{ GeV cm}^{-3}$  denotes the critical energy density of the universe,  $h$  the Hubble rate in the units  $H = h \times 100 \text{ km s}^{-1} \text{ Mpc}^{-1}$  and  $n_\gamma^0 = 410 \text{ cm}^{-3}$  the present number density of the CMB photons. Due to the high temperatures reached in this setup, we do not expect a significant contribution from nonthermal gravitino production. For the parameter example shown in Fig. 5 we find  $\Omega_{\tilde{G}} h^2 \simeq 0.11$ , matching the observed amount of dark matter  $\Omega_{\text{DM}}^{\text{obs}} h^2 \simeq 0.11$  [74]<sup>8</sup>. Note that in the choice of this parameter example  $M_1 = 5.4 \times 10^{11} \text{ GeV}$  was adjusted to obtain this result. Performing a parameter scan over  $\tilde{m}_1$  and  $m_{\tilde{G}}$ , thereby adjusting  $M_1$  to achieve the correct gravitino

<sup>8</sup>The recently published Planck data yields a slightly larger value,  $\Omega_{\text{DM}}^{\text{obs}} h^2 = 0.12$  [76]. The effect of this change on the work presented here is marginal, and in the following we will stay with the value quoted above.

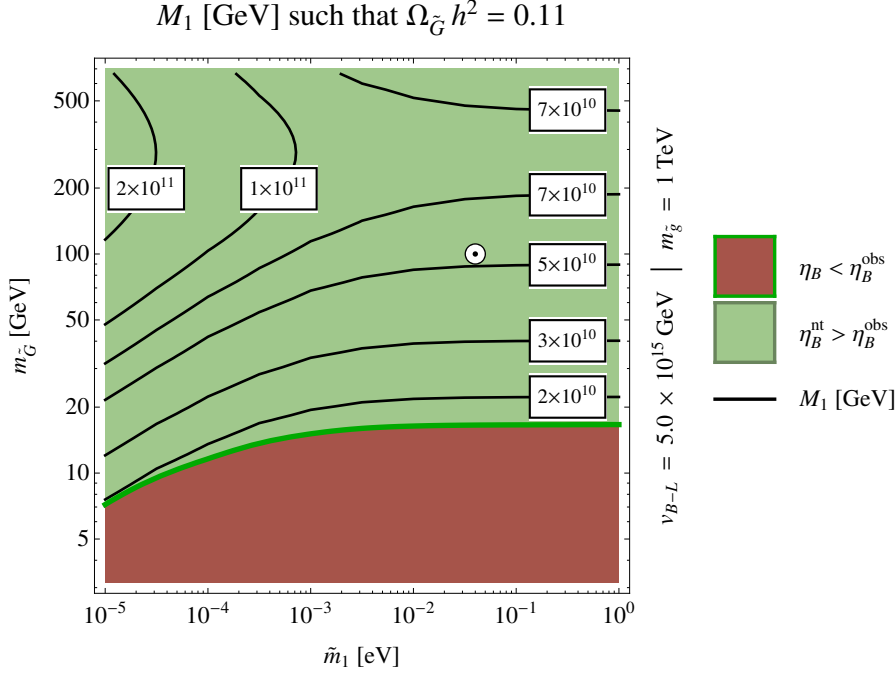


**Fig. 8:** Contour plots of the heavy neutrino mass  $M_1$  as a function of the effective neutrino mass  $\tilde{m}_1$  and the gravitino mass  $m_{\tilde{G}}$  such that the relic density of dark matter is accounted for by gravitinos. In the red region the lepton asymmetry generated by leptogenesis is smaller than the observed one, providing a lower bound on the gravitino mass dependent on  $\tilde{m}_1$ . The small white circle marks the position of the parameter point discussed in Figs. 5 - 7. From Ref. [10].

dark matter abundance, yields the viable parameter space as depicted in Fig. 8. The red shaded region is excluded due to an insufficient production of baryon asymmetry, whereas in the green shaded region we produce a sufficient amount of baryon asymmetry (mainly nonthermally) as well as the correct dark matter abundance. In this region, the reheating temperature ranges from  $\mathcal{O}(10^8)$  to  $\mathcal{O}(10^{10})$  GeV.

As can be seen from Fig. 8, requiring successful leptogenesis as well as the correct dark matter abundance thus yields a lower bound on the gravitino mass  $m_{\tilde{G}}$  in terms of the effective neutrino mass parameter  $\tilde{m}_1$ ,

$$m_{\tilde{G}} \geq 16 \text{ GeV} \left( \frac{m_{\tilde{g}}}{1 \text{ TeV}} \right)^2 \left( \frac{\tilde{m}_1}{10^{-3} \text{ eV}} \right)^{0.25-c}, \quad c = \begin{cases} -0.01 & \text{for } \tilde{m}_1 \lesssim 10^{-3} \text{ eV} \\ 0.21 & \text{for } \tilde{m}_1 \gtrsim 10^{-3} \text{ eV} \end{cases}. \quad (26)$$

with the value of the exponent  $c$  determined by numerically solving the Boltzmann equations. Eq. (26) links a parameter of the neutrino mass sector related to  $B-L$  breaking to a parameter involved in low-energy supersymmetry breaking. Physically, this bound can be understood as follows. For gravitino masses below  $\mathcal{O}(10)$  GeV, a reheating temperature  $T_{\text{RH}}^N \lesssim \mathcal{O}(10^8 - 10^9)$  GeV is required to avoid overproduction of gravitinos. According to our reheating mechanism such low reheating temperatures are associated with relatively small values of the neutrino mass,  $M_1 \lesssim \mathcal{O}(10^{10})$  GeV. The low temperature and low mass then entail a small abundance of (s)neutrinos at the time the asymmetry is generated and a small  $CP$  parameter  $\epsilon_1$ . Both effects combine and result in an insufficient lepton asymmetry, rendering dark matter made of gravitinos with a mass below  $\mathcal{O}(10)$  GeV inconsistent with leptogenesis.

Alternatively, as discussed in Ref. [32], we can assume a hierarchical supersymmetric mass spectrum with the gravitino as the heaviest particle and a neutralino with mass  $m_\chi$  as the LSP,

$$m_\chi \ll m_{\text{squark, slepton}} \ll m_{\tilde{G}}, \quad (27)$$

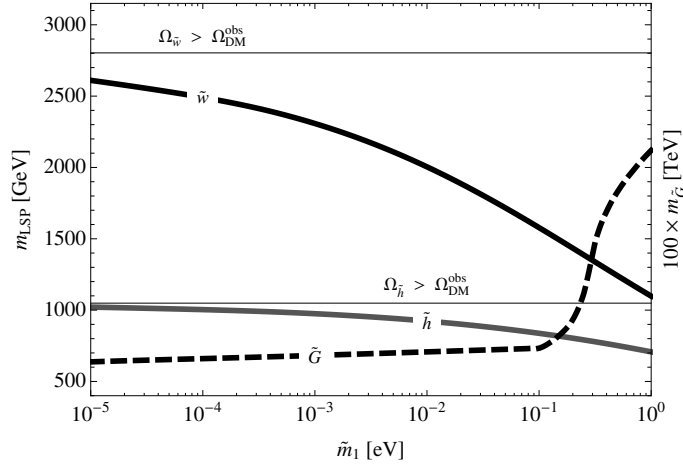


**Fig. 9:** Upper bounds on wino ( $\tilde{w}$ ) and higgsino ( $\tilde{h}$ ) LSP masses imposed by successful leptogenesis as well as absolute lower bound on the gravitino mass according to BBN as functions of the effective neutrino mass  $\tilde{m}_1$ . Wino masses larger than 2.8 TeV and higgsino masses larger than 1.0 TeV result in thermal overproduction of DM. From Ref. [32].

as is found, for instance, in Refs. [77–79]. Due to this hierarchy the LSP is typically a ‘pure’ gaugino or higgsino [80]. Generically, the thermal abundance of a bino LSP is too large. We therefore focus on the possibility of a wino or higgsino LSP<sup>9</sup>. There are then two relevant production channels for neutralino dark matter: thermal production, accompanied by the standard thermal freeze-out mechanism for weakly interacting massive particles (WIMPs), and nonthermal production, as a decay product of the gravitinos produced during the reheating process. In the parameter regime of interest, the resulting thermal and nonthermal abundances can be estimated as  $\Omega_\chi^{\text{th}}$  [83–85] and  $\Omega_\chi^{\tilde{G}}$ , respectively:

$$\begin{aligned} \Omega_\chi^{\text{th}} h^2 &= c_\chi \left( \frac{m_\chi}{1 \text{ TeV}} \right)^2, & c_{\tilde{w}} &= 0.014, & c_{\tilde{h}} &= 0.10 \\ \Omega_\chi^{\tilde{G}} h^2 &= \left( \frac{m_\chi}{m_{\tilde{G}}} \right) \Omega_{\tilde{G}} h^2 \simeq 2.7 \times 10^{-2} \left( \frac{m_\chi}{100 \text{ GeV}} \right) \left( \frac{T_{\text{RH}}^N(M_1, \tilde{m}_1)}{10^{10} \text{ GeV}} \right). \end{aligned} \quad (28)$$

Here  $c_{\tilde{w}}$  and  $c_{\tilde{h}}$  apply to the wino and higgsino case, respectively, and  $\Omega_{\tilde{G}}$  refers to the ‘would-be’ gravitino abundance today if the gravitinos were stable. Requiring the total neutralino LSP abundance to match the observed dark matter abundance constrains the reheating temperature, depending on the value of the neutralino LSP mass  $m_\chi$ . Additionally taking into account the bounds from successful leptogenesis and big bang nucleosynthesis (BBN) on the reheating temperature, we find upper bounds on the neutralino LSP mass and an absolute lower bound on the gravitino mass (for all neutralino LSP masses) depending on the value of  $\tilde{m}_1$ , as depicted in Fig. 9. As in the gravitino LSP case, we thus find relations between the neutrino and superparticle mass spectrum, induced by the key role of the reheating temperature in the efficiency of both leptogenesis and thermal gravitino production.

## 5 Gravitational Waves

So far, we have discussed the birth of the hot early universe in the MSM as well as indirect probes of this mechanism in terms of the resulting neutrino and dark matter properties. We now turn to the possibility of directly probing such early universe physics by measuring the gravitational wave (GW) background

<sup>9</sup>Recently it has been shown that wino DM is strongly constrained by indirect searches using the H.E.S.S. and Fermi gamma-ray telescopes [81, 82].

[86]. GWs are generated by nonspherical, inhomogeneous strong gravitational field dynamics, decouple immediately from their source and to very good approximation propagate freely ever since. Hence, GWs can carry information on the very early universe.

### 5.1 Cosmic gravitational wave background

Gravitational waves are tensor perturbations of the homogeneous background metric. In a flat FRW background, these perturbations can be parametrized as [87]

$$ds^2 = a^2(\tau) (\eta_{\mu\nu} + h_{\mu\nu}) dx^\mu dx^\nu. \quad (29)$$

Here  $\eta_{\mu\nu} = \text{diag}(-1, 1, 1, 1)$  and  $h_{\mu\nu}$  denotes the tensor perturbation.  $x^\mu$  are conformal coordinates with  $x^i, i = 1..3$ , denoting the comoving spatial coordinates and  $\tau = x^0$  the conformal time. These are related to the physical coordinates and the cosmic time as  $\mathbf{x}_{\text{phys}} = a(\tau) \mathbf{x}$  and  $dt = a(\tau) d\tau$ , respectively.

The tensor perturbation evolves dynamically according to the Einstein equation. In the vacuum,  $h_{\mu\nu}$  contains two physical degrees of freedom. A convenient gauge choice is the transverse traceless (TT) gauge, i.e.  $h^{0\mu} = 0, h^i_i = 0$  and  $\partial^j h_{ij} = 0$ . In the weak field approximation, the linearized Einstein equation in momentum space yields the following mode equation for the tensor perturbation around the FRW background in the TT gauge,

$$\tilde{h}''_{ij}(\mathbf{k}, \tau) + \left( k^2 - \frac{a''}{a} \right) \tilde{h}_{ij}(\mathbf{k}, \tau) = 16\pi G a \Pi_{ij}(\mathbf{k}, \tau), \quad (30)$$

describing the generation and propagation of GWs. Here  $\tilde{h}_{ij} = ah_{ij}$ ,  $\Pi_{ij}$  denotes the Fourier transform of the TT part of the anisotropic stress-energy tensor  $T_{\mu\nu}$  of the source,  $k = |\mathbf{k}|$ ,  $\mathbf{k}$  is the comoving wave number, related to the physical wave number through  $\mathbf{k}_{\text{phys}} = \mathbf{k}/a$ , and the prime denotes the derivative with respect to conformal time.

A useful plane wave expansion for freely propagating GWs is given by

$$h_{ij}(\mathbf{x}, \tau) = \sum_{P=+, \times} \int_{-\infty}^{+\infty} \frac{dk}{2\pi} \int d^2\hat{\mathbf{k}} h_P(\mathbf{k}) T_k(\tau) e_{ij}^P(\hat{\mathbf{k}}) e^{-ik(\tau - \hat{\mathbf{k}}\mathbf{x})}, \quad (31)$$

where  $\hat{\mathbf{k}} = \mathbf{k}/k$ ,  $P = +, \times$  labels the two possible polarization states of a GW in the TT gauge and  $e_{ij}^{+, \times}$  are the two corresponding polarization tensors satisfying the normalization condition  $e_{ij}^P e^{ijQ} = 2\delta^{PQ}$ .  $h_P(\mathbf{k})$  denote the coefficients of the expansion after factorizing out the red-shift due to the expansion of the universe, with the latter captured in the so-called transfer function  $T_k(\tau)$ .

An analytical expression for  $T_k$  can be obtained by studying the source-free version of Eq. (30). The resulting mode equation can be easily solved, revealing that the amplitude  $h_{ij}(k)$  of a given mode remains constant in the super-horizon regime,  $k \ll aH$ , while it decreases as  $1/a$  inside the horizon, i.e. for  $k \gg aH$ . Identifying the transfer function  $T_k$  as  $T_k(\tau_*, \tau) = h_{ij}^E(\mathbf{k}, \tau)/h_{ij}^E(\mathbf{k}, \tau_*)$ , with  $h_{ij}^E(\mathbf{k}, \tau)$  denoting the envelope of the oscillating function  $h_{ij}(\mathbf{k}, \tau)$ , we can employ the approximation<sup>10</sup> (see e.g. [88])

$$T_k(\tau_*, \tau_0) \approx \frac{a(\tau_*)}{a(\tau_0)} \quad \text{with } \tau_* = \begin{cases} \tau_i & \text{for sub-horizon sources} \\ \tau_k & \text{for super-horizon sources} \end{cases}. \quad (32)$$

Here,  $\tau_i$  marks the time when the GW was generated and  $\tau_k$  denotes the time when a given mode with wave number  $k$  entered the horizon,  $k = a(\tau_k) H(\tau_k)$ . In Eq. (32), we assume for super-horizon sources

<sup>10</sup>In Sec. 4, we set  $a_{\text{PH}} = 1$ . Another convention used frequently is  $a_0 = 1$ , with  $a_0$  referring to the value of the scale factor today. In this section, we explicitly keep  $a_0$  without specifying a convention. In the end, the dependence on  $a_0$  must drop out of the observables independent of the choice of convention.

that the amplitude is constant until  $\tau = \tau_k$  and then drops as  $1/a$  immediately afterwards. The actual solution to the mode equation yields corrections to both of these assumptions. However, as a numerical check reveals, these two effects roughly compensate each other so that Eq. (32) reproduces the full result very well. For super-horizon sources we will use the more compact notation  $T_k(\tau) = T_k(\tau_k, \tau)$  in the following.

The GW background is a superposition of GWs propagating with all frequencies in all directions. An important observable characterizing the GW background is the ensemble average of the energy density [87], which is expected to be isotropic,

$$\rho_{\text{GW}}(\tau) = \frac{1}{32\pi G} \left\langle \dot{h}_{ij}(\mathbf{x}, \tau) \dot{h}^{ij}(\mathbf{x}, \tau) \right\rangle = \int_{-\infty}^{\infty} d \ln k \frac{\partial \rho_{\text{GW}}(k, \tau)}{\partial \ln k}, \quad (33)$$

with the angular brackets denoting the ensemble average and the dot referring to the derivative with respect to cosmic time. Alternatively, one uses the ratio of the differential energy density to the critical density,

$$\Omega_{\text{GW}}(k, \tau) = \frac{1}{\rho_c} \frac{\partial \rho_{\text{GW}}(k, \tau)}{\partial \ln k}. \quad (34)$$

In the model considered in this paper, the energy density has a part of quantum origin and a part of classical origin,  $\rho_{\text{GW}}(\tau) = \rho_{\text{GW}}^{\text{qu}}(\tau) + \rho_{\text{GW}}^{\text{cl}}(\tau)$ . The former part is due to inflation and is therefore stochastic, whereas the latter part is determined by the contributions to the stress energy tensor from cosmic strings and from tachyonic preheating,  $\rho_{\text{GW}}^{\text{cl}}(\tau) = \rho_{\text{GW}}^{\text{CS}} + \rho_{\text{GW}}^{\text{PH}}(\tau)$ .

For a stochastic GW background the Fourier modes  $h_A(\mathbf{k})$  are random variables and their ensemble average of their two-point function is determined by a time-independent spectral density  $S_h(k)$  [87],

$$\langle h_P(\mathbf{k}) h_Q^*(\mathbf{k}') \rangle = 2\pi \delta(k - k') \frac{1}{4\pi} \delta^{(2)}(\hat{\mathbf{k}} - \hat{\mathbf{k}}') \delta_{PQ} \frac{1}{2} S_h(k). \quad (35)$$

This relation reflects the fact that different modes are uncorrelated and that the background is isotropic. Exploiting Eqs. (31)–(35), we can express the differential energy density due to a stochastic source in terms of the spectral density as

$$\frac{\partial \rho_{\text{GW}}(k, \tau)}{\partial \ln k} = \frac{a^2(\tau_*)}{16\pi^2 G a^4(\tau)} k^3 S_h(k). \quad (36)$$

The classical contribution to the GW energy density is obtained by integrating Eq. (30) from the initial time  $\tau_i$  of GW production until today,

$$h_{ij}(\mathbf{k}, \tau) = 16\pi G \frac{1}{a(\tau)} \int_{\tau_i}^{\tau} d\tau' a(\tau') \mathcal{G}(k, \tau, \tau') \Pi_{ij}(\mathbf{k}, \tau'), \quad (37)$$

where  $\mathcal{G}(k, \tau, \tau')$  is the retarded Green's function of the differential operator on the left-hand side of Eq. (30). For sub-horizon modes, i.e.  $k\tau \gg 1$ , one has  $\mathcal{G}(k, \tau, \tau') = \sin(k(\tau - \tau'))/k$ . With this, one can evaluate the ensemble average  $\langle \dot{h}^2 \rangle$  in terms of  $\langle \Pi^2 \rangle$  by calculating the derivative of Eq. (37) on sub-horizon scales. Assuming translation invariance and isotropy of the source,

$$\langle \Pi_{ij}(\mathbf{k}, \tau) \Pi^{ij}(\mathbf{k}', \tau') \rangle = (2\pi)^3 \Pi^2(k, \tau, \tau') \delta(\mathbf{k} + \mathbf{k}'), \quad (38)$$

the resulting differential energy density simplifies to

$$\frac{\partial \rho_{\text{GW}}(k, \tau)}{\partial \ln k} = \frac{2G}{\pi} \frac{k^3}{a^4(\tau)} \int_{\tau_i}^{\tau} d\tau_1 \int_{\tau_i}^{\tau} d\tau_2 a(\tau_1) a(\tau_2) \cos(k(\tau_1 - \tau_2)) \Pi^2(k, \tau_1, \tau_2), \quad (39)$$

Here, in order to perform the ensemble average, we have also averaged the integrand over a period  $\Delta\tau = 2\pi/k$ , assuming ergodicity.

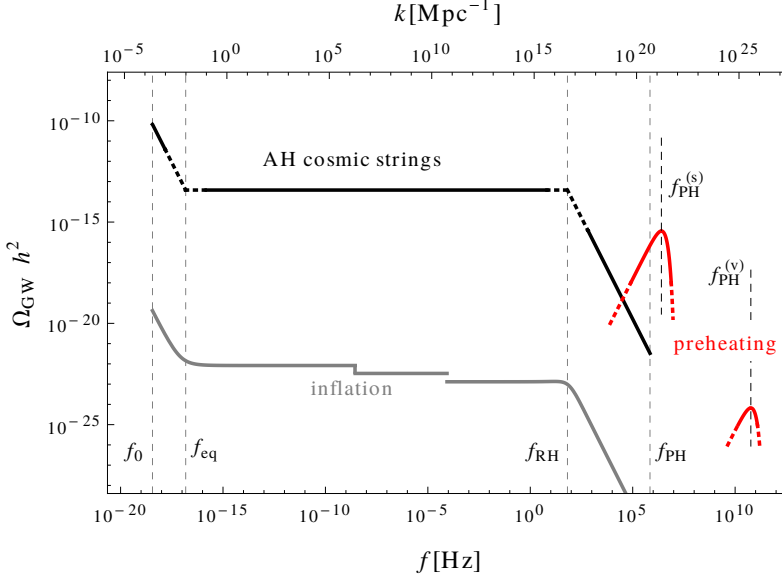


**Fig. 10:** Predicted GW spectrum due to inflation (grey), preheating (red) and Abelian Higgs cosmic strings (black) for  $M_1 = 5.4 \times 10^{10}$  GeV,  $v_{B-L} = 5 \times 10^{15}$  GeV and  $m_S = 3 \times 10^{13}$  GeV, as in Fig. 5.  $f_0$ ,  $f_{\text{eq}}$ ,  $f_{\text{RH}}$  and  $f_{\text{PH}}$  denote the frequencies associated with a horizon-sized wave today, at matter-radiation equality, at reheating and at preheating, respectively.  $f_{\text{PH}}^{(s)}$  and  $f_{\text{PH}}^{(v)}$  denote the positions of the peaks in the GW spectrum associated with the scalar and the vector boson present at preheating. The dashed segments indicate the uncertainties due to the breakdown of the analytical approximations. From Ref. [34].

## 5.2 Gravitational waves from a $B-L$ phase transition

We will now in turn discuss the resulting GW background from inflation, from tachyonic preheating and from cosmic strings in the scaling regime, based on the analysis of Ref. [34]. An overview of the resulting contributions is depicted in Fig. 10.

### Gravitational waves from inflation

During inflation quantum fluctuations of the metric are generated and stretched to ever larger physical scales so that they eventually cross the Hubble horizon and become classical. Outside the horizon, the amplitudes of these metric perturbations remain preserved and they only begin to evolve again once they re-enter the Hubble horizon after the end of inflation. Inflation hence gives rise to a stochastic background of gravitational waves [88–90] with a spectrum which is determined by the properties of the primordial quantum metric fluctuations as well as by the expansion history of the universe, which governs the red-shift of the GWs since horizon re-entry,

$$\Omega_{\text{GW}}(k, \tau) = \frac{A_t}{12} \frac{k^2}{a_0^2 H_0^2} T_k^2(\tau). \quad (40)$$

Here  $A_t$ , controlled by the Hubble parameter during inflation, denotes the amplitude of the primordial tensor perturbations. Evaluating the evolution of the scale factor throughout the cosmic history, i.e. through the epochs of reheating, radiation, matter and vacuum domination, yields the transfer function  $T_k$  and thus

$$\Omega_{\text{GW}}(k) = \frac{A_t^2}{12} \Omega_r \frac{g_*^k}{g_*^0} \left( \frac{g_{*,s}^0}{g_{*,s}^k} \right)^{4/3} \times \begin{cases} \frac{1}{2} (k_{\text{eq}}/k)^2, & k_0 \ll k \ll k_{\text{eq}} \\ 1, & k_{\text{eq}} \ll k \ll k_{\text{RH}} \\ 2 R C_{\text{RH}}^6 (k_{\text{RH}}/k)^2, & k_{\text{RH}} \ll k \ll k_{\text{PH}} \end{cases}, \quad (41)$$

with  $\Omega_r$  denoting the fraction of energy stored in radiation today. The parameters  $C_{\text{RH}}$  and  $R$  account for the deviation from pure matter domination during reheating and the production of relativistic degrees of freedom after  $a_{\text{RH}}$ , respectively, and are numerically found to be typically  $\mathcal{O}(1)$ .<sup>11</sup> As long as a mode with wave number  $k$  re-enters the Hubble horizon during radiation domination,  $g_*^k$  and  $g_{*,s}^k$  denote the usual values of the effective number of degrees of freedom  $g_*(\tau)$  and  $g_{*,s}(\tau)$  at time  $\tau_k$ . On the other hand, during reheating and matter domination  $g_*^k$  and  $g_{*,s}^k$  correspond to  $g_*^{\text{RH}}$  and  $g_{*,s}^{\text{RH}}$  as well as to  $g_*^{\text{eq}}$  and  $g_{*,s}^{\text{eq}}$ , respectively. The wave numbers  $k_{\text{eq}}$ ,  $k_{\text{RH}}$  and  $k_{\text{PH}}$  refer to the modes which crossed the horizon at matter-radiation equality, the end of reheating and at preheating, respectively.  $k_0$  is correspondingly given by the size of the Hubble horizon today. Translated into frequencies  $f = k/(2\pi a_0)$  at which GW experiments could observe the corresponding modes, they are given by

$$f_0 = 3.58 \times 10^{-19} \text{ Hz} \left( \frac{h}{0.70} \right), \quad f_{\text{eq}} = 1.57 \times 10^{-17} \text{ Hz} \left( \frac{\Omega_m h^2}{0.14} \right), \quad (42)$$

$$f_{\text{RH}} = 4.25 \times 10^{-1} \text{ Hz} \left( \frac{T_*}{10^7 \text{ GeV}} \right), \quad f_{\text{PH}} = 1.93 \times 10^4 \text{ Hz} \left( \frac{\lambda}{10^{-4}} \right)^{1/6} \left( \frac{10^{-15} v_{B-L}}{5 \text{ GeV}} \right)^{2/3} \left( \frac{T_*}{10^7 \text{ GeV}} \right)^{1/3}, \quad (43)$$

with  $\Omega_m$  denoting the present value of the fraction of energy stored in matter and  $T_*$  closely related to the reheating temperature, see footnote 12. Evidently, the energy spectrum  $\Omega_{\text{GW}}$  decreases like  $k^{-2}$  at its edges and features a plateau in its center, cf. grey curve in Fig. 10. In the context of cosmological  $B-L$  breaking, the height of the plateau is controlled by the coupling  $\lambda$ , which determines the self-interaction of the  $B-L$  breaking Higgs field, as well as by the  $B-L$  breaking scale,

$$\Omega_{\text{GW}}^{\text{pl}} h^2 = 3.28 \times 10^{-22} \left( \frac{\lambda}{10^{-4}} \right) \left( \frac{v_{B-L}}{5 \times 10^{15} \text{ GeV}} \right)^4 \left( \frac{\Omega_r}{8.5 \times 10^{-5}} \right) \bar{g}^k, \quad (44)$$

where  $\bar{g}^k = (4g_*^k/427)(427/(4g_{*,s}^k))^{4/3}$  is a ratio of energy and entropy degrees of freedom. The small steps visible in the plateau of the grey curve in Fig. 10 represent the change of the number of relativistic degrees of freedom due to the QCD phase transition and the crossing of a typical mass-scale for supersymmetric particles. A remarkable feature of the GW spectrum from inflation is that the position of the kink, which separates the plateau arising for modes which entered during radiation domination and the  $k^{-2}$  behaviour from the reheating regime, is directly related to the reheating temperature, providing a possibility to probe this otherwise experimentally hardly accessible quantity.<sup>12</sup>

### Gravitational waves from preheating

The process of tachyonic preheating forms a classical, sub-horizon source for GWs which is active only for a short time. The resulting GW spectrum can be obtained by calculating the solution to the mode equation, Eq. (37), and inserting it into Eq. (33). The anisotropic stress tensor  $\Pi_{ij}$  entering Eq. (37) is determined by the dynamics of preheating and vanishes after the end of preheating, allowing the GWs to propagate freely for  $\tau \gg \tau_{\text{PH}}$ . The remaining challenge is thus to calculate  $\Pi_{ij}$  during preheating. This task can be performed numerically, see e.g. Ref. [91] for a detailed description of the method and an application to preheating after chaotic inflation, as well as Ref. [92] for an application to tachyonic preheating after hybrid inflation. Based on analytical estimates supported by the results of these simulations [53, 91–94], one finds two high-frequency peaks in the resulting GW spectrum, related to the

<sup>11</sup>For a more detailed discussion of the numerical results, including the precise shape of the ‘kinks’ in the inflationary GW spectrum, cf. Ref. [34].

<sup>12</sup>To be more precise, the quantity which is probed is the temperature  $\hat{T}_{\text{RH}}$  when the energy stored in relativistic degrees of freedom (MSSM particles and nonthermal (s)neutrinos) overcomes the energy stored in the non-relativistic  $B-L$  Higgs bosons. The quantity  $T_*$  appearing in Eq. (43) is related to  $\hat{T}_{\text{RH}}$  via two correction factors  $D$  and  $R$ ,  $T_* = R^{1/2} D^{1/3} \hat{T}_{\text{RH}}$ . Here  $D$  accounts for the entropy production after  $a = a_{\text{RH}}$  and, just as  $R$ , is typically found to be  $\mathcal{O}(1)$  by numerically solving the Boltzmann equations.

mass of the  $B-L$  vector ( $v$ ) and scalar Higgs ( $s$ ) bosons at preheating. The corresponding positions and amplitudes of the peaks in the GW spectrum are given by

$$\begin{aligned}
 f_{\text{PH}}^{(s)} &\simeq 6.3 \times 10^6 \text{ Hz} \left( \frac{M_1}{10^{11} \text{ GeV}} \right)^{1/3} \left( \frac{5 \times 10^{15} \text{ GeV}}{v_{B-L}} \right)^2 \left( \frac{m_S}{3 \times 10^{13} \text{ GeV}} \right)^{7/6}, \\
 \Omega_{\text{GW}}^{(s,\text{max})} h^2 &\simeq 3.6 \times 10^{-16} \frac{c_{\text{PH}}}{0.05} \left( \frac{M_1}{10^{11} \text{ GeV}} \right)^{4/3} \left( \frac{5 \times 10^{15} \text{ GeV}}{v_{B-L}} \right)^{-2} \left( \frac{m_S}{3 \times 10^{13} \text{ GeV}} \right)^{-4/3}, \\
 f_{\text{PH}}^{(v)} &\simeq 7.5 \times 10^{10} \text{ Hz } g \left( \frac{M_1}{10^{11} \text{ GeV}} \right)^{1/3} \left( \frac{m_S}{3 \times 10^{13} \text{ GeV}} \right)^{-1/2}, \\
 \Omega_{\text{GW}}^{(v,\text{max})} h^2 &\simeq 2.6 \times 10^{-24} \frac{1}{g^2} \frac{c_{\text{PH}}}{0.05} \left( \frac{M_1}{10^{11} \text{ GeV}} \right)^{4/3} \left( \frac{5 \times 10^{15} \text{ GeV}}{v_{B-L}} \right)^2 \left( \frac{m_S}{3 \times 10^{13} \text{ GeV}} \right)^2,
 \end{aligned} \tag{45}$$

and are depicted by the red curves in Fig. 10. Here  $g$  is the  $B-L$  gauge coupling and  $c_{\text{PH}}$  is a model-dependent numerical factor, found to be  $c_{\text{PH}} = 0.05$  in Ref. [53].

### Gravitational waves from cosmic strings

We now turn to the third source, namely, cosmic strings in the scaling regime, cf. Sec. 3.2. We here review the calculation of the resulting GW background in the Abelian Higgs (AH) model following Ref. [95]. In Ref. [34], we additionally discuss an alternative approach based on the Nambu-Goto model of cosmic strings. Here, we will merely give the final result of the latter calculation in order to quantify the theoretical uncertainties involved.

The GW background generated by an AH string network can be estimated analytically starting from Eq. (39). Exploiting general properties of the unequal time correlator of a scaling, sub-horizon source as discussed in Ref. [96] and introducing the dimensionless variable  $x = k\tau$ , we can evaluate the unequal time correlator of the AH string network,  $\Pi^2(k, \tau, \tau')$ , as

$$\Pi^2(k, \tau, \tau') = \frac{4v_{B-L}^4}{\sqrt{\tau\tau'}} C^T(x, x'). \tag{46}$$

Here  $C^T(x, x')$  is essentially local in time [96],  $C^T(x, x') \sim \delta(x - x') \tilde{C}(x)$ , with  $\tilde{C}$  some function which falls off rapidly for  $x \gg 1$ , i.e. for modes well inside the horizon. Inserting this into Eq. (39) yields

$$\Omega_{\text{GW}}(k) = \frac{k^2}{3\pi^2 H_0^2 a_0^2} \left( \frac{v_{B-L}}{M_{\text{Pl}}} \right)^4 \int_{x_i}^{x_0} dx \frac{a^2(x/k)}{a_0^2 x} \tilde{C}(x). \tag{47}$$

As a result of the rapid decrease of  $\tilde{C}(x)$  for  $x \gg 1$ , this integral is dominated by its lower boundary. For scales which entered the Hubble horizon after the  $B-L$  phase transition,  $x_i = k\tau_k$  is an  $\mathcal{O}(1)$  constant. Hence, the  $k$ -dependence of Eq. (47) can be traced back to  $a(x/k)$ . For radiation domination, we have  $a(\tau) \simeq \sqrt{\Omega_r} H_0 \tau a_0^2$ , where we have neglected the change in the effective number of degrees of freedom. This yields

$$\int_{x_i}^{x_0} dx \frac{a^2(x/k)}{a_0^2 x} \tilde{C}(x) \simeq \frac{\Omega_r H_0^2 a_0^2}{2k^2} F^r, \tag{48}$$

where  $F^r$  is a constant, and therefore a flat spectrum,  $\Omega_{\text{GW}} \propto k^0$ . For matter domination, one has  $a(x/k) \propto k^{-2}$ , which yields  $\Omega_{\text{GW}} \propto k^{-2}$ .

In summary, we can express today's spectrum of GWs from a scaling network of AH cosmic

strings as<sup>13</sup>

$$\Omega_{\text{GW}}(k) \simeq \Omega_{\text{GW}}^{\text{pl}} \times \begin{cases} (k_{\text{eq}}/k)^2, & k_0 \ll k \ll k_{\text{eq}} \\ 1, & k_{\text{eq}} \ll k \ll k_{\text{RH}} \\ (k_{\text{RH}}/k)^2, & k_{\text{RH}} \ll k \ll k_{\text{PH}} \end{cases}. \quad (49)$$

Here,  $k_{\text{eq}}$ ,  $k_{\text{RH}}$  and  $k_{\text{PH}}$  are determined by Eqs. (42), and (43), and the height of the plateau  $\Omega_{\text{GW}}^{\text{pl}}$  can be estimated using the result of the numerical simulations in Ref. [95],

$$\Omega_{\text{GW}}^{\text{pl}} h^2 = 4.0 \times 10^{-14} \frac{F^r}{F_{\text{FHU}}^r} \left( \frac{v_{B-L}}{5 \times 10^{15} \text{GeV}} \right)^4 \left( \frac{\Omega_r h^2}{4.2 \times 10^{-5}} \right), \quad (50)$$

where  $F_{\text{FHU}}^r = 4.0 \times 10^3$  is the numerical constant determined in Ref. [95] for global cosmic strings. The corresponding constant for local strings is expected to have the same order of magnitude [97].

Eq. (49) strikingly resembles the result found for the stochastic GW background from inflation, cf. Eq. (41), up to an overall normalization factor, cf. Fig. 10. Note, however, that the origin is quite different. On the one hand, in the case of inflation, the GWs can be traced back to vacuum fluctuations of the metric which remain ‘frozen’ outside the horizon. After horizon re-entry, they propagate according to the source-free wave equation in FRW space. The amplitude of the resulting stochastic GW background today is determined by the redshift of these modes after entering the horizon. On the other hand, the GWs from cosmic strings stem from a classical source, which is active until today. Only the nature of the unequal time correlator, with its rapid decrease for  $x \gg 1$ , effectively removes the impact of the source when the corresponding mode is well within the horizon. In more physical terms, this implies that the dominant source for GWs from cosmic strings are Hubble-sized structures of the cosmic string network. This explains why the wave numbers associated with the horizon at  $a_{\text{RH}}$  and  $a_{\text{eq}}$  play crucial roles in the GW spectrum from AH cosmic strings, although the GW modes associated with cosmic strings never actually ‘cross’ the horizon. For cosmic strings the height of the plateau is enhanced by a very large numerical factor  $F^r$ . On the contrary, GWs from inflation are suppressed by the small Yukawa coupling  $\lambda$ . This explains the enormous difference in amplitude between GWs from inflation and cosmic strings.

The calculation presented here, resulting in Eq. (49), was based on the Abelian Higgs (AH) cosmic string model. For comparison, Fig. 11 shows the result obtained in the Nambu-Goto (NG) model, cf. Ref. [34]. In both approaches the radiation-dominated epoch leads to a plateau for intermediate frequencies. Compared to the AH result, the boundaries in the NG case are shifted to higher frequencies by a factor  $1/\alpha$ , where  $\alpha$  denotes the size at which cosmic string loops are formed relative to the respective horizon size.<sup>14</sup> This shift in frequency is directly related to the maximal loop size which is determined by  $\alpha H^{-1}$  in the NG case. Furthermore, the frequency dependence for small and large frequencies differs, which is a consequence of the different mechanisms of gravitational radiation: in the AH model the dominant contribution to the GW background comes from Hubble-sized structures, in the NG model the dominant contribution is due to ‘cusps’ in small cosmic string loops, which are formed when waves moving in opposite directions on the loop collide. The striking difference in amplitude by five orders of magnitude between the AH and NG model is due to the different energy loss mechanisms of the string network in the scaling regime. While the energy loss of AH strings is mainly due to massive radiation, NG strings deposit all their energy into GWs. Hence, these two cases provide lower and upper bounds on the GW background from cosmic strings, and it is conceivable that the true answer corresponds to some intermediate value. Assuming a transition between the AH model at early times and the NG model

<sup>13</sup>Note that in Eq. (49), the normalization of the ‘ $1/k^2$ -flanks’ was obtained by matching to the plateau value for  $k = k_{\text{RH}}$  and  $k = k_{\text{eq}}$ , respectively. However, since close to these points the dominant component of the energy density is not much larger than the other components, a more detailed knowledge of  $\tilde{C}(x)$  is necessary to evaluate Eq. (47) at these points.

<sup>14</sup>Note that  $\alpha$  cannot take arbitrarily small values. A lower bound is given by the requirement that, in the area of application of the NG model, the loop size should be larger than the string width obtained in the AH model (controlled by  $m_S^{-1}, m_G^{-1}$ ) or at the very least larger than  $M_P^{-1}$ .

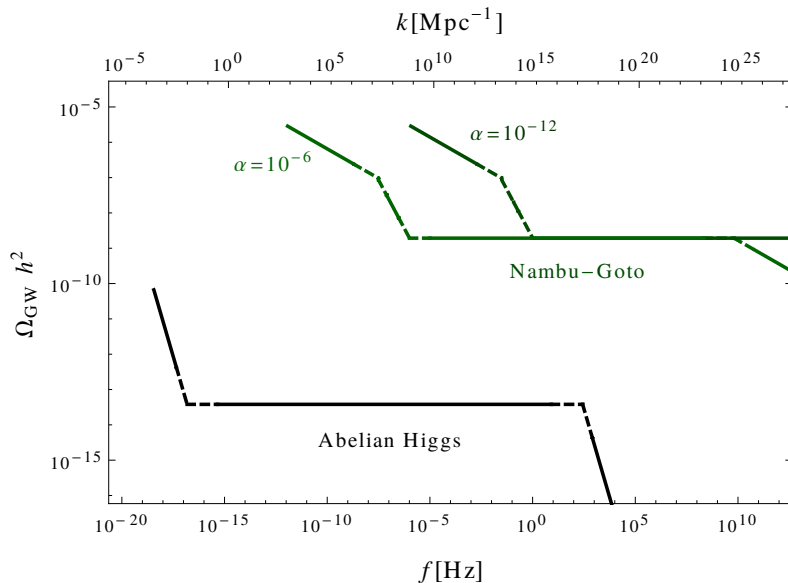


**Fig. 11:** Comparison of the GW spectra predicted by AH strings and NG strings for two values of  $\alpha$  (which governs the initial cosmic string loop size in the NG model). The other parameters are chosen as in Fig. 10, which yields a cosmic string tension of  $G\mu = 2 \times 10^{-7}$ . From Ref. [34].

at later times sometime during radiation domination, a notable point is that, due to the shift of the GW spectrum of NG strings to higher frequencies, the GWs generated at later times in the NG regime might cover up the GWs generated at earlier times in the AH regime. To address this important question of how to correctly describe the evolution of cosmic strings is clearly a theoretical challenge.

## 6 Observational Prospects and Outlook

In this paper we have demonstrated that the MSM, a minimal supersymmetric extension of the Standard Model with right-handed neutrinos and spontaneously broken local  $B-L$  symmetry, is capable of remedying several shortcomings of the Standard Model while at the same time successfully accounting for the earliest phases of the cosmological evolution. While the MSM allows for grand unification and explains the smallness of the observed neutrino masses on the particle physics side, it accommodates inflation and the generation of entropy, baryon asymmetry and dark matter during the reheating process on the cosmology side. These successes of the MSM therefore truly render it a minimal consistent model of particle physics *and* the early universe.

The MSM gives rise to a rich phenomenology that can be probed in on-going and upcoming cosmological observations and high energy physics experiments. First of all, future data on the temperature anisotropies as well as on the polarization of the CMB radiation will test the dynamics of the  $B-L$  breaking sector of the MSM. Dedicated experiments searching for tensor modes in the CMB, such as CMBPol [98] or LiteBIRD [99], have, for instance, the potential to rule out supersymmetric F-term hybrid inflation by measuring a tensor-to-scalar ratio  $r$  of  $\mathcal{O}(10^{-2})$  or larger, cf. Eq. (10). Meanwhile, indications in the CMB for the presence of local cosmic strings could provide evidence in favour of cosmological  $B-L$  breaking, cf. Sec. 3.2. For parameter values compatible with inflation, the AH model of the  $B-L$  phase transition typically predicts a cosmic string tension  $G\mu$  only shortly below the current observational bound,  $G\mu < 3.2 \times 10^{-7}$ . From the perspective of the MSM, it is thus expected that signs of cosmic strings should soon be seen.

Next to the CMB, cosmic strings ought to reveal their existence also in weak and strong lensing

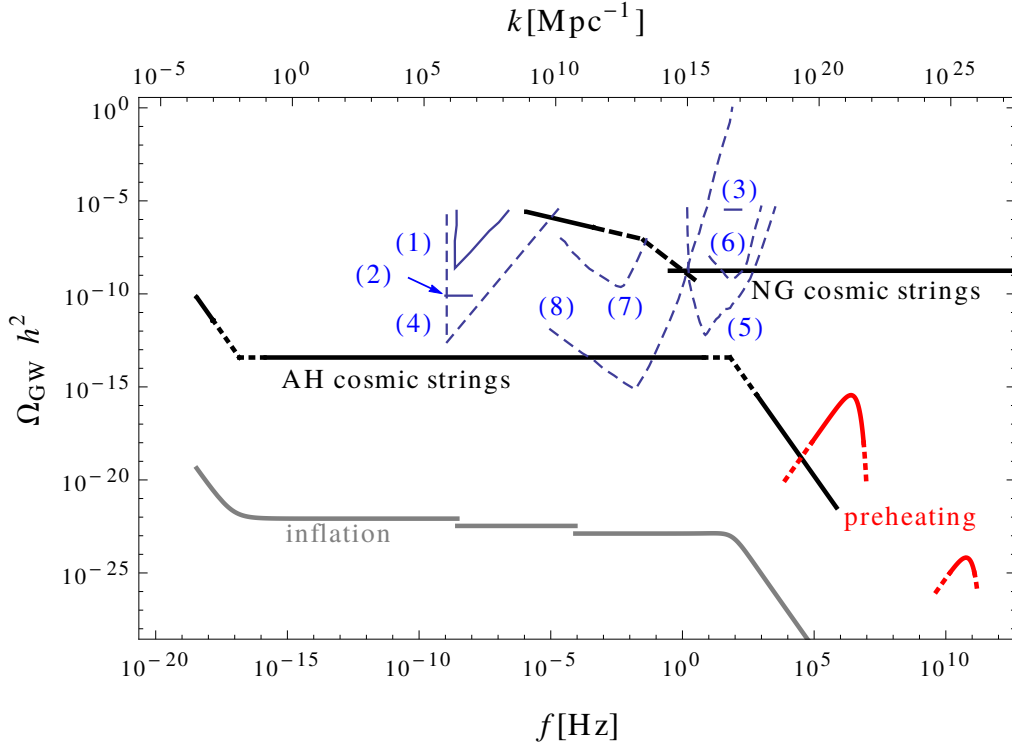


**Fig. 12:** Predicted GW spectrum and the (expected) sensitivity of current and upcoming experiments. The GW spectrum due to inflation (gray), preheating (red) as well as AH and NG cosmic strings (black) is shown for  $v_{B-L} = 5 \times 10^{15}$  GeV,  $M_1 = 10^{11}$  GeV,  $m_S = 3 \times 10^{13}$  GeV, and  $\alpha = 10^{-12}$ . The current bounds on the stochastic GW spectrum from (1) millisecond pulsar timing (taken from Ref. [88], with (2) marking the update from EPTA [100] and (3) LIGO [101] are marked by solid blue lines. The dashed blue lines mark the expected sensitivity of some planned experiments: (4) SKA [102], (5) ET [103], (6) advanced LIGO [103], (7) eLISA [104], (8) BBO and DECIGO [105]. Note that with a correlation analysis ultimate DECIGO has a sensitivity down to  $10^{-18}$ . From Ref. [34]

surveys, in the spectrum of ultra-high-energy cosmic rays and GeV-scale  $\gamma$ -rays and finally also in the spectrum of GWs. In Sec. 5, we discussed this latter characteristic signature of the MSM in more detail. In doing so, we put a particular emphasis on the uncertainties in the theoretical calculations, which we assessed by calculating the spectrum of GWs either emitted by AH or by NG cosmic strings. Our result for the GW spectrum related to cosmological  $B-L$  breaking is shown in Fig. 12, which compares the GW signals that are respectively expected to originate from AH strings, NG strings, inflation and preheating. In addition to that, Fig. 12 also indicates current bounds on  $\Omega_{\text{GW}} h^2$  as well as the expected sensitivity of upcoming GW experiments, cf. Ref. [106] for a review. The observation of a GW signal coming from cosmic strings in the scaling regime in the not too far future is clearly challenging. Depending on the parameters of the AH model, the reheating temperature and the cosmic string loop parameter  $\alpha$ , future experiments will either see a flat plateau in the GW spectrum or detect a kink-type feature related to the transition between two successive stages in the expansion history of the universe. Particularly intriguing in this context is the possibility to determine the reheating temperature by measuring the position of the kink in the GW spectrum that is included by AH strings at frequencies around  $f_{\text{RH}}$ , cf. Eq. (43) and footnote 12. Nonetheless it is important to realize that at present our understanding of the formation, evolution and decay of cosmic strings is still far from complete. For one reason or another, the GW background due to cosmic strings might be suppressed or even absent, cf. Ref. [34] for details, thereby

potentially rendering inflation and preheating the dominant sources of GWs. At least in the case of inflation, the exact shape of the GW spectrum and in particular of its kinks could then be predicted with a much better precision than as for cosmic strings [34]. As both the GW signals from inflation as well as from preheating are however rather faint, a positive observation by any of the planned GW experiments seems to be out of reach.

The dynamics of the neutrino sector in the MSM can be tested on the basis of the parameter relations that we derived in our study of the reheating process, cf. Sec. 4.2. Assuming the gravitino to be the LSP, the requirement of consistency between leptogenesis and gravitino dark matter provided us with relations between the neutrino mass parameters  $\tilde{m}_1$  and  $M_1$  on the one hand and the superparticle masses  $m_{\tilde{G}}$  and  $m_{\tilde{g}}$  on the other hand, cf. Fig. 8. In particular, we found a lower bound on the gravitino mass that scales quadratically with the gluino mass and that at the same time slightly varies with  $\tilde{m}_1$ , cf. Eq. (26). As an alternative to gravitino dark matter, we also considered the possibility of very heavy gravitinos, in the case of which dark matter is accounted for by partly thermally, partly nonthermally produced winos or higgsinos. In this scenario, requiring consistency between leptogenesis, WIMP dark matter and primordial nucleosynthesis, we were able to derive upper bounds on the neutralino mass  $m_{\text{LSP}}$  as well as absolute lower bounds on the gravitino mass as functions of  $\tilde{m}_1$ , cf. Fig. 9.

Owing to these relations and bounds, a determination of  $\tilde{m}_1$ ,  $M_1$ ,  $m_{\tilde{G}}$ ,  $m_{\tilde{g}}$  and/or  $m_{\text{LSP}}$  in present or upcoming experiments would therefore allow to constrain the parameter space of the MSM or even to falsify it. The absolute mass scale of the Standard Model neutrinos, which is closely related to  $\tilde{m}_1$ , is, for instance, probed by low-energy neutrino experiments such as GERDA [107] and KATRIN [108] that are looking for neutrinoless double- $\beta$  decay and studying the  $\beta$ -decay of tritium, respectively. Meanwhile, it is hard to experimentally access the neutrino mass  $M_1$  directly; but fortunately the MSM offers a possibility to determine  $M_1$  indirectly. As reheating after inflation is driven by the decay of heavy (s)neutrinos in the MSM, the plateau temperature  $T_{\text{RH}}^N$  turns out to be a function of  $\tilde{m}_1$  and  $M_1$ , cf. Ref. [10] for details. Once  $\tilde{m}_1$  is known, there thus exists a one-to-one relation between values of  $M_1$  and  $T_{\text{RH}}^N$ , at least as long as all Yukawa couplings are kept fixed. As mentioned above, it is conceivable that the reheating temperature could possibly be determined by means of GW observations. Such an observation would then also allow for a measurement of  $M_1$ .

Depending on the scale of soft supersymmetry breaking and the details of the superparticle mass spectrum, a determination of  $m_{\tilde{G}}$ ,  $m_{\tilde{g}}$  and  $m_{\text{LSP}}$  is potentially within the reach of experiments aiming at the direct or indirect detection of dark matter and/or collider searches for supersymmetry. If dark matter should be composed of gravitino LSPs, direct and indirect detection experiments would actually be bound to yield null observations. However, if  $R$  parity was slightly violated, gravitino dark matter would be unstable [109, 110], which could lead to observable signals in the fluxes of gamma rays, charged cosmic rays and cosmic neutrinos [111]. At the same time, the decays of the next-to-lightest superparticle (NLSP) via its  $R$  parity-violating interactions might be observable in collider experiments in the form of displaced vertices with distinctive decay signatures [112, 113]. A slight violation of  $R$  parity is in fact motivated from cosmology—if  $R$  parity was exactly conserved, the late-time decays of the NLSP could spoil the successful predictions of primordial nucleosynthesis [?, 47]—and hence we are confident that the nature of dark matter is not doomed to remain obscure, even if it is made out of gravitinos. Finally, dark matter composed of partly thermally, partly nonthermally produced winos or higgsinos could soon be seen in indirect detection experiments such as H.E.S.S. and Fermi-LAT, cf. footnote 9. On the other hand, for the hierarchical superparticle mass spectrum in Eq. (27), the prospects for a direct detection of WIMP dark matter via its scattering off heavy nuclei do not look particularly promising, cf. Ref. [32]. Also the discovery of a wino or higgsino LSP at colliders seems to be rather challenging in this scenario. Given the large masses for the gluinos and squarks, the characteristic missing energy signature of events with LSPs in the final state may be absent. On the contrary, the wino- or higgsino-like chargino, almost mass degenerate with its neutral partner, might leave macroscopic charged tracks in the detector, which could increase the discovery potential of this dark matter scenario. In addition to that, monojets caused

by the Drell-Yan production of LSP pairs in association with initial state gluon radiation may also provide a possible discovery channel. We therefore conclude that the MSM is experimentally accessible not only in cosmological observations, but also in a number of high energy physics experiments. Upcoming data will thus shed more light on whether or not the MSM is indeed a good description of particle physics up to the multi-TeV scale as well as of the earliest phases of our universe.

Before concluding, we would still like to compare the MSM with a closely related model, the  $\nu$ MSM [115], the non-supersymmetric minimal Standard Model with right-handed neutrinos, which can also account for inflation, entropy production, baryon asymmetry and dark matter. The  $\nu$ MSM is a model with minimal particle content as well as minimal symmetry. The local symmetry is that of the Standard Model and the global  $B-L$  symmetry is explicitly broken by Majorana masses of the right-handed neutrinos. Baryogenesis via leptogenesis and dark matter require these masses to lie in the keV and GeV range, far below the electroweak scale, which leads to predictions that are experimentally testable in the near future. The Higgs field of electroweak symmetry breaking also plays the role of the inflaton, which requires a large non-minimal coupling to gravity, tuned to account for the observed amplitude of the CMB temperature anisotropies. In the  $\nu$ MSM there is no unification of strong and electroweak interactions. Also the MSM has minimal matter content. However, the symmetry group is enlarged, and in addition to the Standard Model gauge group it contains local  $U(1)_{B-L}$  symmetry and local supersymmetry. Assuming quark and lepton mass matrices compatible with grand unification, and therefore hierarchical right-handed neutrinos, one finds that  $U(1)_{B-L}$  is broken at the GUT scale. The symmetry breaking sector contains an inflaton field and the GUT scale automatically yields the right order of magnitude for the amplitude of CMB temperature anisotropies. The lightest superparticle is the constituent of dark matter, which can be searched for at the Large Hadron Collider as well as with direct and indirect detection experiments. Direct evidence for the MSM may eventually be obtained via the spectrum of relic GWs. In summary, supporting evidence for or falsification of the  $\nu$ MSM or the MSM will decide whether or not physics beyond the Standard Model is tied to symmetries larger than those already revealed by the Standard Model.

## References

- [1] J. Beringer *et al.* [Particle Data Group Collaboration], Phys. Rev. D **86** (2012) 010001.
- [2] G. Aad *et al.* [ATLAS Collaboration], Phys. Lett. B **716** (2012) 1 [arXiv:1207.7214 [hep-ex]].
- [3] S. Chatrchyan *et al.* [CMS Collaboration], Phys. Lett. B **716** (2012) 30 [arXiv:1207.7235 [hep-ex]].
- [4] H. Pagels and J. R. Primack, Phys. Rev. Lett. **48**, 223 (1982).
- [5] H. Goldberg, Phys. Rev. Lett. **50**, 1419 (1983) [Erratum-ibid. **103**, 099905 (2009)].
- [6] J. R. Ellis, J. S. Hagelin, D. V. Nanopoulos, K. A. Olive and M. Srednicki, Nucl. Phys. B **238**, 453 (1984).
- [7] M. Fukugita and T. Yanagida, Phys. Lett. B **174**, 45 (1986).
- [8] E. J. Copeland, A. R. Liddle, D. H. Lyth, E. D. Stewart and D. Wands, Phys. Rev. D **49**, 6410 (1994), [astro-ph/9401011].
- [9] G. R. Dvali, Q. Shafi and R. K. Schaefer, Phys. Rev. Lett. **73**, 1886 (1994), [hep-ph/9406319].
- [10] W. Buchmüller, V. Domcke and K. Schmitz, Nucl. Phys. B **862**, 587 (2012) [arXiv:1202.6679 [hep-ph]].
- [11] W. Buchmüller, K. Schmitz and G. Vertongen, Phys. Lett. B **693**, 421 (2010) [arXiv:1008.2355 [hep-ph]].
- [12] W. Buchmüller, K. Schmitz and G. Vertongen, Nucl. Phys. B **851**, 481 (2011) [arXiv:1104.2750 [hep-ph]].
- [13] M. Plumacher, Nucl. Phys. B **530**, 207 (1998), [hep-ph/9704231].

- [14] W. Buchmuller, P. Di Bari and M. Plumacher, *Annals Phys.* **315**, 305 (2005), [hep-ph/0401240].
- [15] G. Lazarides and Q. Shafi, *Phys. Lett. B* **258**, 305 (1991).
- [16] T. Asaka, K. Hamaguchi, M. Kawasaki and T. Yanagida, *Phys. Lett. B* **464**, 12 (1999), [hep-ph/9906366].
- [17] T. Asaka, K. Hamaguchi, M. Kawasaki and T. Yanagida, *Phys. Rev. D* **61**, 083512 (2000), [hep-ph/9907559].
- [18] F. Hahn-Woernle and M. Plumacher, *Nucl. Phys. B* **806**, 68 (2009), arXiv:0801.3972 [hep-ph].
- [19] H. Murayama, H. Suzuki, T. Yanagida and J. Yokoyama, *Phys. Rev. Lett.* **70**, 1912 (1993).
- [20] J. R. Ellis, M. Raidal and T. Yanagida, *Phys. Lett. B* **581**, 9 (2004), [hep-ph/0303242].
- [21] S. Antusch, M. Bastero-Gil, S. F. King and Q. Shafi, *Phys. Rev. D* **71**, 083519 (2005), [hep-ph/0411298].
- [22] S. Antusch, J. P. Baumann, V. F. Domcke and P. M. Kostka, *JCAP* **1010**, 006 (2010), arXiv:1007.0708 [hep-ph].
- [23] V. N. Senoguz and Q. Shafi, hep-ph/0512170.
- [24] S. Weinberg, *Phys. Rev. Lett.* **48**, 1303 (1982).
- [25] J. R. Ellis, D. V. Nanopoulos and S. Sarkar, *Nucl. Phys. B* **259**, 175 (1985).
- [26] M. Kawasaki, K. Kohri and T. Moroi, *Phys. Lett. B* **625**, 7 (2005), [astro-ph/0402490].
- [27] M. Kawasaki, K. Kohri and T. Moroi, *Phys. Rev. D* **71**, 083502 (2005), [astro-ph/0408426].
- [28] K. Jedamzik, *Phys. Rev. D* **74**, 103509 (2006), [hep-ph/0604251].
- [29] M. Bolz, W. Buchmuller and M. Plumacher, *Phys. Lett. B* **443**, 209 (1998), [hep-ph/9809381].
- [30] T. Gherghetta, G. F. Giudice and J. D. Wells, *Nucl. Phys. B* **559** (1999) 27 [hep-ph/9904378].
- [31] M. Ibe, R. Kitano, H. Murayama and T. Yanagida, *Phys. Rev. D* **70** (2004) 075012 [hep-ph/0403198].
- [32] W. Buchmuller, V. Domcke and K. Schmitz, *Phys. Lett. B* **713**, 63 (2012) [arXiv:1203.0285 [hep-ph]].
- [33] G. N. Felder, J. Garcia-Bellido, P. B. Greene, L. Kofman, A. D. Linde and I. Tkachev, *Phys. Rev. Lett.* **87**, 011601 (2001) [hep-ph/0012142].
- [34] W. Buchmuller, V. Domcke, K. Kamada and K. Schmitz, arXiv:1305.3392 [hep-ph].
- [35] P. A. R. Ade *et al.* [Planck Collaboration], arXiv:1303.5082 [astro-ph.CO].
- [36] A. D. Linde and A. Riotto, *Phys. Rev. D* **56**, 1841 (1997) [hep-ph/9703209].
- [37] K. Schmitz, arXiv:1307.3887 [hep-ph].
- [38] P. A. R. Ade *et al.* [Planck Collaboration], arXiv:1303.5085 [astro-ph.CO].
- [39] W. Buchmuller, L. Covi and D. Delepine, *Phys. Lett. B* **491**, 183 (2000) [hep-ph/0006168].
- [40] K. Nakayama, F. Takahashi and T. T. Yanagida, *JCAP* **1012**, 010 (2010) [arXiv:1007.5152 [hep-ph]].
- [41] C. Pallis and Q. Shafi, arXiv:1304.5202 [hep-ph].
- [42] M. Bastero-Gil, S. F. King and Q. Shafi, *Phys. Lett. B* **651**, 345 (2007) [hep-ph/0604198].
- [43] M. Kawasaki, F. Takahashi and T. T. Yanagida, *Phys. Lett. B* **638**, 8 (2006) [hep-ph/0603265].
- [44] M. Endo, F. Takahashi and T. T. Yanagida, *Phys. Lett. B* **658**, 236 (2008) [hep-ph/0701042].
- [45] M. Y. Khlopov and A. D. Linde, *Phys. Lett. B* **138**, 265 (1984).
- [46] J. R. Ellis, J. E. Kim and D. V. Nanopoulos, *Phys. Lett. B* **145**, 181 (1984).
- [47] T. Moroi, H. Murayama and M. Yamaguchi, *Phys. Lett. B* **303**, 289 (1993).

- [48] W. Buchmüller, V. Domcke, K. Kamada and K. Schmitz, in preparation
- [49] T. W. B. Kibble, *J. Phys. A* **9**, 1387 (1976).
- [50] E. J. Copeland, S. Pascoli and A. Rajantie, *Phys. Rev. D* **65**, 103517 (2002) [hep-ph/0202031].
- [51] J. Garcia-Bellido, M. Garcia Perez and A. Gonzalez-Arroyo, *Phys. Rev. D* **67**, 103501 (2003) [hep-ph/0208228].
- [52] J. Garcia-Bellido and E. Ruiz Morales, *Phys. Lett. B* **536**, 193 (2002) [hep-ph/0109230].
- [53] J. Garcia-Bellido and D. G. Figueroa, *Phys. Rev. Lett.* **98**, 061302 (2007) [astro-ph/0701014].
- [54] J. Berges, D. Gelfand and J. Pruschke, *Phys. Rev. Lett.* **107**, 061301 (2011) [arXiv:1012.4632 [hep-ph]].
- [55] A. Vilenkin, Cambridge University Press (1994).
- [56] M. Hindmarsh, *Prog. Theor. Phys. Suppl.* **190**, 197 (2011) [arXiv:1106.0391 [astro-ph.CO]].
- [57] F. Lenz, *Lect. Notes Phys.* **659**, 7 (2005) [hep-th/0403286].
- [58] C. T. Hill, H. M. Hodges and M. S. Turner, *Phys. Rev. Lett.* **59**, 2493 (1987).
- [59] H. J. de Vega and F. A. Schaposnik, *Phys. Rev. D* **14**, 1100 (1976).
- [60] M. Hindmarsh, S. Stuckey and N. Bevis, *Phys. Rev. D* **79**, 123504 (2009) [arXiv:0812.1929 [hep-th]].
- [61] S. Kuroyanagi, K. Miyamoto, T. Sekiguchi, K. Takahashi and J. Silk, *Phys. Rev. D* **87**, 023522 (2013) [arXiv:1210.2829 [astro-ph.CO]].
- [62] G. Sigl, K. Jedamzik, D. N. Schramm and V. S. Berezhinsky, *Phys. Rev. D* **52**, 6682 (1995) [astro-ph/9503094].
- [63] R. J. Protheroe and T. Stanev, *Phys. Rev. Lett.* **77**, 3708 (1996) [Erratum-ibid. **78**, 3420 (1997)] [astro-ph/9605036].
- [64] P. Bhattacharjee, Q. Shafi and F. W. Stecker, *Phys. Rev. Lett.* **80**, 3698 (1998) [hep-ph/9710533].
- [65] G. Sigl, S. Lee, P. Bhattacharjee and S. Yoshida, *Phys. Rev. D* **59**, 043504 (1999) [hep-ph/9809242].
- [66] U. F. Wichoski, J. H. MacGibbon and R. H. Brandenberger, *Phys. Rev. D* **65**, 063005 (2002) [hep-ph/9805419].
- [67] J. N. Moore, E. P. S. Shellard and C. J. A. P. Martins, *Phys. Rev. D* **65**, 023503 (2002) [hep-ph/0107171].
- [68] G. Vincent, N. D. Antunes and M. Hindmarsh, *Phys. Rev. Lett.* **80**, 2277 (1998) [hep-ph/9708427].
- [69] A. Albrecht and N. Turok, *Phys. Rev. D* **40**, 973 (1989).
- [70] V. Vanchurin, K. D. Olum and A. Vilenkin, *Phys. Rev. D* **74**, 063527 (2006) [gr-qc/0511159].
- [71] K. D. Olum and V. Vanchurin, *Phys. Rev. D* **75**, 063521 (2007) [astro-ph/0610419].
- [72] J. J. Blanco-Pillado, K. D. Olum and B. Shlaer, *Phys. Rev. D* **83**, 083514 (2011) [arXiv:1101.5173 [astro-ph.CO]].
- [73] W. Buchmüller, R. D. Peccei and T. Yanagida, *Ann. Rev. Nucl. Part. Sci.* **55**, 311 (2005) [hep-ph/0502169].
- [74] E. Komatsu *et al.* [WMAP Collaboration], *Astrophys. J. Suppl.* **192**, 18 (2011) [arXiv:1001.4538 [astro-ph.CO]].
- [75] W. Buchmüller, V. Domcke and K. Schmitz, *JHEP* **1203**, 008 (2012) [arXiv:1111.3872 [hep-ph]].
- [76] P. A. R. Ade *et al.* [Planck Collaboration], arXiv:1303.5076 [astro-ph.CO].
- [77] M. Ibe and T. T. Yanagida, *Phys. Lett. B* **709**, 374 (2012) [arXiv:1112.2462 [hep-ph]].
- [78] K. S. Jeong, M. Shimosuka and M. Yamaguchi, *JHEP* **1209**, 050 (2012) [arXiv:1112.5293 [hep-ph]].
- [79] S. Krippendorf, H. P. Nilles, M. Ratz and M. W. Winkler, *Phys. Lett. B* **712**, 87 (2012) [arXiv:1201.4857 [hep-ph]].

- [80] S. P. Martin, In \*Kane, G.L. (ed.): Perspectives on supersymmetry II\* 1-153 [hep-ph/9709356].
- [81] T. Cohen, M. Lisanti, A. Pierce and T. R. Slatyer, arXiv:1307.4082 [hep-ph].
- [82] J. Fan and M. Reece, arXiv:1307.4400 [hep-ph].
- [83] N. Arkani-Hamed, A. Delgado and G. F. Giudice, Nucl. Phys. B **741**, 108 (2006) [hep-ph/0601041].
- [84] J. Hisano, S. Matsumoto, M. Nagai, O. Saito and M. Senami, Phys. Lett. B **646**, 34 (2007) [hep-ph/0610249].
- [85] M. Cirelli, A. Strumia and M. Tamburini, Nucl. Phys. B **787**, 152 (2007) [arXiv:0706.4071 [hep-ph]].
- [86] B. Allen, In \*Les Houches 1995, Relativistic gravitation and gravitational radiation\* 373-417 [gr-qc/9604033].
- [87] M. Maggiore, Oxford University Press, October 2007. 572p. (ISBN-13: 978-0-19-857074-5)
- [88] T. L. Smith, M. Kamionkowski and A. Cooray, Phys. Rev. D **73**, 023504 (2006) [astro-ph/0506422].
- [89] M. S. Turner, M. J. White and J. E. Lidsey, Phys. Rev. D **48**, 4613 (1993) [astro-ph/9306029].
- [90] K. Nakayama, S. Saito, Y. Suwa and J. 'i. Yokoyama, JCAP **0806**, 020 (2008) [arXiv:0804.1827 [astro-ph]].
- [91] J. F. Dufaux, A. Bergman, G. N. Felder, L. Kofman and J. -P. Uzan, Phys. Rev. D **76**, 123517 (2007) [arXiv:0707.0875 [astro-ph]].
- [92] J. -F. Dufaux, G. Felder, L. Kofman and O. Navros, JCAP **0903**, 001 (2009) [arXiv:0812.2917 [astro-ph]].
- [93] G. N. Felder and L. Kofman, Phys. Rev. D **75**, 043518 (2007) [hep-ph/0606256].
- [94] J. -F. Dufaux, D. G. Figueroa and J. Garcia-Bellido, Phys. Rev. D **82**, 083518 (2010) [arXiv:1006.0217 [astro-ph.CO]].
- [95] D. G. Figueroa, M. Hindmarsh and J. Urrestilla, Phys. Rev. Lett. **110**, 101302 (2013) [arXiv:1212.5458 [astro-ph.CO]].
- [96] R. Durrer, M. Kunz and A. Melchiorri, Phys. Rev. D **59**, 123005 (1999) [astro-ph/9811174].
- [97] M. Hindmarsh, private communication.
- [98] D. Baumann *et al.* [CMBPol Study Team Collaboration], AIP Conf. Proc. **1141**, 10 (2009) [arXiv:0811.3919 [astro-ph]].
- [99] LiteBIRD project, <http://cmb.kek.jp/litebird/index.html>; M. Hazumi, AIP Conf. Proc. **1040**, 78 (2008).
- [100] R. van Haasteren, Y. Levin, G. H. Janssen, K. Lazaridis, M. K. B. W. Stappers, G. Desvignes, M. B. Purver and A. G. Lyne *et al.*, arXiv:1103.0576 [astro-ph.CO].
- [101] C. Palomba [LIGO Scientific and Virgo Collaborations], arXiv:1201.3176 [astro-ph.IM].
- [102] M. Kramer, astro-ph/0409020.
- [103] M. Abarnathy, F. Acernese, P. Ajith *et al.* [ET Science Team], "Einstein gravitational wave Telescope - Conceptual Design Study," ET-0106C-10, European Gravitational Observatory, 2011.
- [104] P. Amaro-Seoane, S. Aoudia, S. Babak, P. Binetruy, E. Berti, A. Bohe, C. Caprini and M. Colpi *et al.*, arXiv:1201.3621 [astro-ph.CO].
- [105] L. Alabidi, K. Kohri, M. Sasaki and Y. Sendouda, JCAP **1209**, 017 (2012) [arXiv:1203.4663 [astro-ph.CO]].
- [106] M. Maggiore, Phys. Rept. **331**, 283 (2000) [gr-qc/9909001].
- [107] M. Agostini *et al.* [GERDA Collaboration], arXiv:1307.4720 [nucl-ex].
- [108] [for the KATRIN Collaboration], arXiv:1307.5486 [physics.ins-det].
- [109] F. Takayama and M. Yamaguchi, Phys. Lett. B **485**, 388 (2000) [hep-ph/0005214].
- [110] W. Buchmuller, L. Covi, K. Hamaguchi, A. Ibarra and T. Yanagida, JHEP **0703**, 037 (2007) [hep-

ph/0702184 [HEP-PH]].

[111] M. Grefe, arXiv:1111.6779 [hep-ph].

[112] S. Bobrovskiy, W. Buchmuller, J. Hajer and J. Schmidt, JHEP **1109**, 119 (2011) [arXiv:1107.0926 [hep-ph]].

[113] S. Bobrovskiy, J. Hajer and S. Rydbeck, JHEP **1302**, 133 (2013) [arXiv:1211.5584 [hep-ph]].

[114] A. de Gouvea, T. Moroi and H. Murayama, Phys. Rev. D **56**, 1281 (1997) [hep-ph/9701244].

[115] For a review and references, see M. Shaposhnikov, Phys. Part. Nucl. **41** (2010) 862.



# Black Hole Macro-Quantumness

Gia Dvali<sup>a, b, c</sup> and Cesar Gomez<sup>a, d, \*</sup>

<sup>a</sup>Arnold Sommerfeld Center for Theoretical Physics, Department für Physik,  
Ludwig-Maximilians-Universität München, Theresienstr. 37, 80333 München, Germany

<sup>b</sup>Max-Planck-Institut für Physik, Föhringer Ring 6, 80805 München, Germany

<sup>c</sup>Center for Cosmology and Particle Physics, Department of Physics, New York University, 4  
Washington Place, New York, NY 10003, USA

<sup>d</sup>Instituto de Física Teórica UAM-CSIC, C-XVI, Universidad Autónoma de Madrid, Cantoblanco,  
28049 Madrid, Spain

## Abstract

It is a common wisdom that properties of macroscopic bodies are well described by (semi)classical physics. As we have suggested [1–3] this wisdom is not applicable to black holes. Despite being macroscopic, black holes are quantum objects. They represent Bose-Einstein condensates of  $N$ -soft gravitons at the quantum critical point, where  $N$  Bogoliubov modes become gapless. As a result, physics governing arbitrarily-large black holes (e.g., of galactic size) is a quantum physics of the collective Bogoliubov modes. This fact introduces a new intrinsically-quantum corrections in form of  $1/N$ , as opposed to  $e^{-N}$ . These corrections are unaccounted by the usual semiclassical expansion in  $\hbar$  and cannot be recast in form of a quantum back-reaction to classical metric. Instead the metric itself becomes an approximate entity. These  $1/N$  corrections abolish the presumed properties of black holes, such as non existence of hair, and are the key to nullifying the so-called information paradox.

## 1 Essence of Macro-Quantumness

It is a common wisdom that the properties derived in idealized semi-classical treatment, such as, e.g., Hawking's exact thermality [5] [6] and absence of hair [7], must be well-applicable to the real macroscopic black holes. From the first glance, this sounds reasonable. After all, the common effective-field-theoretic sense tells us that for large objects all the microscopic quantum physics averages out in effective macroscopic characteristics, which are classical. When applying this reasoning to ordinary macroscopic objects such as planets, stars or galaxies, no apparent paradoxes or inconsistencies appear. For example, treating the earth as a semi-classical gravitating source gives a consistent picture.

In contrast, when applying the same common sense to realistic macroscopic black holes of finite mass, one ends up with puzzles and paradoxes, perhaps the most prominent being Hawking's information paradox [8]. The purpose of this short note is not to discuss the existing puzzles one by one, but instead to point out the misconception that underlies all of them. Namely, the quantum effects for the macroscopic black holes are much more important than what is suggested by straightforward application of semi-classical reasoning. This is the lesson from the recently-developed black hole quantum portrait [1–4]. In this respect there is nothing new in the present note, but we shall provide a sharper focus and specifically reiterate the key point that we believe sources the black hole mysteries. We would like to explain why it happens that some macroscopic bodies are more quantum than others.

The short answer is that despite being macroscopic, black holes are systems at the critical point of a *quantum* phase transition [3]. As a result, no matter how large and heavy, they can never be treated

---

\*E-mail: cesar.gomez@uam.es

fully classically. Indeed the very nature of the phase transition as quantum requires a great amount of quantumness in the form of entanglement. Of course, for some aspects (e.g., large distance gravitational effects on probe bodies) the semi-classical treatment is fine, but is non-applicable for other aspects, such as information storage and processing.

In order to explain this profound difference, let us compare a black hole to an ordinary macroscopic object, e.g., a planet or a bucket of water. Of course the common property of all the macroscopic objects, that allows to treat them in long-distance regimes classically, is the large number of quantum constituents,  $N$ . Property,  $N \gg 1$  is universally shared by all the macroscopic bodies of our interest.

For such objects we can define some quantum characteristics, such as,  $N$  (e.g., number of atoms in the bucket of water) and their *quantum* coupling strengths. However, in ordinary objects with size much bigger than the de-Broglie wave-lengths of the constituents, the coupling  $\alpha_{ij}$  between a pair of constituents  $i$  and  $j$  strongly depends on the relative positions of the constituents (for example, a nearest neighbor coupling in atomic systems ) and cannot be defined universally.

In contrast, an universal coupling can be defined in the systems in which everyone talks to everyone at an equal strength. Such is the property of Bose-Einstein condensates (BECs) where all the constituents are in a common quantum state. In particular, the black holes represent such condensates of gravitons. For such a system we can define a very useful parameter,

$$\lambda \equiv N\alpha, \tag{1}$$

which is somewhat analogous to the 't Hooft coupling for gauge theories with  $N$ -colors [9]. Despite the crucial difference that in our case  $N$  is not an input of the theory, but rather a characteristic of a particular BEC, we shall refer to  $\lambda$  as the 't Hooft coupling.

This parameter plays the central role in our considerations since it determines how close is the system from *quantum* criticality. Thus, level of classicality of the system is not determined by only how large  $N$  is, but most importantly how far it is from the critical value  $N = 1/\alpha$ . This is the fundamental difference between black holes and other macroscopic bodies with many constituents. For the ordinary macroscopic objects, such as planets, the analog of the 't Hooft's coupling either cannot be defined or it is far from quantum criticality. This is why the ordinary macroscopic objects can be treated classically with a very good approximation, without encountering any seeming paradoxes. Contrary, as we have shown, black holes are always at the quantum critical point  $N\alpha = 1$  up to  $1/N$  corrections. As a result, black holes can never be treated classically. There are certain quantum effects (such as mass gap and degeneracy of Bogoliubov modes) that for large black holes become extremely important. In particular, at the quantum critical point small subsystems are maximally entangled i.e the entanglement entropy for the reduced one particle density matrix is maximal.

We thus, have outlined the following sequence of macroscopic systems with increasing level of quantumness:

**Ordinary macroscopic objects (e.g., planets or buckets of water).**

Quantum Characteristics :  $N$  exists,  $\lambda$  cannot be defined.



**Generic (non-critical) Bose-Einstein-Condensates.**

Quantum Characteristics : Both  $N$  and  $\lambda$  are well defined, but  $\lambda \neq 1$ .



**Black holes: Bose-Einstein condensates stuck at the quantum critical point.**

Quantum Characteristics : Both  $N$  and  $\lambda$  are well defined, and  $\lambda = 1$ .

In order to explain this profound difference, let us consider a hypothetical gravitating source of the mass of a neutron star. We shall use an oversimplified model in which we shall approximate the source by a collection of  $N_B$  particles of baryonic mass,  $m_B \sim \text{GeV}$ , stabilized by some non-gravitational forces. We shall ignore the contribution to the energy from the stabilizing force. Then by dialing the strength of the stabilizing force, we can bring the system to the critical point of black hole formation. In the classical approximation such a "neutron star" outside produces a gravitational field identical to the one produced by a classical Schwarzschild black hole. So why is the case that for the neutron star the quantum effects are not important whereas for a black hole of the same mass they are absolutely crucial?

In order to answer this question let us reduce the quantum portrait of the above system to its bare essentials. We are dealing with a source, represented by a multi-baryon state of occupation number  $N_B \sim 10^{57}$  and size  $L \sim 10^6$  cm. This source is not a Bose-Einstein condensate, since baryons (even if spin-0) are not in the same state, and in particular their de Broglie wave-lengths are much shorter than the size of the system. However, these baryons source gravity and produce gravitational field that contains approximately  $N \sim 10^{77}$  gravitons. The two occupation numbers are related as,

$$N = N_B^2 (m_B/M_P)^2, \quad (2)$$

where  $M_P$  is the Planck mass, and we shall also define the Planck length  $L_P \equiv \hbar/M_P$ . Unlike baryons, these gravitons are much closer to being a Bose-Einstein condensate, because the majority of them occupy the same state, and in particular have comparable characteristic wave-lengths  $L$  given by the size of the baryonic source,  $L \sim L_{star}$ . Due to this, in contrast to the baryonic constituents of the star, for gravitons we can define an universal quantum coupling,

$$\alpha \equiv (L_P/L)^2 \quad (3)$$

and the corresponding 't Hooft's coupling  $\lambda$  given by (1). The only caveat is that the graviton condensate is not self-sustained as long as  $L_{star} > r_g$ . That is, the gravitational mass (self-energy) of the graviton condensate  $M_{gr} = N\hbar/L$  is below the mass of the baryonic source  $M_{star} = N_B m_B$  and alone is not enough to keep the gravitons together. Classically, we think of this situation as the size of the source  $L_{star}$  being larger than the corresponding gravitational radius  $r_g \equiv M_{star} L_P^2/\hbar$ , but we see that the quantum-mechanical reason is that the 't Hooft coupling is far from criticality. Indeed, expressing  $N$  and  $\alpha$  through their dependence on  $L$  and  $r_g$ , we have,

$$\lambda \equiv N\alpha = (r_g/L)^2 = (r_g/L_{star})^2. \quad (4)$$

Thus, the classical statement that a given source is not a black hole ( $r_g < L_{star}$ ), quantum-mechanically translates as the condition that the 't Hooft coupling of graviton condensate is weak,  $\lambda < 1$ . Thus, the standard semi-classical expansion in powers of  $r_g/L$  is nothing but an expansion in the 't Hooft coupling  $\lambda$ . This expansion ignores additional  $1/N$ -effects. That is, it represents a planar approximation:

$$\lambda = \text{fixed}, \quad N = \infty. \quad (5)$$

Such approximation is justified *only* as long as  $\lambda$  is sub-critical.

Now imagine that by changing the parameters of the model (say, by decreasing a stabilizing force) we bring the source to the point  $L_{star} = r_g$ . Classically, we think of this point as a point of classical black hole formation, but in reality this is a critical point of a *quantum* phase transition! As we have shown [3], there are dramatic quantum effects which take place at this point. In particular, of order  $N$  Bogoliubov modes of the graviton condensate become gapless and nearly degenerate. The condensate starts a quantum depletion, leakage and a subsequent collapse. This is the underlying quantum-mechanical nature of the process that semi-classically is viewed as Hawking evaporation. But, Hawking's semi-classical limit in our language corresponds to planar limit, in which only  $\lambda$ -corrections are kept whereas

$1/N$ -corrections are not taken into the account. In reality every act of emission differs from this idealized approximation by  $1/N$ -corrections. Our point is to stress the extreme importance of these corrections.

In other words for a generic BEC the quantity  $1/N$  measures the *quantum noise* of the system. For  $N \gg 1$  these effects can be thought as very tiny and effectively negligible. This is in fact the case provided the constituents of the system are not entangled. However, and this is the key of the quantum phase transition, quantum noise makes a dramatic difference when the constituents are maximally entangled i.e at the quantum critical point. In fact at this point the entanglement entropy for the reduced one particle density matrix becomes maximal and a new branch of light Bogoliubov modes appear [10]. This is something completely alien to any classical system. In this sense black holes are intrinsically quantum objects. This phenomenon is fully missed in classical or semi-classical analysis. Its discovery requires a microscopic quantum view.

*Thus, even macroscopic black holes are quantum.*

This is a very general message we wanted to bring across in this short note.

## 2 Quantumness Versus Semi-Classicality

Can the quantum effects we are pointing out be somehow read off in the standard semi-classical treatment? We shall now explain why the answer is negative.

In standard treatment the black holes are introduced through the metric  $g_{\mu\nu}(x)$ , which is an intrinsically-classical entity. The effects of quantum gravity are then thought to be accounted in terms of quantum corrections to metric, without abandoning the very concept of the (classical) metric. In other words, both before and after the quantum corrections the metric itself is treated as a background classical field. The role of the quantum gravity is reduced to understanding the rules of corrections according to which this classical entity changes, without abolishing the very concept of a background metric. We claim that for certain macroscopic systems, such as black holes, the above treatment is inconsistent.

It is absolutely crucial to understand that  $1/N$ -corrections are intrinsically-quantum and can never be recast in form of some quantum-back-reacted metric. Instead the very notion of the metric needs to be abandoned and be treated as approximate. In order to explain this, let us go through the three levels of quantumness:

$$\begin{aligned} \text{Classical: } \hbar = 0, \frac{1}{N} = 0; \\ \downarrow \\ \text{Semi-Classical: } \hbar \neq 0, \frac{1}{N} = 0; \\ \downarrow \\ \text{Quantum: } \hbar \neq 0, \frac{1}{N} \neq 0. \end{aligned}$$

Consider a light test body and a heavy source of energy momentum tensors  $\tau_{\mu\nu}$  and  $T_{\mu\nu}$  respectively. In classical GR a scattering of a probe on a source can be understood in terms of a propagation of the former in a background classical metric created by the latter, with an amplitude,

$$A_{Cl} = \int_x g_{\mu\nu}(x)\tau^{\mu\nu}(x), \quad (6)$$

where integration is performed over a four-dimensional space-time volume. The metric  $g_{\mu\nu}$  is obtained by solving the classical Einstein equation with the source  $T_{\mu\nu}$ . It is well-known that exactly the same amplitude can be reproduced by summing up the infinite series of tree-level Feynman diagrams with intermediate graviton lines,

$$A = G_N \int_{x,y} T(x)\Delta(x-y)\tau(y) +$$

$$G_N^2 \int_{x,y,z,w} T(x)T(y)\Delta(x-w)\Delta(y-w)\Delta(z-w)O(w)\tau(z) + \dots \quad (7)$$

Here  $\Delta(x)$  is a graviton propagator, and tensorial indexes are suppressed. These series are non-zero despite the fact that we are working in  $\hbar = 0$  limit, and they fully reproduce the result obtained by considering the motion in the classical metric (6). In fact, order by order the above series reproduce the expansion of a classical solution of Einstein equation in series of  $G_N$ . For example, for a spherical source of mass  $M$ , the above series reproduce the expansion of Schwarzschild metric in series of  $\frac{r_g}{r}$  where  $r_g \equiv 2G_N M$  is the gravitational radius of the source and  $r$  is a radial coordinate [11].

Let us now move towards the quantum picture,  $\hbar \neq 0$ . The standard idea about how to take into the account quantum gravity effects is to integrate out loops and write down the  $\hbar$ -corrected effective action for  $g_{\mu\nu}(x)$ . The action obtained in this way will in general contain an infinite series of curvature invariants, with each power of curvature being accompanied by a factor of  $L_P^2$  (in absence of other input scales). The effective quantum-corrected metric is then represented as a solution to the equations obtained by varying the effective action. In this philosophy, the quantum gravity effects are accounted in form of a back reaction to the classical metric. The quantum-corrected metric obtained in such a way, although formally includes  $\hbar$ -effects is still treated as a classical entity:

$$g_{\mu\nu}(x) \rightarrow g'_{\mu\nu} = g_{\mu\nu}(x) + \delta g_{\mu\nu}(x, \hbar). \quad (8)$$

In particular, the quantum-corrected scattering of a probe over the source in this limit can still be reduced to the effects of propagation in the background metric obtained by replacing in (6)  $g_{\mu\nu}$  by  $g'_{\mu\nu}$ .

As a result, such an analysis is not really quantum, but rather *semi-classical*, as it never resolves the quantum constituents of the metric ( $1/N = 0$ ).

*This is the essence of semi-classical approximation: It reduces quantum effects to the  $\hbar$ -correction of classical entities, without resolving their constituency.*

We thus claim, that the above treatment of quantum gravity misses out the  $1/N$ -corrections, which are absolutely crucial for black holes. The physics generated by these corrections, is impossible to be reproduced by any quantum corrections to the classical metric. Instead, the very notion of the metric must be abandoned and only treated as approximate.

In our language it is clear why this is the only consistent treatment. Indeed, it is impossible to keep all three quantities  $M, L_P$  and  $\hbar$  finite, and simultaneously keep  $1/N = 0$ . Putting it differently,  $r_g$ -corrections are corrections in terms of series in 't Hooft coupling  $\lambda = (\alpha N)$ , which are different from  $1/N$ -series. Naively, it seems that one can consistently keep the former while discarding the latter by taking the planar limit (5). However, this is an illusion, since in this limit also the black hole evaporation time ( which scales as  $N^{3/2}$ ) becomes infinite, so that the integrated effect is still finite.

Notice, that  $1/N$  corrections are present already in the tree-level scattering of a probe over a black hole and come from the processes in which the probe exchanges the momentum with individual constituent of the graviton condensate. Because the condensate is at the quantum critical point, such exchanges cost  $1/N$  as opposed to  $e^{-N}$ .

The resulting quantum scattering amplitude  $A_Q$  differs from its classical counterpart by  $1/N$ -effects,

$$A_Q = A_{Cl} + \mathcal{O}(1/N). \quad (9)$$

However, the crucial point is that, unlike the semi-classical case, these effects cannot be recast in form of propagation in any new corrected metric. That is, the quantum amplitude  $A_Q$  does not admit any representation in form of

$$A_Q = \int_x g_{\mu\nu}(x)' \tau^{\mu\nu}, \quad (10)$$

where  $g_{\mu\nu}(x)^l$  could be any sensible metric. Such representation of the amplitude ceases to exist as soon as we correctly account for  $1/N$ -effects.<sup>1</sup>

### 3 $1/N$ -Corrections Account for Information

Obviously, the  $1/N$ -corrections to semi-classical results are much stronger than the naively-expected  $e^{-N}$ -correction. However, from the first glance these enhanced corrections still look very small. This smallness is an illusion and in reality  $1/N$ -corrections are precisely what one needs for the correct accounting of information-retrieval in black hole decay.

The reason is that  $1/N$ -corrections to planar results are taking place for each act of emission. Over a black hole half-lifetime this deviation accumulates to order-one effect, which is sufficient to start resolving the information at order-one rate. As we have shown [2], this reproduces Page's time [12], which automatically follows from our picture.

It is crucial that  $N$  is not a fixed characteristics of the theory (unlike in gauge theories with  $N$ -colors) but rather a characteristic of a particular black hole. Moreover, it is a good characteristic only during the time  $\sim \sqrt{N}L_P$ , during which the black hole depletes and leaks decreasing  $N$  by one unit. This process continues self-similarly

$$N \rightarrow N - 1 \rightarrow N - 2 \dots \quad (11)$$

Each elementary step of the cascade reveals a distinct feature (information) encoded in a  $1/N$ -suppressed deviation from the Hawking's idealized semi-classical result. To resolve this feature immediately is extremely improbable, but this is not an issue. Unitarity does not require the information to be resolvable immediately. It only requires that information is resolvable on the time-scale of black hole evaporation.

This is exactly the case, since probability to recognize the given feature over the black hole half-lifetime, which scales as  $\sim N^{3/2}L_P$ , is of order one. In other words, the increase of  $N$  suppresses the probability of decoding a given feature per emission time as  $N^{-3/2}$ , but correspondingly the black hole life-time increases as  $N^{3/2}$ , so that the product is always of order one. As a result, for arbitrarily large  $N$  the information starts to be recognizable at order-one rate after a half-lifetime of a black hole.

To reiterate the picture, let us imagine a situation when Alice is observing evaporation of a solar mass black hole. For simplicity, we shall exclude all non-gravitational species from the theory. Then from our point of view, such a black hole is a BEC of approximately kilometer wavelength gravitons of occupation number  $N \sim 10^{76}$ , with  $\sim N$  gapless Bogoliubov modes. From the point of view of the quantum information this black hole is a message encoded in a  $N \sim 10^{76}$  long sequence of 0-s and 1-s,

$$BH = (0, 0, 1, 0, 1, 1, 1, \dots), \quad (12)$$

where, the sequence is determined by the state of Bogoliubov modes.

After every time interval of approximately  $\Delta\tau \sim \sqrt{N}L_P \sim 10^{-5}$  sec the message emits a graviton and becomes shorter by one unit. In the semi-classical (planar) approximation (5) Alice thinks that she sees a thermal evaporation of a black hole with a featureless (exactly thermal) spectrum. However, in reality she sees a depletion and leakage of graviton BEC, with features encoded in sub-leading  $1/N$ -corrections. As we know [1, 2], this correction to the black hole rate goes as  $\Gamma_{feature} \sim N^{-3/2}L_P^{-1}$ . Thus, probability for Alice to recognize the feature per emission time is  $\Delta P = \Gamma_{feature}\Delta\tau \sim 1/N$ . For a solar mass black hole this probability is  $10^{-71}$  and is tiny. However, the time-scale available for Alice to resolve the feature is also enormous, and is given by the black hole life-time  $\tau = N\Delta\tau \sim N^{3/2}L_P \sim 10^{73}$ sec! The probability to resolve the feature during this time is

$$P \sim \Delta PN \sim 1. \quad (13)$$

<sup>1</sup>The quantity  $N$  defined in [1] as a measure of classicality also emerges in [14]. However, there this quantity is unrelated to any quantum resolution of the constituents of the metric.

Notice, that by then Alice has witnessed  $\sim N$  acts of emission and had of order  $\tau \sim N^{3/2}L_P$  time for analyzing each of them. Consequently she accumulated order one knowledge about roughly the half of the structure of the message. This knowledge brings her to the point starting from which she begins to resolve information with order one probability.

It is important to stress that we are not modifying Hawking's entanglement at each step of the emission process by a factor  $\frac{1}{N} \ln 2$ . This would not do the job of reproducing Page's time [13]. What we are instead doing is to use  $1/N$  effects ( at the quantum critical point ) to trigger depletion of *one* bit of information with probability  $1/N$  in *each step* of the evaporation process.

This completes our point of nullifying the information paradox. Notice, that increasing  $N$  is not changing the final answer, since although it suppresses the feature per emission time, it also increases the available time for resolving it so that the two effects always balance each other.

This analysis also makes clear the fundamental mistake in the standard semi-classical reasoning. If the features were suppressed by  $e^{-N}$  instead of  $1/N$ , Alice would have never had enough time for resolving these features, and the paradox would follow. It is now clear that this "paradox" was a result of our misconception about the quantum properties of macroscopic black holes.

In summary the Bose-Einstein condensate approach to the black hole information paradox lies on the following basic points:

- Black hole emission is due to quantum depletion triggered by quantum noise. This quantum emission is not based on any form of Hawking pair creation in the near horizon geometry. It is a perfectly unitary process with a rate determined by the microscopic dynamics of the condensate.
- This emission rate is modified by  $1/N$  effects.
- In particular if we tag a subset of  $N_B$  quanta the rate of leakage of any form of information encoded in those quanta ( as could be a baryon number of the black hole ) goes like  $\frac{N_B}{N^{3/2}}$ . This in particular means that the black hole can successfully hide some information as its baryon number – or any other form of message encoded within the tagged quanta – but only until reaching the half-evaporation point. The *observable* prediction of this picture is  $1/N$  hair. In case of baryon number this hair can have observable effects for astrophysical black holes, that are mostly made out of baryons.

In this respect we need to stress the following. Of course, one could argue that a general believe that unitary quantum gravity should not result in information paradox implicitly assumes that some mechanism should purify Hawking radiation. However, an issue that has never been addressed previously is how this potential purification of Hawking radiation affects the *folk dictum* that in any consistent theory of gravity there are no global symmetries. We want to stress that in the Bose-Einstein portrait approach to the mechanism of information retrieval, gravity is perfectly consistent with global symmetries [2]. Obviously, how purification affects the *dictum* depends on the strength of the corrections used to purify the emitted quanta. Our  $1/N$ -corrections revoke the *dictum*.

In short, semi-classicality breaks down whenever quantum noise  $1/N$ -effects become significant. This is unavoidably the case at the quantum phase transition point. The black hole emits as a normal quantum system, but its identity card is to be at a *quantum phase transition point*.

Finally, we wish to note on a possible avenue of probing the large  $N$ -picture. Recently, Veneziano [15] suggested a very interesting stringy computation that reveals  $1/N$ -hair in string - string-hole scattering. Viewed as a black hole of occupation number  $N = 1/g_s^2$  ( $g_s \equiv$  string coupling), this result represents a manifestation of  $1/N$ -hair suggested by black hole quantum  $N$ -portrait.

## Acknowledgements

We thank Gabriele Veneziano for discussions and for sharing his preliminary results with us. It is a pleasure to thank Stanley Deser, Daniel Flassig, Andrei Gruzinov, Alex Pritzel and Nico Wintergerst for discussions. The work of G.D. was supported in part by Humboldt Foundation under Alexander von Humboldt Professorship, by European Commission under the ERC advanced grant 226371, by TRR 33 “The Dark Universe” and by the NSF grant PHY-0758032. The work of C.G. was supported in part by Humboldt Foundation and by Grants: FPA 2009-07908, CPAN (CSD2007-00042) and HEPHACOS P-ESP00346.

## References

- [1] G. Dvali, C. Gomez, Black Hole’s Quantum N-Portrait, arXiv:1112.3359 [hep-th]; Landau-Ginzburg Limit of Black Hole’s Quantum Portrait: Self Similarity and Critical Exponent, arXiv:1203.3372 [hep-th].
- [2] G. Dvali, C. Gomez, “Black Hole’s 1/N Hair,” arXiv:1203.6575 [hep-th].
- [3] G. Dvali, C. Gomez Black Holes as Critical Point of Quantum Phase Transition. arXiv:1207.4059 [hep-th]
- [4] Some generalizations of these portrait for cosmological spaces was discussed in [1] and in, P. Binetruy, Vacuum energy, holography and a quantum portrait of the visible Universe, arXiv:1208.4645 [gr-qc].
- [5] S. W. Hawking, *Comm. Math. Phys.* 43 (1975) 199
- [6] J. D. Bekenstein, *Phys. Rev. D* 7 (1973) 2333
- [7] W. Israel, *Phys. Rev.* **164** (1967) 1776; *Commun. Math. Phys.* **8**, (1968) 245; B. Carter, *Phys. Rev. Lett.* **26** (1971) 331. J. Hartle, *Phys. Rev. D* **3** (1971) 2938. J. Bekenstein, *Phys. Rev. D* **5**, 1239 (1972); *Phys. Rev. D* **5**, (1972) 2403; *Phys. Rev. Lett.* **28** (1972) 452. C. Teitelboim, *Phys. Rev. D* **5** (1972) 294.
- [8] S.W. Hawking The Unpredictability of Quantum Gravity. *Commun.Math.Phys.* 87 (1982) 395-415
- [9] G. ’t Hooft, A Planar Diagram Theory for Strong Interactions. *Nucl.Phys.* B72 (1974) 461
- [10] D. Flassig, A. Pritzel and N. Wintergerst, "Black Holes and Quantumness on Macroscopic Scales", to appear. For the analysis of other aspects see: F .Berkhahn and F. Niedermann; Microscopic picture of non-relativistic classicalons, to appear
- [11] M. J. Duff, "Quantum Tree Graphs and the Schwarzschild Solution," *Phys. Rev. D* 7, 2317-2326 (1973); "Covariant gauges and point sources in general relativity," *Annals Phys.* 79, 261-275 (1973)
- [12] D.N. Page, Information in black hole radiation. *Phys.Rev.Lett.* 71 (1993) 3743-3746; hep-th/9306083
- [13] S. D. Mathur, The Information paradox: A Pedagogical introduction, *Class.Quant.Grav.* 26 (2009) 224001, 0909.1038. The information paradox: conSSicts and resolutions, hep-th/12012079
- [14] R. Brustein, Origin of the blackhole information paradox, arXiv:1209.2686 [hep-th]
- [15] G. Veneziano, "Quantum hair and the string - black hole correspondence", to appear.

# Massive spin-2 theories

Sarah Folkerts\*, Cristiano Germani<sup>†</sup> and Nico Wintergerst<sup>‡</sup>

Arnold Sommerfeld Center, Ludwig-Maximilians-Universität, Theresienstr. 37, 80333 München, Germany

## Abstract

We give an introduction to massive spin-2 theories (including massive gravity) and the problem of their non-linear completion. We review the Boulware-Deser ghost problem and two ways to circumvent classic no-go theorems. In turn, massive spin-2 theories are not uniquely defined. In the case of truncated theories, we show that the Boulware-Deser ghost may only be avoided if the derivative structure of the theory is not tuned to be Einsteinian.

## 1 Introduction

If low energy physics is described by the language of effective field theory (EFT), an important question to ask is what (interacting) degrees of freedom can in principle be used on four-dimensional Minkowski space.

In a Poincaré invariant theory, such as an EFT constructed on a four-dimensional flat space, different degrees of freedom as well as their corresponding one-particle states may be labelled by their mass and spin, which are Casimir operators of the Poincaré group.

This classification is of course most useful when the one-particle states under consideration are eigenstates of the full Hamiltonian. However, in almost all cases diagonalization of the interacting Hamiltonian is extremely involved. Therefore, one introduces the concept of *asymptotic states*, eigenstates of the quadratic part of the Hamiltonian. This is due to the fact that a typical measurement involves a scattering experiment where the experimental apparatus may only monitor the *in* and *out* states far away from the scattering interactions. This brings about the concept of the S-matrix

$$P(in, out) = \langle in|S|out \rangle, \quad (1)$$

where  $P \leq 1$  is the probability that the *in* asymptotic (far away from the scattering process) state scatters into the *out* asymptotic state where, importantly, *in* and *out* states are eigenstates of the *free* Hamiltonian. In almost all cases, these states are also eigenstates of the Casimir operators of the Poincaré group, thus allowing the above classification on the asymptotic states. Here, we will follow this trend.

Fundamental theories must have that for all processes  $P \leq 1$ . This condition is what is commonly called the unitarity bound. In an EFT instead, the considered action is only an approximation to the full quantum effective action; it corresponds to the first terms of a perturbative expansion in terms of the dimensionless parameters  $E/\Lambda_s$  and  $\phi/\Lambda_s$ , where  $E$  is the energy,  $\phi$  represents any field content and  $\Lambda_s$  is the so-called cut-off or strong coupling scale. Of course, if  $\Lambda_s \rightarrow \infty$ , the theory is valid up to any energy scale and it is called *renormalizable*.

Whenever the perturbative expansion breaks down, for sufficiently high transfer-energies  $E > \Lambda_s$ , one obtains  $P > 1$ . In this case, if one insists on this theory still being described in terms of a perturbative expansion, it must be rewritten in terms of new degrees of freedom materializing at an energy scale  $E > \Lambda_s$ . This is what is commonly called a Wilsonian UV completion.

---

\*E-mail: Sarah.Folkerts@physik.uni-muenchen.de

<sup>†</sup>E-mail: cristiano.germani@lmu.de

<sup>‡</sup>E-mail: nico.wintergerst@physik.uni-muenchen.de

Theories with massive and massless spin 0 and spin 1/2 fields together with massless spin 1 fields can be constructed without violation of unitarity. This is, in fact, the content of the Standard Model of particle physics.

Any other degrees of freedom will inexorably violate unitarity at some energy scale (non-renormalizable theories). If it was not for gravity, a massless spin 2 particle, we could just ignore these other degrees of freedom. However, as gravitational interactions *do* exist, one may ask whether other non-renormalizable degrees of freedom also exist up to energy scales that are not experimentally probed yet.

A self-interacting massive vector field with mass  $m$  has a typical strong coupling scale  $\Lambda \sim m$ . The violation of unitarity is due to the fact that the longitudinal mode of the vector, which is non-physical in the massless case, has a polarization  $\vec{\epsilon} \propto \frac{\vec{k}}{m}$ . Thus, the larger is the mass, the later we need to postpone the completion necessary to restore unitarity.

This can be understood by (schematically) considering the interaction in Fourier space

$$\int d^4x A_\mu J^\mu \sim \int dt d^3k J_{\mu;(\mathbf{k})} \sum_{\lambda=1}^3 \epsilon_{\mathbf{k},\lambda}^\mu A_{\mathbf{k}}, \quad (2)$$

where the sum extends over the three polarizations defined by the conditions

$$\begin{aligned} \mathbf{k}_\mu \epsilon_{\mathbf{k},\lambda}^\mu &= 0, \\ \epsilon_{\mu;\mathbf{k},\lambda} \epsilon_{\mathbf{k},\lambda}^\mu &= 1. \end{aligned} \quad (3)$$

The spatial part of the longitudinal polarization is defined to be parallel to the three-momentum, i.e.  $\epsilon_{\mathbf{k},3}^i \propto \mathbf{k}^i$ . Explicitly, it takes on the form

$$\epsilon_{\mathbf{k},3}^\mu = \left( \frac{|\mathbf{k}|}{m}, \frac{\mathbf{k}}{|\mathbf{k}|} \frac{E_{\mathbf{k}}}{m} \right), \quad (4)$$

thus giving rise to a vertex

$$J_{\mu;(\mathbf{k})} \epsilon_{\mathbf{k},3}^\mu A_{\mathbf{k}} \quad (5)$$

which becomes strong at energies of order  $m$ .

Note that for large  $|\mathbf{k}|$ ,

$$\epsilon_{\mathbf{k},3}^\mu \approx \frac{1}{m} k^\mu. \quad (6)$$

This signals a straightforward way to avoid the violation of unitarity. If the source  $J_\mu$  is conserved,  $\partial_\mu J^\mu = 0$ , in the large momentum limit  $J_{\mu;(\mathbf{k})} \epsilon_{\mathbf{k},3}^\mu \rightarrow 0$ .

We can understand this effect in a different way. We can construct one particle states by defining creation and annihilation operators  $a_{\mathbf{k}}^\lambda$ , generating the eigenstates of the non-interacting Hamiltonian. We write

$$A_\mu^\lambda = \int \frac{d^3k}{\sqrt{2E_{\mathbf{k}}}} \epsilon_\mu^\lambda(\mathbf{k}) \left( a_{\mathbf{k}}^\lambda e^{i\mathbf{k}\cdot\mathbf{x}} + a_{\mathbf{k}}^{\dagger\lambda} e^{-i\mathbf{k}\cdot\mathbf{x}} \right). \quad (7)$$

At the same time we can define a new scalar field  $\phi$  as

$$\phi = \int \frac{d^3k}{\sqrt{2E_{\mathbf{k}}}} \left[ \left( i a_{\mathbf{k}}^{(3)} \right) e^{i\mathbf{k}\cdot\mathbf{x}} + \left( i a_{\mathbf{k}}^{(3)\dagger} \right) e^{-i\mathbf{k}\cdot\mathbf{x}} \right]. \quad (8)$$

On an asymptotic state  $|\mathbf{k}\rangle$  of four-momentum  $k^\mu$  one has

$$\partial_\mu \phi |\mathbf{k}\rangle = \frac{1}{\sqrt{2E_{\mathbf{k}}}} k_\mu \left( a_{\mathbf{k}}^{(3)} e^{i\mathbf{k}\cdot\mathbf{x}} + a_{\mathbf{k}}^{\dagger(3)} e^{-i\mathbf{k}\cdot\mathbf{x}} \right) |\mathbf{k}\rangle. \quad (9)$$

Henceforth

$$\left( A_\mu^{(3)} - \frac{1}{m} \partial_\mu \phi \right) |\mathbf{k}\rangle \underset{\mathbf{k} \gg m}{\sim} \frac{m}{|\mathbf{k}|} \hat{k}_\mu a_{\mathbf{k}}^{(3)} |\mathbf{k}\rangle \underset{\mathbf{k} \rightarrow \infty}{\rightarrow} 0. \quad (10)$$

Here,  $\hat{k}_\mu$  is the unit vector pointing in the direction of  $\mathbf{k}$ . We thus see that the longitudinal polarization in the high energy limit is well described by a scalar field up to corrections  $\mathcal{O}\left(\frac{m}{\mathbf{k}}\right)$ . This is the essence of the Stückelberg decomposition of the massive vector. There, the field is decomposed into a massless vector and a scalar where the scalar is nothing else than the re-incarnation of the gauge direction of the massless case.

To be precise, in the massless case the action is invariant under the gauge transformation

$$A_\mu \rightarrow A_\mu + \frac{\partial_\mu \phi}{m}, \quad (11)$$

for any  $\phi$  and some mass scale  $m$ . In the massive case however  $\phi$  represents the extra polarization at high energies as in (10). In this case, we can decompose

$$A_\mu = \tilde{A}_\mu + \frac{\partial_\mu \phi}{m}. \quad (12)$$

As a consequence,  $A_\mu$ , and hence any action constructed from it, is invariant under transformations of  $\tilde{A}_\mu$  of the type (11) (U(1)) if the change is absorbed by a shift in the scalar  $\phi$ . We see that the interaction of the scalar degrees of freedom to external conserved sources  $J^\mu$  is absent:

$$\int d^4x A_\mu J^\mu = \int d^4x \tilde{A}_\mu J^\mu + \frac{1}{m} \text{boundary}. \quad (13)$$

Thus a massive linearly interacting vector can exist without unitarity problems. The would be strong coupling scale appears in fact only in the boundary term.

The question is now whether interacting higher spins  $s \geq 3/2$  can be consistently constructed. First of all, one notes that, because of the non-trivial tensorial structure of  $s \geq 3/2$  fields, all interactions must be unitarity violating [1]. Furthermore, in the case of massive fields, the extra longitudinal polarization does not decouple in the massless limit even if the field interacts with a conserved source. This is simply due to the fact that these extra polarizations always carry contributions which are not proportional to the four-momentum even in the high-energy limit.

Let us take as an example a massive spin 2 field  $h_{\alpha\beta}$ . Similar to the massive vector field discussed above, the properties of this theory can also be investigated through a helicity or *linear* Stückelberg decomposition.

The decomposition of the field into helicity eigenmodes is in complete analogy to the massive vector. For high energies the helicity-1 component (or vectorial polarization) can be described by the derivative of a Lorentz vector ( $A_\mu$ ), whereas the helicity-0 component (or longitudinal polarization) can be described by a scalar field  $\chi$  [2,3]. The helicity-2 component (the transverse polarization) is described by a tensor  $\tilde{h}_{\mu\nu}$ .

One then decomposes the massive spin-2 field as

$$h_{\mu\nu} = \tilde{h}_{\mu\nu} + \frac{\partial_{(\mu} A_{\nu)}}{m} + \frac{1}{3} \left( \frac{\partial_\mu \partial_\nu \chi}{m^2} + \frac{1}{2} \eta_{\mu\nu} \chi \right). \quad (14)$$

Here we used the symmetrization convention  $a_{(\mu} b_{\nu)} = \frac{1}{2}(a_\mu b_\nu + a_\nu b_\mu)$ .

Similar to the massive vector, interactions of the longitudinal polarization violate unitarity. The coupling to the energy momentum tensor is of the form (recall that the energy momentum tensor must be of dimension 4)

$$\frac{1}{\Lambda_s} \int d^4x h_{\alpha\beta} T^{\alpha\beta} = \frac{1}{6\Lambda_s} \int d^4x \chi T + \dots, \quad (15)$$

and violates unitarity at the scale  $\Lambda_s$ .

If we were instead considering a non-conserved source  $J^{\mu\nu}$  of mass dimension  $d \geq 2$ <sup>1</sup> we would have in addition the interaction

$$\int d^4x h_{\alpha\beta} J^{\alpha\beta} = \frac{\Lambda^{3-d}}{3m^2} \int d^4x \partial_{\mu\nu} \chi \tilde{J}^{\mu\nu} + \dots, \quad (16)$$

where  $\Lambda$  is the mass scale of the source  $J$  and  $\tilde{J} = J/\Lambda^{3-d}$  is the dimensionless source. This interaction creates a strong coupling scale  $\Lambda_s \equiv (\frac{3m^2}{\Lambda^{3-d}})^{\frac{1}{d-1}}$  proportional to the mass  $m$ .

What we thus see is that theories describing interactions of fields of spin  $s \geq 3/2$ , as EFTs on a Minkowski background, cannot be fundamental (unless free) and must be UV completed in the Wilsonian sense if they are to be described in perturbation theory. For a different route to UV completion see, e.g. [4–6].

A Poincaré invariant consistent theory of massless spin-2, at least at the lowest momentum expansion, must be Einstein's theory [7, 8]. Therefore, at least in the low momentum limit, a massless spin-2 theory is unique up to a strong coupling scale  $\Lambda_s$ . The question we would like to address is whether a similar "uniqueness" theorem holds for a massive spin 2 at least up to a generic strong coupling scale  $\Lambda_s$ . As we shall demonstrate, this is not the case.

## 2 Massive spin-2 without self-interactions

The action of a free massive spin-2 particle is given by what is commonly called the Fierz-Pauli action and is unique [9].

Its construction can be understood most easily by considering the aforementioned helicity or Stückelberg decomposition. Demanding the absence of higher derivatives, which signal the appearance of new degrees of freedom, removes all arbitrariness in the action; only the Fierz-Pauli form allows for this property. It is given by

$$S = \int d^4x \mathcal{L} = \int d^4x \left( \partial_\mu h^{\mu\nu} \partial_\nu h - \partial_\mu h^{\rho\sigma} \partial_\rho h_\sigma^\mu + \frac{1}{2} \partial_\mu h^{\rho\sigma} \partial^\mu h_{\rho\sigma} - \frac{1}{2} \partial_\mu h \partial^\mu h - \frac{1}{2} m^2 (h^{\mu\nu} h_{\mu\nu} - h^2) \right), \quad (17)$$

where  $h \equiv h_\mu^\mu$ .

Inserting (14) into the quadratic action (17) leads to

$$\begin{aligned} \mathcal{L}_{\text{PF}} &= \tilde{h}^{\mu\nu} \mathcal{E}_{\mu\nu}^{\rho\sigma} \tilde{h}_{\rho\sigma} - \frac{1}{8} F_{\mu\nu} F^{\mu\nu} + \frac{1}{12} \chi \square \chi - \frac{1}{2} m^2 \left( \tilde{h}^{\mu\nu} \tilde{h}_{\mu\nu} - \tilde{h}^2 \right) + \frac{1}{6} m^2 \chi^2 \\ &+ \frac{1}{2} m^2 \chi \tilde{h} + m \left( \tilde{h} \partial_\mu A^\mu - \tilde{h}^{\mu\nu} \partial_\mu A_\nu \right) + \frac{m}{2} \chi \partial_\mu A^\mu, \end{aligned} \quad (18)$$

where  $\tilde{h}^{\mu\nu} \mathcal{E}_{\mu\nu}^{\rho\sigma} \tilde{h}_{\rho\sigma} = \partial_\mu \tilde{h}^{\mu\nu} \partial_\nu \tilde{h} - \partial_\mu \tilde{h}^{\rho\sigma} \partial_\rho \tilde{h}_\sigma^\mu + \frac{1}{2} \partial_\mu \tilde{h}^{\rho\sigma} \partial^\mu \tilde{h}_{\rho\sigma} - \frac{1}{2} \partial_\mu \tilde{h} \partial^\mu \tilde{h}$  describes the linear part of the Einstein action. For  $k^2 \gg m^2$ , the action becomes diagonal in field space. The individual kinetic terms for  $\tilde{h}_{\mu\nu}$  and  $A_\mu$  correspond to massless linearized Einstein and Maxwell theory, respectively. Thus, in the limit where the mixing of the individual fields can be neglected,  $\tilde{h}_{\mu\nu}$  carries precisely the two helicity-2,  $A_\mu$  the two helicity-1 and  $\chi$  the single helicity-0 degrees of freedom.

Note that requiring the diagonalization of the kinetic term fixes the relative factor of 1/2 between the  $\chi$ -terms in (14). Similarly, the factors of  $m$  in (14) normalize the kinetic terms. The coefficient of the kinetic term for  $\chi$  is determined by the coupling of  $h_{\mu\nu}$  to sources:  $\int d^4x T^{\mu\nu} h_{\mu\nu}$ . The propagator of a massive spin-2 field  $h_{\mu\nu}$  between two conserved sources  $T_{\mu\nu}$  and  $\tau_{\mu\nu}$  is given by

<sup>1</sup>For dimension  $d < 2$  we just have kinetic or mass mixing.

$$\begin{aligned}
T^{\mu\nu} D_{\mu\nu,\rho\sigma} \tau^{\rho\sigma} &= T^{\mu\nu} \frac{(\eta_{\mu\rho}\eta_{\nu\sigma} + \eta_{\mu\sigma}\eta_{\nu\rho} - \frac{2}{3}\eta_{\mu\nu}\eta_{\rho\sigma})}{p^2 - m^2} \tau^{\rho\sigma} \\
&= T^{\mu\nu} \frac{(\eta_{\mu\rho}\eta_{\nu\sigma} + \eta_{\mu\sigma}\eta_{\nu\rho} - \frac{1}{2}\eta_{\mu\nu}\eta_{\rho\sigma})}{p^2 - m^2} \tau^{\rho\sigma} + T^{\mu\nu} \frac{1}{6} \frac{\eta_{\mu\nu}\eta_{\rho\sigma}}{p^2 - m^2} \tau^{\rho\sigma}. \quad (19)
\end{aligned}$$

The first term in the last line corresponds to the helicity-2 state  $\tilde{h}_{\mu\nu}$ . The second term is an additional interaction from the extra scalar degree of freedom  $\chi$  and fixes the overall normalization of it in our helicity decomposition. By considering non-conserved sources one can accordingly fix the normalization of  $A_\mu$  in (14).

For  $m = 0$ , the action (17) describes linearized Einstein gravity and is invariant under linearized diffeomorphisms,

$$h_{\mu\nu} \rightarrow h_{\mu\nu} + \frac{1}{2}(\partial_\mu \xi_\nu + \partial_\nu \xi_\mu), \quad (20)$$

where  $\xi_\mu(x)$  defines the linear coordinate transformation. The gauge redundancy fixes the relative coefficients of the two-derivative terms. Since both vector and scalar appear with derivatives in the Stückelberg decomposition, the only way for their equations of motion to be second order is for these derivative terms to drop out from the two-derivative kinetic term for  $h_{\mu\nu}$ . In other words, we impose on the kinetic part of the Lagrangian the condition

$$\mathcal{L}(h_{\mu\nu}) = \mathcal{L}(h_{\mu\nu} + \partial_{(\mu} \tilde{A}_{\nu)} + \partial_{\mu\nu} \tilde{\chi}) + \text{boundaries}, \quad (21)$$

where  $\tilde{A}_\mu$  and  $\tilde{\chi}$  are respectively a vector and a scalar. This is equivalent to the gauge invariance (20) for a specific  $\xi_\mu$ .

The uniqueness of said structure can also be understood from a Hamiltonian analysis. Let us first examine the kinetic term. After having integrated by parts such that  $h_{00}$  and  $h_{0i}$  do not appear with time derivatives, the canonical momenta of the Lagrangian (17) are

$$\pi_{ij} = \frac{\partial \mathcal{L}}{\partial \dot{h}_{ij}} = \dot{h}_{ij} - \dot{h}_{ii} \delta_{ij} - 2\partial_{(i} h_{j)0}. \quad (22)$$

The other canonical momenta ( $\pi_{00}$  and  $\pi_{0i}$ ) are zero due to the integration by parts. Inverting (22), one obtains

$$\dot{h}_{ij} = \pi_{ij} - \pi_{kk} \delta_{ij} + 2\partial_{(i} h_{j)0}. \quad (23)$$

Performing the Legendre transformation and rewriting the Lagrangian in terms of the canonical momenta yields

$$\begin{aligned}
\mathcal{L} &= \pi_{ij} \dot{h}_{ij} - \mathcal{H} + 2h_{0i} \partial_j \pi_{ij} + h_{00} (\nabla^2 h_{ii} - \partial_i \partial_j h_{ij}), \\
\text{where } \mathcal{H} &= \frac{1}{2} \pi_{ij}^2 - \frac{1}{4} \pi_{ii}^2 + \frac{1}{2} \partial_k h_{ij} \partial_k h_{ij} - \partial_i h_{jk} \partial_j h_{ik} + \partial_i h_{ij} \partial_j h_{kk} - \frac{1}{2} \partial_i h_{jj} \partial_i h_{kk}. \quad (24)
\end{aligned}$$

The canonical momenta for  $h_{00}$  and  $h_{0i}$  are zero and the variables themselves appear only linearly in terms without time-derivatives. They are Lagrange multipliers which give the constraint equations  $\nabla^2 h_{ii} - \partial_i \partial_j h_{ij} = 0$  and  $\partial_j \pi_{ij} = 0$ . All these constraints commute, in the sense of Poisson brackets, with each other. Hence, the constraints are first class (for an introduction to constrained systems see for example [10, 11]). This is characteristic for theories with a gauge symmetry. The constraints together with the gauge transformations reduce the physical phase space to a four dimensional hypersurface,

which is described by the canonical coordinates of the two physical polarizations of the massless spin-2 graviton and their conjugate momenta.

Adding a mass term to the analysis changes the Hamiltonian and the Lagrangian of (25) in the following way

$$\begin{aligned} \mathcal{L} &= \pi_{ij}\dot{h}_{ij} - \mathcal{H} + m^2 h_{0i}^2 + 2h_{0i}\partial_j\pi_{ij} + h_{00}(\nabla^2 h_{ii} - \partial_i\partial_j h_{ij} - m^2 h_{ii}), \\ \text{where } \mathcal{H} &= \frac{1}{2}\pi_{ij}^2 - \frac{1}{4}\pi_{ii}^2 + \frac{1}{2}\partial_k h_{ij}\partial_k h_{ij} - \partial_i h_{jk}\partial_j h_{ik} + \partial_i h_{ij}\partial_j h_{kk} \\ &\quad - \frac{1}{2}\partial_i h_{jj}\partial_i h_{kk} + \frac{1}{2}(h_{ij}h_{ij} - h_{ii}^2). \end{aligned} \quad (25)$$

Note that the conjugate momenta are unchanged by the additional mass term. However, the structure of the Lagrangian is different and  $h_{0i}$  is no longer a Lagrange multiplier. Nevertheless, it is still non-dynamical and its equation of motion yields the algebraic relation

$$h_{0i} = -\frac{1}{m^2}\partial_i\pi_{ij}. \quad (26)$$

$h_{00}$  still is a Lagrange multiplier and it enforces the constraint

$$\nabla^2 h_{ii} - \partial_i\partial_j h_{ij} - m^2 h_{ii} = 0 \quad (27)$$

which is now of second class. Requiring that the constraint is conserved in time, i.e. that it commutes with the Hamiltonian, gives rise to a secondary constraint. Since  $h_{0i}$  is determined by (26) and  $h_{00}$  gives two second class constraints (one primary and one secondary), the resulting physical phase space is then ten dimensional describing the five physical polarizations of the massive spin-2 particle and their conjugate momenta. Departing from the Fierz-Pauli mass term introduces nonlinearities in  $h_{00}$  and the constraint which fixes the trace  $h_{ii}$  to zero is lost resulting in either a tachyonic or ghost-like sixth degree of freedom [12, 13].

Let us briefly mention coupling to sources. Adding a source term to the Lagrangian (17) of the form  $h_{\mu\nu}T^{\mu\nu}$  does not change the linear constraint analysis. No matter whether the source is conserved,  $\partial_\mu T^{\mu\nu} = 0$ , or not, the source coupling will only introduce  $h_{00}$  and  $h_{0i}$  linearly and without time derivatives and therefore it will not affect the number of constraints. Note that this holds true for any linear coupling of  $h_{\mu\nu}$  to sources.

### 3 Self-interacting theories

We now focus on the question of self-interactions in massive spin-2 theories. We address subtleties in the construction and inquire whether uniqueness theorems can exist similar to the case of the Einstein theory for a massless spin-2 field.

#### 3.1 Boulware-Deser ghost

Boulware and Deser (BD) argued in [13] that simply introducing a mass term for the full nonlinear theory of general relativity reintroduces the sixth degree of freedom which could be tuned away in the Fierz-Pauli theory. Although this result turned out to be not generic, it is instructive to see their reasoning.

Let us first consider pure general relativity. Using the ADM formalism [14] in which a general metric can be re-written as

$$ds^2 = g_{\alpha\beta}dx^\alpha dx^\beta = -N^2 dt^2 + \gamma_{ij}(dx^i + N^i dt)(dx^j + N^j dt), \quad (28)$$

where  $\gamma_{ij} \equiv g_{ij}$ ,  $N \equiv (-g^{00})^{-\frac{1}{2}}$  (lapse),  $N_i \equiv g_{0i}$  (shift). The full action reads (for simplicity we set the Planck mass to one)

$$S = \int d^4x \sqrt{-g} R = \int d^4x (\pi_{ij} \dot{\gamma}_{ij} - NR^{(0)} - N_i R^i - 2(\pi^{ij} N_j - \frac{1}{2} \pi N^i + N^{|i} \sqrt{\gamma})_{|j}), \quad (29)$$

All curvatures are functions of  $\gamma_{ij}$  and  $\pi_{ij}$ , but do not depend on  $N$  or  $N_i$ .  $R$  is the four dimensional Ricci scalar and  $-R^{(0)} \equiv {}^3R + \gamma^{-\frac{1}{2}} (\frac{1}{2} \pi^2 - \pi_{ij} \pi^{ij})$  and  ${}^3R$  is the three dimensional Ricci scalar with respect to the metric  $\gamma_{ij}$ .  $R^i = -2\pi^i_{|j}$ , where the bar “|” denotes covariant differentiation with respect to the spatial metric  $\gamma_{ij}$ .

In the massless theory,  $N$  and  $N_i$  are Lagrange multiplier which enforce first class constraints on the system, thereby eliminating four (and correspondingly eight phase space) degrees of freedom yielding 2 propagating helicities of the massless spin-2 particle. We now introduce the Minkowski background by expanding

$$g_{\alpha\beta} = \eta_{\alpha\beta} + h_{\alpha\beta}, \quad (30)$$

where  $\eta_{\alpha\beta}$  is the Minkowski metric and  $h_{\alpha\beta}$  is a tensor on the flat background. Its indices are consequently raised and lowered by the Minkowski metric. The inverse metric  $g^{\alpha\beta}$  is given by an infinite series of  $h_{\alpha\beta}$  and can be obtained from  $g^{\alpha\mu} g_{\mu\beta} = \delta_{\mu}^{\alpha}$ . At linear order  $N = 1 - \frac{1}{2} h_{00}$  and  $N_i = h_{0i}$  and one recovers the result of the previous section. At nonlinear order, however,

$$N^2 = (1 - h_{00}) - h_{0i} h_{0j} g^{ij}, \quad (31)$$

whereas  $N_i$  remains unchanged.

The Fierz-Pauli mass term  $f = (h_{\mu\nu} h^{\mu\nu} - h^2)$  can nevertheless easily be expressed in terms of  $N_i$  and the nonlinear  $N$  [13],

$$f = h_{ij}^2 - h_{ii}^2 - 2N_i^2 + 2h_{ii}(1 - N^2 - N_i N^i). \quad (32)$$

In contrast to the linear case, here  $N$  (which to linear order is equivalent to  $h_{00}$ ) appears quadratically in the mass term although still appearing linearly in the full non-linear derivative (Einstein) structure of the theory. Therefore now neither  $N$  nor  $N_i$  are Lagrange multipliers.

Thus, at the full non-linear level, the trace  $h_{ii}$  is no longer constrained since the constraint was related to the fact that  $N$  was a Lagrange multiplier. Therefore, there are six degrees of freedom propagating: The so-called Bouleware-Deser ghost propagates on top of the five degrees of freedom of the Fierz-Pauli massive spin-2. We will see that this conclusion, although correct generically, can be avoided for specific theories.

The simplest example is the free Fierz-Pauli theory discussed above. There, since the expansion is truncated at the linear level we have that  $N = 1 - \frac{1}{2} h_{00}$  and the mass term in the Lagrangian is

$$f = h_{ij}^2 - h_{ii}^2 - 2N_i^2 + 2h_{ii}(1 - 2N). \quad (33)$$

Thus, as in the derivative part of the action (the linearized Einstein-Hilbert Lagrangian),  $N$  only appears linearly. In other words, the lapse is here again a Lagrange multiplier, as in General Relativity.

The philosophy of avoiding the BD ghost will be the same for interacting theories: we will search for theories that can be written in terms of a linear lapse function acting as a Lagrange multiplier. In order to do that and to avoid the BD conclusions, we will have to either deform the derivative structure of the massless theory and/or the non-derivative structure.

### 3.2 Cubic interactions for a massive spin-2 particle

We will start by considering the simplest possible interaction, a cubic interaction as described in [2].

There, the idea was to consider a cubic interaction that keeps the structure of the *linear* Fierz-Pauli action. In other words, by deviating from the Einsteinian derivative structure at the cubic order,  $N = 1 - \frac{1}{2}h_{00}$  remains a Lagrange multiplier also in the nonlinear theory. Non-derivative interactions can then be constructed that preserve this property.

This construction can straightforwardly be achieved by considering the most general cubic interaction with at most two derivatives on  $h_{\mu\nu}$ . Demanding linearity in  $h_{00}$  fixes all coefficients besides respective prefactors of the zero- and two-derivative terms.

The unique structure is found to be [2]

$$\begin{aligned} \mathcal{L}^{(3)} = & \frac{k_1}{\Lambda^7} (h^{\alpha\beta} \partial_\alpha h^{\mu\nu} \partial_\beta h_{\mu\nu} - h^{\alpha\beta} \partial_\alpha h \partial_\beta h + 4h^{\alpha\beta} \partial_\beta h \partial_\mu h_\alpha^\mu - 2h^{\mu\nu} \partial_\alpha h \partial^\alpha h_{\mu\nu} + h \partial_\mu h \partial^\mu h \\ & - 3h^{\mu\nu} \partial_\alpha h_\mu^\alpha \partial_\beta h_\nu^\beta - 4h^{\mu\nu} \partial_\nu h_\mu^\alpha \partial_\beta h_\alpha^\beta + 3h \partial_\mu h^{\mu\nu} \partial_\alpha h_\nu^\alpha + 2h^{\mu\nu} \partial^\alpha h_{\mu\nu} \partial_\beta h_\alpha^\beta \\ & - 2h \partial_\alpha h \partial_\beta h^{\alpha\beta} + h^{\mu\nu} \partial_\alpha h_{\nu\beta} \partial^\beta h_\mu^\alpha + 2h^{\mu\nu} \partial_\beta h_{\nu\alpha} \partial^\beta h_\mu^\alpha - h \partial_\alpha h_{\mu\nu} \partial^\nu h^{\mu\alpha} - h \partial_\alpha h^{\mu\nu} \partial^\alpha h_{\mu\nu}) \\ & + \frac{k_2}{\Lambda^5} (2h_\nu^\mu h_\rho^\nu h_\mu^\rho - 3h h_{\mu\nu} h^{\mu\nu} + h^3). \end{aligned} \quad (34)$$

In terms of the components of  $h_{\mu\nu}$ , for example, the non-derivative part is given by

$$\mathcal{L} = \frac{3k_2}{2} h_{00} (h_{ii}^2 - h_{ij}^2) + \text{terms independent on } h_{00}. \quad (35)$$

Hence,  $h_{00}$  and  $h_{0i}$  appear in the same way as in the free action. We do not display the explicit expression for the derivative part because the expression is rather lengthy. Still, one can easily check that also there  $h_{0i}$  remains non-dynamical and can be solved for algebraically, yielding 3 constraints on  $h_{\mu\nu}$ . Furthermore,  $h_{00}$  appears as a Lagrange multiplier in (34) and accordingly eliminates another two degrees of freedom [2].

The fact that the action (34) propagates five degrees of freedom can also be checked in the helicity decomposition (14). Inserting the decomposition into (34) reveals that the corresponding equations of motion are free of higher time derivatives on the helicity components.

Indeed, this is in direct correspondence to the Hamiltonian analysis outlined above. The components  $h_{00}$  and  $h_{0i}$  are exactly those components of  $h_{\mu\nu}$  which can introduce higher time derivatives on the equations of motion as, in terms of helicities, these correspond to  $\partial_0^2 \chi$ ,  $\partial_0 A_0$ ,  $\partial_0 \partial_i \chi$  and  $\partial_0 A_i$ . Therefore, any action free of higher derivatives on the helicities, requires  $h_{00}$  to be a Lagrange multiplier and  $h_{0i}$  to be nondynamical.

Up to boundary terms, one can rewrite the above Lagrangian in a compact form [15] as follows

$$\mathcal{L}^{(3)} = k_1 \epsilon^{\alpha_1 \dots \alpha_4} \epsilon^{\beta_1 \dots \beta_4} \partial_{\alpha_1} \partial_{\beta_1} h_{\alpha_2 \beta_2} \dots h_{\alpha_4 \beta_4} + k_2 \epsilon^{\alpha_1 \dots \alpha_3 \sigma_4} \epsilon_{\sigma_4}^{\beta_1 \dots \beta_3} h_{\alpha_1 \beta_1} \dots h_{\alpha_3 \beta_3}. \quad (36)$$

$\epsilon^{\alpha_1 \dots \alpha_4}$  denotes the totally antisymmetric four-tensor in four dimension. From its antisymmetry properties it is then simple to conclude that the constraint structure of the free Lagrangian is preserved. If there is one  $h_{00}$  in (36), then there cannot be any other factor of it in that term. Therefore,  $h_{00}$  can only appear as a Lagrange multiplier. Terms with  $h_{0i}$  can carry at most one time derivative and one power of  $h_{0i}$  or only spatial derivatives and at most two powers of  $h_{0i}$ ; all other terms have spatial indices. Variation with respect to  $h_{0i}$ , thus, leads to a constraint equation for itself which defines it algebraically in terms of the components  $h_{ij}$ .

### 3.3 Resummed theories

The second possible route to find nonlinear extensions of the Fierz-Pauli theory is to retain the Einsteinian derivative structure and construct a nonlinear extension of the mass term. In this case one searches for a theory preserving a similar constraint structure of the lapse for the full Einstein theory. This approach was taken in [16].

What we learned from the analysis of BD is that the lapse  $N$  cannot be a Lagrange multiplier if the two following assumptions co-exist

- The derivative structure is Einsteinian
- $N$  and  $N^i$  are independent variables.

As we are interested in the class of theories that fulfill the former assumption, one needs to relax the latter, thereby keeping  $N$  as a Lagrangian multiplier such to eliminate the BD ghost. The theory with this property has been found by [16], the so-called dRGT massive gravity.

In other words, the theory of [16] is a deformation of General Relativity with non-derivative term such that [17]

- The derivative structure is Einsteinian.
- $N^i$  can be fully traded by a new variable  $n^i(N, N^i, h_{ij})$ .
- After the field redefinition,  $N$  only appears linearly in the action and without derivatives.

The second condition forces the redefinition to be of type

$$N^i = (\delta_j^i + ND_j^i) n^j, \quad (37)$$

where  $D_j^i$  is an appropriate matrix independent upon  $N$ .<sup>2</sup> Of course, any truncation in powers of  $h_{ij}$  of this construction would bring back the BD ghost.

For our purposes, we adopt the notation of [17]. We write the resummed theory of [16] in terms of the inverse metric  $g^{-1}$  and an auxiliary background metric  $\eta$ . The action of dRGT massive gravity can then be written according to [17] (here we re-introduce the Planck mass  $M_P$ )

$$S = M_P^2 \int d^4x \sqrt{-g} \left[ R(g) + 2m^2 \sum_{n=0}^2 \beta_n e_n(\sqrt{g^{-1}\eta}) \right], \quad (38)$$

where  $m$  is the graviton mass and the  $e_n(\mathbb{X})$  are functions of matrix traces given by

$$e_0(\mathbb{X}) = 1, e_1(\mathbb{X}) = [\mathbb{X}], e_2(\mathbb{X}) = \frac{1}{2}([\mathbb{X}]^2 - [\mathbb{X}^2]). \quad (39)$$

The square brackets denote the trace and  $\beta_0 = 6$ ,  $\beta_1 = -3$  and  $\beta_2 = 1$  for dRGT massive gravity [16,17]. Note that the coefficients are chosen such that the action describes a flat background without a cosmological constant. The matrix  $\sqrt{g^{-1}\eta}$  is defined by  $\sqrt{g^{-1}\eta}\sqrt{g^{-1}\eta} = g^{\mu\nu}\eta_{\nu\rho}$ . Since  $\eta_{\mu\nu}$  transforms as a rank-two tensor, the action (38) is invariant under general coordinate transformations.

Expanding the action (38) to second order in the metric perturbations  $g_{\mu\nu} = \eta_{\mu\nu} + h_{\mu\nu}$ , one recovers the Fierz-Pauli action (17).

As suggested in [16] and later shown in [17–20], the action (38) indeed only propagates five degrees of freedom. In order to see this, one can redefine the shift as (37). This has been also done for the full nonlinear action in [17]. We will briefly discuss their findings.

<sup>2</sup>Note that we would get exactly the same results by not doing the field redefinition. This field redefinition only makes manifest that the lapse is a Lagrange multiplier.

A constraint analysis is most conveniently carried out by using the ADM decomposition [14]. Using (28), the Lagrangian (38) is given by

$$M_P^{-2}\mathcal{L} = \pi^{ij}\partial_t\gamma_{ij} + NR^0 + R_iN^i + 2m^2\sqrt{\det\gamma}N\sum_{n=0}^2\beta_n e_n\left(\sqrt{g^{-1}\eta}\right). \quad (40)$$

The mass term includes  $N$  in a non-linear way and is, therefore, responsible for the seeming loss of the constraint. However, one can redefine the shift  $N_i$  by (37) and finds the following Lagrangian [17, 19]

$$M_P^{-2}\mathcal{L} = \pi^{ij}\partial_t\gamma_{ij} - \mathcal{H}_0(\pi^{ij}, \gamma_{ij}, n_j) + N\mathcal{C}(\pi^{ij}, \gamma_{ij}, n_j), \quad (41)$$

where  $\mathcal{H}_0$  is the Hamiltonian and  $\mathcal{C}$  is the additional constraint ensuring that only five of the six components of  $\gamma_{ij}$  are propagating. Thus, we have established that there are three independent variables  $n_i$  which are not propagating and algebraically determined by their equations of motion and there is one Lagrange multiplier  $N$  which yields a constraint equation for  $\pi^{ij}$  and  $\gamma_{ij}$ . Therefore, there are only five propagating independent degrees of freedom which constitute the massive graviton.

It is, however, important to note that the redefinition (37) can only be used when considering the full non-linear action (38). Whenever truncating the theory, this ceases to be valid and thus one is left with six propagating degrees of freedom.

One might be puzzled by analyzing the action (38) in terms of the helicity decomposition (14). There, indeed, are higher derivatives (apparently signaling new degrees of freedom) appearing on the equations of motion of, e.g., the scalar helicity  $\chi$  for the nonlinear terms [2]. The lowest suppression scale of these terms is  $\Lambda_5 = (m^4 M_P)^{\frac{1}{5}}$ . In the full theory, however, this scale is redundant and can be removed by a field redefinition [18]<sup>3</sup>. With this field redefinition also the higher derivative terms disappear. It can be shown that this happens for all scales below  $\Lambda_3 = (m^2 M_P)^{\frac{1}{3}}$  [18], such that the theory in terms of the redefined fields is free of higher derivative interactions. Note, however, that when truncating the theory to any finite order this is no longer the case.

In works subsequent to [16, 17], it was furthermore shown that the absence of the sixth ghost like degree of freedom can also be confirmed in the Stückelberg language [20].

## 4 Conclusions

Within this work we have addressed the question whether theories of a single interacting massive-spin 2 field obey similar uniqueness theorems as in the massless case.

For a long time, it was doubtful whether there even exists one consistent theory that describes self-interactions of a massive spin-2 particle. The fact that adding the Fierz-Pauli mass term to the Einstein-Hilbert action introduces nonlinearities in the lapse into the action was taken as the basis of a no-go-theorem for nonlinear extensions of Fierz-Pauli theory. It was argued that any such extension necessarily leads to the appearance of a sixth unphysical and ghost-like polarization in the theory, the Boulware-Deser ghost.

We have reviewed two possible ways to circumvent this apparent theorem. One is to sacrifice the Einsteinian derivative structure, such that the (00)-component of the tensor field  $h_{\mu\nu}$  enters the action only linearly even when self-interactions are added. This ensures that only five degrees of freedom are propagating. We have shown that this property can equivalently be checked in a helicity decomposition of the massive tensor. The found action is characterized by the absence of higher derivatives on the helicity components. It is the unique theory with this property.

<sup>3</sup>Note that this field redefinition is in fact necessary in order to define a Hamiltonian in terms of the helicities. Without it, the relation between the canonical momenta and time derivatives of fields is not invertible. This reflects the redundancy of the coupling in the full theory.

The second route is to leave the derivative structure untouched, but instead adding a potential for the massive spin-2 field in such a way that guarantees the presence of a Lagrange multiplier in the system. By casting the action into an appropriate form, this Lagrange multiplier is once again given by the lapse.

The latter approach, since it relies on redundancies of the full action, requires a full resummation of the theory. Any truncation to finite order appears to propagate more than five degrees of freedom. However, the scale at which this additional degree of freedom appears coincides with the scale at which nonlinearities become important. Henceforth, conclusions can only be drawn from the resummed theory.

We have further addressed the issue of higher derivatives in the helicity decomposition in the latter class of theories. While these are present, the fact that redundancies are present prevents one from constructing a Hamiltonian. A field redefinition is necessary in order to be able to invert the canonical momenta; after this redefinition, no more higher derivatives are present. The Hamiltonian of the theory does not suffer from an Ostrogradski linear instability.

The experimental viability of either theory is unknown. The former deviates from the well probed Einsteinian cubic vertex and is therefore not viable as a massive graviton. The latter has the correct vertex structure. However, choosing its mass to be of the order of the Hubble scale leads to a strong coupling already at very low energies,  $\Lambda_s = (m^2 M_P)^{1/3} \sim (1000 \text{ km})^{-1}$ .

Either theory could in principle describe self-interactions of a massive spin-2 meson and could therefore be of different phenomenological interest.

## References

- [1] S. Weinberg and E. Witten, *Phys. Lett. B* **96**, 59 (1980).
- [2] S. Folkerts, A. Pritzel and N. Wintergerst, arXiv:1107.3157 [hep-th].
- [3] K. Hinterbichler, *Rev. Mod. Phys.* **84**, 671 (2012) [arXiv:1105.3735 [hep-th]].
- [4] G. Dvali and C. Gomez, arXiv:1005.3497 [hep-th].
- [5] G. Dvali, S. Folkerts and C. Germani, *Phys. Rev. D* **84**, 024039 (2011) [arXiv:1006.0984 [hep-th]].
- [6] G. Dvali, G. F. Giudice, C. Gomez and A. Kehagias, *JHEP* **1108**, 108 (2011) [arXiv:1010.1415 [hep-ph]].
- [7] S. Weinberg, *Phys. Rev.* **135**, B1049 (1964). S. Weinberg, *Phys. Rev.* **138**, B988 (1965).
- [8] V. I. Ogievetsky, I. V. Polubarinov, *Annals of Physics*, Volume 35, Issue 2, November 1965, Pages 167-208,
- [9] M. Fierz and W. Pauli, *Proc. Roy. Soc. Lond. A* **173**, 211 (1939).
- [10] M. Henneaux and C. Teitelboim, Princeton, USA: Univ. Pr. (1992) 520 p
- [11] Dirac, P. A. Maurice, DoverPublications.com, 2001
- [12] P. Van Nieuwenhuizen, *Nucl. Phys. B* **60**, 478 (1973).
- [13] D. G. Boulware and S. Deser, *Phys. Rev. D* **6**, 3368 (1972).
- [14] R. L. Arnowitt, S. Deser and C. W. Misner, *Phys. Rev.* **117**, 1595 (1960). R. L. Arnowitt, S. Deser and C. W. Misner, *Gen. Rel. Grav.* **40**, 1997 (2008) [gr-qc/0405109].
- [15] K. Hinterbichler, arXiv:1305.7227 [hep-th].
- [16] C. de Rham, G. Gabadadze and A. J. Tolley, *Phys. Rev. Lett.* **106**, 231101 (2011) [arXiv:1011.1232 [hep-th]].
- [17] S. F. Hassan and R. A. Rosen, *Phys. Rev. Lett.* **108**, 041101 (2012) [arXiv:1106.3344 [hep-th]].
- [18] C. de Rham, G. Gabadadze and A. J. Tolley, *JHEP* **1111**, 093 (2011) [arXiv:1108.4521 [hep-th]].
- [19] S. F. Hassan and R. A. Rosen, *JHEP* **1204**, 123 (2012) [arXiv:1111.2070 [hep-th]].
- [20] C. de Rham, G. Gabadadze and A. J. Tolley, *Phys. Lett. B* **711**, 190 (2012) [arXiv:1107.3820 [hep-th]].



# Higgs, Top, and Bottom Mass Predictions in Finite Unified Theories

Sven Heinemeyer<sup>a,\*</sup>, Myriam Mondragón<sup>b,†</sup> and George Zoupanos<sup>c,d,‡</sup>

<sup>a</sup> Instituto de Física de Cantabria (CSIC-UC), Edificio Juan Jorda, Avda. de Los Castros s/n, 39005 Santander, Spain

<sup>b</sup> Instituto de Física, Universidad Nacional Autónoma de México, Apdo. Postal 20-364, México 01000 D.F., México

<sup>c</sup> Institut für Theoretische Physik, Universität Heidelberg, Philosophenweg 16, D-69120 Heidelberg, Germany

<sup>d</sup> On leave of absence from Physics Department, National Technical University, Zografou Campus: Heroon Polytechniou 9, 15780 Zografou, Athens, Greece

## Abstract

All-loop Finite Unified Theories (FUTs) are  $N = 1$  supersymmetric Grand Unified Theories (GUTs) based on the principle of reduction of couplings, which have a remarkable predictive power. The reduction of couplings implies the existence of renormalization group invariant relations among them, which guarantee the vanishing of the beta functions at all orders in perturbation theory in particular  $N = 1$  GUTs. In the soft breaking sector these relations imply the existence of a sum rule among the soft scalar masses. The confrontation of the predictions of a  $SU(5)$  FUT model with the top and bottom quark masses and other low-energy experimental constraints leads to a prediction of the light Higgs-boson mass in the range  $M_h \sim 121 - 126$  GeV, in remarkable agreement with the discovery of the Higgs boson with a mass around  $\sim 125.7$  GeV. Also a relatively heavy spectrum with coloured supersymmetric particles above  $\sim 1.5$  TeV is predicted, consistent with the non-observation of those particles at the LHC.

## 1 Introduction

In the last thirty years a large and sustained effort has been made to achieve a unified description of all interactions. Among the main efforts in this direction are superstring theories, and non-commutative geometry. The two approaches have common unification targets and share similar hopes for exhibiting improved renormalization properties in the ultraviolet (UV) as compared to ordinary field theories. Among the numerous important developments in both frameworks, it is worth noting two conjectures of utmost importance that signal the developments in certain directions in string theory. The conjectures refer to (i) the duality among the 4-dimensional  $N = 4$  supersymmetric Yang-Mills theory and the type IIB string theory on  $AdS_5 \times S^5$  [1]; the former being the maximal  $N = 4$  supersymmetric Yang-Mills theory is known to be UV all-loop finite theory [2, 3], (ii) the possibility of “miraculous” UV divergence cancellations in 4-dimensional maximal  $N = 8$  supergravity leading to a finite theory, as has been confirmed in a remarkable 4-loop calculation [4–8]. However, despite the importance of having frameworks to discuss quantum gravity in a self-consistent way and possibly to construct there finite theories, it is very interesting too to search for the minimal realistic framework in which finiteness can take place. In addition, the main goal expected from a unified description of interactions by the particle physics community is to understand the present day large number of free parameters of the Standard Model (SM) in terms of a few fundamental ones. In other words, to achieve *reduction of couplings* at a more fundamental level.

---

\*E-mail: Sven.Heinemeyer@cern.ch

†E-mail: myriam@fisica.unam.mx

‡E-mail: George.Zoupanos@cern.ch

To reduce the number of free parameters of a theory, and thus render it more predictive, one is usually led to introduce a symmetry. Grand Unified Theories (GUTs) are very good examples of such a procedure [9–13]. GUTs can also relate the Yukawa couplings among themselves, again  $SU(5)$  provided an example of this by predicting the ratio  $M_\tau/M_b$  [14] in the SM. A natural extension of the GUT idea is to find a way to relate the gauge and Yukawa sectors of a theory, that is to achieve Gauge–Yukawa Unification (GYU) [15–17]. This can be done by searching for renormalization group invariant (RGI) relations [16–35] holding below the Planck scale down to the GUT scale, leading to more predictive theories as compared to supersymmetric GUTs [16, 21–26]. An outstanding feature of the use of RGI relations is that one can guarantee their validity to all-orders in perturbation theory by studying the uniqueness of the resulting relations at one-loop [27, 28]. Even more remarkable is the fact that it is possible to find RGI relations among couplings that guarantee finiteness to all-orders in perturbation theory [29–31].

The above programme, called Gauge–Yukawa unification scheme, applied in the dimensionless couplings of supersymmetric GUTs, such as gauge and Yukawa couplings, predicted correctly, among others, the top quark mass in the finite and in the minimal  $N = 1$  supersymmetric  $SU(5)$  GUTs [21–23].

The search for RGI relations was extended to the soft supersymmetry breaking sector (SSB) of these theories [26, 36], which involves parameters of dimension one and two. The  $\beta$ -functions of the parameters of the softly broken theory can be expressed in terms of partial differential operators involving the dimensionless parameters of the unbroken theory, which in turn can be transformed into total derivative operators [37–40]. It is possible to do this in the RGI surface which is defined by the solution of the reduction equations.

Concerning the boundary conditions for the soft breaking terms, the first attempts involved using a “universal” value for the scalar masses, but this led to phenomenological problems, of which the worst was a they lead to charge and/or colour breaking minima deeper than the standard vacuum [41]. Then it was realized that in  $N = 1$  Gauge–Yukawa unified theories there exists a RGI sum rule for the soft scalar masses at lower orders; at one-loop for the non-finite case [42] and at two-loops for the finite case [32]. The sum rule manages to overcome the phenomenological problems of the universal boundary conditions. It was also proven [40] that the sum rule for the soft scalar masses is RGI to all-orders for both the general as well as for the finite case.

In here we review an  $SU(5)$  finite model and its predictions coming both from the dimensionless sector, namely the top and quark masses and  $\tan\beta$ , as well as the ones coming from the dimensionful sector, which are the SUSY spectrum and the Higgs masses. We take into account the restrictions resulting from the low-energy observables [35, 43], which include the recent values of  $\text{BR}(B_s \rightarrow \mu^+\mu^-)$  and the value of the light Higgs boson mass.

## 2 Finiteness

Finiteness can be understood by considering a chiral, anomaly free,  $N = 1$  globally supersymmetric gauge theory based on a group  $G$  with gauge coupling constant  $g$ . The superpotential of the theory is given by

$$W = \frac{1}{2} m^{ij} \Phi_i \Phi_j + \frac{1}{6} C^{ijk} \Phi_i \Phi_j \Phi_k, \quad (1)$$

where  $m^{ij}$  (the mass terms) and  $C^{ijk}$  (the Yukawa couplings) are gauge invariant tensors and the matter field  $\Phi_i$  transforms according to the irreducible representation  $R_i$  of the gauge group  $G$ . All the one-loop  $\beta$ -functions of the theory vanish if the  $\beta$ -function of the gauge coupling  $\beta_g^{(1)}$ , and the anomalous dimensions of the Yukawa couplings  $\gamma_i^{j(1)}$ , vanish, i.e.

$$\sum_i \ell(R_i) = 3C_2(G), \quad \frac{1}{2} C_{ipq} C^{j pq} = 2\delta_i^j g^2 C_2(R_i), \quad (2)$$

where  $\ell(R_i)$  is the Dynkin index of  $R_i$ , and  $C_2(G)$  is the quadratic Casimir invariant of the adjoint representation of  $G$ . These conditions are also enough to guarantee two-loop finiteness [44]. A striking fact is the existence of a theorem [29–31] that guarantees the vanishing of the  $\beta$ -functions to all-orders in perturbation theory. This requires that, in addition to the one-loop finiteness conditions (2), the Yukawa couplings are reduced in favour of the gauge coupling to all-orders (see [34] for details). Alternatively, similar results can be obtained [45–47] using an analysis of the all-loop NSVZ gauge beta-function [48, 49].

Next consider the superpotential given by (1) along with the Lagrangian for soft supersymmetry breaking (SSB) terms

$$-\mathcal{L}_{\text{SB}} = \frac{1}{6} h^{ijk} \phi_i \phi_j \phi_k + \frac{1}{2} b^{ij} \phi_i \phi_j + \frac{1}{2} (m^2)_i^j \phi^{*i} \phi_j + \frac{1}{2} M \lambda \lambda + \text{h.c.}, \quad (3)$$

where the  $\phi_i$  are the scalar parts of the chiral superfields  $\Phi_i$ ,  $\lambda$  are the gauginos and  $M$  their unified mass,  $h^{ijk}$  and  $b^{ij}$  are the trilinear and bilinear dimensionful couplings respectively, and  $(m^2)_i^j$  the soft scalars masses. Since we would like to consider only finite theories here, we assume that the gauge group is a simple group and the one-loop  $\beta$ -function of the gauge coupling  $g$  vanishes. We also assume that the reduction equations admit power series solutions of the form

$$C^{ijk} = g \sum_n \rho_{(n)}^{ijk} g^{2n}. \quad (4)$$

According to the finiteness theorem of ref. [29–31, 50], the theory is then finite to all orders in perturbation theory, if, among others, the one-loop anomalous dimensions  $\gamma_i^{j(1)}$  vanish. The one- and two-loop finiteness for  $h^{ijk}$  can be achieved through the relation [51]

$$h^{ijk} = -MC^{ijk} + \dots = -M\rho_{(0)}^{ijk} g + O(g^5), \quad (5)$$

where  $\dots$  stand for higher order terms.

In addition it was found that the RGI SSB scalar masses in Gauge-Yukawa unified models satisfy a universal sum rule at one-loop [42]. This result was generalized to two-loops for finite theories [32], and then to all-loops for general Gauge-Yukawa and finite unified theories [40]. From these latter results, the following soft scalar-mass sum rule is found [32]

$$\frac{(m_i^2 + m_j^2 + m_k^2)}{MM^\dagger} = 1 + \frac{g^2}{16\pi^2} \Delta^{(2)} + O(g^4) \quad (6)$$

for  $i, j, k$  with  $\rho_{(0)}^{ijk} \neq 0$ , where  $m_{i,j,k}^2$  are the scalar masses and  $\Delta^{(2)}$  is the two-loop correction

$$\Delta^{(2)} = -2 \sum_l [(m_l^2 / MM^\dagger) - (1/3)] \ell(R_l), \quad (7)$$

which vanishes for the universal choice, i.e. when all the soft scalar masses are the same at the unification point. This correction also vanishes in the models considered here.

### 3 $SU(5)$ Finite Unified Theories

Finite Unified Models have been studied for already two decades. A realistic two-loop finite  $SU(5)$  model was presented in [52], and shortly afterwards the conditions for finiteness in the soft susy breaking sector at one-loop [44] were given. Since finite models usually have an extended Higgs sector, in order to make them viable a rotation of the Higgs sector was proposed [53]. The first all-loop finite theory was studied in [21, 22], without taking into account the soft breaking terms. Naturally, the concept of finiteness was extended to the soft breaking sector, where also one-loop finiteness implies two-loop

finiteness [51], and then finiteness to all-loops in the soft sector of realistic models was studied [38, 54], although the universality of the soft breaking terms lead to a charged lightest SUSY particle (LSP). This fact was also noticed in [55], where the inclusion of an extra parameter in the Higgs sector was introduced to alleviate it. With the derivation of the sum-rule in the soft supersymmetry breaking sector and the proof that it can be made all-loop finite the construction of all-loop phenomenologically viable finite models was made possible [32, 40].

Here we will study an all-loop Finite Unified theories with  $SU(5)$  gauge group, where the reduction of couplings has been applied to the third generation of quarks and leptons. An extension to three families, and the generation of quark mixing angles and masses in Finite Unified Theories has been addressed in [56], where several examples are given. These extensions are not considered here. Realistic Finite Unified Theories based on product gauge groups, where the finiteness implies three generations of matter, have also been studied [57].

The particle content of the model we will study consists of the following supermultiplets: three  $(\bar{\mathbf{5}} + \mathbf{10})$ , needed for each of the three generations of quarks and leptons, four  $(\bar{\mathbf{5}} + \mathbf{5})$  and one  $\mathbf{24}$  considered as Higgs supermultiplets. When the gauge group of the finite GUT is broken the theory is no longer finite, and we will assume that we are left with the MSSM.

Thus, a predictive Gauge-Yukawa unified  $SU(5)$  model which is finite to all orders, in addition to the requirements mentioned already, should also have the following properties:

1. One-loop anomalous dimensions are diagonal, i.e.,  $\gamma_i^{(1)j} \propto \delta_i^j$ .
2. Three fermion generations, in the irreducible representations  $\bar{\mathbf{5}}_i, \mathbf{10}_i$  ( $i = 1, 2, 3$ ), which obviously should not couple to the adjoint  $\mathbf{24}$ .
3. The two Higgs doublets of the MSSM should mostly be made out of a pair of Higgs quintet and anti-quintet, which couple to the third generation.

The superpotential which describes the model is [21, 22, 32]

$$\begin{aligned}
 W &= \sum_{i=1}^3 \left[ \frac{1}{2} g_i^u \mathbf{10}_i \mathbf{10}_i H_i + g_i^d \mathbf{10}_i \bar{\mathbf{5}}_i \bar{H}_i \right] \\
 &+ g_{23}^u \mathbf{10}_2 \mathbf{10}_3 H_4 + g_{23}^d \mathbf{10}_2 \bar{\mathbf{5}}_3 \bar{H}_4 + g_{32}^d \mathbf{10}_3 \bar{\mathbf{5}}_2 \bar{H}_4 \\
 &+ \sum_{a=1}^4 g_a^f H_a \mathbf{24} \bar{H}_a + \frac{g^\lambda}{3} (\mathbf{24})^3, \tag{8}
 \end{aligned}$$

where  $H_a$  and  $\bar{H}_a$  ( $a = 1, \dots, 4$ ) stand for the Higgs quintets and anti-quintets.

After the reduction of couplings, the symmetry is enhanced, and we are left with the following superpotential [58], we will from now on refer to this model as **FUTB**

$$\begin{aligned}
 W &= \sum_{i=1}^3 \left[ \frac{1}{2} g_i^u \mathbf{10}_i \mathbf{10}_i H_i + g_i^d \mathbf{10}_i \bar{\mathbf{5}}_i \bar{H}_i \right] + g_{23}^u \mathbf{10}_2 \mathbf{10}_3 H_4 \\
 &+ g_{23}^d \mathbf{10}_2 \bar{\mathbf{5}}_3 \bar{H}_4 + g_{32}^d \mathbf{10}_3 \bar{\mathbf{5}}_2 \bar{H}_4 + g_2^f H_2 \mathbf{24} \bar{H}_2 + g_3^f H_3 \mathbf{24} \bar{H}_3 + \frac{g^\lambda}{3} (\mathbf{24})^3, \tag{9}
 \end{aligned}$$

The non-degenerate and isolated solutions to  $\gamma_i^{(1)} = 0$  give us:

$$\begin{aligned}
 (g_1^u)^2 &= \frac{8}{5} g^2, \quad (g_1^d)^2 = \frac{6}{5} g^2, \quad (g_2^u)^2 = (g_3^u)^2 = \frac{4}{5} g^2, \\
 (g_2^d)^2 &= (g_3^d)^2 = \frac{3}{5} g^2, \quad (g_{23}^u)^2 = \frac{4}{5} g^2, \quad (g_{23}^d)^2 = (g_{32}^d)^2 = \frac{3}{5} g^2, \tag{10}
 \end{aligned}$$

$$(g^\lambda)^2 = \frac{15}{7}g^2, (g_2^f)^2 = (g_3^f)^2 = \frac{1}{2}g^2, (g_1^f)^2 = 0, (g_4^f)^2 = 0,$$

and from the sum rule we obtain:

$$\begin{aligned} m_{H_u}^2 + 2m_{\mathbf{10}}^2 &= M^2, m_{H_d}^2 - 2m_{\mathbf{10}}^2 = -\frac{M^2}{3}, \\ m_{\mathbf{5}}^2 + 3m_{\mathbf{10}}^2 &= \frac{4M^2}{3}, \end{aligned} \quad (11)$$

i.e., we have only two free parameters  $m_{\mathbf{10}} \equiv m_{\mathbf{10}_3}$  and  $M$  for the dimensionful sector.

As already mentioned, after the  $SU(5)$  gauge symmetry breaking we assume we have the MSSM, i.e. only two Higgs doublets. This can be achieved by introducing appropriate mass terms that allow to perform a rotation of the Higgs sector [21, 22, 52, 53, 59], in such a way that only one pair of Higgs doublets, coupled mostly to the third family, remains light and acquire vacuum expectation values. To avoid fast proton decay the usual fine tuning to achieve doublet-triplet splitting is performed. Notice that, although similar, the mechanism is not identical to minimal  $SU(5)$ , since we have an extended Higgs sector.

Thus, after the gauge symmetry of the GUT theory is broken we are left with the MSSM, with the boundary conditions for the third family given by the finiteness conditions, while the other two families are not restricted.

#### 4 Predictions of Low Energy Parameters

Since the gauge symmetry is spontaneously broken below  $M_{\text{GUT}}$ , the finiteness conditions do not restrict the renormalization properties at low energies, and all it remains are boundary conditions on the gauge and Yukawa couplings, see Eq. (10), the  $h = -MC$  relation, see Eq. (5), and the soft scalar-mass sum rule at  $M_{\text{GUT}}$ , as applied in the model Eq. (11). Thus we examine the evolution of these parameters according to their RGEs up to two-loops for dimensionless parameters and at one-loop for dimensionful ones with the relevant boundary conditions. Below  $M_{\text{GUT}}$  their evolution is assumed to be governed by the MSSM. We further assume a unique supersymmetry breaking scale  $M_s$  (which we define as the geometric mean of the stop masses) and therefore below that scale the effective theory is just the SM.

We now review the predictions of the model with the experimental data, starting with the heavy quark masses see ref. [35] for more details. We use for the top quark the value for the pole mass [60]

$$m_t^{\text{exp}} = (173.2 \pm 0.9) \text{ GeV}, \quad (12)$$

and we recall that the theoretical prediction for  $m_t$  of the present framework may suffer from a correction of  $\sim 4\%$  [15, 16, 33, 61]. For the bottom quark mass we use the value at  $M_Z$  [62]

$$m_b(M_Z) = (2.83 \pm 0.10) \text{ GeV}, \quad (13)$$

to avoid uncertainties that come from the further running from the  $M_Z$  to the  $m_b$  mass.

In fig.1 we show the **FUTB** model predictions for  $m_t$  and  $m_b(M_Z)$  as a function of the unified gaugino mass  $M$ , for the two cases  $\mu < 0$  and  $\mu > 0$ . In the value of the bottom mass  $m_b$ , we have included the corrections coming from bottom squark-gluino loops and top squark-chargino loops [63], known usually as the  $\Delta_b$  effects. The bounds on the  $m_b(M_Z)$  and the  $m_t$  mass clearly single out the sign  $\mu < 0$ , as the solution most compatible with this experimental constraints. Although  $\mu < 0$  is already challenged by present data of the anomalous magnetic moment of the muon  $a_\mu$  [64, 65], a heavy SUSY spectrum as the one we have here (see below) gives results for  $a_\mu$  very close to the SM result, and thus cannot be excluded.

We now analyze the impact of further low-energy observables on the model **FUTB** with  $\mu < 0$ . As additional constraints we consider the following observables: the rare  $b$  decays  $\text{BR}(b \rightarrow s\gamma)$  and  $\text{BR}(B_s \rightarrow \mu^+\mu^-)$ .

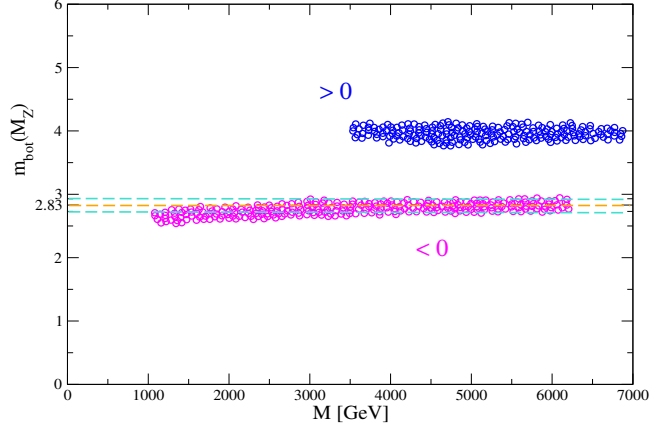


**Fig. 1:** The bottom quark mass at the  $Z$  boson scale (left) and top quark pole mass (right) are shown as function of  $M$ , the unified gaugino mass.

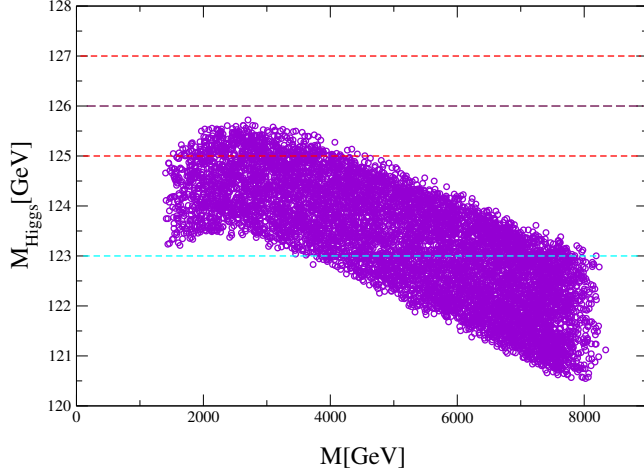


**Fig. 2:** The lightest Higgs mass,  $M_h$ , as function of  $M$  for the model **FUTB** with  $\mu < 0$ , see text.

For the branching ratio  $\text{BR}(b \rightarrow s\gamma)$ , we take the value given by the Heavy Flavour Averaging Group (HFAG) is [66]

$$\text{BR}(b \rightarrow s\gamma) = (3.55 \pm 0.24_{-0.10}^{+0.09} \pm 0.03) \times 10^{-4}. \quad (14)$$

For the branching ratio  $\text{BR}(B_s \rightarrow \mu^+\mu^-)$ , the SM prediction is at the level of  $3 \times 10^{-9}$ , while we use an experimental upper limit of

$$\text{BR}(B_s \rightarrow \mu^+\mu^-) = 4.5 \times 10^{-9} \quad (15)$$

at the 95% C.L. [67] This is in relatively good agreement with the recent direct measurement of this quantity by CMS and LHCb [68]. As we do not expect a sizable impact of the new measurement on our results, we stick for our analysis to the simple upper limit.

For the lightest Higgs mass prediction we use the code `FeynHiggs` [69–72]. The prediction for  $M_h$  of **FUTB** with  $\mu < 0$  is shown in Fig. 2, where the constraints from the two  $B$  physics observables are taken into account. The lightest Higgs mass ranges in

$$M_h \sim 121 - 126 \text{ GeV}, \quad (16)$$

where the uncertainty comes from variations of the soft scalar masses. To this value one has to add at least  $\pm 2$  GeV coming from unknown higher order corrections [71].<sup>1</sup> We have also included a small variation, due to threshold corrections at the GUT scale, of up to 5% of the FUT boundary conditions. The masses of the heavier Higgs bosons are found at higher values in comparison with our previous analyses [35, 74–76]. This is due to the more stringent bound on  $\text{BR}(B_s \rightarrow \mu^+ \mu^-)$ , which pushes the heavy Higgs masses beyond  $\sim 1$  TeV, excluding their discovery at the LHC. We furthermore find in our analysis that the lightest observable SUSY particle (LOSP) is either the stau or the second lightest neutralino, with mass starting around  $\sim 500$  GeV.

As the crucial new ingredient we take into account the recent observations of the Higgs boson discovered at LHC [77–80]. We impose a constraint on our results to the Higgs mass of

$$M_h \sim 126.0 \pm 1 \pm 2 \text{ GeV}, \quad (17)$$

where  $\pm 1$  comes from the experimental error and  $\pm 2$  corresponds to the theoretical error, and see how this affects the SUSY spectrum.<sup>2</sup> Constraining the allowed values of the Higgs mass this way puts a limit on the allowed values of the unified gaugino mass, as can be seen from Fig. 2. The red lines correspond to the pure experimental uncertainty and restrict  $2 \text{ TeV} \lesssim M \lesssim 5 \text{ TeV}$ . The blue line includes the additional theory uncertainty of  $\pm 2$  GeV. Taking this uncertainty into account no bound on  $M$  can be placed. However, a substantial part of the formerly allowed parameter points are now excluded. This in turn restricts the lightest observable SUSY particle (LOSP), which turns out to be the light scalar tau. In Fig. 3 the effects on the mass of the LOSP are demonstrated. Without any Higgs mass constraint all coloured points are allowed. Imposing  $M_h = 126 \pm 1$  GeV only the green (light shaded) points are allowed, restricting the mass to be between about 500 GeV and 2500 GeV. The lower values might be experimentally accessible at the ILC with 1000 GeV center-of-mass energy or at CLIC with an energy up to  $\sim 3$  TeV. Taking into account the theory uncertainty on  $M_h$  also the blue (dark shaded) points are allowed, permitting the LOSP mass up to  $\sim 4$  TeV. If the upper end of the parameter space were realized the light scalar tau would remain unobservable even at CLIC.

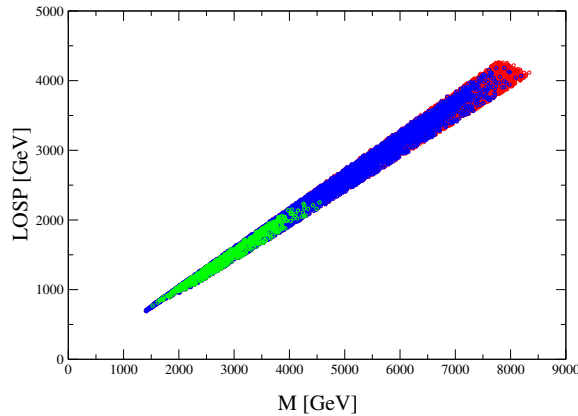


**Fig. 3:** The mass of the LOSP is presented as a function of  $M$ . Shown are only points that fulfill the  $B$  physics constraints. The green (light shaded) points correspond to  $M_h = 126 \pm 1$  GeV, the blue (dark shaded) points have  $M_h = 126 \pm 3$  GeV, and the red points have no  $M_h$  restriction.

<sup>1</sup>We have not yet taken into account the improved  $M_h$  prediction presented in [73] (and implemented into the most recent version of FeynHiggs), which will lead to an upward shift in the Higgs boson mass prediction.

<sup>2</sup>In this analysis the new  $M_h$  evaluation [73] may have a relevant impact on the restrictions on the allowed SUSY parameter space shown below.

|               |       |           |       |
|---------------|-------|-----------|-------|
| Mbot( $M_Z$ ) | 2.74  | Mtop      | 174.1 |
| Mh            | 125.0 | MA        | 1517  |
| MH            | 1515  | MH $^\pm$ | 1518  |
| Stop1         | 2483  | Stop2     | 2808  |
| Sbot1         | 2403  | Sbot2     | 2786  |
| Mstau1        | 892   | Mstau2    | 1089  |
| Char1         | 1453  | Char2     | 2127  |
| Neu1          | 790   | Neu2      | 1453  |
| Neu3          | 2123  | Neu4      | 2127  |
| Mgluino       | 3632  |           |       |

**Table 1:** A representative spectrum of a light **FUTB**,  $\mu < 0$  spectrum, compliant with the  $B$  physics constraints. All masses are in GeV.

The full particle spectrum of model **FUTB** with  $\mu < 0$ , compliant with quark mass constraints and the  $B$ -physics observables is shown in Fig. 4. In the upper (lower) plot we impose  $M_h = 126 \pm 3(1)$  GeV. Without any  $M_h$  restrictions the coloured SUSY particles have masses above  $\sim 1.8$  TeV in agreement with the non-observation of those particles at the LHC [81–83]. Including the Higgs mass constraints in general favours the lower part of the SUSY particle mass spectra, but also cuts away the very low values. Neglecting the theory uncertainties of  $M_h$  (as shown in the lower plot of Fig. 4) permits SUSY masses which would remain unobservable at the LHC, the ILC or CLIC. On the other hand, large parts of the allowed spectrum of the lighter scalar tau or the lighter neutralinos might be accessible at CLIC with  $\sqrt{s} = 3$  TeV. Including the theory uncertainties, even higher masses are permitted, further weakening the discovery potential of the LHC and future  $e^+e^-$  colliders. A numerical example of the lighter part of the spectrum is shown in Table 1. If such a spectrum were realized, the coloured particles are at the border of the discovery region at the LHC. Some uncoloured particles like the scalar taus, the light chargino or the lighter neutralinos would be in the reach of a high-energy Linear Collider.

## 5 Conclusions

It is a remarkable fact that many interesting ideas that have survived various theoretical and phenomenological tests, as well as the solution to the UV divergencies problem, find a common ground in the framework of  $N = 1$  Finite Unified Theories, which we have briefly described here. These theories, which are based on the principle of reduction of couplings (expressed via RGI relations among couplings and masses) show very promising features. From the theoretical side they solve the problem of ultraviolet divergencies in a minimal way, whereas on the phenomenological side, they provide strict selection rules for choosing realistic models which lead to testable predictions. The success of predicting the top-quark mass [21–24, 26, 84] was extended to the predictions of the Higgs masses and the supersymmetric spectrum of the MSSM [35]. The predictions of the **FUTB**  $SU(5)$  finite model in light of the recent discovery of a Higgs-like state at the LHC and on the new bounds on the branching ratio  $\text{BR}(B_s \rightarrow \mu^+ \mu^-)$  shows that compared to our previous analysis [35], the new bound on  $\text{BR}(B_s \rightarrow \mu^+ \mu^-)$  excludes values for the heavy Higgs bosons masses below  $1 \sim \text{TeV}$ , and in general allows only a very heavy SUSY spectrum. The Higgs mass constraint favours the lower part of this spectrum, with SUSY masses ranging from  $\sim 500$  GeV up to the multi-TeV level, where the lower part of the spectrum could be accessible at the ILC or CLIC [43].

## Acknowledgements

G.Z. thanks the Institut für Theoretische Physik, Heidelberg, for its generous support and warm hospitality. The work of G.Z. was supported by the Research Funding Program ARISTEIA, Higher Order

Calculations and Tools for High Energy Colliders, HOCTools (co-financed by the European Union (European Social Fund ESF) and Greek national funds through the Operational Program Education and Lifelong Learning of the National Strategic Reference Framework (NSRF)) and the European Union's ITN programme HIGGSTOOLS. The work of M.M. was supported by mexican grants PAPIIT IN113712 and Conacyt 132059. The work of S.H. was supported in part by CICYT (grant FPA 2010-22163-C02-01) and by the Spanish MICINN's Consolider-Ingenio 2010 Program under grant MultiDark CSD2009-00064.

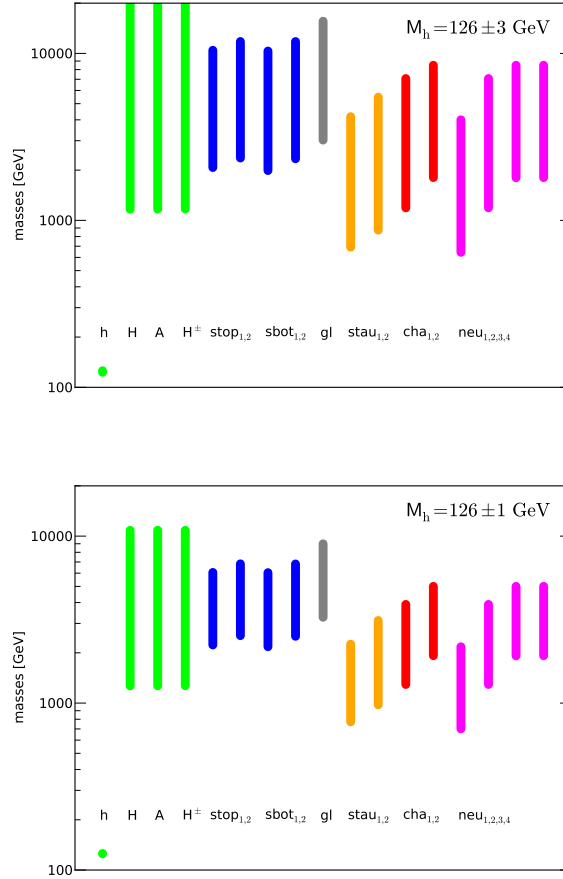


**Fig. 4:** The upper (lower) plot shows the spectrum after imposing the constraint  $M_h = 126 \pm 3$  ( $1$ ) GeV of model **FUTB** with  $\mu < 0$ , where the points shown are in agreement with the quark mass constraints and the  $B$ -physics observables. The light (green) points on the left are the various Higgs boson masses. The dark (blue) points following are the two scalar top and bottom masses, followed by the lighter (gray) gluino mass. Next come the lighter (beige) scalar tau masses. The darker (red) points to the right are the two chargino masses followed by the lighter shaded (pink) points indicating the neutralino masses.

## References

- [1] J. M. Maldacena, Adv. Theor. Math. Phys. **2**, 231 (1998), [hep-th/9711200].
- [2] S. Mandelstam, Nucl. Phys. **B123**, 149 (1983).
- [3] L. Brink, O. Lindgren and B. E. W. Nilsson, Phys. Lett. **B123**, 323 (1983).

- [4] Z. Bern, J. J. Carrasco, L. J. Dixon, H. Johansson and R. Roiban, *Phys. Rev. Lett.* **103**, 081301 (2009), [0905.2326].
- [5] R. Kallosh, *JHEP* **09**, 116 (2009), [0906.3495].
- [6] Z. Bern *et al.*, *Phys. Rev. Lett.* **98**, 161303 (2007), [hep-th/0702112].
- [7] Z. Bern, L. J. Dixon and R. Roiban, *Phys. Lett.* **B644**, 265 (2007), [hep-th/0611086].
- [8] M. B. Green, J. G. Russo and P. Vanhove, *Phys. Rev. Lett.* **98**, 131602 (2007), [hep-th/0611273].
- [9] J. C. Pati and A. Salam, *Phys. Rev. Lett.* **31**, 661 (1973).
- [10] H. Georgi and S. L. Glashow, *Phys. Rev. Lett.* **32**, 438 (1974).
- [11] H. Georgi, H. R. Quinn and S. Weinberg, *Phys. Rev. Lett.* **33**, 451 (1974).
- [12] H. Fritzsch and P. Minkowski, *Ann. Phys.* **93**, 193 (1975).
- [13] H. Georgi, *Particles and Fields: Williamsburg 1974*. AIP Conference Proceedings No. 23, American Institute of Physics, New York, 1974, ed. Carlson, C. E.
- [14] A. J. Buras, J. R. Ellis, M. K. Gaillard and D. V. Nanopoulos, *Nucl. Phys.* **B135**, 66 (1978).
- [15] J. Kubo, M. Mondragon, M. Olechowski and G. Zoupanos, *Nucl. Phys.* **B479**, 25 (1996), [hep-ph/9512435].
- [16] J. Kubo, M. Mondragon and G. Zoupanos, *Acta Phys. Polon.* **B27**, 3911 (1997), [hep-ph/9703289].
- [17] T. Kobayashi, J. Kubo, M. Mondragon and G. Zoupanos, *Acta Phys. Polon.* **B30**, 2013 (1999).
- [18] E. Ma, *Phys. Rev.* **D17**, 623 (1978).
- [19] E. Ma, *Phys. Rev.* **D31**, 1143 (1985).
- [20] S. Nandi and W.-C. Ng, *Phys. Rev.* **D20**, 972 (1979).
- [21] D. Kapetanakis, M. Mondragon and G. Zoupanos, *Z. Phys.* **C60**, 181 (1993), [hep-ph/9210218].
- [22] M. Mondragon and G. Zoupanos, *Nucl. Phys. Proc. Suppl.* **37C**, 98 (1995).
- [23] J. Kubo, M. Mondragon and G. Zoupanos, *Nucl. Phys.* **B424**, 291 (1994).
- [24] J. Kubo, M. Mondragon, N. D. Tracas and G. Zoupanos, *Phys. Lett.* **B342**, 155 (1995), [hep-th/9409003].
- [25] J. Kubo, M. Mondragon, M. Olechowski and G. Zoupanos, hep-ph/9510279.
- [26] J. Kubo, M. Mondragon and G. Zoupanos, *Phys. Lett.* **B389**, 523 (1996), [hep-ph/9609218].
- [27] W. Zimmermann, *Commun. Math. Phys.* **97**, 211 (1985).
- [28] R. Oehme and W. Zimmermann, *Commun. Math. Phys.* **97**, 569 (1985).
- [29] C. Lucchesi, O. Piguet and K. Sibold, *Helv. Phys. Acta* **61**, 321 (1988).
- [30] O. Piguet and K. Sibold, *Int. J. Mod. Phys.* **A1**, 913 (1986).
- [31] C. Lucchesi and G. Zoupanos, *Fortschr. Phys.* **45**, 129 (1997), [hep-ph/9604216].
- [32] T. Kobayashi, J. Kubo, M. Mondragon and G. Zoupanos, *Nucl. Phys.* **B511**, 45 (1998), [hep-ph/9707425].
- [33] T. Kobayashi, J. Kubo, M. Mondragon and G. Zoupanos, *Surveys High Energ. Phys.* **16**, 87 (2001).
- [34] S. Heinemeyer, M. Mondragon and G. Zoupanos, 1101.2476.
- [35] S. Heinemeyer, M. Mondragon and G. Zoupanos, *JHEP* **07**, 135 (2008), [0712.3630].
- [36] I. Jack and D. R. T. Jones, *Phys. Lett.* **B349**, 294 (1995), [hep-ph/9501395].
- [37] D. I. Kazakov, *Phys. Lett.* **B449**, 201 (1999), [hep-ph/9812513].
- [38] D. I. Kazakov, *Phys. Lett.* **B421**, 211 (1998), [hep-ph/9709465].
- [39] I. Jack, D. R. T. Jones and A. Pickering, *Phys. Lett.* **B426**, 73 (1998), [hep-ph/9712542].
- [40] T. Kobayashi, J. Kubo and G. Zoupanos, *Phys. Lett.* **B427**, 291 (1998), [hep-ph/9802267].
- [41] J. A. Casas, A. Lleyda and C. Munoz, *Phys. Lett.* **B380**, 59 (1996), [hep-ph/9601357].
- [42] Y. Kawamura, T. Kobayashi and J. Kubo, *Phys. Lett.* **B405**, 64 (1997), [hep-ph/9703320].

- [43] S. Heinemeyer, M. Mondragon and G. Zoupanos, Phys.Lett. **B718**, 1430 (2013), [1211.3765].
- [44] D. R. T. Jones, L. Mezincescu and Y. P. Yao, Phys. Lett. **B148**, 317 (1984).
- [45] A. V. Ermushev, D. I. Kazakov and O. V. Tarasov, Nucl. Phys. **B281**, 72 (1987).
- [46] D. I. Kazakov, Mod. Phys. Lett. **A2**, 663 (1987).
- [47] R. G. Leigh and M. J. Strassler, Nucl. Phys. **B447**, 95 (1995), [hep-th/9503121].
- [48] V. A. Novikov, M. A. Shifman, A. I. Vainshtein and V. I. Zakharov, Nucl. Phys. **B229**, 407 (1983).
- [49] M. A. Shifman, Int. J. Mod. Phys. **A11**, 5761 (1996), [hep-ph/9606281].
- [50] C. Lucchesi, O. Piguet and K. Sibold, Phys. Lett. **B201**, 241 (1988).
- [51] I. Jack and D. R. T. Jones, Phys. Lett. **B333**, 372 (1994), [hep-ph/9405233].
- [52] D. R. T. Jones and S. Raby, Phys. Lett. **B143**, 137 (1984).
- [53] J. Leon, J. Perez-Mercader, M. Quiros and J. Ramirez-Mittelbrunn, Phys. Lett. **B156**, 66 (1985).
- [54] D. I. Kazakov, M. Y. Kalmykov, I. N. Kondrashuk and A. V. Gladyshev, Nucl. Phys. **B471**, 389 (1996), [hep-ph/9511419].
- [55] K. Yoshioka, Phys. Rev. **D61**, 055008 (2000), [hep-ph/9705449].
- [56] K. S. Babu, T. Enkhbat and I. Gogoladze, Phys. Lett. **B555**, 238 (2003), [hep-ph/0204246].
- [57] E. Ma, M. Mondragon and G. Zoupanos, JHEP **12**, 026 (2004), [hep-ph/0407236].
- [58] M. Mondragon and G. Zoupanos, J.Phys.Conf.Ser. **171**, 012095 (2009).
- [59] S. Hamidi and J. H. Schwarz, Phys. Lett. **B147**, 301 (1984).
- [60] Tevatron Electroweak Working Group, 0903.2503, Tevatron Electroweak Working Group, arXiv:0903.2503 [hep-ex].
- [61] M. Mondragon and G. Zoupanos, Acta Phys. Polon. **B34**, 5459 (2003).
- [62] Particle Data Group, K. Nakamura *et al.*, J.Phys. **G37**, 075021 (2010).
- [63] M. S. Carena, D. Garcia, U. Nierste and C. E. M. Wagner, Nucl. Phys. **B577**, 88 (2000), [hep-ph/9912516].
- [64] T. Moroi, Phys.Rev. **D53**, 6565 (1996), [hep-ph/9512396].
- [65] Muon G-2 Collaboration, G. Bennett *et al.*, Phys.Rev. **D73**, 072003 (2006), [hep-ex/0602035].
- [66] Heavy Flavour Averaging Group, see: [www.slac.stanford.edu/xorg/hfag/](http://www.slac.stanford.edu/xorg/hfag/).
- [67] LHCb collaboration, R. Aaij *et al.*, Phys.Rev.Lett. **108**, 231801 (2012), [1203.4493].
- [68] CMS and LHCb Collaborations, (2013), <http://cdsweb.cern.ch/record/1374913/files/BPH-11-019-p>
- [69] S. Heinemeyer, W. Hollik and G. Weiglein, Comput. Phys. Commun. **124**, 76 (2000), [hep-ph/9812320].
- [70] S. Heinemeyer, W. Hollik and G. Weiglein, Eur. Phys. J. **C9**, 343 (1999), [hep-ph/9812472].
- [71] G. Degrassi, S. Heinemeyer, W. Hollik, P. Slavich and G. Weiglein, Eur. Phys. J. **C28**, 133 (2003), [hep-ph/0212020].
- [72] M. Frank *et al.*, JHEP **02**, 047 (2007), [hep-ph/0611326].
- [73] T. Hahn, S. Heinemeyer, W. Hollik, H. Rzehak and G. Weiglein, 1312.4937.
- [74] S. Heinemeyer, M. Mondragon and G. Zoupanos, 0810.0727.
- [75] S. Heinemeyer, M. Mondragon and G. Zoupanos, J.Phys.Conf.Ser. **171**, 012096 (2009).
- [76] S. Heinemeyer, M. Mondragon and G. Zoupanos, 1201.5171.
- [77] ATLAS Collaboration, G. Aad *et al.*, Phys.Lett. **B716**, 1 (2012), [1207.7214].
- [78] ATLAS Collaboration, (2013), ATLAS-CONF-2013-014, ATLAS-COM-CONF-2013-025.
- [79] CMS Collaboration, S. Chatrchyan *et al.*, Phys.Lett. **B716**, 30 (2012), [1207.7235].
- [80] CMS Collaboration, S. Chatrchyan *et al.*, 1303.4571.
- [81] CMS Collaboration, S. Chatrchyan *et al.*, Phys.Lett. **B713**, 68 (2012), [1202.4083].

- [82] ATLAS Collaboration, P. Pravalorio, Talk at SUSY2012 (2012).
- [83] CMS Collaboration, C. Campagnari, Talk at SUSY2012 (2012).
- [84] J. Kubo, M. Mondragon, S. Shoda and G. Zoupanos, Nucl. Phys. **B469**, 3 (1996), [hep-ph/9512258].

# Beyond the Standard Model of Physics with Astronomical Observations

Raul Jimenez\*

ICREA & ICC, University of Barcelona (IEEC-UB), Marti i Franques 1, Barcelona 08028, Spain  
Theory Group, Physics Department, CERN, CH-1211, Geneva 23, Switzerland

## Abstract

There has been significant recent progress in observational cosmology. This, in turn, has provided an unprecedented picture of the early universe and its evolution. In this review I will present a (biased) view of how one can use these observational results to constraint fundamental physics and in particular physics beyond the standard model.

## 1 Introduction

Over the last two decades we have seen phenomenal progress in our observational understanding of the Universe. It was in the early 90s that the first image of the fluctuation of the Cosmic Microwave Background (CMB) was obtained by the COBE satellite. It was around the same time that the first survey of galaxies was carried out by the CfA. Twenty years later we have had our knowledge of the cosmos revolutionised by the outstanding data collected by two galaxy surveys: 2dF and SDSS and by two CMB satellites WMAP & Planck, which have provided both full sky temperature and polarization measurements of the CMB. In fact, Planck has already obtained all information in the temperature power spectrum that is available in the scale (cosmic variance limited) at angular scales larger than  $5'$ . While these datasets have had a profound impact on our understanding of the cosmos, they also provide an invaluable tool to extract information about fundamental physics. The future is even brighter, because there are current and future cosmological experiments planned to map out the whole sky at all wavelengths. Further, the promise of detecting gravitational waves should be realised during this decade with advanced ground-based observatories like LIGO, and therefore a new window will open at mapping the Universe. In this talk, I will give a (presenter biased) view of some insights into fundamental physics that have been obtained using cosmological observations. Namely: constraints on dark energy, neutrino masses and hierarchy and beyond the standard model physics. Most of the material shown here has been presented elsewhere in many of my own referred publications, but is presented here coherently to give a panchromatic view of how to shed light on beyond the standard model physics with cosmology.

## 2 Dark energy

Direct supernova measurements of the deceleration parameter [1], as well as indirect measurements based upon a combination of results from the cosmic microwave background (CMB) [2], large-scale structure (LSS) [3,4], and the Hubble constant [5] indicate that the expansion is accelerating. This suggests either that gravity on the largest scales is described by some theory other than general relativity and/or that the Universe is filled with some sort of negative-pressure “dark energy” that drives the accelerated expansion [6]; either way, it requires new physics beyond general relativity and the standard model of particle physics. These observations have garnered considerable theoretical attention as well as observational and experimental efforts to learn more about the new physics coming into play.

The simplest possibility is to extend Einstein’s equation with a cosmological constant, or equivalently, to hypothesize a fluid with an equation-of-state parameter  $w \equiv p/\rho = -1$  (with  $p$  and  $\rho$  the pressure and energy density, respectively). However, it may well be that the cosmological “constant” actually evolves with time, in which case  $w \neq -1$ , and there are a variety of theoretical reasons [7] to

---

\*E-mail: raul.jimenez@icc.ub.edu

believe that this is the case. Precise measurement of  $w(z)$  (with, in general, a parameterized redshift dependence) or, equivalently, the cosmic expansion history, has thus become a central goal of physical cosmology [8, 10].

Among the techniques to determine the cosmic expansion history are supernova searches, baryon acoustic oscillations (BAO) [11, 12, 14, 15], weak lensing [16], and galaxy clusters [17]. These techniques all have different strengths, and they all also suffer from a different set of weaknesses. As argued in the ESO/ESA and Dark Energy Task Force reports [8, 10], robust conclusions about the cosmic expansion history will likely require several avenues to allow for cross checks. There may also still be room for other ideas for determining the expansion history.

A common weakness of supernova searches, BAO (at least the angular clustering), weak lensing, and cluster-based measurements is that they rely largely on integrated quantities. For example supernovae probe the luminosity distance,

$$d_L(z) = (1+z) \int_z^0 (1+z') \frac{dt}{dz'} dz'. \quad (1)$$

The other probes rely on similar quantities, which depend on an integral of the expansion history, to determine the expansion history, rather than the expansion history itself. The purpose of the differential-age technique [18] is to circumvent this limitation by measuring directly the integrand,  $dt/dz$ , or in other words, the change in the age of the Universe as a function of redshift. This can be achieved by measuring ages of galaxies with respect to a fiducial model, thus circumventing the need to compute absolute ages. From Galactic globular clusters age-dating we know that relative ages are much more accurately determined than absolute ages (e.g., Refs. [19–21]). A preliminary analysis, with archival data, has already been carried out [22, 23], and the results applied to constrain dark-energy theories (e.g., Refs. [24]).

The challenge with the differential-age measurement is to find a population of standard clocks and accurately date them. There is now growing observational evidence that the most massive galaxies contain the oldest stellar populations up to redshifts of  $z \sim 1-2$  [25–29]. Refs. [28] and [30] have shown that the most massive galaxies have less than 1% of their present stellar mass formed at  $z < 1$ . Ref. [29] shows that star formation in massive systems in high-density regions — i.e., galaxy clusters — ceased by redshift  $z \sim 3$  and Ref. [31] shows that massive systems, those with stellar masses  $> 5 \times 10^{11} M_\odot$ ,

| $z$    | BC03 models |                 |                 |                |         | MaStro models |                 |                 |                |         |
|--------|-------------|-----------------|-----------------|----------------|---------|---------------|-----------------|-----------------|----------------|---------|
|        | $H(z)$      | $\sigma_{stat}$ | $\sigma_{syst}$ | $\sigma_{tot}$ | % error | $H(z)$        | $\sigma_{stat}$ | $\sigma_{syst}$ | $\sigma_{tot}$ | % error |
| 0.1791 | 75          | 3.8             | 0.5             | 4              | 5%      | 81            | 4.1             | 2.5             | 5              | 6%      |
| 0.1993 | 75          | 4.9             | 0.6             | 5              | 7%      | 81            | 5.2             | 2.6             | 6              | 7%      |
| 0.3519 | 83          | 13              | 4.8             | 14             | 17%     | 88            | 13.9            | 7.9             | 16             | 18%     |
| 0.5929 | 104         | 11.6            | 4.5             | 13             | 12%     | 110           | 12.3            | 7.5             | 15             | 13%     |
| 0.6797 | 92          | 6.4             | 4.3             | 8              | 9%      | 98            | 6.8             | 7.1             | 10             | 11%     |
| 0.7812 | 105         | 9.4             | 6.1             | 12             | 12%     | 88            | 8               | 7.4             | 11             | 13%     |
| 0.8754 | 125         | 15.3            | 6               | 17             | 13%     | 124           | 14.3            | 8.7             | 17             | 14%     |
| 1.037  | 154         | 13.6            | 14.9            | 20             | 13%     | 113           | 10.1            | 11.7            | 15             | 14%     |

**Table 1:**  $H(z)$  measurements (in units of  $[\text{kms}^{-1}\text{Mpc}^{-1}]$ ) and their errors; the columns in the middle report the relative contribution of statistical and systematic errors, and the last ones the total error (estimated by summing in quadrature  $\sigma_{stat}$  and  $\sigma_{syst}$ ). These values have been estimated respectively with BC03 and MaStro stellar population synthesis models. This dataset can be downloaded at the address [http://www.astronomia.unibo.it/Astronomia/Ricerca/Progetti+e+attivita/cosmic\\_chronometers.htm](http://www.astronomia.unibo.it/Astronomia/Ricerca/Progetti+e+attivita/cosmic_chronometers.htm) (alternatively <http://start.at/cosmicchronometers>).

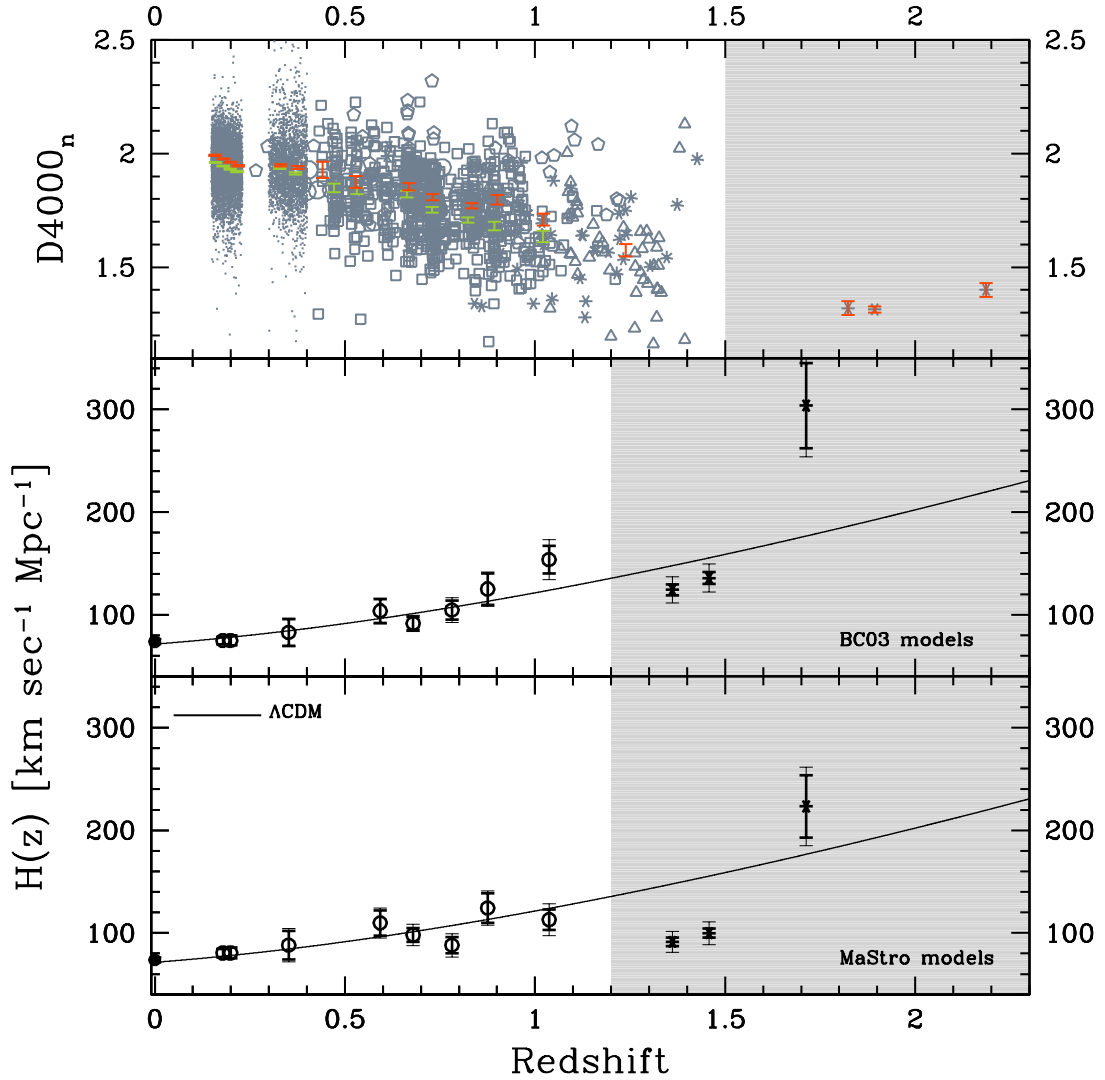


**Fig. 1:** The  $H(z)$  measurement from a sample of passively evolving galaxies. The points at  $z > 1$  are taken from Ref. [33], while the point at  $z = 0$  is from the Hubble Key Project [5]. The solid line is the  $\Lambda\text{CDM}$  model.

have finished their star-formation activity by  $z \sim 2$ . There is thus considerable empirical evidence for a population of galaxies, harboured in the highest-density regions of galaxy clusters, that has formed its stellar population at high redshift,  $z > 2$ , and that since that time this population has been evolving passively, without further episodes of star formation. These galaxies trace the “red envelope,” and are the oldest objects in the Universe at every redshift. The differential ages of these galaxies should thus be a good indicator for the rate of change of the age of the Universe as a function of redshift.

The most recent measurements of the expansion history obtained from the ages of passively-evolving galaxies in galaxy clusters at  $z < 2.0$  have been reported by [32–34] (see Fig. 1 and Table 1). Such observations provide a promising new cosmological constraint, particularly for understanding the evolution of the dark-energy density (Fig. II). The current measurements already provide valuable constraints [35–37], and the success of this effort should motivate further measurements along these lines

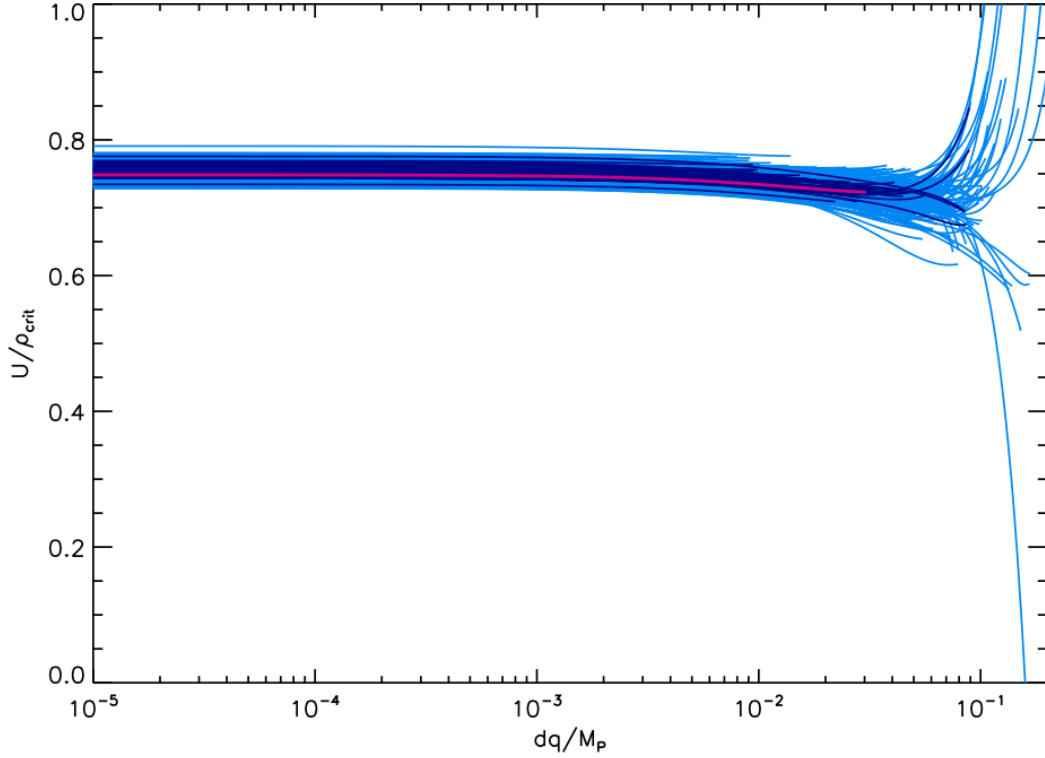


**Fig. II:** The effective potential of accelerated expansion  $U(q)$  in units of the critical density  $\rho_{\text{crit}}$  as function of the displacement of the field  $q$  in  $M_p$  units. Different tracks are plotted for values with 68% confidence (dark blue lines) and 95% confidence (light blue lines). The best-fit model is shown as a solid red line, which is better described physically as a pseudo-Goldstone boson. The trajectories correspond to how much the field has moved in the full redshift range of the observational data ( $0 < z < 1.1$ ). Note that the potential is very flat at the few  $\sigma$  level and that for many models the field displacement is very small. The data strongly favor a flat potential.

as well as a more intensive investigation of the theoretical underpinnings of the calculations and the associated uncertainties. Further, there has been significant advancement in the last few years in modelling stellar populations of LRG galaxies and the differential technique has been recently applied very successfully to determine the metallicity of LRGs.

*The main highlight is that the expansion history of the Universe is consistent with that predicted by a flat potential, i.e. a cosmological constant. The data do not require extra parameters beyond a constant term in the Lagrangian to explain the current accelerated expansion.* Further, deviations in the potential from a constant are constrained to be below 6%. Observational constraints allow the parameters describing the Lagrangian to vary only within certain limits; the relative range of the allowed variation of the parameters confirms a well defined hierarchy where the linear and quadratic terms dominate over higher-order terms, justifying the basic assumption of the effective theory approach. Observational constraints also give some indications of the relevant energy scales involved. Because a direct determination of a Lagrangian allows us to determine the underlying symmetries in the theory, our results can be used to shed light on this as well.

Additional effort on both the theoretical and observational side may ultimately promote the differential-age technique as an important new dark-energy avenue which complements supernova searches, weak lensing, baryon acoustic oscillations, and cluster abundances. The differential-age technique can po-

tentially provide *model independent* measurements of the expansion history of the universe at the % level [38–41]. Also, absolute ages of stellar ages have proven very valuable to establish possible deviations from the  $\Lambda$ CDM model [42, 43]

### 3 Measuring the neutrino mass and its hierarchy

In the past decade, there has been great progress in neutrino physics. It has been shown that atmospheric neutrinos exhibit a large up-down asymmetry in the SuperKamiokande (SK) experiment. This was the first significant evidence for a finite neutrino mass [44] and hence the incompleteness of the Standard Model of particle physics. Accelerator experiments [45, 46] have confirmed this evidence and improved the determination of the neutrino mass splitting required to explain the observations. The Sudbury Neutrino Observatory (SNO) experiment has shown that the solar neutrinos change their flavors from the electron type to other active types (muon and tau neutrinos) [47]. Finally, the KamLAND reactor anti-neutrino oscillation experiments reported a significant deficit in reactor anti-neutrino flux over approximately 180 km of propagation [48]. Combining results from the pioneering Homestake experiment [49] and Gallium-based experiments [50], the decades-long solar neutrino problem [51] has been solved by the electron neutrinos produced at Sun’s core propagating adiabatically to a heavier mass eigenstate due to the matter effect [52].

As a summary, two hierarchical neutrino mass splittings and two large mixing angles have been measured, while only a bound on a third mixing angle has been established. Furthermore the standard model has three neutrinos and the motivation for considering deviations from the standard model in the form of extra neutrino species has now disappeared [54, 55].

New neutrino experiments aim to determine the remaining parameters of the neutrino mass matrix and the nature of the neutrino mass. Meanwhile, relic neutrinos produced in the early universe are hardly detectable by weak interactions but new cosmological probes offer the opportunity to detect relic neutrinos and determine neutrino mass parameters.

It is very relevant that the maximal mixing of the solar mixing angle is excluded at a high significance. The exclusion of the maximal mixing by SNO [47] has an important impact on a deep question in neutrino physics: “are neutrinos their own anti-particle?”. If the answer is yes, then neutrinos are Majorana fermions; if not, they are Dirac. If neutrinos and anti-neutrinos are identical, there could have been a process in the Early Universe that affected the balance between particles and anti-particles, leading to the matter anti-matter asymmetry we need to exist [56]. This question can, in principle, be resolved if neutrinoless double beta decay is observed. Because such a phenomenon will violate the lepton number by two units, it cannot be caused if the neutrino is different from the anti-neutrino (see [53] and references therein). Many experimental proposals exist that will increase the sensitivity to such a phenomenon dramatically over the next ten years (e.g., [57] and references therein).

The crucial question cosmology can address is if a negative result from such experiments can lead to a definitive statement about the nature of neutrinos. Within three generations of neutrinos, and given all neutrino oscillation data, there are three possible mass spectra: a) degenerate, with mass splitting smaller than the neutrino masses, and two non-degenerate cases, b) normal hierarchy, with the larger mass splitting between the two more massive neutrinos and c) inverted hierarchy, with the smaller spitting between the two higher mass neutrinos. For the inverted hierarchy, a lower bound can be derived on the effective neutrino mass [53]. The bound for the degenerate spectrum is stronger than for inverted hierarchy. Unfortunately, for the normal hierarchy, one cannot obtain a similar rigorous lower limit.

Neutrino oscillation data have measured the neutrino squared mass differences, which are hierarchical. Given the smallness of neutrino masses and the hierarchy in mass splittings, we can characterize the impact of neutrino masses on cosmological observables and in particular on the the matter power spectrum by two parameters: the total mass  $\Sigma$  and the ratio of the largest mass splitting to the total mass,  $\Delta$ . One can safely neglect the impact of the solar mass splitting in cosmology. In this approach, two

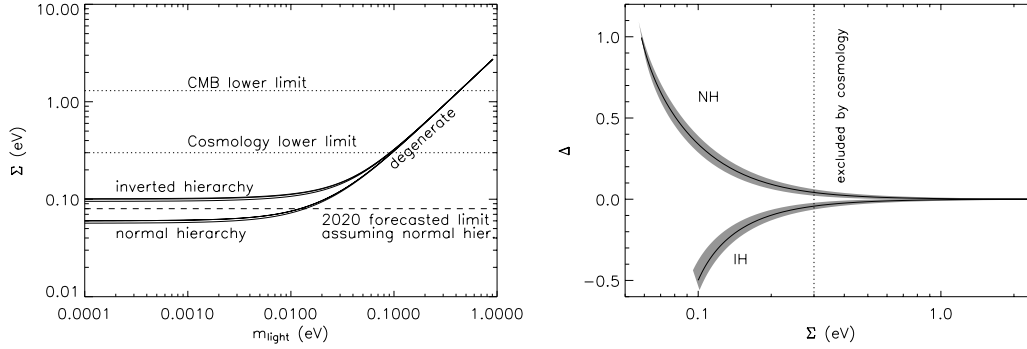


**Fig. III:** Left: constraints from neutrino oscillations and from cosmology in the  $m$ - $\Sigma$  plane. Right: constraints from neutrino oscillations (shaded regions) and from cosmology in the  $\Sigma$ - $\Delta$  plane. In this parameterization the sign of  $\Delta$  specifies the hierarchy.

masses characterize the neutrino mass spectrum, the lightest one,  $m$ , and the heaviest one,  $M$ .

Neutrino oscillation data are unable to resolve whether the mass spectrum consists in two light states with mass  $m$  and a heavy one with mass  $M$ , named normal hierarchy (NH) or two heavy states with mass  $M$  and a light one with mass  $m$ , named inverted hierarchy (IH). Near future neutrino oscillation data may resolve the neutrino mass hierarchy if

one of the still unknown parameters that relates flavor with mass states is not too small. On the contrary, if that mixing angle is too small, oscillation data may be unable to solve this issue. Analogously, a total neutrino mass determination from cosmology will be able to determine the hierarchy only if the underlying model is normal hierarchy and  $\Sigma < 0.1$  eV (see e.g., Fig III). If neutrinos exist in either an inverted hierarchy or are degenerate, (and if the neutrinoless double beta decay signal is not seen within the bounds determined by neutrino oscillation data), then the three light neutrino mass eigenstates (only) will be found to be Dirac particles.

Massive neutrinos affect cosmological observations in a variety of different ways. For example, cosmic microwave background (CMB) data alone constrain the total neutrino mass  $\Sigma < 1.3$  eV at the 95% confidence level [58]. Neutrinos with mass  $< 1$  eV become non-relativistic after the epoch of recombination probed by the CMB, thus massive neutrinos alter matter-radiation equality for a fixed  $\Omega_m h^2$ . After neutrinos become non-relativistic, their free streaming damps the small-scale power and modifies the shape of the matter power spectrum below the free-streaming length. Combining large-scale structure and CMB data, at present the sum of masses is constrained to be  $\Sigma < 0.3$  eV [59]. Forthcoming large-scale structure data promise to determine the small-scale ( $0.1 < k < 1$  h/Mpc) matter power spectrum exquisitely well and to yield errors on  $\Sigma$  well below 0.1 eV (e.g., [60–62]).

The effect of neutrino mass on the CMB is related to the physical density of neutrinos, and therefore the mass difference between eigenstates can be neglected. However individual neutrino masses can have an effect on the large-scale shape of the matter power spectrum. In fact, neutrinos of different masses have different transition redshifts from relativistic to non-relativistic behavior, and their individual masses and their mass splitting change the details of the radiation-domination to matter-domination regime. As a result the detailed shape of the matter power spectrum on scales  $k \sim 0.01$  h/Mpc is affected. In principle therefore a precise measurement of the matter power spectrum shape can give information on both the sum of the masses and individual masses (and thus the hierarchy), even if the second effect is much smaller than the first.

We define the relation between the neutrino masses  $m$  and  $M$  and the parameters  $\Sigma$  and  $\Delta$  as

$$\text{NH : } \quad \Sigma = 2m + M \quad \Delta = (M - m)/\Sigma \quad (2)$$

$$\text{IH : } \quad \Sigma = m + 2M \quad \Delta = (m - M)/\Sigma \quad (3)$$

(recall that  $m$  denotes the lightest neutrino mass and  $M$  the heaviest).

In Fig III we show the current constraints on neutrino mass properties in the  $m$ - $\Delta$  and  $\Sigma$ - $\Delta$  planes. While many different parameterizations have been proposed in the literature to account for neutrino mass splitting in a cosmological context [63, 65, 66] here we advocate using the  $\Delta$  parameterization for the following reasons.  $\Delta$  changes continuously through normal, degenerate and inverted hierarchies;  $\Delta$  is positive for NH and negative for IH. Finally, see Ref. [64], cosmological data are sensitive to  $\Delta$  in an easily understood way through the largest mass splitting (i.e., the absolute value of  $\Delta$ ), while the direction of the splitting (the sign of  $\Delta$ ) introduces a sub-dominant correction to the main effect. This parameterisation is strictly only applicable for  $\Sigma > 0$ , but oscillations experiments already set  $\Sigma > M > 0.05\text{eV}$ .

It is important to note that not the entire parameter space in the  $\Sigma$ - $\Delta$  plane (or of any other parameterization of the hierarchy used in the literature) is allowed by particle physics constraints and should be explored: only the regions around the normal and inverted hierarchies allowed by neutrino oscillation experiments should be considered (see Fig III).

To gain a physical intuition on the effect of neutrino properties on cosmological observables, such as the shape of the matter power spectrum, it is useful to adopt the following analytical approximation, as described in Ref. [65]. The matter power spectrum can be written as:

$$\frac{k^3 P(k; z)}{2\pi^2} = \Delta_R^2 \frac{2k^2}{5H_0^2 \Omega_m^2} D_\nu^2(k, z) T^2(k) \left(\frac{k}{k_0}\right)^{(n_s-1)}, \quad (4)$$

where  $\Delta_R^2$  is the primordial amplitude of the fluctuations,  $n_s$  is the primordial power spectrum spectral slope,  $T(k)$  denotes the matter transfer function and  $D_\nu(k, z)$  is the scale-dependent linear growth function, which encloses the dependence of  $P(k)$  on non-relativistic neutrino species.

Each of the three neutrinos contributes to the neutrino mass fraction  $f_{\nu,i}$  where  $i$  runs from 1 to 3,

$$f_{\nu,i} = \frac{\Omega_{\nu,i}}{\Omega_m} = 0.05 \left(\frac{m_{\nu_i}}{0.658\text{eV}}\right) \left(\frac{0.14}{\Omega_m h^2}\right) \quad (5)$$

and has a free-streaming scale  $k_{\text{fs},i}$ ,

$$k_{\text{fs},i} = 0.113 \left(\frac{m_{\nu_i}}{\text{1eV}}\right)^{1/2} \left(\frac{\Omega_m h^2}{0.14} \frac{5}{1+z}\right)^{1/2} \text{Mpc}^{-1}. \quad (6)$$

Analogously, one can define the corresponding quantities for the combined effect of all species, by using  $\Sigma$  instead of  $m_{\nu_i}$ . Since we will only distinguish between a light and a heavy eigenstate we will have e.g.,  $f_{\nu,m}$ ,  $f_{\nu,\Sigma}$ ,  $k_{\text{fs},m}$ ,  $k_{\text{fs},\Sigma}$  etc., where in the expression for  $f_{\nu,m}$  one should use the mass of the eigenstate (which is the mass of the individual neutrino, or twice as much depending on the hierarchy) while in  $k_{\text{fs},m}$  one should use the mass of the individual neutrino.

The dependence of  $P(k)$  on non-relativistic neutrino species is in  $D_\nu(k, z)$ , given by

$$D_{\nu_i}(k, z) \propto (1 - f_{\nu_i}) D(z)^{1-p_i} \quad (7)$$

where  $k \gg k_{\text{fs},i}(z)$  and  $p_i = (5 - \sqrt{25 - 24f_{\nu_i}})/4$ . The standard linear growth function  $D(z)$  fitting formula is taken from [67].

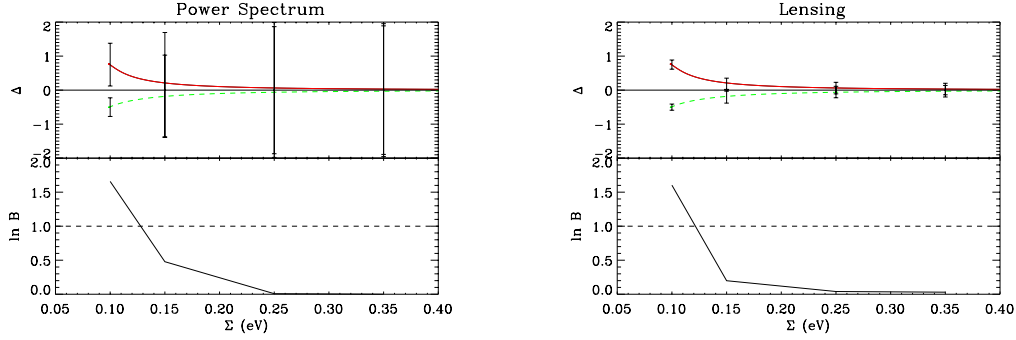


**Fig. IV:** LSS (left) and Weak Lensing (right) forecasts for neutrino mass parameters  $\Sigma$  and  $\Delta$ . We assume the LSS survey consists of a comoving volume of  $600 \text{ Gpc}^3$  at  $z = 2$  and  $2000 \text{ Gpc}^3$  at  $z = 5$ . The Weak Lensing survey covers  $40,000 \text{ sq. deg.}$  with a median redshift of  $3.0$  and a number density of  $150$  galaxies per square arcminute. Several fiducial models  $(\Sigma, \Delta)$  were used to derive by Fisher matrix approach the expected errors. The upper panel shows the  $1\text{-}\sigma$  errors on  $\Delta$  and  $\Sigma$ , the errors in  $\Sigma$  are so small that are barely visible. The lower panel shows the expected evidence ratio between the normal and inverted constraints as a function of neutrino mass. The dashed line shows the  $\ln B = 1$  level: in Jeffrey's scale  $\ln B < 1$  is 'inconclusive' evidence, and  $1 < \ln B < 2.5$  corresponds to 'substantial' evidence.

In summary there are three qualitatively different regimes in  $k$ -space that are introduced by the neutrino mass splitting

$$D_\nu(k, z) = D(k, z) \quad k < k_{\text{fs},m} \quad (8)$$

$$D_\nu(k, z) = (1 - f_{\nu,m})D(z)^{(1-p_m)} \quad k_{\text{fs},m} < k < k_{\text{fs},\Sigma} \quad (9)$$

$$D_\nu(k, z) = (1 - f_{\nu,\Sigma})D(z)^{(1-p_\Sigma)} \quad k > k_{\text{fs},\Sigma}, \quad (10)$$

where the subscript  $m$  refers to the light neutrino eigenstate and  $\Sigma$  to the sum of all masses.

This description is, however, incomplete: the transitions between the three regimes is done sharply in  $k$  while in reality the change is very smooth. In addition, the individual masses change the details of the matter-radiation transition which (keeping all other parameters fixed) adds an additional effect at scales  $k > k_{\text{fs},\Sigma}$ .

In order to explore what constraints can be placed on  $\Delta$  and  $\Sigma$  for a given survey set-up we can use a Fisher matrix approach. The elements of  $\mathbf{F}$ , the Fisher information matrix [68], are given by

$$F_{\theta\gamma} = -2 \left\langle \frac{\partial^2 \ln L}{\partial \theta \partial \gamma} \right\rangle \quad (11)$$

where  $\theta$  and  $\gamma$  denote cosmological parameters (and the Fisher matrix element's indices) and  $L$  denotes the likelihood of the data given the model. Marginalised errors on a parameter are computed as  $\sigma^2(\theta) = (\mathbf{F}^{-1})_{\theta\theta}$ . We can also calculate expected Bayesian evidence for cosmological parameters using the approach of Ref. [69, 70]. In the case that we are considering we use the formula from [70] for the expectation value of the evidence, in this case the expected Bayes factor is simply the log of ratio of the Fisher determinants.

Following Ref. [71] the Fisher matrix for the galaxy power spectrum is

$$F_{\theta\gamma} = \frac{V_s}{8\pi^2} \int_{-1}^1 d\mu \int_{k_{\text{min}}}^{k_{\text{max}}} k^2 dk N \frac{\partial \ln P(k, \mu)}{\partial \theta} \frac{\partial \ln P(k, \mu)}{\partial \gamma} \quad (12)$$

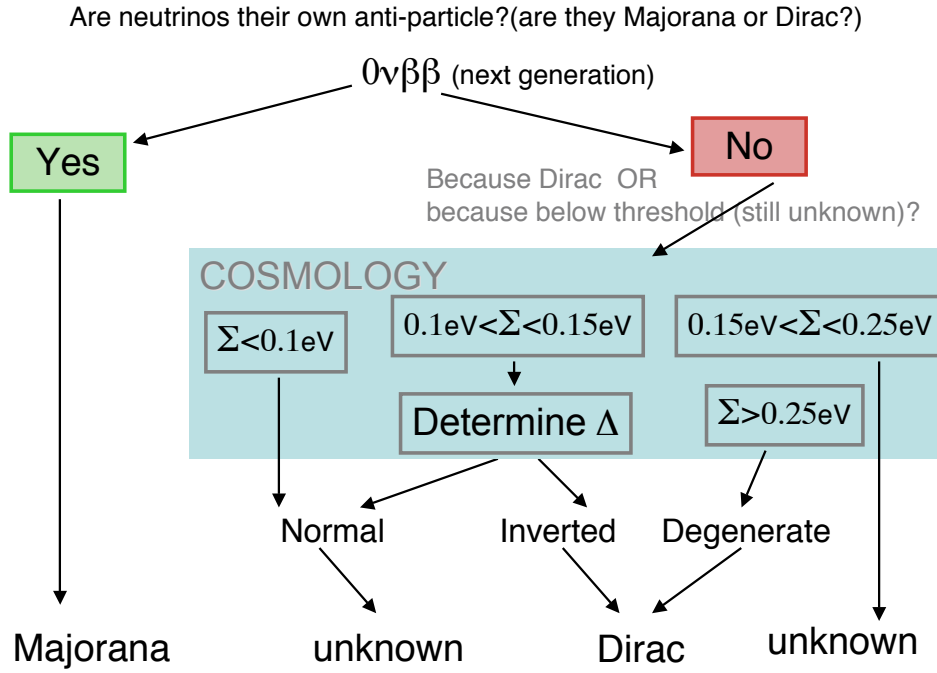


**Fig. V:** Role of cosmology in determining the nature of neutrino mass. Future neutrinoless double beta decay ( $0\nu\beta\beta$ ) experiments and future cosmological surveys will be highly complementary in addressing the question of whether neutrinos are Dirac or Majorana particles. Next generation means near future experiments whose goal is to reach a sensitivity to the neutrinoless double beta decay effective mass of 0.01 eV. We can still find two small windows where this combination of experiments will not be able to give a definite answer, but this region is much reduced by combining  $0\nu\beta\beta$  and cosmological observations.

with  $N = [nP(k, \mu)/(nP(k, \mu) + 1)]^2$  and  $V_s$  is the volume of the survey. The integration over the projected angle along the light of sight <sup>1</sup>  $\mu$  is analytical and the maximum and minimum wavenumbers allowed depend on the survey characteristics with the constraint that  $k_{\max}$  must be in the linear regime. The derivatives are computed at the fiducial model chosen.

The degeneracies between  $\Sigma$  and  $\Delta$  are small, and the very small constraint on  $\Sigma$  results in the constraints being effectively un-correlated in the  $\Sigma$ - $\Delta$  plane. We note that the constraints on  $\Delta$  around the IH and NH peaks are tighter for weak lensing than LSS, this is due to lensing providing constraints on both the geometry and the growth of structure, which provides a smaller raw constraint and a more orthogonal constraint to the CMB resulting in smaller errors. Interestingly, even though the weak lensing constraints on  $\Delta$  are smaller than for the power spectrum, the evidence ratio is comparable (see Fig. IV), because, due to the multi-dimensional degeneracy directions, a naive correspondence between error-bars and evidence is not applicable (it is to a first approximation the difference between the two error bars that is important).

Note that the evidence calculation explicitly assumes two isolated peaks, and so is only applicable when the fiducial points are separated by multiple-sigma. As a result of this, the evidence calculations may be slightly optimistic for large masses. However, for  $\Sigma < 0.2$  eV, the  $\chi^2$  difference between the

<sup>1</sup>As it is customary,  $\mu$  denotes the cosine of the angle with respect to the line of sight.

two minima becomes noticeable as well as the shift between the location of one of the two minima and the central  $\Delta$  value for the oscillations experiments (which induces an additional  $\chi^2$  difference). While this information is not fully accounted for in a Bayesian approach to forecasting the evidence, it may be included at the moment of analyzing the data, using different approaches such as the likelihood ratio, and may slightly improve the significance for the hierarchy determination.

While we have used the oscillation results to center the Fisher and evidence calculations on the NH and IH, combining the oscillation experiments constraints will not improve the evidence; in fact, oscillation experiments give symmetric errors on  $\Delta$  (i.e. they do not depend on the sign of  $\Delta$ ). The final scheme is shown in Fig. V which illustrates how the hierarchy can be determined in future cosmology experiments.

Better perspectives at measuring the neutrino hierarchy from the sky can be attained by exploiting the non-linear part of the power spectrum of galaxies as was shown by Ref. [72]. Non-linearities enhance the dependence of the power spectrum on the different neutrino hierarchies, thus making the observational signature more pronounced. If all other cosmological parameters are known (including the sum of neutrino masses  $\Sigma$ ), the two hierarchies can be distinguished with confidence, as illustrated in Fig. VII as function of the maximum  $k$  considered, making the effect potentially measurable. We have assumed an effective volume of  $1 (\text{Gpc}/h)^3$  at  $z = 0$  (red lines) and  $10 (\text{Gpc}/h)^3$  at  $z = 1$  (blue lines).<sup>2</sup> Whether degeneracies with other cosmological parameters and systematic effects (galaxy bias, baryonic physics, observational limitations etc.) will cancel the detectability of the effect remains to be explored.

Cosmology has the potential of determining the neutrino hierarchy in the interesting window  $\Sigma \gtrsim 0.1\text{eV}$ . Signal-to-noise estimates done using linear theory predictions indicated that if  $\Sigma$  happens to be in the window  $0.15\text{eV} < \Sigma < 0.25\text{eV}$ , cosmology could not help determine the hierarchy and thus the nature of neutrino masses [64], leaving an important gap in our knowledge of neutrino properties. The fact that non-linearities enhance the effect compared to the linear prediction, will potentially enable cosmology to determine the hierarchy in a wider  $\Sigma$  range and possibly close the gap.

As an aside and already noted in Ref. [64], cosmology is more sensitive to  $|\Delta|$  than to its sign: a measurement of  $|\Delta|$  in agreement with that predicted by oscillations experiments for the measured  $\Sigma$  would provide a convincing consistency check for the total neutrino mass constraint from cosmology.

#### 4 Using astronomical distances to constraint beyond the standard model physics

Cosmological observations provide constraints on different distance measures: luminosity distance (as provided e.g., by supernovae), angular diameter distance (as provided e.g., by baryon acoustic oscillations) and even on the expansion rate or the Hubble parameter as a function of redshift  $z$ . Both luminosity distance and angular diameter distance are functions of the Hubble parameter. While combining these measurements helps to break parameter degeneracies and constrain cosmological parameters, comparing them helps to constrain possible deviations from the assumptions underlying the standard cosmological model (e.g. isotropy), or to directly constrain physics beyond the standard model of particle physics (e.g. couplings of photons to scalar or pseudo-scalar matter).

The Etherington relation [73] implies that, in a cosmology based on a metric theory of gravity, distance measures are unique: the luminosity distance is  $(1+z)^2$  times the angular diameter distance. This is valid in any cosmological background where photons travel on null geodesics and where, crucially, photon number is conserved.

There are several scenarios in which the Etherington relation would be violated: for instance we can have deviations from a metric theory of gravity, photons not traveling along unique null geodesics, variations of fundamental constants, etc. Here we want to restrict our attention to violations of the Etherington relation arising from the violation of photon conservation.

<sup>2</sup>These volumes roughly correspond to the volume out to  $z = 0.5$  and between  $z = 0.5$  and  $z = 1.5$  in 1/10 of the sky respectively in a standard  $\Lambda$ CDM universe.

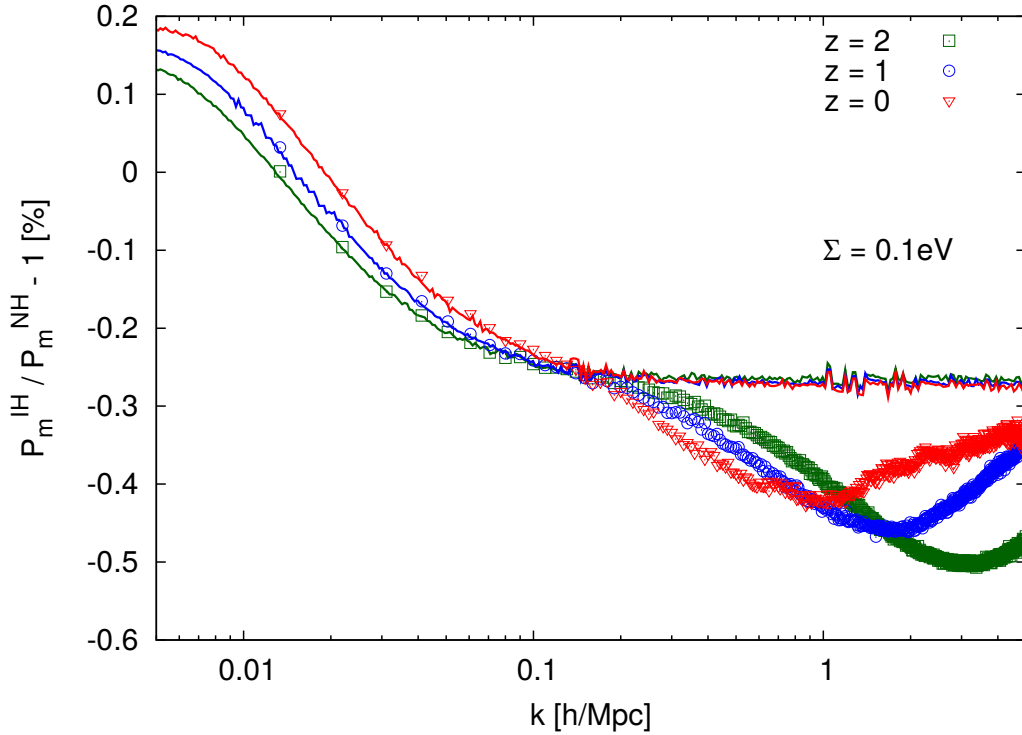


**Fig. VI:** Fractional difference in the total matter power spectrum (CDM+baryons+massive neutrinos) of the inverted hierarchy and normal hierarchy run (the sum of neutrino masses is kept fixed and only the mass splitting is varied). Note that also in this case, non-linearities enhance the effect on mildly non-linear scales compared to linear theory predictions (solid lines).

A change in the photon flux during propagation towards the Earth will affect the Supernovae (SNe) luminosity distance measures but not the determinations of the angular diameter distance. Photon conservation can be violated by simple astrophysical effects or by exotic physics. Amongst the former we find, for instance, attenuation due to interstellar dust, gas and/or plasmas. Most known sources of attenuation are expected to be clustered and can be typically constrained down to the 0.1% level [74, 75]. Unclustered sources of attenuation are however much more difficult to constrain. For example, gray dust [76] has been invoked to explain the observed dimming of Type Ia Supernovae without resorting to cosmic acceleration.

More exotic sources of photon conservation violation involve a coupling of photons to particles beyond the standard model of particle physics. Such couplings would mean that, while passing through the intergalactic medium, a photon could disappear –or even (re)appear!– interacting with such exotic particles, modifying the apparent luminosity of sources. Here we consider the mixing of photons with scalars, known as axion-like particles, and the possibility of mini-charged particles which have a tiny, and unquantised electric charge. A recent review [77] highlights the rich phenomenology of these weakly-interacting-sub-eV-particles (WISPs), whose effects have been searched for in a number of laboratory experiments and astronomical observations. In particular, the implications of these particles on the SN luminosity have been described in a number of publications [78–82].

One of the most interesting features of these models is that the exotic opacity involved could in principle “mimic” the value of a non-zero cosmological constant inferred from SNe measurements.

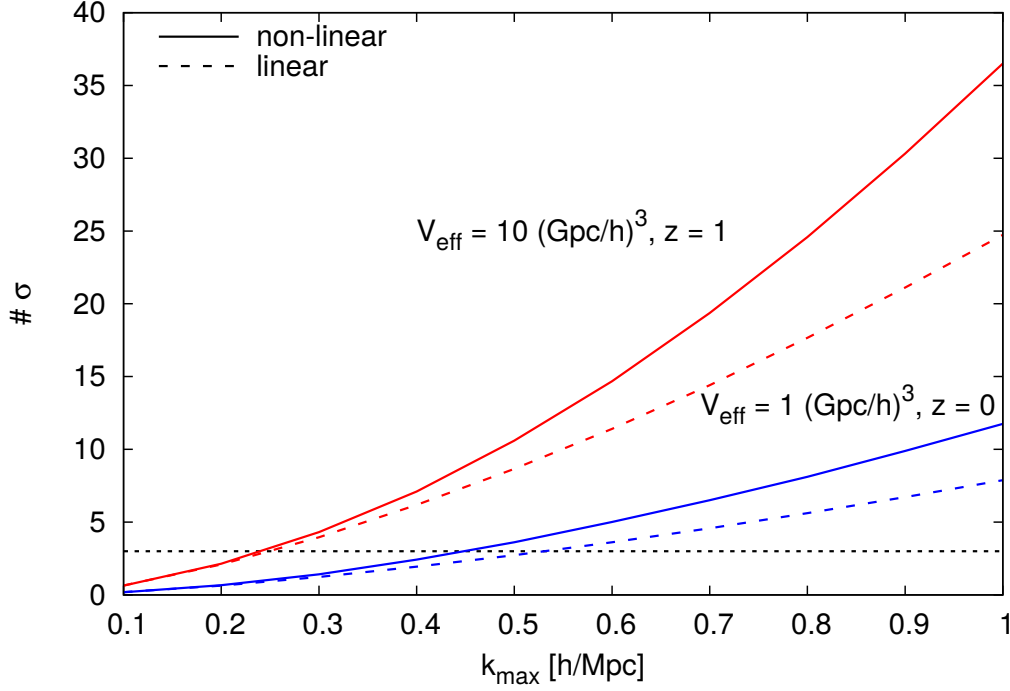


**Fig. VII:** Forecast of the number of sigmas separating the two hierarchies for  $\Sigma = 0.1\text{eV}$  as a function of the maximum  $k$  vector considered and for two effective volumes  $1$  and  $10 (\text{Gpc}/h)^3$  at  $z = 0$  and  $z = 1$  respectively. It is assumed that all other cosmological parameters are known. The horizontal dotted line indicates the  $3 - \sigma$  level.

However, this possibility can already be excluded (at least in the simplest WISP models) by the absence of distortions in the CMB or the spectra of quasars for axion-like-particles, and by arguments of stellar evolution in the case of mini-charged particles.

#### 4.1 Calculating cosmic opacity

In reference [93], the authors use Type Ia SN brightness data (namely the SCP Union 2008 compilation [94]) in combination with measurements of cosmic expansion  $H(z)$  from differential aging of luminous red galaxies (LRGs) [23,95] to obtain constraints on non-trivial opacity, at cosmological scales. The basic idea is to study possible violations from the “Etherington relation” [73], the distance duality between luminosity distance,  $d_L$ , and angular diameter distance,  $d_A$ :

$$d_L(z) = (1 + z)^2 d_A(z). \quad (13)$$

This identity depends only on photon number conservation and local Lorentz invariance. It holds for general metric theories of gravity, where photons travel along unique null geodesics. Since Lorentz violation is strongly constrained for the low energies corresponding to optical observations [83], the study of possible violations of Eq. (13) through SN observations directly constrains photon number violation. Any such systematic violations can then be interpreted as an opacity effect in the observed luminosity distance, parametrised through a generic opacity parameter,  $\tau(z)$ , as:

$$d_{L,obs}^2 = d_{L,true}^2 e^{\tau(z)}. \quad (14)$$

Note that this ‘‘opacity’’ can have in principle both signs. In other words, this parametrisation also allows for apparent *brightening* of light sources, as would be the case, for example, if exotic particles were also emitted from the source and converted into photons along the line of sight [81]. From Eq. (14) it is clear that the inferred distance moduli for the observed SNe picks an extra term which is linear in  $\tau(z)$ :

$$DM_{obs}(z) = DM_{true}(z) + 2.5[\log e]\tau(z). \quad (15)$$

On the other hand, one can also use other determinations of distance measures, which are independent of  $\tau$ , to constrain possible deviations from Eq. (13). This approach was initiated in reference [92] (see also [84–87] for related earlier work) where the authors used measurements [88] of the baryon acoustic oscillation (BAO) scale at two redshifts, namely  $z = 0.20$  and  $z = 0.35$ , to obtain a parameterization-independent upper-bound for the difference in opacity between these two redshifts,  $\Delta\tau < 0.13$  at 95% confidence. In reference [93] this constraint was improved (and also extended over a wider redshift range, but for a general parameterised form for  $\tau$ ) by using, instead of measurements of the BAO scale at these two redshifts, measurements of cosmic expansion  $H(z)$  from differential aging of LRGs at redshifts  $z < 2$ . This method of distance determination relies on the detailed shapes of galaxy spectra but not on galaxy luminosities, so it is independent of  $\tau$ .

In particular, the authors introduced a parameter  $\epsilon$  to study deviations from the Etherington relation of the form:

$$d_L(z) = d_A(z)(1+z)^{2+\epsilon}, \quad (16)$$

and constrained this parameter to be  $\epsilon = -0.01_{-0.09}^{+0.08}$  at 95% confidence. Restricted to the redshift range  $0.2 < z < 0.35$ , where  $\tau(z) = 2\epsilon z + \mathcal{O}(\epsilon z^2)$ , this corresponds to  $\Delta\tau < 0.02$  at 95% confidence. Below, we will apply similar constraints on different parametrisations of  $\tau$  which correspond to particular models of exotic matter-photon coupling, namely axion-like particles (ALPs), chameleons, and mini-charged particles (MCPs).

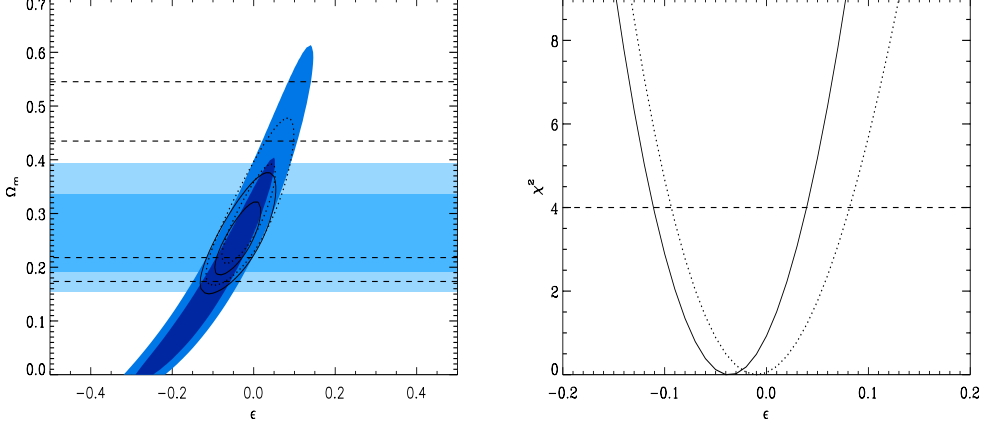
Before moving to these models, we briefly update the above constraint on  $\epsilon$  using the latest  $H(z)$  data [32], which include two extra data points at redshifts  $z = 0.48$  and  $z = 0.9$ , as well as the latest determination of  $H_0$  [89]. Even though the addition of these two extra data points alone significantly improves the constraints of reference [93], the effect of  $H_0$  is also quite significant, because it acts as an overall scale in the distance measures, which is marginalised over a Gaussian prior, and the measurement error in this determination is about half of that of the HST Key Project determination [90] used in [93].

Fig. VIII shows the updated constraints obtained using the above data in combination with the SCP Union 2008 Compilation [94] of type Ia Supernova data, compared to the previous constraints of reference [93]. On the left, the darker blue contours correspond to the (two-parameter) 68% and 95% joint confidence levels obtained from SN data alone, while lighter blue contours are the corresponding confidence levels for  $H(z)$  data. Solid-line transparent contours are for joint SN+ $H(z)$  data. For comparison we also show the previous  $H(z)$  and SN+ $H(z)$  contours in dotted and dashed lines respectively. On the right we show one-parameter (marginalized over all other parameters) constraints on  $\epsilon$ , again for the current analysis (solid line) and for that of reference [93] (dotted). For the reader familiar with Bayesian methods, this plot corresponds to the posterior

$$P(\epsilon|S, E) = \int_{\Omega_m} \int_{H_0} P(\Omega_m, H_0|E)P(\epsilon, \Omega_m, H_0|S) d\Omega_m dH_0, \quad (17)$$

where  $P(\Omega_m, H_0|E)$  and  $P(\epsilon, \Omega_m, H_0|S)$  are the posterior probabilities for the corresponding model parameters, given the  $H(z)$  (Expansion) and SN (Supernovae) data respectively. These are given by the likelihoods of the two data sets in the model parameters, assuming Gaussian errors and using flat priors on all three parameters. In particular, we have taken  $\epsilon \in [-0.5, 0.5]$ ,  $\Omega_m \in [0, 1]$  and  $H_0 \in [74.2 - 3 \times 3.6, 74.2 + 3 \times 3.6]$  (Riess et. al. [89]), all spaced uniformly over the relevant intervals, in a flat  $\Lambda$ CDM model. Similarly, the solid line transparent contours on the left plot of Fig. VIII correspond to

taking only the integral over  $H_0$  in the right hand side of Eq. (17), yielding, therefore, the two-parameter posterior  $P(\epsilon, \Omega_m | \mathcal{S}, \mathcal{E})$ .



**Fig. VIII:** Updated constraints of reference [93], using  $H(z)$  data [32] and the Riess et al. determination of  $H_0$  [89] in combination with the SCP Union 2008 SN Ia compilation. *Left:* Two-parameter constraints on the  $\epsilon - \Omega_m$  plane. Darker blue contours correspond to 68% and 95% confidence levels obtained from SN data alone, lighter blue contours are for  $H(z)$  data, and solid line transparent contours are for joint SN+ $H(z)$ . Previous  $H(z)$  and joint SN+ $H(z)$  from [93] are shown in dashed and dotted lines respectively. *Right:* One-parameter joint constraints on  $\epsilon$  for the current analysis (solid line) and that of reference [93] (dotted line). The dashed line shows the 95% confidence level,  $\Delta\chi^2 = 2$ .

As seen in Fig. VIII, the improvement in these constraints is significant. The new result on  $\epsilon$ , marginalised over all other parameters, is  $\epsilon = -0.04^{+0.08}_{-0.07}$  at 95% confidence, which for redshifts between 0.2 and 0.35 (currently probed by BAO data), corresponds to a transparency (i.e.,  $\tau \geq 0$ ) bound  $\Delta\tau < 0.012$ , a factor of two tighter than the result in reference [93]<sup>3</sup>. We now move on to study more general parametrisations of cosmic opacity, tailored for particular models of exotic matter coupled to photons.

#### 4.2 Axion-like Particles and Chameleons

New scalar or pseudo scalar particles from physics beyond the standard model, here denoted as  $\phi$ , may couple to photons through

$$\mathcal{L}_{scalar} = \frac{1}{4M} F_{\mu\nu} F^{\mu\nu} \phi \quad (18)$$

and

$$\mathcal{L}_{pseudo-scalar} = \frac{1}{8M} \epsilon_{\mu\nu\lambda\rho} F^{\mu\nu} F^{\lambda\rho} \phi \quad (19)$$

where  $M$  is the energy scale of the coupling (another widely used notation is  $g_{\phi\gamma} = 1/M$ ),  $F_{\mu\nu}$  the electromagnetic field strength and  $\epsilon_{\mu\nu\lambda\rho}$  the Levi-Civita symbol in four dimensions. Such fields are collectively known as Axion-Like Particles (ALPs), as a coupling of the form (19) arises for the axion introduced by Peccei and Quinn (PQ) to solve the strong CP problem [96]. Interestingly, these fields also arise naturally in string theory (for a review see [97]).

Axions, or axion-like-particles, can arise from field theoretic extensions of the standard model as Goldstone bosons when a global shift symmetry, present in the high energy sector, is spontaneously

<sup>3</sup>Note that the data slightly favour negative  $\epsilon$  (thus the much stronger constraint on a positive  $\Delta\tau$ ), but only at  $< 1\text{-}\sigma$  level.

broken. In the PQ axion case, this symmetry is colour anomalous and the explicit breaking makes the axion pick up a small mass. This mass is, up to a model-independent constant, proportional to the coupling (19). For a generic ALP, however, the mass is in principle independent of the strength of its coupling, and in particular can be zero if the related shift symmetry remains intact. That is, for instance, the case of Arions [98], the orthogonal combination of the PQ axion, if there are *two* independent colour anomalous shift symmetries.

Chameleon scalar fields are another very interesting type of ALPs [99]. They were originally invoked in [100, 101] to explain the current accelerated expansion of the Universe with a quintessence field which can couple to matter without giving rise to large fifth forces or unacceptable violations of the weak equivalence principle. The chameleon achieves this because its mass depends on the local energy density. The environmental dependence of the mass of the chameleon means that it avoids many of the constraints on the strength of the coupling, which normally apply to standard scalar and pseudo-scalar fields as they are derived from physics in dense environments. For a more detailed discussion see [102]. The cosmology of the chameleon was explored in detail in [103], the possibility of the chameleon coupling to photons was first discussed in [104] and such a coupling was shown to be generic in [99].

The Lagrangian terms given above mean that ALPs can affect the propagation of photons; in particular, if photons traverse a magnetic field there is a non-zero probability that they will oscillate into ALPs [105]. Notice however that only photons polarized perpendicular (parallel) to the magnetic field mix with scalar (pseudo-scalar) particles. Therefore, the interactions between photons and ALPs in the presence of a magnetic field not only imply that photon number is not conserved, but can also alter the polarization of the light beam. Both effects have been exploited in many searches for ALPs both in the laboratory and in astronomical observations, see [77] for a recent review.

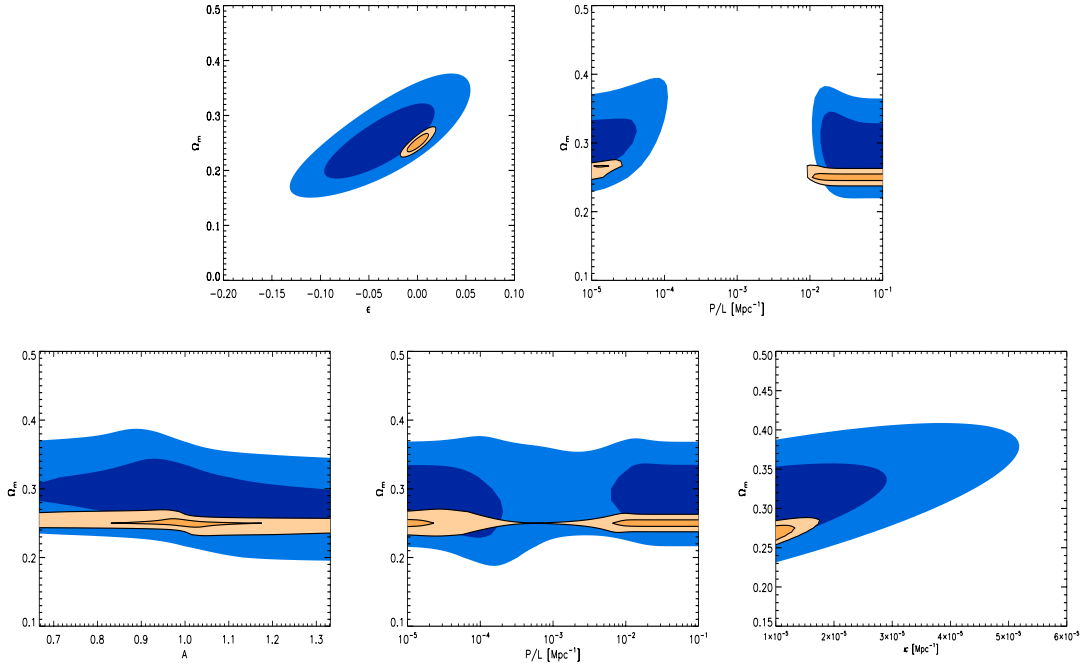


**Fig. IX:** Forecast constraints from joint EUCLID (orange scale), shown together with the corresponding constraints from current data, namely SN (Union08) joint with chronometer  $H(z)$  (blue scale). Dark and light contours correspond to 1- and 2- $\sigma$  respectively. From top left to bottom right: constraints on the opacity parameter  $\epsilon$ , parameter  $P/L$  for the simple ALP model of section, parameters  $A$  &  $P/L$  for chameleons, and parameter  $\kappa$  for MCPs see Ref. [106] for more details.

If new particles from physics beyond the standard model couple to photons then the propagation of light may be altered. We have reviewed two scenarios for exotic particles which can significantly modify the propagation of photons as they pass through magnetic fields. Measurements of cosmic opacity are a strong tool to constrain such scenarios, as interactions between photons and exotic particles in the magnetic fields of the intergalactic medium leads to a new source of cosmic opacity. Uniform deviations from cosmic transparency (i.e. opacity) can be constrained through their effects on distance duality, by parameterizing possible deviations from the Etherington relation.

More exotic sources of photon-conservation violation involve a coupling of photons to particles beyond the standard model of particle physics. We have focused on axion-like particles, new scalar or pseudo scalar fields which couple to the kinetic terms of photons, and mini-charged particles which are hidden sector particles with a tiny electric charge. Photons passing through intergalactic magnetic fields may be lost by pair production of light mini-charged particles. If the mixing between axion-like particles and photons is significant, then interactions in the intergalactic magnetic fields will also lead to a loss of photons due to conversion into ALPs. However if the coupling between photons and ALPs is sufficiently strong, one-third of any initial flux will be converted into ALPs, and two-thirds into photons, resulting in a redshift-independent dimming of supernovae which we cannot constrain or exclude with cosmic opacity bounds.

The improved measurement of the cosmic opacity found here leads to improved bounds on these exotic physics scenarios which are summarised in Fig. IX. Future measurements of baryon acoustic oscillations, and an increase in the number of observations of high redshift supernovae will lead to further improvements in the constraints on physics beyond the standard model.

## References

- [1] S. Perlmutter *et al.* [Supernova Cosmology Project Collaboration], *Astrophys. J.* **517** (1999) 565 [arXiv:astro-ph/9812133]; A. G. Riess *et al.* [Supernova Search Team Collaboration], *Astron. J.* **116** (1998) 1009 [arXiv:astro-ph/9805201].
- [2] G. Jungman, M. Kamionkowski, A. Kosowsky and D. N. Spergel, *Phys. Rev. D* **54** (1996) 1332 [arXiv:astro-ph/9512139]; G. Jungman, M. Kamionkowski, A. Kosowsky and D. N. Spergel, *Phys. Rev. Lett.* **76** (1996) 1007 [arXiv:astro-ph/9507080]; P. de Bernardis *et al.* [Boomerang Collaboration], *Nature* **404** (2000) 955 [arXiv:astro-ph/0004404]; A. D. Miller *et al.*, *Astrophys. J.* **524** (1999) L1 [arXiv:astro-ph/9906421]; S. Hanany *et al.*, *Astrophys. J.* **545** (2000) L5 [arXiv:astro-ph/0005123]; A. H. Jaffe *et al.* [Boomerang Collaboration], *Phys. Rev. Lett.* **86** (2001) 3475 [arXiv:astro-ph/0007333]; N. W. Halverson *et al.*, *Astrophys. J.* **568** (2002) 38 [arXiv:astro-ph/0104489]; B. S. Mason *et al.*, *Astrophys. J.* **591** (2003) 540 [arXiv:astro-ph/0205384]; A. Benoit *et al.* [the Archeops Collaboration], *Astron. Astrophys.* **399** (2003) L25 [arXiv:astro-ph/0210306]; J. H. Goldstein *et al.*, *Astrophys. J.* **599** (2003) 773 [arXiv:astro-ph/0212517]; D. N. Spergel *et al.* [WMAP Collaboration], *Astrophys. J. Suppl.* **148** (2003) 175 [arXiv:astro-ph/0302209]; C. L. Reichardt *et al.*, *Astrophys. J.* **694** (2009) 1200 [arXiv:0801.1491 [astro-ph]]; C. L. Reichardt *et al.*, arXiv:0801.1491 [astro-ph]; D. N. Spergel *et al.* [WMAP Collaboration], *Astrophys. J. Suppl.* **170** (2007) 377 [arXiv:astro-ph/0603449]; J. Dunkley *et al.* [WMAP Collaboration], *Astrophys. J. Suppl.* **180** (2009) 306 [arXiv:0803.0586 [astro-ph]].
- [3] W. J. Percival *et al.* [The 2dFGRS Collaboration], *MNRAS* **327** (2001) 1297 [arXiv:astro-ph/0105252].
- [4] S. Dodelson *et al.* [SDSS Collaboration], *Astrophys. J.* **572** (2001) 140 [arXiv:astro-ph/0107421].
- [5] W. L. Freedman *et al.* [HST Collaboration], *Astrophys. J.* **553** (2001) 47 [arXiv:astro-ph/0012376].
- [6] P. J. E. Peebles and B. Ratra, *Rev. Mod. Phys.* **75**, 559 (2003) [arXiv:astro-ph/0207347]; T. Padmanabhan, *Phys. Rept.* **380** (2003) 235 [arXiv:hep-th/0212290]; E. J. Copeland, M. Sami and S. Tsujikawa, *Int. J. Mod. Phys. D* **15** (2006) 1753 [arXiv:hep-th/0603057]; J. Frieman, M. Turner

- and D. Huterer, *Ann. Rev. Astron. Astrophys.* **46** (2008) 385 [arXiv:0803.0982 [astro-ph]]; E. V. Linder, *Rept. Prog. Phys.* **71** (2008) 056901 [arXiv:0801.2968 [astro-ph]]; R. R. Caldwell and M. Kamionkowski, arXiv:0903.0866 [astro-ph.CO];
- [7] B. Ratra and P. J. E. Peebles, *Phys. Rev. D* **37** (1988) 3406; R. R. Caldwell, R. Dave and P. J. Steinhardt, *Phys. Rev. Lett.* **80**, 1582 (1998) [arXiv:astro-ph/9708069].
- [8] J. A. Peacock, P. Schneider, G. Efstathiou, J. R. Ellis, B. Leibundgut, S. J. Lilly and Y. Mellier, arXiv:astro-ph/0610906.
- [9] D. Stern, R. Jimenez, L. Verde, S. A. Stanford and M. Kamionkowski, *Astrophys. J. Suppl.*, **188**, (2010) 280
- [10] A. Albrecht *et al.*, arXiv:astro-ph/0609591;
- [11] W. J. Percival, S. Cole, D. J. Eisenstein, R. C. Nichol, J. A. Peacock, A. C. Pope and A. S. Szalay, *MNRAS* **381** (2007) 1053 [arXiv:0705.3323 [astro-ph]].
- [12] D. J. Eisenstein *et al.* [SDSS Collaboration], *Astrophys. J.* **633** (2005) 560 [arXiv:astro-ph/0501171].
- [13] J. B. Oke *et al.*, *Publ. Astrophys. Soc. Pac.* **107** (1995) 375
- [14] H. J. Seo and D. J. Eisenstein, *Astrophys. J.* **598** (2003) 720 [arXiv:astro-ph/0307460].
- [15] J. R. Pritchard, S. R. Furlanetto and M. Kamionkowski, *MNRAS* **374** (2007) 159 [arXiv:astro-ph/0604358].
- [16] A. Refregier, *Ann. Rev. Astron. Astrophys.* **41** (2003) 645 [arXiv:astro-ph/0307212].
- [17] Z. Haiman, J. J. Mohr and G. P. Holder, *Astrophys. J.* **553** (2000) 545 [arXiv:astro-ph/0002336].
- [18] R. Jimenez and A. Loeb, *Astrophys. J.* **573** (2002) 37 [arXiv:astro-ph/0106145].
- [19] B. Chaboyer, *Astrophys. J.* **444** (1995) L9 [arXiv:astro-ph/9412015].
- [20] R. Jimenez, U. G. Jorgensen, P. Thejll and J. MacDonald, *MNRAS* **275** (1995) 1245 [arXiv:astro-ph/9502050].
- [21] L. M. Krauss and B. Chaboyer, *Science* **299** (2003) 65.
- [22] R. Jimenez, L. Verde, T. Treu and D. Stern, *Astrophys. J.* **593**, 622 (2003) [arXiv:astro-ph/0302560].
- [23] J. Simon, L. Verde and R. Jimenez, *Phys. Rev. D* **71** (2005) 123001 [arXiv:astro-ph/0412269].
- [24] M. Sahlen, A. R. Liddle and D. Parkinson, *Phys. Rev. D* **72** (2005) 083511 [arXiv:astro-ph/0506696]; L. Samushia and B. Ratra, *Astrophys. J.* **650** (2006) L5 [arXiv:astro-ph/0607301]; R. Lazkoz, *AIP Conf. Proc.* **960** (2007) 3 [arXiv:0710.2872 [astro-ph]]; N. E. Mavromatos and V. A. Mitsou, *Astropart. Phys.* **29** (2008) 442 [arXiv:0707.4671 [astro-ph]]; F. C. Carvalho, E. M. Santos, J. S. Alcaniz and J. Santos, *JCAP* **0809** (2008) 008 [arXiv:0804.2878 [astro-ph]]; E. Fernandez-Martinez and L. Verde, *JCAP* **0808** (2008) 023 [arXiv:0806.1871 [astro-ph]]; A. Kurek, O. Hrycyna and M. Szydlowski, *Phys. Lett. B* **659** (2008) 14 [arXiv:0707.0292 [astro-ph]]; A. A. Sen and R. J. Scherrer, *Phys. Lett. B* **659** (2008) 457 [arXiv:astro-ph/0703416]; H. Zhang and Z. H. Zhu, *JCAP* **0803** (2008) 007 [arXiv:astro-ph/0703245]; B. Ratra and M. S. Vogeley, *Publ. Astron. Soc. Pac.* **120** (2008) 235 [arXiv:0706.1565 [astro-ph]];
- [25] J. Dunlop, J. Peacock, H. Spinrad, A. Dey, R. Jimenez, D. Stern and R. Windhorst, *Nature* **381** (1996) 581.
- [26] H. Spinrad, A. Dey, D. Stern, J. Dunlop, J. Peacock, R. Jimenez and R. Windhorst, *Astrophys. J.* **484** (1997) 581. arXiv:astro-ph/9702233.
- [27] L. L. Cowie, A. Songaila and A. J. Barger, "Density for  $z < 1$ ," *Astron. J.* **118** (1999) 603 [arXiv:astro-ph/9904345].
- [28] A. Heavens, B. Panter, R. Jimenez and J. Dunlop, *Nature* **428** (2004) 625 [arXiv:astro-ph/0403293].
- [29] D. Thomas, C. Maraston, R. Bender and C. M. de Oliveira, *Astrophys. J.* **621** (2005) 673

- [arXiv:astro-ph/0410209].
- [30] B. Panter, R. Jimenez, A. F. Heavens and S. Charlot, *MNRAS* **378** (2007) 1550 [arXiv:astro-ph/0608531].
- [31] T. Treu *et al.*, *Astrophys. J.* **633**, 174 (2005) [arXiv:astro-ph/0503164].
- [32] Stern, D., Jimenez, R., Verde, L., Kamionkowski, M., Stanford, S. A. 2010. *JCAP* 2, 8.
- [33] Moresco M., Jimenez R., Cimatti A., Pozzetti L., 2011, *JCAP*, 3, 45
- [34] Moresco M., et al., 2012, *JCAP*, 8, 6
- [35] Moresco M., Verde L., Pozzetti L., Jimenez R., Cimatti A., 2012, *JCAP*, 7, 53
- [36] Jimenez R., Talavera P., Verde L., Moresco M., Cimatti A., Pozzetti L., 2012, *JCAP*, 3, 14
- [37] Moresco M., Jimenez R., Cimatti A., Pozzetti L., 2011, *JCAP*, 3, 45
- [38] Bellini E., Jimenez R., 2013, arXiv, arXiv:1306.1262
- [39] de Putter R., Verde L., Jimenez R., 2013, *JCAP*, 2, 47
- [40] Hoyle B., Tojeiro R., Jimenez R., Heavens A., Clarkson C., Maartens R., 2013, *ApJ*, 762, L9
- [41] Heavens A. F., Jimenez R., Maartens R., 2011, *JCAP*, 9, 35
- [42] Verde L., Jimenez R., Feeney S., 2013, arXiv, arXiv:1303.5341
- [43] Verde L., Protopapas P., Jimenez R., 2013, arXiv, arXiv:1306.6766
- [44] Y. Fukuda *et al.*, *Phys. Rev. Lett.* **81**, 1562 (1998).
- [45] Ahn, M. H., *et al.*, *Phys. Rev. D* **74**, 072003 (2006).
- [46] Adamson P., *et al.*, *Phys. Rev. Lett.* **101**, 221804 (2008)
- [47] Q. R. Ahmad *et al.*, *Phys. Rev. Lett.* **89**, 011301 (2002).
- [48] K. Eguchi *et al.*, *Phys. Rev. Lett.* **90**, 021802 (2003).
- [49] B. T. Cleveland *et al.*, *Astrophys. J.* **496**, 505 (1998).
- [50] E. Bellotti, Talk at VIIIth International Conference on Topics in Astroparticle and Underground Physics (TAUP03), Seattle, (Sep 5-9, 2003); V. Gavrin, *ibid.*
- [51] J. N. Bahcall, *Phys. Rev. Lett.* **12**, 300 (1964); R. Davis, *Phys. Rev. Lett.* **12**, 303 (1964).
- [52] L. Wolfenstein, *Phys. Rev. D* **17**, 2369 (1978); S. P. Mikheev and A. Y. Smirnov, *Sov. J. Nucl. Phys.* **42**, 913 (1985).
- [53] H. Murayama and C. Pena-Garay, *Phys. Rev. D* **69**, 031301 (2004).
- [54] Melchiorri, A., Mena, O., Palomares-Ruiz, S., Pascoli, S., Slosar, A., & Sorel, M., *JCAP*, 1, 36 (2009)
- [55] A. A. Aguilar-Arevalo et al., *Phys. Rev. Lett.* 98, 231801 (2007).
- [56] M. Fukugita and T. Yanagida, *Phys. Lett. B* **174**, 45 (1986).
- [57] Cremonesi, O. 2010, arXiv:1002.1437
- [58] E. Komatsu *et al.*, *Astrophys. J. Suppl.* **180** (2009) 330.
- [59] Reid, B. A., Verde, L., Jimenez, R., & Mena, O. 2010, *JCAP*, 1, 3
- [60] LSST Science Collaborations: Paul A. Abell, et al. 2009, arXiv:0912.0201
- [61] Hannestad, S. 2010, arXiv:1003.4119
- [62] Refregier, A., Amara, A., Kitching, T. D., Rassat, A., Scaramella, R., Weller, J., & Euclid Imaging Consortium, f. t. 2010, arXiv:1001.0061
- [63] Slosar, A. 2006, *Phys. Rev. D.*, 73, 123501
- [64] Jimenez, R., Kitching, T., Peña-Garay, C., Verde, L. 2010. *JCAP* 5, 35.
- [65] M. Takada, E. Komatsu and T. Futamase, *Phys. Rev. D* **73**, 083520 (2006).
- [66] de Bernardis, F., Kitching, T. D., Heavens, A., & Melchiorri, A. 2009, *PRD*, 80, 123509
- [67] D. J. Eisenstein and W. Hu, *Astrophys. J.* **511** (1997) 5.

- [68] Fisher, R. A. 1932, Proceedings of the Cambridge Philosophical Society, 28, 257
- [69] Heavens, A. F., Kitching, T. D., & Verde, L. 2007, MNRAS, 380, 1029
- [70] Taylor, A. N., & Kitching, T. D. 2010, arXiv:1003.1136
- [71] H. J. Seo and D. J. Eisenstein, *Astrophys. J.* **598**, 720 (2003).
- [72] Wagner C., Verde L., Jimenez R., 2012, *ApJ*, 752, L31
- [73] Etherington, J. M. H. 1933, *Phil. Mag.*, 15, 761
- [74] Ménard, B. et al. 2008, MNRAS, 385, 1053
- [75] Bovy, J., Hogg, D. W., & Moustakas, J. 2008, *ApJ*, 688, 198
- [76] Aguirre, A. N. 1999, *ApJL*, 512, L19
- [77] Jaeckel, J., & Ringwald, A., arXiv:1002.0329 [hep-ph]
- [78] Csáki, C., Kaloper, N., & Terning, J., *Phys. Rev. Lett.* **88** (2002) 161302
- [79] Mörtzell, E., Bergström, L., & Goobar, A., *Phys. Rev. D* **66** (2002) 047702
- [80] Mirizzi, A., Raffelt, G. G., & Serpico, P. D., *Lect. Notes Phys.* **741**, 115 (2008) [arXiv:astro-ph/0607415]
- [81] Burrage, C., *Phys. Rev. D* **77** (2008) 043009 [arXiv:0711.2966 [astro-ph]]
- [82] Ahlers, M., *Phys. Rev. D* **80** (2009) 023513 [arXiv:0904.0998 [hep-ph]]
- [83] Kostelecky, V. A., & Russell, N. 2008, arXiv:0801.0287 [hep-ph]
- [84] Bassett B. A., & Kunz, M., *Astrophys. J.* **607**, 661 (2004)
- [85] Bassett B. A., & Kunz, M., *Phys. Rev. D* **69**, 101305 (2004)
- [86] Uzan, J. P. *Gen. Rel. Grav.* **39** (2007) 307 [arXiv:astro-ph/0605313]
- [87] Lazkoz, R., Nesseris, S. & Perivolaropoulos, L. 2008, *JCAP* **0807** 012 [arXiv:0712.1232 [astro-ph]]
- [88] Percival, W. J. et al. 2007, MNRAS, 381, 1053
- [89] Riess, A.G., *et al.*, *Astrophys. J.* **699** (2009) 539 [arXiv:0905.0695 [astro-ph.CO]]
- [90] Freedman, W. L., *et al.* 2001, *ApJ*, 553, 47
- [91] Song, Y. S., & Hu, W., *Phys. Rev. D* **73** (2006) 023003 [arXiv:astro-ph/0508002]
- [92] More, S., Bovy, J., & Hogg, D. W. 2008, arXiv:0810.5553
- [93] Avgoustidis, A., Verde, L., & Jimenez, R., *JCAP* **0906** (2009) 012 [arXiv:0902.2006 [astro-ph.CO]]
- [94] Kowalski *et al.* 2008, *ApJ*, 686, 749
- [95] Jimenez, R., Verde, L., Treu, T., & Stern, D., 2003, *ApJ*, 593, 622
- [96] Peccei, R. D., & Quinn, H. R., *Phys. Rev. Lett.* **38** (1977) 1440.
- [97] Svrcek, P., & Witten, E., *JHEP* **0606** (2006) 051 [arXiv:hep-th/0605206]
- [98] Anselm, A. A., & Uraltsev, N. G., *Phys. Lett.* **B114** (1982) 39-41.
- [99] Brax, P., Burrage, C., Davis, A. C., Seery, D., & Weltman, A., arXiv:0911.1267 [hep-ph]
- [100] Khoury, J., & Weltman, A., *Phys. Rev. Lett.* **93** (2004) 171104 [arXiv:astro-ph/0309300]
- [101] Khoury, J., & Weltman, A., *Phys. Rev. D* **69** (2004) 044026 [arXiv:astro-ph/0309411]
- [102] Burrage, C., Davis, A. C., & Shaw, D. J., *Phys. Rev. D* **79** (2009) 044028 [arXiv:0809.1763 [astro-ph]]
- [103] Brax, P., van de Bruck, C., Davis, A. C., Khoury, J., & Weltman, A., *Phys. Rev. D* **70** (2004) 123518 [arXiv:astro-ph/0408415]
- [104] Brax, P., van de Bruck, C., & Davis, A. C., *Phys. Rev. Lett.* **99** (2007) 121103 [arXiv:hep-ph/0703243]
- [105] Raffelt, G., & Stodolsky, L., *Phys. Rev. D* **37** (1988) 1237.

[106] Avgoustidis, A., Burrage, C., Redondo, J., Verde, L., Jimenez, R. 2010. JCAP 10, 24.

# Neutrinos and Physics Beyond Electroweak and Cosmological Standard Models

Daniela Kirilova\*

Institute of Astronomy and NAO, Bulgarian Academy of Sciences, Tsarigradsko Shosse, 72, Sofia, Bulgaria

## Abstract

This is a short review of the established and the proposed by physics beyond Standard Electroweak Model and beyond Standard Cosmological Model neutrino characteristics. In particular, cosmological effects of and cosmological constraints on: extra neutrino families, neutrino mass differences and mixing, lepton asymmetry in the neutrino sector, neutrino masses, light sterile neutrino, are discussed.

## 1 Introduction

Astrophysical and cosmological observational data require Physics beyond Standard Electroweak Model (EWM) and beyond Standard Cosmological Model (SCM) (called further Beyond Standard Models (BSMs)) to explain the dark energy (DE), dark matter (DM) and dark radiation (DR) components of our Universe and their nature. BSMs physics is needed also for the explanation of the peculiar initial conditions of the pre-Friedmann epoch: its flatness, homogeneity, isotropy, etc., initial anisotropies providing the pattern of observed today structures, and also the locally observed baryon asymmetry. I.e. BSMs physics is necessary for revealing the nature and the characteristics of inflation and CPV or/and BV mechanism in baryogenesis models.

Alas, there is no firm *experimental detection* of BSMs candidates for DM and DE, only experimental and observational constraints on the hypothetical candidates or/and theories exist.

In neutrino sector, however, *BSM was established experimentally*: Experimental data on neutrino oscillations firmly determined three neutrino mixing angles and three mass differences. Cosmology provides complementary knowledge: Neutrino had a considerable influence on the processes in the Universe during different cosmological epochs - they were dynamically important ingradient during radiation stage of the Universe, influenced light elements synthesis during Big Bang Nucleosynthesis (BBN), Cosmic Microwave Background (CMB) anisotropies, and played a role in the formation of galaxies and their structures. Thus, BBN, CMB and LSS provide information and stringent constraints on neutrino characteristics.

In this work we present cosmological constraints on BSMs neutrino properties, namely, on the number of neutrino families, neutrino mass differences and mixing, lepton asymmetry hidden in the neutrino sector, neutrino masses and sterile neutrino characteristics, and discuss DR problem.

## 2 Established and Predicted Neutrino Properties by EWM and SCM

**Neutrinos in EWM:** In standard EWM neutrinos are massless, spin 1/2 fermions,  $SU(2)_W$  doublets. There are 3 neutrino flavors of light neutrinos,  $\nu_e$ ,  $\nu_\mu$  and  $\nu_\tau$ . The experimental measurement of the number of light (with  $m < m_Z/2$ ) neutrino types was provided by LEP experiments:  $N_\nu = 2.984 \pm 0.008$ .

Experimental evidence for BSM physics in the neutrino sector exists: Neutrinos oscillate, there exist neutrino mixing and there are non-zero neutrino mass differences. The origin of neutrino masses is

---

\*E-mail: dani@astro.bas.bg

not known, it is predicted by various mass generation mechanisms, usually involving the introduction of extra BSMs particles.

BSM physics, like GUT models, models with large extra dimensions, Manyfold Universe models, mirror matter models, etc., predicts "sterile" neutrinos  $\nu_s$ , i.e.  $SU(2)_W$  singlets.

**SCM neutrinos:** SCM predicts massless relic neutrinos, with equilibrium Fermi-Dirac distribution, zero chemical potential and neutrinos energy density at RD stage comparable to that of photons:

$$\rho_\nu = 7/8(T_\nu/T)^4 N_{eff} \rho_\gamma(T). \quad (1)$$

where  $N_{eff}$  is the effective number of the relativistic neutrino species. Then neutrino were dynamically important, because the expansion rate at RD is determined by the relativistic density  $H \sim \sqrt{8\pi G_N \rho}/3$ .

At  $T > 1$  MeV neutrinos were in equilibrium, since neutrino weak interaction rates were fast enough  $\Gamma_w \sim \sigma(E)n_\nu(T) > H$ .  $\Gamma_w$  decreased faster than  $H$  with the cooling of the universe, hence at  $T \sim 1$  MeV neutrino interactions froze out and cosmic neutrino background (CNB) was formed. Due to the extreme smallness of neutrino mass, neutrinos kept their equilibrium FD distribution after decoupling.

In SCM, since  $T \sim m_e$  neutrino temperature became lower than the photons one  $T_\nu = (4/11)^{1/3} T_\gamma$  due to photons heating by  $e^+e^-$ -annihilation. However, neutrino shared a small part of the entropy release due to non-instantaneous decoupling, QED finite temperature effects and flavor neutrino oscillations [1, 2]. Thus, the cosmology predicts the exact number of neutrino species  $N_\nu = 3.046$ , CNB temperature today -  $T = 1.9$  K, total neutrino number density  $n_\nu = 339.3 \text{ cm}^{-3}$ , neutrino energy density  $\Omega_\nu(t_0) = 2 \times 7/8 \times (\pi^2/30) T_{\nu,0}^4 / \rho_c \sim 10^{-5}$ .

Though CNB neutrinos have been only indirectly detected till now, SCM puts numerous constraints on neutrino and physics BSM neutrino characteristics due to neutrino cosmological effects on processes which have left observable relics.

### 3 Neutrino Beyond Standard Models - established and hypothetical

#### 3.1 Neutrino Oscillations

It has been observationally and experimentally proved that neutrinos oscillate, i.e. there exists flavor neutrino mixing in vacuum and neutrino mass eigenstates  $\nu_j$  do not coincide with the flavor eigenstates  $\nu_f$ ,

$$\nu_f = \sum_{i=1}^3 U_{fi} \nu_i, \quad \delta m_{ij}^2 = m_j^2 - m_i^2 \neq 0, \quad (i \neq j) \quad (2)$$

This implies BSM characteristics for neutrino: non-zero neutrino mass and mixing and non-conservation of the individual lepton charges  $L_f$ .

Neutrino oscillations occur also in medium, called matter oscillation. The data from solar neutrino detectors showed evidence for matter effects in the solar  $\nu_e$  transitions. For the early Universe, matter oscillations were studied as well [3].

The medium changes the oscillation pattern: suppresses oscillations by decreasing their amplitude or enhances oscillation, when a resonant condition between the oscillation parameters and the characteristics of the medium holds. In the equilibrium situation when working in terms of mean neutrino energy, the resonant condition is:

$$Q \mp L = \cos 2\vartheta. \quad (3)$$

where  $Q = -bET^4/(\delta m^2 M_W^2)$ ,  $L = -aET^3 L^\alpha/(\delta m^2)$ ,  $L^\alpha$  is given through the fermion asymmetries of the plasma,  $a$  and  $b$  are positive constants different for the different neutrino types,  $-L$  corresponds

to the neutrino and  $+L$  to the antineutrino case. For  $Q = 0$  this is the well known Mikheev-Smirnov-Wolfenstein effect [4]. In non-equilibrium case the spectrum distribution of neutrino in the early universe must be taken into account and the resonance condition and the description of neutrino propagation is more complicated [5, 6].

### 3.2 Neutrino masses

Two non-zero mass differences are measured by neutrino oscillation experiments, so at least 2 neutrino types have different and non-zero masses. (The discussion of the indications for a third mass difference in  $\sim eV^2$  range is presented in the next section.)

Neutrinos with a definite mass can be Dirac fermions or Majorana particles. The mass pattern, *normal*  $m_1 < m_2 \ll m_3$  or *inverted hierarchy*  $m_3 \ll m_1 < m_2$ , is also still unknown. The absolute neutrino masses have not been measured yet. Atmospheric neutrino oscillations data point to at least one neutrino type with mass  $m > 0.048$  eV and put lower limit on the relic neutrino density today:  $\Omega_\nu > 0.003$ , where  $\Omega_\nu = 3m/(93.14h^2 eV^2)$ .

Cosmology provides the most stringent constraints on the total neutrino density and mass  $\Omega_\nu < 0.02$ ,  $m < 0.66$  eV. The constraints are obtained from the analysis of neutrino role in structure formation of the Universe: Flavor neutrino are hot dark matter and predicted LSS in a Universe filled with hot DM is incompatible with observations.

Neutrinoless double beta decay and beta decay experiments give the limit  $m < 2.05$  eV at 95% C.L.

### 3.3 Active-sterile neutrino oscillations

Though solar and atmospheric neutrino anomalies are well described in terms of flavor neutrino oscillations, there exist some indications of sub-leading active-sterile oscillations [25–28, 62]. The phenomenology of sterile neutrino and the experimental, astrophysical and cosmological constraints on them can be found in ref. [8, 9].

In case of active-sterile oscillations beyond SCM physics is expected: i) excitation of additional light particles into equilibrium [10–12], i.e. 4 or more neutrino families, instead of 3 may exist; ii) distortion of the neutrino energy spectrum from the equilibrium FD form, in case of oscillations after neutrino decoupling [13–15]. iii) change in neutrino-antineutrino asymmetry of the medium: either *suppress pre-existing asymmetry* [12, 17] or *enhance it* (in MSW resonant active-sterile oscillations) [14, 16, 18] <sup>1</sup> iv) neutrino oscillations may be changed by L: *may be suppressed* [5, 18] or *enhanced* [5, 6]. v) Sterile neutrino, produced by neutrino oscillations, may be DM candidate [19]: 1 – 2 KeV mass sterile neutrino are warm DM candidates, compatible to cosmological observational data [20, 21]. vi) Sterile neutrinos are employed in leptogenesis models, where CP violating  $\nu_s$  decays produce the locally observed baryon asymmetry of the Universe.

In BBN with active-sterile neutrino oscillations spectrum distortion and L generation lead to different nucleon kinetics, and modified BBN element production. BBN stringent limits on oscillation parameters exist [29–34], and are discussed in more detail in the next section. Active-sterile oscillations may play important role for neutrino involved processes in the Universe also during CMB and LSS formation.

### 3.4 Neutrino-antineutrino asymmetry

Lepton asymmetry of the Universe,  $L = (n_l - n_{\bar{l}})/n_\gamma$ , may be contained mainly in the neutrino sector. Its value is not directly measured, it is only constrained by cosmology.

<sup>1</sup>More precisely, there exists interplay between neutrino oscillations and asymmetry L of the medium in the early universe plasma [22]

L increases the radiation energy density:  $\Delta N_{eff} = 15/7[(\xi/\pi)^4 + 2(\xi/\pi)^2]$ , where  $\xi = \mu/T$  is the  $\nu$  degeneracy parameter. Hence, L leads to faster expansion, delaying matter/radiation equality epoch, thus influencing BBN, CMB, LSS. Besides, BBN feels also *the kinetic effect of electron neutrino asymmetry* and provides more restrictive constraints on  $L_e$  (see ref. [35] and refs there in.)

L with much smaller values,  $L \ll 0.01$  may influence BBN through its interplay with electron-sterile neutrino oscillations, *indirect kinetic effect* [5, 6]. Thus, CMB, LSS and BBN constrain L due to its cosmological effects.

#### 4 Cosmological Constraints on BSMs Neutrino

Most precise constraints on many BSMs characteristics of neutrino are obtained from BBN considerations.

*BBN is theoretically well established and observationally and experimentally supported* (see for example [38]). The inputs include: the neutron lifetime  $\tau_n = 885.7 \pm 0.8$ , the gravitational constant  $G_N = 6.7087 \pm 0.001 \times 10^{-39} \text{ GeV}^{-2}$ , the baryon-to-photon number density  $\eta = n_B/n_\gamma$  and the nuclear rates. Precise data on nuclear processes rates from laboratory experiments at low energy (10 KeV - 1 MeV) is available.  $\eta$  until recently was considered as the only parameter of the standard BBN and was estimated from the data on the primordial abundances of the 4 elements, produced during BBN. Today  $\eta$  is known from the analysis of CMB anisotropies (which corresponds, however, to the epoch of CMB formation).

In standard BBN 4 light nuclides: D, He-3, He-4, Li-7 are produced in non-negligible quantities during the first few minutes of the RD stage, between 1 - 0.01 MeV. *Precise astrophysical data on the predicted by BBN theory light elements abundances exists.* The accepted today primordial values are:  $D/H = (2.87 \pm 0.22) \times 10^{-5}$ ,  $Y_p = 0,2534 \pm 0,0083$  [36],  $Li/H = (1.23_{-0.16}^{0.34}) \times 10^{-10}$ . BBN abundances predictions are consistent with observations. D and He-4 are used as most reliable probes for BSMs physics.

In general BBN depends on all known interactions and thus cosmology can be used to constrain their BSM modifications. In particular, BBN produced abundances, besides on the baryon-to-photon ratio, depend on i) the expansion rate ii) weak interaction rates and neutron lifetime. The nucleons freezing, and hence, the primordial yields, depend strongly on the competition between the weak rates of n-p transitions and the expansion rate  $H(N_{eff})$ . Thus, BBN is used as a probe of non-standard physics leading to changes in  $H$ ,  $\Gamma_w$ , pre-BBN nucleon kinetics or BBN itself. BBN probes any additional light i.e.  $m < MeV$ , relativistic during BBN, particles species, nonstandard interactions relevant at BBN epoch, departures from equilibrium distributions of particle densities of nucleons and leptons (caused by neutrino oscillations, lepton asymmetry, inhomogeneous distribution of baryons, etc.) BBN produced He-4 is known to be the best speedometer and is usually used to constrain additional radiation. It is also the most exact leptometer at the early stage.

Due to the closeness of the BBN epoch and the epoch of formation of the CNB, and due to the strong influence of neutrino on BBN, BBN constraints on BSM neutrino characteristics are the most stringent one.

##### 4.1 Cosmological Constraints on $N_{eff}$

BBN constrains most strongly the effective number of relativistic species  $N_{eff}$  [38]. BBN constraints, based on recent  $He - 4$  data [36], read:  $\delta N_{eff} = 0.66 \pm 0.46$ ,  $N_{eff} = 3.71_{-0.45}^{+0.47}$ . [39, 42]. Much stringent bound follows from BBN D abundance and CMB data:  $N_{eff} = 3.53 + 0.66 - 0.63$  [41]. Recent BBN analysis [42] favors  $\delta N_{eff} \sim 1$ , while  $\delta N_{eff} \sim 2$  is disfavored at more than 95% C.L.

The BBN bounds on  $N_{eff}$  are tightened in the presence of active sterile oscillations [24].

CMB experiments provide the constraint:  $N_{eff} = 3.361_{-0.64}^{+0.68}$  at 95% C.L. [45]. Higher than the

standard value  $\delta N_{eff} > 0$  is favored. In case of no entropy release between BBN and CMB epochs, CMB+BBN constraints holds, namely:  $N_{eff} = 3.41 \pm 0.3$  (68% Planck +WP+high l+Y(Aver et al.))

CMB data allow simultaneous constraints on extra radiation and the total flavor neutrino mass: for massless sterile case:  $N_{eff} = 3.29^{+0.67}_{-0.64}$  (95% Planck +WP+high l) and  $m < 0.6$  eV. The bounds are marginally compatible with fully thermalized sterile neutrino with sub-eV mass  $m_s < 0.5$  eV, necessary to explain the oscillations anomalies, called DR.

#### 4.2 Cosmological Effects and Constraints of Active-Sterile Neutrino Oscillations

*Active-sterile neutrino oscillation, effective before neutrino decoupling*, introduce extra relativistic particles [7, 11, 12] and change the expansion rate and the BBN production of He-4.

*Active-sterile neutrino oscillation, effective after neutrino decoupling*, cause deviations of neutrino energy spectrum from the equilibrium FD form, and influence electron neutrino and antineutrino number densities and/or spectrum, thus effecting the weak rates  $\Gamma_w \sim G_F E_\nu n_{\nu_e}$  of n-p transitions.

Active-sterile oscillations may cause the following kinetic effects: i) *change of the particle densities of electron neutrino and antineutrino* by fast electron-sterile neutrino oscillations [11,12]; ii) *distortion in the energy spectrum distribution of electron neutrino* caused by late electron-sterile neutrino oscillations, proceeding after decoupling [13–16]; iii) *change of the asymmetry*: production of  $L > 0.01$  (capable to influence n-p kinetics) in the electron neutrino sector by fast resonant electron-sterile oscillations [14, 16, 18], or suppression of a preexisting L, and thus changing the BBN in comparison with the case of absence of oscillations and finally to iv) *indirect kinetic effect* due to oscillations-asymmetry interplay, in case of small L. This influences the oscillations pattern, which reflects in change of BBN.

Hence, due to these effects of neutrino oscillations BBN is the sensitive probe to neutrino oscillation parameters. Most recent constraints on the neutrino oscillation parameters in case of relatively fast oscillations have been obtained in ref [31]. BBN constraints on electron-sterile oscillations, effective after neutrino decoupling, are considered in refs. [16, 29, 30, 32, 33]. The precise account of the energy spectrum distribution of oscillating neutrino allows to extend the BBN constraints towards very small mass differences - down to  $10^{-9}$  eV<sup>2</sup>.

#### 4.3 Cosmological constraints on L

BBN provides the most stringent constraints on L. In BBN with the known flavor neutrino oscillations, degeneracies in different neutrino sectors equilibrate before BBN due to flavor neutrino oscillations. Hence, the stringent BBN constraint on  $L_e$  applies to other neutrino types [23]. Thus the contemporary BBN bound is  $L < 0.1$ . CMB and LSS provide looser bounds [46].

In the case of modified BBN with active-sterile neutrino oscillations, very stringent constraints on L are possible [5,6,47]. As far as in such non-standard BBN  $L > \delta m^2$  inhibits oscillations, the detection of active-sterile oscillations will provide the bound  $L < \delta m^2$  [6, 22]. For example, from the indications for active-sterile oscillations with  $\delta m^2 \sim 10^{-5}$  [25] follows BBN upper limit  $L < 10^{-3.3}$ . BBN with late electron-sterile neutrino oscillations can measure tiny L with close to the baryon asymmetry values [6].

#### 4.4 Dark radiation and eV neutrino saga

*Different types of cosmological indications suggested additional relativistic density*: BBN [36,48], CMB and LSS data, as well as their combined analysis pointed to excess radiation [49–51].

Besides, *different neutrino oscillations experiments (reactor, LSND, MiniBooNe, Gallium) data presented indications for neutrino oscillations with 1 or 2 sterile neutrinos with sub-eV masses* [26–28, 62]. Recent analyses of neutrino data prefer 3+1 models [27].

Hence, beyond SMC models, including extra neutrinos, were studied. Analysis of different type of cosmological data provided during the last years showed that the sub-eV neutrinos would have been

brought into thermal equilibrium before BBN [53–56], and thus restricted by BBN. Besides, sub-eV neutrinos produce too much hot dark matter [52, 57]. Thus, two additional  $\nu_s$  are in tension both with BBN and with LSS and are difficult to realize in SCM [52, 58–60]. Cosmology favors one additional sterile neutrino, but prefers it to be lighter than eV [45, 58]. Accepting  $m = 0.6$  eV and allowing for massive sterile neutrino the following CMB constraints on extra radiation and sterile neutrino mass have been obtained:  $N_{eff} < 3.91$  (95% Planck +WP+high l) and  $m_s < 0.59$  eV.

To relax the cosmological constraints, modifications of SCM have been explored. It was shown that excess radiation cannot be explained by degenerate BBN [65]. However, the presence of L may be the solution in case its value is large enough to suppress active-sterile oscillations and prevent the thermalization of the sterile neutrinos and circumvent BBN constraints [22, 61].

Other possible explanations employing decays of heavy neutrinos were discussed in refs. [63, 64].

## 5 Conclusions

BBN, CMB and LSS cosmological data provides a powerful test for BSM neutrino characteristics. In particular, cosmology provides the most stringent constraints on neutrino masses, neutrino active-sterile oscillations, the extra radiation, the neutrino families, lepton asymmetry or/and neutrino chemical potentials, sterile neutrino, etc. Hopefully, future terrestrial physical experiments and future cosmic missions and surveys will discover not only BSMs neutrino physics but also solve the DM, DE, inflation and matter-antimatter asymmetry quests.

## Acknowledgements

The author is glad to thank the organizers and especially prof. G. Djorjievic for the kind invitation to the SEENET-MTP Workshop: Beyond the Standard Models - BW2013, Vrnjacka Banja, Serbia, and acknowledges the financial support for participation into it.

## References

- [1] Dolgov, A., Hansen S., Semikoz, D., *Nucl. Phys. B* **503**, 426 (1997)
- [2] Mangano, G., Miele, G., Pastor, S., Pinto, T., Pisanti, O., Serpico, P., *Nucl. Phys. B* **729**, 221 (2005)
- [3] D. Notzold, G. Raffelt, *Nucl. Phys.* **B307**, 924 (1988)
- [4] S. Mikheyev, A. Smirnov, *Sov. J. Nucl. Phys.* **42**, 913 (1985); *Nuovo Cimento* **9C**, 17 (1986); L. Wolfenstein, *Phys. Rev.* **D17**, 2369 (1978).
- [5] Kirilova, D., Chizhov M., *Nucl. Phys. B* **534**, 447 (1998) 2000 in *Verbier 2000, Cosmology and particle physics* 433, astro-ph/0101083.
- [6] Kirilova D., *JCAP* **06**, 007 (2012)
- [7] Dolgov, A., *Sov. J. Nucl. Phys.* **33**, (1981) 700.
- [8] M. Drewers, arXiv: 1303.6912
- [9] Kusenko A., *Physics Reports*, **481**, 1 (2009)
- [10] G. Mangano, G. Miele, S. Pastor, T. Pinto, O. Pisanti, P. Serpico, *Nucl. Phys.* **B729**, 221-234 (2005)
- [11] Barbieri, R., Dolgov, A., *Phys. Lett. B* **237**, 440 (1990).
- [12] Enqvist K., Kainulainen K., Thompson M., *Nucl. Phys. B* **373**, 498 (1992).
- [13] Kirilova, D., *JINR preprint E2-88-301*, (1988)
- [14] Kirilova, D., Chizhov, M., in *Neutrino96*, 478 (1996)
- [15] Kirilova, D., *Int. J. Mod. Phys.* **D 13**, 831 (2004).
- [16] Kirilova, D., Chizhov, M., *Phys. Lett. B* **393**, 375 (1997).
- [17] R. Foot, R. R. Volkas *Phys.Rev.Lett.* **75** 4350 (1995); *Phys.Rev.* **D55** 5147 (1997); *Phys.Rev.* **D56** 6653 (1997); *Phys.Rev.* **D59** 029901 (1999)

- [18] Foot R., Thomson, M., Volkas R. 1996: *Phys. Rev. D* **53**, R5349; X. Shi, *Phys. Rev. D* **54** 2753 (1996)
- [19] A. Boyarsky, D. Iakubovskiy, O. Ruchayskiy, Physics of the Dark Universe, V.1, Issue 1, 136-154 (2012)
- [20] T.Asaka, M. Laine, M. Shaposhnikov, JNEP 01,091 (2007)
- [21] A. Boyarsky, J. Lesgourgues, O Ruchayskiy, M.Viel, JCAP 0905, 012 (2009).
- [22] Kirilova D., *Hyperfine Interact.* **215** 1-3, 111-118, (2013); *Proc. 5th International Symposium on Symmetries in Subatomic Physics* 18-22 June, 2012, Groningen (2012).
- [23] A. Dolgov, S. Hansen, S. Pastor, S.Petcov, G.Raffelt, D.Semikoz, 2002, *Nucl. Phys. B* **632**, 363; Y.Y.Y. Wong, *Phys. Rev. D***66**, 025015 (2002)
- [24] Kirilova D., *Prog. Part. Nucl. Phys.* (2010)
- [25] P. Holanda, A. Smirnov *Phys.Rev.D* **83** 113011 (2011)
- [26] K.N. Abazajian et al. htSterile Neutrinos: A White Paper e-Print: arXiv:1204.5379 (2012)
- [27] C. Giunti, M. Laveder, PRD 84, 093006 (2011); PRD 84, 073008 (2011)Phys.Lett B706, 200 (2011)
- [28] Maltoni M., T. Schwetz, PRD 76, 093005 (2007); J. Kopp, M. Maltoni, T. Schwetz, Phys.Rev.Lett. 107, 091801 (2011)
- [29] Kirilova, D., Chizhov, M., *Phys. Rev. D* **58**, 073004 (1998)
- [30] Kirilova, D., Chizhov, M., *Nucl. Phys. B* **591**, 457 (2000).
- [31] Dolgov A., Villante F., *Nucl. Phys. B* **679**, 261 (2004).
- [32] Kirilova D., *Int. J. Mod. Phys. D* **16**, 1197, (2007)
- [33] Kirilova D., Panayotova M., *JCAP*, **12**, 014 (2006)
- [34] Panayotova M., *Bulg.J.Phys.* **38**, 341 (2011)
- [35] Simha, G. Steigman, *JCAP***0808** 011 (2008)
- [36] Yu. I. Izotov, T. X. Thuan, *ApJ* **710** L67 (2010)
- [37] Steigman, G., *JCAP* **04** 029 (2010)
- [38] Iocco, F., Mangano, G., Miele, G., Pisanti, O., Serpico, P. D., *Phys. Rept.* **472**, 1(2009)
- [39] Mangano G.,Serpico P., PLB 701, 296 (2011)
- [40] E. Komatsu et al.?(WMAP 7 year) ApJ Suppl. 192, 18 (2011)
- [41] N ollet K., Holder G., arXiv: 1112.2683
- [42] Steigman arXiv: 1208.0032, 2012
- [43] A. Cuocco, J. Lesgourgues, G. Mangano, S. Pastor, *PRD* 71, 123501 (2005)
- [44] M. Shiraishi, K. Ichikava, K. Ichiki, N Sugiyama, M. Yannaguchi, JCAP 0907, 005 (2009)
- [45] Planck Collaboration, arXiv: 1303.5076
- [46] Lesgourgues, J., Pastor, S., *Physics Reports*, **429**, 307 (2006).
- [47] Kirilova D. *Prog. Part. Nucl. Phys.***66**, 260 (2011)
- [48] Aver,E., Olive, K.A., Skillman, E.D., *JCAP* 05, 003 (2010a); arXiv:1012.2385 v1. et al. 2010
- [49] Komatsu et al. 2011, arXiv:1001.4538;Komatsu et al. (WMAP),*Astrophys. J. Suppl.***180**, 330 (2009)
- [50] R. Keisler et al., *Ap.J* **743**, 28 (2011); arXiv:1105.3182
- [51] Dunkley J. et al., *A.J* **739**, 52 (2011); arXiv:1009.0866; Hou Z. et al., arXiv:1104.2333
- [52] Hamman et al. 2012; Hamman J. et al., *JCAP* **1109**, 034 (2011); arXiv:1108.4136 J. Hamann, et. al. (2010) *Phys. Rev. Lett.* **105** 181301.
- [53] P. Di Bari, *PRD* 65, 043509 (2002)
- [54] K. Abazajian, *Ap.Phys.* 19, 303 (2003)

- [55] M. Cirelli, G. Marandella, A. Strumia, F. Vissani, *NPB* 708, 215 (2005)
- [56] S. Hannestad, I. Tamborra, T. Tram, *JCAP* 1207, 025 (2012); arXiv:1204.5861
- [57] Dodelson S., Melchiorri A., Slosar A., *Phys. Rev. Lett.* **97**, 14130 (2006); astro/ph 0511500
- [58] Giusarma E. et al, *Phys. Rev. D* **83** 115023 (2011); arXiv:1102.4774
- [59] Nollet K., Holder G., 1112.2683
- [60] Hou Z. et al., arXiv:1104.2333
- [61] Mirizzi A. et al., arXiv:1206.1046; S. Hannestad, I Tamborra, T. Tram, arXiv:1204.5861
- [62] Karagiorgi G., *PRD* 80,073001 (2009); arXiv:1110.3735 (2011)
- [63] Dolgov A., Kirilova D., *Int.J.Mod.Phys.* **A3**, 267 (1988); Kirilova D., School and Workshop on Space Plasma Physics, 83-89, AIP Conf. Proc., 1121, 31.08-07.09, Sozopol, Bulgaria, ed.I. Zhelyazkov, 2009
- [64] O. Ruchayskiy, A. Ivashko, arXiv:1202.2841 (2012)
- [65] Mangano G., G. Miele, S. Pastor, O. Pisanti, S. Sarikas, *JCAP* **11**, 035 (2011);
- [66] Barenboim G., Borissov L., Lykken J., Smirnov A., *JHEP*, 0210, 001 (2002)

# Is there a fundamental cosmological dipole?

Leandros Perivolaropoulos\*

Department of Physics, University of Ioannina, 45110 Ioannina, Greece

## Abstract

Early hints for deviation from the cosmological principle and statistical isotropy are being accumulated. After reviewing these hints, I focus on four cosmologically observed axes which appear to be either marginally consistent or in conflict with the standard  $\Lambda$ CDM isotropic and homogeneous cosmology. These axes are abnormally aligned with each other and include: (a) The Fine Structure Constant  $\alpha$  Dipole (b) the Dark Energy Dipole (c) the Dark Velocity Flow and (d) the CMB Maximum Temperature Asymmetry. I also discuss a simple physical model (extended topological quintessence) that has the potential to explain the existence and alignment of these axes. The model is based on the recent formation of a global monopole with Hubble scale core by an  $O(3)$  symmetric scalar field, non-minimally coupled to electromagnetism.

## 1 Introduction

The consistency level of the standard cosmological model ( $\Lambda$ CDM) with geometric and dynamical cosmological observations has been increasing during the past decade [1]. However, there are some puzzling conflicts between the predictions of  $\Lambda$ CDM and specific observations. These observations include peculiar velocity bulk flows on scales larger than  $100h^{-1}Mpc$  ( $z \geq 0.03$ ) [2–4], planarity and alignment of the quadrupole and octopole CMB map moments [5] and alignment of quasar optical polarization along a particular cosmological axis. Most of the observations that are in tension with the standard model  $\Lambda$ CDM involve the existence of preferred cosmological axes which appear to be anomalously close to each other [6–8] given that these observations should be mutually uncorrelated.

Hints for two new cosmological dipoles have emerged during the past five years. They include the Fine Structure Constant  $\alpha$  Dipole which deviates about  $4\sigma$  from isotropy [8, 9] and the Dark Energy Dipole which deviates about  $2\sigma$  from isotropy [8].

Quasar absorption line spectra can determine the value of the fine structure constant at various cosmological redshifts and directions. The Keck+VLT sample consists of 295 absorbers at a redshift range  $0.2 < z < 4.2$  and indicates a spatially varying fine structure constant  $\alpha$  with dipole angular distribution. Isotropy is found to be  $4.1\sigma$  away from the best fit dipolar angular distribution [8, 9].

Correspondingly, the distance moduli residuals from the  $\Lambda$ CDM best fit also exhibit a dipole anisotropy. In this case isotropy is found to be  $2\sigma$  away from the best fit dipolar angular distribution. This Dark Energy dipole is obtained [8] from the 557 Type Ia supernovae (SNIa) of the Union2 sample [10] ( $0 < z < 1.4$ ).

In view of the existence of these new cosmological dipoles, the following questions emerge:

1. What is the alignment level of these dipoles?
2. What is the probability to produce the observed combination of these two dipoles in a homogeneous-isotropic cosmological model where the two dipoles are uncorrelated?
3. What physical model has the potential to predict the existence of the above combined dipoles?

The detailed presentation of the answers to these questions will be the focus of this brief review. These answers may be briefly stated as follows [8]:

---

\*E-mail: leandros@uoi.gr

1. The Dark Energy dipole and the  $\alpha$  dipole are abnormally aligned with each other (angular separation  $11.3^\circ \pm 11.8^\circ$ ).
2. The probability that the combined quasar absorber and SnIa data are obtained in the context of a homogeneous and isotropic cosmology with no correlation between the datasets, is less than one part in  $10^6$ .
3. There is a physical model based on a Hubble scale topological defect non-minimally coupled to electromagnetism that has the potential to explain the observed aligned dipoles

The structure of this brief review is the following: In section II I review the derivation of the  $\alpha$  and Dark Energy dipoles and obtain the probability that these dipoles would be produced in the context of isotropic cosmology. In section III I review the physical model that has the potential to explain the aligned cosmic dipoles and discuss additional hints for a CMB temperature asymmetry axis that appears to be abnormally aligned with the  $\alpha$  and Dark energy dipoles. The connection of this CMB axis with the proposed physical model is also discussed. Finally in section IV I conclude and briefly discuss future extensions of this research programme.

## 2 Cosmic Dipoles

### 2.1 The $\alpha$ Dipole

Consider a quasar emitting a continuous emission spectrum of radiation at a redshift  $z_{em}$  (see Fig. 1).

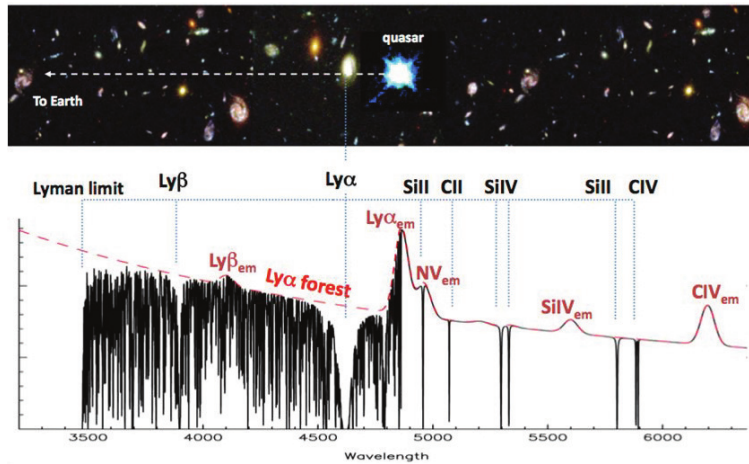


**Fig. 1:** The absorption spectrum of a galaxy gas cloud absorber superposed on the emission spectrum of a quasar can provide information about the value of the fine structure constant  $\alpha$  at the time and location where the radiation was absorbed (courtesy of J. Webb).

If this radiation goes through a gas cloud in a galaxy before it is observed on Earth, an absorption spectrum will emerge. From the absorption lines we can find both the absorber redshift and the fine structure constant  $\alpha = e^2/hc$  at the time and location of the absorption. While cosmological redshift shifts the spectral lines always towards larger wavelengths, variation of  $\alpha$  shifts spectral lines in both directions (Fig. 2) depending on the atom (or ion) and the energy levels involved. The sensitivity in determining  $\alpha$  from the absorption lines is significantly improved by using the Many Multiplet Method where several absorption lines of different atoms and ions (eg iron and magnesium) are used simultaneously to determine  $\alpha$  [11].

Using the Many Multiplet Method in quasar absorber northern hemisphere data from the Keck Telescope in Hawaii, Webb et. al. [11] found a statistically significant ( $3\sigma$ ) variation of  $\alpha$  at high redshifts ( $z > 1$ ). The value of  $\alpha$  was found to be smaller in the past as shown in Fig. 3.

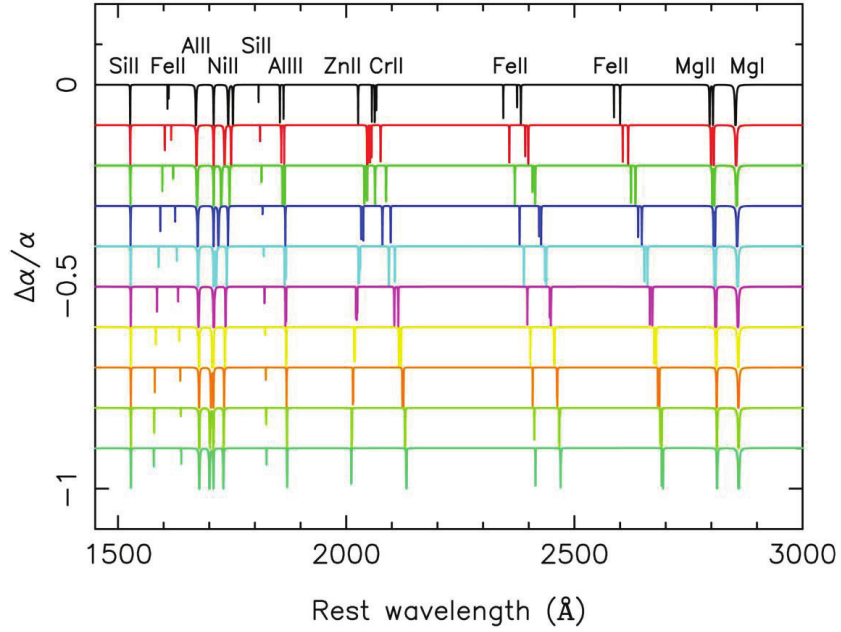


**Fig. 2:** While cosmological redshift shifts the spectral lines always towards larger wavelengths, variation of  $\alpha$  shifts spectral lines in both directions depending on the atom (or ion) and the energy levels involved. The shift of various absorption lines for specific values of  $\alpha$  are shown (courtesy of J. Webb).

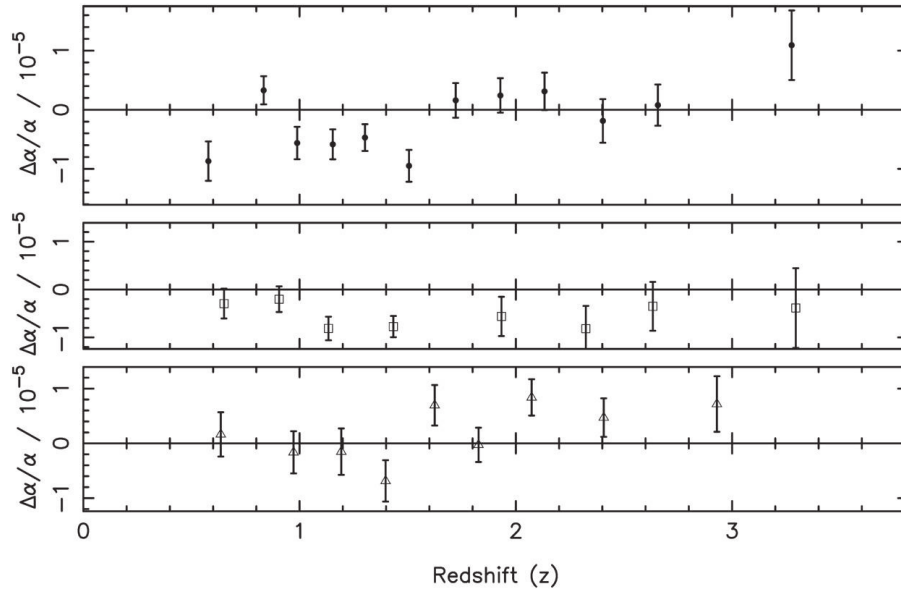


**Fig. 3:** Using quasar absorbers from the Keck Telescope in Hawaii (Northern hemisphere), the values of  $\alpha$  were found to be smaller in the past at higher redshift bins (middle panel) while using quasar absorbers from the VLT in Chile (Southern hemisphere), the values of  $\alpha$  were found to be larger in the past (lower panel). The combined sample results are shown in the upper panel (courtesy of J. Webb)

Using the same method and a full sky combination of Northern Hemisphere quasar absorber data (Keck in Hawaii) and Southern Hemisphere data (VLT in Chile), Webb et. al. [9] found that the values of  $\alpha$  have a non-isotropic variation across the sky. This angular variation is well described by a dipole.

The Keck+VLT dataset used by Webb et. al. consists of 295 absorbers. The best fit dipole distribution was found to be  $4.1\sigma$  away from isotropy (Fig. 4).

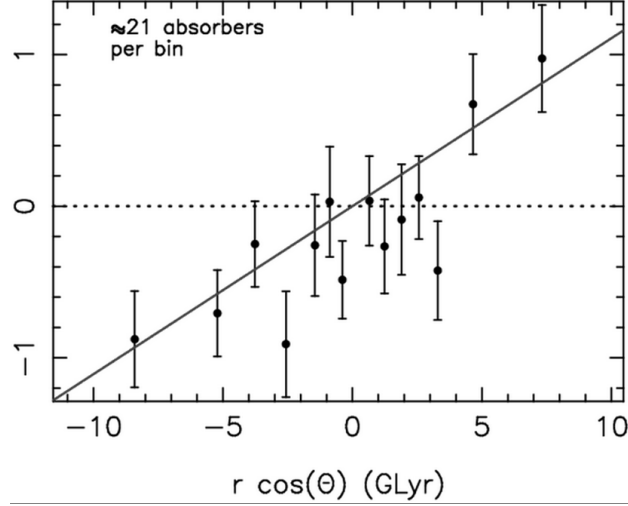


**Fig. 4:** The combination of Keck+VLT data indicated a spatial variation of  $\alpha$  described well by a dipole. (from Ref. [9])

The current constraints on variation of  $\alpha$  are summarized in Table 1 (from Ref. [12]). The hints for cosmological variation of  $\alpha$  come from studies using the Many Multiplet Method while all other studies are consistent with no variation of  $\alpha$ . Particularly strong bounds are those coming from the Oklo natural reactor [13–15] which has operated for about 2 billion years. The Oklo bounds are obtained using the extremely low resonance energy ( $E_r = 97.3\text{meV}$ ) of the reaction



It implies that the abundance of  $^{149}\text{S}_m$  (one of the nuclear fission products of  $^{235}\text{U}$ ) observed at the Oklo can be a good probe of the variability of the coupling constants [16]. Note however that the strong *time* variation bounds on  $\alpha$  obtained from Oklo are consistent with a *spatial* variation of  $\alpha$  obtained by the Keck+VLT data. A sample of the 295 quasar absorber Keck+VLT data are shown in Fig. 5 [9]. The important columns are the J2000-name which includes the equatorial coordinates of each quasar,  $z_{abs}$  which gives the absorber redshift,  $da/a$  and  $err$  which provide the derived variation of  $\alpha$  and its corresponding error estimate. In Fig. 6 we show the locations of the absorbers in galactic coordinates with the corresponding  $\alpha$  variation denoted by color variation. This dataset was fit to a dipole plus monopole angular distribution in Refs [8,9] using the maximum likelihood method. We find the cartesian coordinates of the unit vectors  $\hat{n}_i$  corresponding to each quasar with galactic coordinates  $(l, b)$ . We thus have

$$\hat{n}_i = \cos(b_i) \cos(l_i) \hat{i} + \cos(b_i) \sin(l_i) \hat{j} + \sin(b_i) \hat{k} \quad (2)$$

We then use the dipole+monopole angular distribution model

$$\left( \frac{\Delta\alpha}{\alpha} \right) = A \cos \theta + B \quad (3)$$

where  $\cos \theta$  is the angle with the dipole axis defined by the vector

$$\vec{D} \equiv c_1 \hat{i} + c_2 \hat{j} + c_3 \hat{k} \quad (4)$$

such that

$$\hat{n}_i \cdot \vec{D} = A \cos \theta_i \quad (5)$$

|   | redshift        | $\Delta\alpha/\alpha$               | $\dot{\alpha}/\alpha(\text{yr}^{-1})$ |
|---|-----------------|-------------------------------------|---------------------------------------|
| Atomic Clock(Yb <sup>+</sup> /Hg <sup>+</sup> /H) [18]    | 0               |                                     | $(-0.3 \pm 2.0) \times 10^{-15}$      |
| Atomic Clock(Hg <sup>+</sup> /Yb <sup>+</sup> /H) [19]    | 0               |                                     | $(-0.55 \pm 0.95) \times 10^{-15}$    |
| Atomic Clock(Sr/Hg <sup>+</sup> /Hg <sup>+</sup> /H) [20] | 0               |                                     | $(-3.3 \pm 3.0) \times 10^{-16}$      |
| Atomic Clock(Al <sup>+</sup> /Hg <sup>+</sup> ) [21]      | 0               |                                     | $(-1.6 \pm 2.3) \times 10^{-17}$      |
| Atomic Clock( <sup>162</sup> Dy/ <sup>163</sup> Dy) [22]  | 0               |                                     | $(-2.7 \pm 2.6) \times 10^{-15}$      |
| Oklo(Damour-Dyson [15])                                   | 0.16            | $(-0.9 \sim 1.2) \times 10^{-7}$    | $(-6.7 \sim 5.0) \times 10^{-17}$     |
| Oklo(Fujii et al. [13])                                   | 0.16            | $(-0.18 \sim 0.11) \times 10^{-7}$  | $(0.2 \pm 0.8) \times 10^{-17}$       |
| Oklo(Petrov et al. [14])                                  | 0.16            | $(-0.56 \sim 0.66) \times 10^{-7}$  | $(-3.7 \sim 3.1) \times 10^{-17}$     |
| Oklo(Gould et al. [23])                                   | 0.16            | $(-0.24 \sim 0.11) \times 10^{-7}$  | $(-0.61 \sim 1.3) \times 10^{-17}$    |
| Re/Os bound [24]  | 0.43            | $(-0.25 \pm 1.6) \times 10^{-6}$    | $(-4.0 \sim 2.9) \times 10^{-14}$     |
| HI 21 cm [26]   | 1.8             | $(3.5 \pm 5.5) \times 10^{-6}$      | $(-3.3 \pm 5.2) \times 10^{-16}$      |
| HI 21 cm [25]   | 0.25,0.68       | $< 1.7 \times 10^{-5}$              |                                       |
| QSO absorption line(SiIV) [26]                            | 2.67 – 3.55     | $< 3.5 \times 10^{-4}$              |                                       |
| QSO absorption line(MM) [27]                              | 0.5 – 1.6       | $(-1.09 \pm 0.36) \times 10^{-5}$   |                                       |
| QSO absorption line(MM) [28]                              | 0.5 – 3.5       | $(-0.72 \pm 0.18) \times 10^{-5}$   |                                       |
| QSO absorption line(SiIV) [29]                            | 2.01 – 3.03     | $(-0.5 \pm 1.3) \times 10^{-5}$     |                                       |
| QSO absorption line(MM) [30]                              | 0.2 – 3.7       | $(-0.543 \pm 0.116) \times 10^{-5}$ |                                       |
| QSO absorption line(MM) [31]                              | 0.2 – 4.2       | $(-0.573 \pm 0.113) \times 10^{-5}$ |                                       |
| OH [32]   | 0.247671        | $(0.51 \pm 1.26) \times 10^{-5}$    | $(-1.7 \pm 4.3) \times 10^{-15}$      |
| OH [33]   | 0.247           | $(-3.1 \pm 1.2) \times 10^{-6}$     | $(1.1 \pm 0.4) \times 10^{-15}$       |
| QSO absorption line(MgII/FeII) [34]                       | 0.4 – 2.3       | $(-0.06 \pm 0.06) \times 10^{-5}$   |                                       |
| QSO absorption line(MgII/FeII) [35]                       | 0.4 – 2.3       | $(-0.44 \pm 0.16) \times 10^{-5}$   |                                       |
| QSO absorption line(SiIV) [36]                            | 1.59 – 2.92     | $(0.15 \pm 0.43) \times 10^{-5}$    |                                       |
| QSO absorption line(FeII) [37]                            | 1.84            | $(5.66 \pm 2.67) \times 10^{-6}$    | $(-5.51 \pm 2.60) \times 10^{-16}$    |
| QSO absorption line(FeII) [37]                            | 1.15            | $(-0.12 \pm 1.79) \times 10^{-6}$   | $(0.14 \pm 2.11) \times 10^{-16}$     |
| QSO absorption line(FeII) [38]                            | 1.15            | $(0.5 \pm 2.4) \times 10^{-6}$      | $(-0.6 \pm 2.8) \times 10^{-16}$      |
| QSO absorption line(FeII) [39]                            | 1.58            | $(-1.5 \pm 2.6) \times 10^{-6}$     | $(1.5 \pm 2.7) \times 10^{-16}$       |
| CMB [40]  | 10 <sup>3</sup> | $-0.06 \sim 0.01$                   | $< 5 \times 10^{-12}$                 |
| CMB [41]  | 10 <sup>3</sup> | $-0.013 \sim 0.015$                 | $< 1 \times 10^{-12}$                 |
| BBN [42]  | 10 <sup>9</sup> | $< 6 \times 10^{-2}$                | $< 4.4 \times 10^{-12}$               |

**Table 1:** Summary of the experimental bounds on the time variation of the fine structure constant.  $\Delta\alpha/\alpha \equiv (\alpha_{\text{then}} - \alpha_{\text{now}})/\alpha_{\text{now}}$  (from Ref. [12]).

Finally, we minimize

$$\chi^2(\vec{D}, B) = \sum_{i=1}^{295} \frac{[(\frac{\Delta\alpha}{\alpha})_i - A \cos \theta_i - B]^2}{\sigma_i^2 + \sigma_{rand}^2} \quad (6)$$

where  $(\frac{\Delta\alpha}{\alpha})_i$  and  $\sigma_i$  are obtained from the Keck+VLT dataset [9] and  $\sigma_{rand}$  is an internal random error, assumed to be the same for all data points and representing an estimate of the aggregation of all additional random errors. The magnitude and direction of the best fit dipole in galactic coordinates is obtained from the best fit  $c_i$  coordinates (e.g.  $A = \sqrt{c_1^2 + c_2^2 + c_3^2}$ ).

We find  $A_{fs} = (1.02 \pm 0.25) \times 10^{-5}$  with direction ( $b = -11.7^\circ \pm 7.5^\circ$ ,  $l = 320.5^\circ \pm 11.8^\circ$ ) while for the best fit monopole term we have  $B_{fs} = (-2.2 \pm 1.0) \times 10^{-6}$ . This result shows that the isotropic model  $A = 0$  is more than  $4\sigma$  away from the best fit value of the dipole magnitude. The Keck+VLT dataset along with the best fit direction of the dipole in galactic coordinates is shown in Fig. 6. By the definition of  $(\frac{\Delta\alpha}{\alpha})$  and the construction of the dipole model, the obtained dipole direction shown in Fig. 6

| # | # N | J2000_name     | z_em | z_abs   | da/a   | err   | Sample | Source |
|---|-----|----------------|------|---------|--------|-------|--------|--------|
| 1 | 1   | J000520+052410 | 1.90 | 0.85118 | -0.340 | 1.284 | A      | Keck   |
| 2 | 2   | J012017+213346 | 1.49 | 0.72913 | 0.041  | 1.297 | A      | Keck   |
| 3 | 3   | J012017+213346 | 1.49 | 1.0479  | -0.202 | 2.199 | A      | Keck   |

**Fig. 5:** A sample of the 295 quasar absorber Keck+VLT data.

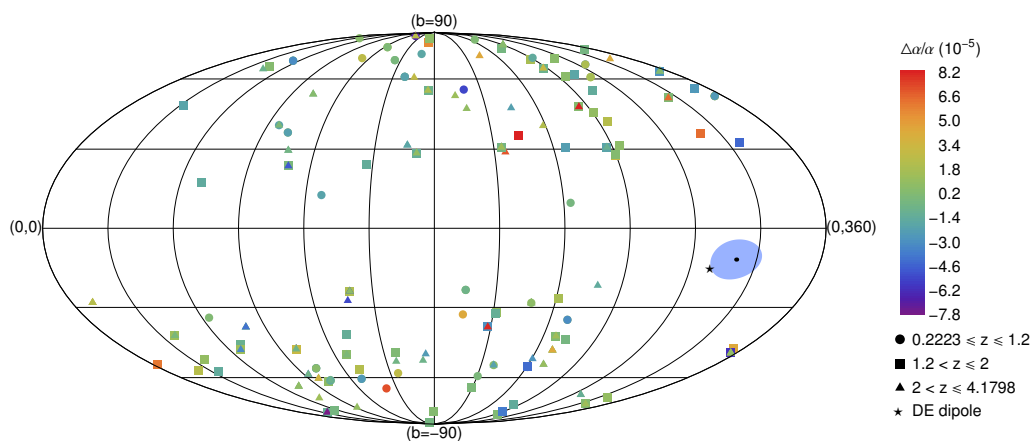


**Fig. 6:** Keck+VLT datapoints and  $\alpha$ -dipole direction. Datapoints in three different redshift bins are represented with different shapes. For comparison the direction of the Dark Energy dipole obtained from the best fit of the Union2 data is shown with a star. The light blue blob represents the  $1\text{-}\sigma$  error on the  $\alpha$ -dipole direction.

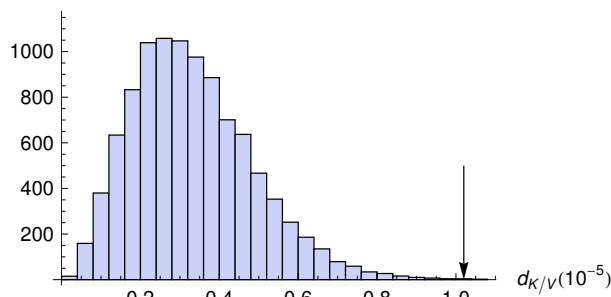


**Fig. 7:** Distribution of  $\alpha$ -dipole magnitudes obtained from the Monte Carlo simulation. The arrow points to the position of the observed best fit value for the  $\alpha$ -dipole magnitude.

is the direction towards larger values of the fine structure constant  $\alpha$ .

This deviation from isotropy can also be verified by considering  $10^4$  Monte Carlo simulations obtained from the Keck+VLT dataset under the assumption of an isotropic monopole model [8]. The distribution of the dipole magnitudes  $d_{K/V}$  obtained in these simulations are shown in Fig. 7. The arrow points to the observed magnitude  $A_{fs} = (1.02 \pm 0.25) \times 10^{-5}$  of the dipole. Clearly, none of the isotropic simulated Keck+VLT datasets had a dipole magnitude as large as the observed. Therefore, the probability to obtain the observed value for the dipole magnitude is less than one part in  $10^4$  (about  $3.9\sigma$ ) in agreement with the  $4\sigma$  result obtained with the covariance matrix in the context of the maximum likelihood approach.

## 2.2 The Dark Energy Dipole

The Union2 dataset provides 557 distance moduli of SnIa along with their  $1\sigma$  errors and their redshift. The galactic coordinates of each SnIa may be found in Refs. [6, 43]. The distance modulus is connected with the Hubble free luminosity distance  $D_L(z)$  as

$$\mu_{th} \equiv m_{th} - M = 5 \log_{10}(D_L(z)) + \mu_0 \quad (7)$$

where  $m_{th}$  and  $M$  are the apparent and absolute magnitudes,  $\mu_0 = 42.3 - 5 \log_{10} h$  and

$$D_L(z) = (1+z) \int_0^z dz' \frac{H_0}{H(z', \Omega_{0m})} \quad (8)$$

where  $H(z', \Omega_{0m})$  is the Hubble parameter ansatz for  $\Lambda$ CDM.

Assuming a  $\Lambda$ CDM parametrization of the expansion rate

$$H(z)^2 = H_0^2 [\Omega_{0m}(1+z)^3 + (1 - \Omega_{0m})] \quad (9)$$

the best fit distance modulus  $\bar{\mu}(z)$  is determined by minimizing

$$\chi^2(\Omega_{0m}, \mu_0) = \sum_{i=1}^{557} \frac{[\mu_{obs}(z_i) - \mu_{th}(z_i)]^2}{\sigma_{\mu_i}^2} \quad (10)$$

where  $\sigma_{\mu_i}^2$  are the distance modulus uncertainties which include both the observational and the intrinsic random magnitude scatter.

A dipole+monopole fit may be performed [8] using the Union2 data. Instead of  $(\frac{\Delta\alpha}{\alpha})$  which corresponds to fine structure constant deviations from its earth measured value we use the distance modulus deviation from its best fit  $\Lambda$ CDM value

$$\left( \frac{\Delta\mu(z)}{\bar{\mu}(z)} \right) \equiv \frac{\bar{\mu}(z) - \mu(z)}{\bar{\mu}(z)} \quad (11)$$

where  $\bar{\mu}$  is the best fit distance modulus in the context of  $\Lambda$ CDM. A minimization of  $\chi^2(\Omega_{0m}, \mu_0)$  using the Union2 dataset leads to the best fit parameter values  $\Omega_{0m} = 0.269 \pm 0.020$  and  $\mu_0 = 43.16 \pm 0.01$  which completely specify  $\bar{\mu}(z_i)$  and therefore also

$$\left( \frac{\Delta\mu(z_i)}{\bar{\mu}(z_i)} \right)_{obs} \equiv \frac{\bar{\mu}(z_i) - \mu(z_i)}{\bar{\mu}(z_i)} \quad (12)$$

for all Union2 datapoints.

In performing the same analysis as for the Keck+VLT data, we replace the  $(\frac{\Delta\alpha}{\alpha})$  datapoints by the  $(\frac{\Delta\mu(z)}{\bar{\mu}(z)})$  datapoints. In the SnIa we set  $\sigma_{rand} = 0$  since the random intrinsic magnitude scatter has already been included in the distance moduli errors  $\sigma_i$ . We find the direction of the dark energy dipole to be  $(b = -15.1^\circ \pm 11.5^\circ, l = 309.4^\circ \pm 18.0^\circ)$ . The magnitudes of the dipole and monopole terms are found to be

$$A_{de} = (1.3 \pm 0.6) \times 10^{-3} \quad (13)$$

$$B_{de} = (2.0 \pm 2.2) \times 10^{-4} \quad (14)$$

The statistical significance of the dark energy dipole is at the  $2\sigma$  level (significantly smaller than the  $4\sigma$  of the fine structure constant dipole) but its direction is only  $11^\circ$  away from the corresponding direction of the fine structure constant dipole. The direction of the dark energy dipole along with the Union2 data

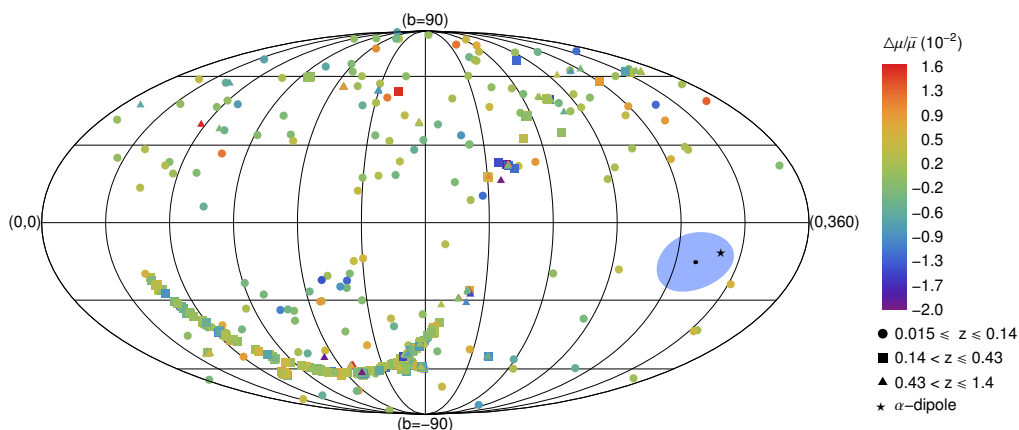


**Fig. 8:** Union2 datapoints and Dark Energy dipole direction. Datapoints in three different redshift bins are represented with different shapes. For comparison the direction of the  $\alpha$ -dipole obtained from the best fit of the Keck-VLT data is shown with a star. The light blue blob represents the  $1\text{-}\sigma$  error on the Dark Energy dipole direction.

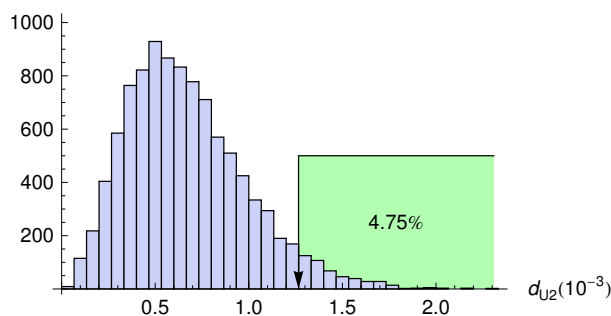


**Fig. 9:** Distribution of dark Energy dipole magnitudes obtained from the Monte Carlo simulation. The arrow points to the position of the observed best fit value and the light green area indicates fraction of the Monte Carlo datasets that give a dipole magnitude bigger than the observed best fit one.

$\left(\frac{\Delta\mu(z_i)}{\bar{\mu}(z_i)}\right)_{obs}$  are shown in Fig. 8 in galactic coordinates. The proximity of the two dipole directions is also made apparent in the same plot as well as by comparing with Fig. 6.

The direction of the dipole in Fig. 8 points towards brighter SnIa compared to best fit isotropic  $\Lambda$ CDM. This implies less accelerating expansion in that direction (assuming isotropic  $\mu_0$ ).

The  $2\sigma$  deviation of the Dark energy dipole from isotropy may also be confirmed by using a Monte Carlo simulation consisting of  $10^4$  Union2 datasets constructed under the assumption of isotropic  $\Lambda$ CDM.

In an effort to determine the likelihood of the observed dark energy dipole magnitude combined with its angular proximity to the fine structure dipole we have performed a Monte Carlo simulation consisting of  $10^4$  Union2 datasets constructed under the assumption of isotropic  $\Lambda$ CDM. In Fig. 9 we show the probability distribution of the dark energy dipole magnitude in the context of isotropic  $\Lambda$ CDM along with the observed dipole magnitude indicated by an arrow. As expected from eq. (13) only 4.75% of the simulated isotropic datasets had a dark energy dipole magnitude larger than the observed value. This is consistent with eq. (13) which indicates that the statistical significance of the existence of a dark energy dipole is about  $2\sigma$ .

In Fig. 10 we show the probability distribution of the angular distance of the isotropic simulated

dipoles from the observed fine structure constant dipole. Only 6.12% of the Monte Carlo datasets had such an angular distance smaller than the observed one. The probability for a Monte Carlo isotropic Union2 dataset to have both a dipole magnitude larger than the observed one and an angular separation from the fine structure dipole smaller than the observed one is 0.98%. This is larger than the anticipated value of  $0.0612 \times 0.0475 = 0.29\%$  due to the nonuniform distribution of the SnIa in the sky. We conclude that obtaining simultaneously the observed magnitude of the  $\alpha$  dipole (0.01%) *and* the observed magnitude and alignment of the Dark Energy dipole (1%) is  $(0.01\% \times 1\% = 0.0001\%)$  ie one part in  $10^6$ .

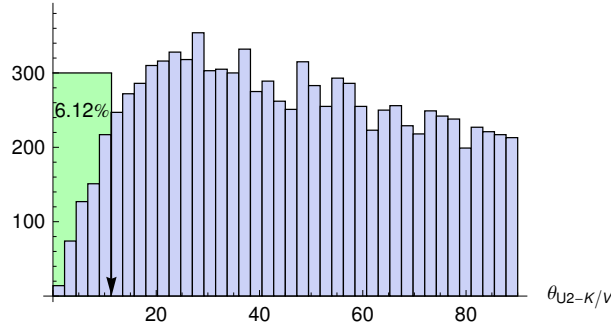


**Fig. 10:** Angular distances between the observed  $\alpha$ -dipole direction and the dipole direction obtained from the Monte Carlo simulations on the Union2 data. The arrow points to observed angular distance value and the light green area represents the Monte Carlo datasets that give an angular distance smaller than the observed one.

### 2.3 Redshift Tomography

It is interesting to identify the redshift range that contributes mostly to the large dipole magnitudes and to their alignment. To achieve this goal we use two approaches: a redshift bin approach and a variable upper redshift cutoff approach. In the redshift bin approach, we divide each dataset in three redshift bins of approximately equal number of datapoints and perform a separate dipole magnitude and alignment analysis in each bin. Thus we compare the results of each bin with respect to the quality of data (errorbar sizes), the dipole magnitudes and the dipole directions. In the variable upper redshift approach we start with truncated datasets with an upper redshift cutoff consisting of about 1/2 of the datapoints. Then we increase the upper redshift cutoff in five steps so that in the final step the full dataset is obtained in each case. We analyse each one of the six cumulative dataset parts with respect to their dipole magnitudes and their directions.

The directions of the best fit dipoles for each one of the redshift ranges is shown in Fig. 11 (the cumulative redshift parts are separately connected in increasing redshift order).

In Fig. 12 we show the angular separation of each Union2 redshift bin from the best fit dipole direction of the full Keck+VLT dataset, as a function of redshift range for each Union2 bin. Clearly, the lowest redshift bin which also has the smallest angular separation error is the one that has its dipole best aligned with the Keck+VLT dipole. In Fig. 13 we show the angular separation of each Keck+VLT redshift bin from the best fit dipole direction of the full Union2 dataset, as a function of redshift range for each bin. Clearly, the highest redshift bin has the lowest error and good alignment with the Union2 dipole. In this case however, the best fit dipole direction appears to be more consistent among the three redshift bins while the directional errorbars are significantly smaller than the Union2 case.

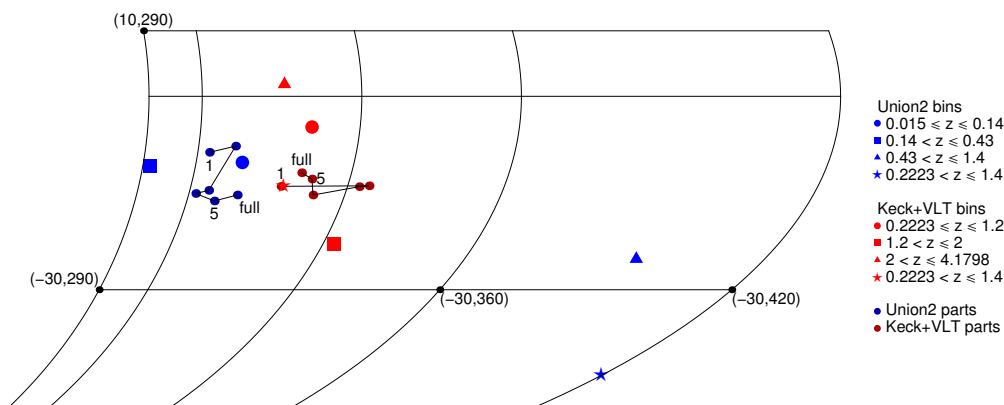


**Fig. 11:** Fine structure  $\alpha$  and Dark Energy dipole directions for the different redshift bins. The 'stars' denote the bins corresponding to the redshift range that is common to the Keck+VLT and Union2 samples. For this range however, the dipole uncertainty obtained from the Union2 data is very large.

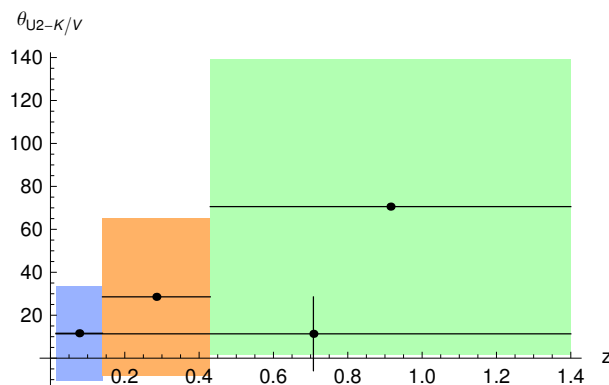


**Fig. 12:** Angular distances (with errors) between the Dark Energy dipole obtained in the different redshift bins and the  $\alpha$ -dipole obtained from the full redshift range Keck+VLT data. Notice that the lowest Union2 redshift bin dipole has the best alignment with the Keck+VLT dipole and also has the smallest error.

### 3 Physical Mechanism: Extended Topological Quintessence

#### 3.1 Global Monopole

If the observed coincident large dipole anisotropies are due to a physical mechanism and not to systematic or statistical fluctuations, then it is of particular interest to investigate what could be a physical model that could give rise simultaneously to these coincident dipoles. Such a mechanism could involve for example an inhomogeneous scalar field which couples to electromagnetism through a non-minimal coupling and whose potential energy could provide the dark energy required for accelerating expansion. Due to negative pressure such a scalar field would tend to quickly become homogenous and isotropic on Hubble scales. However, nontrivial topology would naturally generate sustainable inhomogeneity [44] of such a scalar field.

For a proper potential, the scale of the inhomogeneity would be the observationally required Hubble scale. In such a Hubble scale topological defect, an off center observer would observe aligned dipoles in both dark energy and the fine structure constant. For a large enough core scale, such a defect would become effectively homogenous and indistinguishable from  $\Lambda$ CDM. The dipole nature of observations of off-center observers located in spherically symmetric inhomogeneities has been discussed in detail in

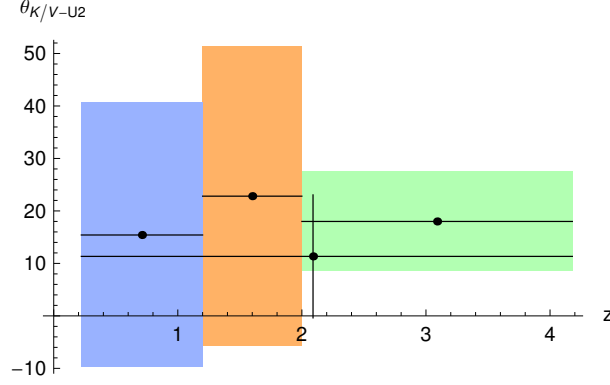


**Fig. 13:** Angular distances (with errors) between the  $\alpha$ -dipole obtained in the different redshift bins and the Dark Energy dipole obtained from the full redshift range Union2 data. Notice that the alignment of all Keck+VLT redshift bin dipoles with the full Union2 dipole is consistent with each other and similar to the alignment of the full Keck+VLT dataset.

Refs [45, 46]

Consider the action

$$S = \int \left[ \frac{1}{2} M_p^2 R - \frac{1}{2} (\partial_\mu \Phi^a)^2 - V(\Phi) + \frac{1}{4} B(\Phi) F_{\mu\nu}^2 + \mathcal{L}_m \right] \sqrt{-g} d^4x, \quad (15)$$

where  $M_p^{-2} = 8\pi G$  is the reduced Planck mass,  $\mathcal{L}_m$  is the Lagrangian density of matter fields,  $\Phi^a$  ( $a = 1, 2, 3$ ) is an  $O(3)$  symmetric scalar field,  $B(\Phi)$  is a non-minimal coupling to electromagnetism and

$$V(\Phi) = \frac{1}{4} \lambda (\Phi^2 - \eta^2)^2, \quad \Phi \equiv \sqrt{\Phi^a \Phi^a}. \quad (16)$$

We assume the existence of a Hubble scale global monopole formed during a recent cosmological phase transition. The vacuum energy density in the monopole core and the size of the core are determined by the two parameters of the model  $\eta$  (the vacuum expectation value) and  $\lambda$  (the coupling constant). The global monopole field configuration is described by the hedgehog ansatz

$$\Phi^a = \Phi(r, t) \hat{r}^a \equiv \Phi(r, t) (\sin \theta \cos \varphi, \sin \theta \sin \varphi, \cos \theta) \quad (17)$$

with boundary conditions

$$\Phi(0, t) = 0, \quad \Phi(\infty, t) = \eta, \quad (18)$$

where  $\eta$  is the scale of symmetry breaking assumed to be such that [44]

$$\frac{\lambda \eta^2}{3H_0^2} \gtrsim 1 \quad (19)$$

In eq. (17) we have allowed for a time dependence having in mind a cosmological setup of an expanding background.

Consider now a non-minimal coupling of the form

$$B(\Phi) = 1 - \xi \frac{\Phi^2}{\eta^2} \quad (20)$$

where  $\xi$  is constant. The fine structure ‘constant’ is related to the coupling  $B(\Phi)$  as

$$\alpha(\Phi) = \frac{e_0^2}{4\pi B(\Phi)^2} \quad (21)$$

where  $e_0$  is the bare charge that remains constant throughout the cosmological evolution. Therefore for small values of  $\Phi/\eta$  we have

$$\left(\frac{\Delta\alpha}{\alpha}\right) \simeq 2\xi \frac{(\Phi^2 - \Phi_0^2)}{\eta^2} \quad (22)$$

where  $\Phi_0$  is the field magnitude at the location of the observer. The dipole directions shown in Figs. 6 and 8 correspond to higher value of  $\alpha$  and lower accelerating expansion (brighter SnIa compared to  $\Lambda$ CDM) respectively. Thus, in the extended topological quintessence picture, for an off-center observer, this would be the direction pointing away from the global monopole core where the potential energy of the monopole is lower and the field magnitude  $\Phi$  is larger. In order to have a higher value of the fine structure constant in the same direction we need  $\xi > 0$ .

In Fig. 14 we illustrate the location of an off-centre observer with respect to the monopole core. In Fig. 14a we plot the observer location along with the field magnitude and direction denoted by the arrows at each point of the  $x - y$  plane. Clearly, the field magnitude is smaller towards the centre of the monopole and this justifies the variation of  $\alpha$  in that direction. Similarly, in Fig. 14b we show the energy density distribution of the global monopole and the location of the observer. Clearly, there is higher dark energy density towards the monopole centre and this justifies the higher acceleration rate in that direction.

### 3.2 Global Vortex

The extended topological quintessence monopole discussed above is distinct from the *varying  $\alpha$  defects* [47] based on Bekensteins's theory [48]. According to this model, the electric charge  $e$  (and therefore also the fine structure constant  $\alpha$ ) is promoted to a dimensionless scalar field  $\varphi \sim \ln e$  with zero potential and a kinetic term multiplied by a large dimensionful parameter  $\omega$ . This is similar to the corresponding extension of General Relativity along the lines of the Brans-Dicke theory where Newton's constant is promoted to a scalar field. As in the Brans-Dicke theory, the parameter  $\omega$  is used to partly *freeze* the dynamics of  $\varphi$  so that the charge variation in spacetime becomes consistent with observational and experimental constraints [12, 49]. The dynamics of the charge field  $\varphi$  affects the dynamics of the gauge field  $A_\mu$  which in turn affects the dynamics of any scalar field  $\Phi$  that couples to  $A_\mu$  via a gauge symmetry. Varying  $\alpha$  defects [47] are gauged defects formed if the vacuum manifold of  $\Phi$  has a non-trivial homotopy group and their dynamics is *indirectly* affected by the dynamics of the fine structure constant (and of  $\varphi$ ). A potential source of severe constraints for this class of defects is that they predict massive photons (spontaneous breaking of electromagnetism) in regions away from the defect core.

In contrast to these varying  $\alpha$  defects, in extended topological quintessence, the defect is global and is formed by the same field that represents  $\alpha$ . These are global defects non-minimally coupled to electromagnetism. As a simple example in Minkowski spacetime, consider a global vortex non-minimally coupled to electromagnetism. The dynamics of the complex scalar field  $\Phi$ , is determined by the Lagrangian density

$$\mathcal{L} = (\partial_\mu \Phi)^* (\partial^\mu \Phi) - \frac{1}{4} B(\Phi) F_{\mu\nu} F^{\mu\nu} - V(\Phi), \quad (23)$$

The field equations obtained by variation of  $\Phi^*$  and  $A_\mu$  are

$$\partial_\mu \partial^\mu \Phi = -\frac{\partial V}{\partial \Phi^*} - \frac{1}{4} \frac{\partial B(\Phi)}{\partial \Phi^*} F_{\mu\nu} F^{\mu\nu}. \quad (24)$$

and

$$\partial_\nu [B(\Phi) F^{\mu\nu}] = 0, \quad (25)$$

For a non-minimally coupled global vortex to form we set

$$V(\Phi) = \frac{\lambda}{4} (\Phi^* \Phi - \eta^2)^2, \quad (26)$$

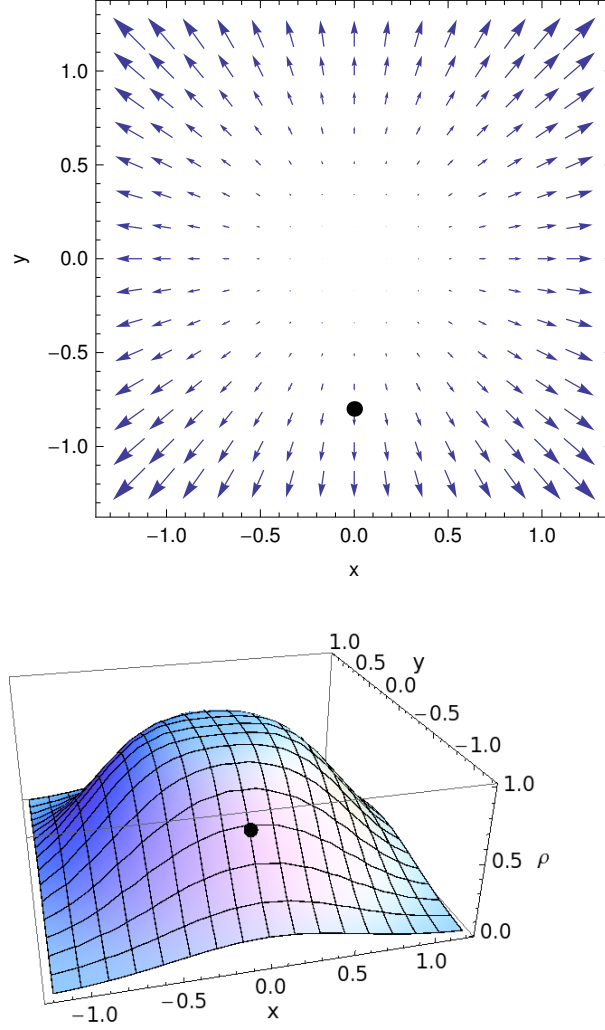


**Fig. 14:** (a) The observer location (thick dot) along with the field magnitude and direction denoted by the arrows at each point of the  $x - y$  plane. Clearly, the field magnitude is smaller towards the centre of the monopole and this justifies the variation of  $\alpha$  in that direction. (b) The energy density ( $\rho$ ) distribution of the global monopole and the location of the observer. Clearly, there is higher dark energy density towards the monopole centre and this justifies the higher acceleration rate in that direction.

and

$$B(\Phi) = 1 - \xi \frac{|\Phi|^2}{\eta^2} \quad (27)$$

We now use the global vortex the ansatz allowing for a coaxial magnetic field

$$\Phi = f(r) e^{in\theta}, \quad (28)$$

$$A_\theta = a(r), \quad (29)$$

where  $f(r)$  and  $a(r)$  are real functions of  $r$  and all other components of  $a_\mu$  are set to zero. We thus obtain the static field equations for  $f(r)$  and  $a(r)$  as

$$\frac{1}{r} \frac{d}{dr} \left( r \frac{df}{dr} \right) - \left( \frac{n^2}{r^2} - \frac{\eta^2 \lambda}{2} + \frac{\lambda}{2} f^2 \right) f - \frac{1}{2} \frac{dB(f^2)}{df} \left( \frac{1}{r} \frac{d}{dr} (ra) \right)^2 = 0, \quad (30)$$

$$\frac{d}{dr} \left( B(f^2) \frac{1}{r} \frac{d}{dr} (ra) \right) = 0, \quad (31)$$

since

$$F_{\mu\nu} F^{\mu\nu} = 2F^{r\theta} F_{r\theta} = 2 \left[ \frac{1}{r} \frac{d}{dr} (ra) \right]^2. \quad (32)$$

The corresponding energy density of the vortex is:

$$\rho = \left( \frac{df}{dr} \right)^2 + \frac{1}{2r^2} B(f^2) \left( \frac{d(ra)}{dr} \right)^2 + \frac{n^2}{r^2} f^2 + \frac{\lambda}{4} (f^2 - \eta^2)^2. \quad (33)$$

If there is no external source of electromagnetic field and if  $B(f^2) > 0$  everywhere, we obtain the usual global vortex solution  $f(r) = f_0(r)$ ,  $a(r) = 0$ . However, if there are regions of space where  $B(f^2) < 0$ , an instability develops which proceeds with spontaneous creation of electromagnetic field in the region where  $B(f^2) < 0$ . For example for  $B(f^2) = 1 - qV(f^2)/\eta^4$ , an instability develops in the core, for large enough values of  $q$ .

If there is an external source of electromagnetic fields (e.g. a localised magnetic field in the  $z$  direction), then the profile of  $f(r)$  will be affected in accordance with eq. (30) and a local additional variation of  $\alpha$  will occur. Thus, a robust prediction of this class of models is a correlation between regions of strong electromagnetic fields and variation of  $\alpha$ . The non-observation of such variation could impose strong constraints on the form of the coupling  $B(f^2)$ . The detailed investigation of these constraints and their consistency with the form of  $B(f^2)$  required to explain the observed  $\alpha$  dipole represents an interesting extension of this project.

### 3.3 Signatures on the CMB

Extended Topological Quintessence is expected to also produce a dipole asymmetry in CMB maps. In these maps however, the dipole term is dominated by our motion with respect to the CMB frame and therefore it has been removed completely. This removal has also swept away any subdominant cosmological contribution to the dipole. However any axial cosmological anisotropy that is not perfectly described by a dipole could have left a trace after the removal of the dipole. The detection of this trace may be possible by using specially designed statistical tests. In an effort to identify this trace we consider three large scale Healpix pixelizations of the WMAP7 ILC map and identify those pairs of opposite pixels in the sky that correspond to Maximum Temperature Difference. We compare the magnitude of this Maximum Temperature Asymmetry (MTA) with that expected from an isotropic model using gaussian simulated CMB maps. We also compare the direction of the MTA with the direction of the other observed cosmic asymmetry axes (Dark Flow, Dark Energy Dipole and  $\alpha$  Dipole). We find the likelihood that the observed magnitude and alignment would occur by chance in an isotropic model with no correlation between the CMB and the other observables.

We thus construct a Temperature Difference Map (TDM) obtained by assigning to each pixel a number equal to the difference between its temperature value and the value of the temperature of the opposite pixel in the sky. Thus we have

$$D^-(\hat{n}_i) = (T(\hat{n}_i) - T(-\hat{n}_i)), \quad (34)$$

where  $\hat{n}_i$  is the direction of the  $i^{th}$  Healpix pixel. In the context of the Healpix pixelization the opposite pixel is always simply defined and identified. By construction, opposite pixels of the TDM are assigned to opposite values. In the TDM we select the pixel  $D_{max}^-(\hat{n}_k)$  with the maximum absolute value. This pixel along with the pixel located opposite to it defines the axis of MTA. The direction of the MTA is then compared with the directions of other cosmic asymmetry axes ( $\alpha$  dipole, Dark Energy dipole and dark flow) and the corresponding angular differences are identified.

The WMAP7 ILC maps using Healpix pixelizations with  $N_{side} = 4, 8, 16$  (pixel size  $\sqrt{4\pi/(12N_{side}^2)}$  rad i.e. about  $14.7^\circ, 7.3^\circ$  and  $3.7^\circ$  respectively) are shown in Figure 15 along with the MTA pixels. The original map has  $N_{side} = 512$ .

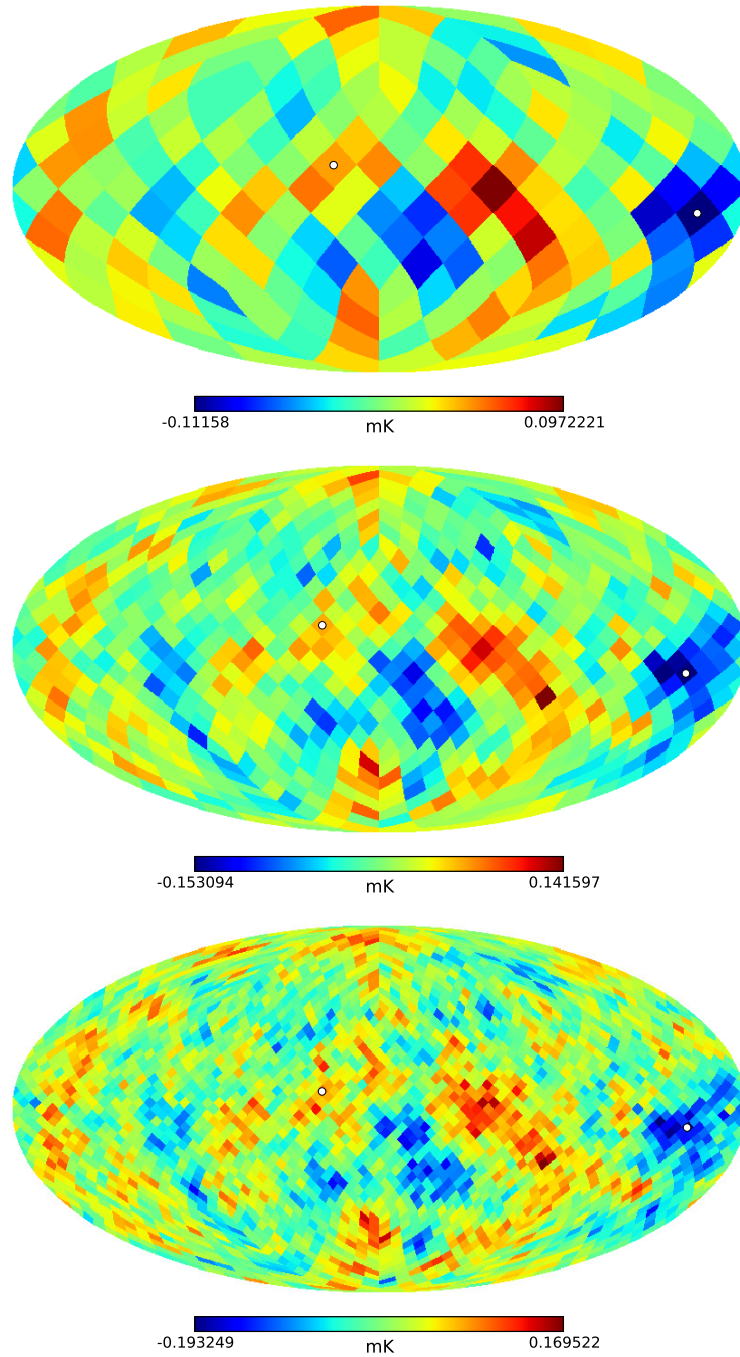


**Fig. 15:** Degraded temperature maps obtained from the 7 years ILC CMB map with  $N_{side} = 4, 8, 16$ . The white dots define the maximum temperature differences direction.

In Figure 16 we show the four cosmic asymmetry directions ( $\alpha$  dipole, Dark energy Dipole, Dark Flow and MTA) in a Mollweide projection. The filled contours around each direction correspond to the

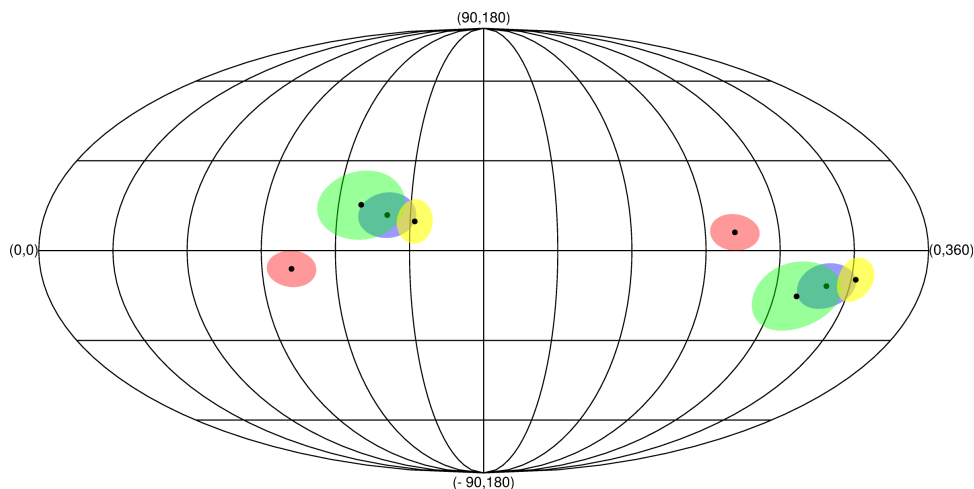


**Fig. 16:** Directions in galactic coordinates for the  $\alpha$  (blue) and Dark Energy (green) dipoles, for the Dark Flow direction (red) and for the direction of MTA in the 7 years ILC CMB map degraded to  $N_{side} = 8$  (yellow).

$1\sigma$  error regions.

The alignment between the four asymmetry axes is remarkable. A Monte Carlo simulation [51] of  $10^4$  ILC maps based on the best fit  $\Lambda$ CDM model has indicated that the probability of a larger than observed magnitude of the MTA and alignment with the  $\alpha$  dipole in the context of  $\Lambda$ CDM is between 0.1% and 0.5%.

In view of these observational results indicating alignment of the four basic cosmic asymmetries and the physical model of Extended Topological Quintessence that has the potential to explain this alignment, an important question remains to be answered: *What are the detailed quantitative predictions of Extended Topological Quintessence and how do they compare with the corresponding data?* The search for the answer to this question is currently in progress.

#### 4 Conclusion - Outlook

I have reviewed early observational hints for deviation from the cosmological principle and statistical isotropy. This appears to be one of the most likely directions that may lead to new fundamental physics in the coming years. Four independent cosmologically observed asymmetry axes appear to be mutually aligned at a level that is not consistent with homogeneous isotropic cosmology. These axes include the Fine Structure Constant Dipole ( $4\sigma$  away from isotropy), the Dark energy Dipole ( $2\sigma$  away from isotropy), the Dark Flow Axis ( $3\sigma$  away from isotropy) and the CMB Maximum Temperature Asymmetry Axis ( $1.5\sigma$  away from isotropy).

A simple mechanism that has the potential to give rise to such an alignment of cosmological axes assumes that we are off-center observers in an approximately spherical dark energy inhomogeneity induced by non-minimally coupled to electromagnetism, topologically non-trivial scalar field (Extended Topological Quintessence). The detailed quantitative predictions of this mechanism constitute an important extension of this research programme.

**Publicly Available Files:** The PowerPoint file of the talk is available at: <http://leandros.physics.uoi.gr/talks/fund-dipole.pptx>. The numerical analysis files used for the construction of all the figures are available through Refs. [8, 51].

## References

- [1] P. J. E. Peebles and B. Ratra, *Rev. Mod. Phys.* **75**, 559 (2003) [arXiv:astro-ph/0207347]; T. Padmanabhan, *Phys. Rept.* **380**, 235 (2003) [arXiv:hep-th/0212290]; S. M. Carroll, *Living Rev. Rel.* **4**, 1 (2001) [arXiv:astro-ph/0004075]; V. Sahni, *Class. Quant. Grav.* **19**, 3435 (2002) [arXiv:astro-ph/0202076].
- [2] R. Watkins, H. A. Feldman and M. J. Hudson, arXiv:0809.4041 [astro-ph]; H. A. Feldman, R. Watkins and M. J. Hudson, *Mon. Not. Roy. Astron. Soc.* **407**, 2328 (2010) [arXiv:0911.5516 [astro-ph.CO]].
- [3] G. Lavaux, R. B. Tully, R. Mohayaee and S. Colombi, *Astrophys. J.* **709**, 483 (2010) [arXiv:0810.3658 [astro-ph]].
- [4] A. Kashlinsky, F. Atrio-Barandela, D. Kocevski and H. Ebeling, *Astrophys. J.* **686**, L49 (2009) [arXiv:0809.3734 [astro-ph]]; A. Kashlinsky, F. Atrio-Barandela and H. Ebeling, arXiv:1202.0717 [astro-ph.CO]; A. Kashlinsky, F. Atrio-Barandela, H. Ebeling, A. Edge and D. Kocevski, *Astrophys. J.* **712**, L81 (2010) [arXiv:0910.4958 [astro-ph.CO]]; F. Atrio-Barandela, A. Kashlinsky, H. Ebeling and D. Kocevski, arXiv:1211.4345 [astro-ph.CO].
- [5] M. Tegmark, A. de Oliveira-Costa and A. Hamilton, *Phys. Rev. D* **68**, 123523 (2003) [astro-ph/0302496]; A. de Oliveira-Costa and M. Tegmark, *Phys. Rev. D* **74**, 023005 (2006) [astro-ph/0603369]; J. P. Ralston and P. Jain, *Int. J. Mod. Phys. D* **13**, 1857 (2004) [astro-ph/0311430].
- [6] I. Antoniou and L. Perivolaropoulos, *JCAP* **1012**, 012 (2010) [arXiv:1007.4347 [astro-ph.CO]].
- [7] L. Perivolaropoulos, arXiv:0811.4684 [astro-ph].
- [8] A. Mariano and L. Perivolaropoulos, *Phys. Rev. D* **86**, 083517 (2012) [arXiv:1206.4055 [astro-ph.CO]].
- [9] J. K. Webb, J. A. King, M. T. Murphy, V. V. Flambaum, R. F. Carswell and M. B. Bainbridge, *Phys. Rev. Lett.* **107**, 191101 (2011) [arXiv:1008.3907 [astro-ph.CO]]; J. A. King, J. K. Webb, M. T. Murphy, V. V. Flambaum, R. F. Carswell, M. B. Bainbridge, M. R. Wilczynska and F. E. Koch, arXiv:1202.4758 [astro-ph.CO].
- [10] R. Amanullah *et al.*, *Astrophys. J.* **716**, 712 (2010) [arXiv:1004.1711 [astro-ph.CO]].
- [11] J. K. Webb, V. V. Flambaum, C. W. Churchill, M. J. Drinkwater and J. D. Barrow, *Phys. Rev. Lett.* **82**, 884 (1999) [astro-ph/9803165]; M. T. Murphy, J. K. Webb, V. V. Flambaum, V. A. Dzuba, C. W. Churchill, J. X. Prochaska, J. D. Barrow and A. M. Wolfe, *Mon. Not. Roy. Astron. Soc.* **327**, 1208 (2001) [astro-ph/0012419]; M. T. Murphy, J. K. Webb and V. V. Flambaum, *Mon. Not. Roy. Astron. Soc.* **345**, 609 (2003) [astro-ph/0306483].
- [12] T. Chiba, *Prog. Theor. Phys.* **126**, 993 (2011) [arXiv:1111.0092 [gr-qc]].
- [13] Y. Fujii, A. Iwamoto, T. Fukahori, T. Ohnuki, M. Nakagawa, H. Hikida, Y. Oura and P. Möller, *Nucl. Phys.* **B 573** (2000) 377.
- [14] Yu. V. Petrov, A. I. Nazarov, M. S. Onegin, V. Y. Petrov and E. G. Sakhnovsky, *Phys. Rev. C* **74** (2006) 064610.
- [15] T. Damour and F. Dyson, *Nucl. Phys.* **B 480** (1996) 37.
- [16] A.I. Shlyakhter, *Nature* **264** (1976) 340.
- [17] S. Bize *et al.*, *Phys. Rev. Lett.* **90** (2003) 150802.
- [18] E. Peik *et al.*, *Phys. Rev. Lett.* **93** (2004) 170801.
- [19] T.M. Fortier *et al.*, *Phys. Rev. Lett.* **98** (2007) 070801.
- [20] S. Blatt *et al.*, *Phys. Rev. Lett.* **100** (2008) 140801.
- [21] T. Rosenband *et al.*, *Science* **319** (2008) 808.
- [22] A. Cingöz *et al.*, *Phys. Rev. Lett.* **938** (2007) 040801.
- [23] C. R. Gould, E. I. Sharapov and S. K. Lamoreaux, *Phys. Rev. C* **74** (2006) 024607.

- [24] Y. Fujii and A. Iwamoto, Phys. Rev. Lett. **91** (2003) 261101.
- [25] C.L. Carilli et al., Phys. Rev. Lett. **85** (2000) 5511.
- [26] L.L. Cowie and A. Songaila, Astrophys.J. **453** (1995) 596.
- [27] J.K. Webb et al., Phys. Rev. Lett. **82** (1999) 884.
- [28] J.K. Webb et al., Phys. Rev. Lett. **87** (2001) 091301.
- [29] M.T. Murphy, J.K. Webb, V.V. Flambaum, J.X. Prochaska, A.M. Wolfe, Mon.Not.Roy.Astron.Soc. **327** (2001) 1237.
- [30] M.T. Murphy, J.K. Webb and V.V. Flambaum, Mon.Not.Roy.Astron.Soc. **345** (2003) 609.
- [31] M.T. Murphy, J.K. Webb and V.V. Flambaum, Lec. Not. Phys. **648** (2004) 131.
- [32] J. Daring, Astrophys.J. **612** (2004) 58.
- [33] N. Kanekar, J. Chengalur, and T. Ghosh, Astrophys.J. **716** (2010) L23.
- [34] R. Srianand, H. Chand, P. Petitjean and B. Aracil, Phys. Rev. Lett. **92** (2004) 121302; H. Chand, R. Srianand, P. Petitjean and B. Aracil, Astron. Astrophys. **417** (2004) 853.
- [35] M.T. Murphy, J.K. Webb and V.V. Flambaum, Phys. Rev. Lett. **99** (2007) 239001; M.T. Murphy, J.K. Webb and V.V. Flambaum, Mon.Not.Roy.Astron.Soc. **384** (2008) 1053.
- [36] H. Chand, P. Petitjean, R. Srianand and B. Aracil, Astron. Astrophys. **430** (2005) 47.
- [37] P. Molaro, D. Reimers, I.I. Agafonova and S.A. Levshakov, Eur. Phys. J. ST **163** (2008) 173.
- [38] H. Chand, R. Srianand, P. Petitjean, B. Aracil, R. Quast and D. Reimers, Astron. Astrophys. **451** (2006) 45.
- [39] I.I. Agafonova, P. Molaro, S.A. Levshakov and J.L. Hou, Astron. Astrophys. **529** (2011) 28.
- [40] C.J.A. Martins et al., Phys. Lett. B **585** (2004) 29.
- [41] E. Menegoni, S. Galli, J. G. Bartlett, C. J. A. Martins and A. Melchiorri, Phys. Rev. D **80** (2009) 087302.
- [42] R.H. Cyburt, B.D. Fields, K.A. Olive, and E.D. Skillman Astropart. Phys. **23** (2005) 313.
- [43] M. Blomqvist, E. Mortsell and S. Nobili, JCAP **0806**, 027 (2008) [arXiv:0806.0496 [astro-ph]]; M. Blomqvist, J. Enander and E. Mortsell, JCAP **1010**, 018 (2010) [arXiv:1006.4638 [astro-ph.CO]].
- [44] J. C. Bueno Sanchez and L. Perivolaropoulos, Phys. Rev. D **84**, 123516 (2011) [arXiv:1110.2587 [astro-ph.CO]].
- [45] J. Grande and L. Perivolaropoulos, Phys. Rev. D **84**, 023514 (2011) [arXiv:1103.4143 [astro-ph.CO]].
- [46] H. Alnes and M. Amarguioui, Phys. Rev. D **74**, 103520 (2006) [astro-ph/0607334].
- [47] J. Magueijo, H. Sandvik and T. W. B. Kibble, Phys. Rev. D **64**, 023521 (2001); J. Menezes, P. P. Avelino and C. Santos, Int. J. Mod. Phys. A **21**, 3295 (2006) [gr-qc/0601007]; J. Menezes, P. P. Avelino and C. Santos, Phys. Rev. D **72**, 103504 (2005) [hep-ph/0509326]; J. Menezes da Silva, arXiv:0808.3274 [hep-ph].
- [48] J. D. Bekenstein, Phys. Rev. D **25**, 1527 (1982); H. B. Sandvik, J. D. Barrow, and J. Magueijo, Phys. Rev. Lett. **88**, 031302 (2002); D. F. Mota and J. D. Barrow, Phys. Lett. B **81**, 141 (2004); D. F. Mota and J. D. Barrow, Mon. Not. Roy. Astron. Soc. **349**, 291 (2004); D. Kimberly and J. Magueijo, Phys. Lett. B **584**, 8 (2004); J. D. Barrow, J. Magueijo and H. B. Sandvik, Phys. Rev. D **66**, 043515 (2002); P. P. Avelino, C. J. A. P. Martins, and J. C. R. E. Oliveira, Phys. Rev. D **70**, 083506 (2004); J. D. Barrow and S. Z. W. Lip, Phys. Rev. D **85**, 023514 (2012) [arXiv:1110.3120 [gr-qc]].
- [49] R. Srianand, H. Chand, P. Petitjean, and B. Aracil, Phys. Rev. Lett. **92**, 121302 (2004); K. A. Olive et al., Phys. Rev. D **69**, 027701 (2004); D. J. Shaw and J. D. Barrow, Phys. Lett. B **639**, 596 (2006); J. D. Barrow, Phys. Rev. D **71**, 083520 (2005); T. Damour, "Varying constants", gr-qc/0306023 (2003);
- [50] T. Damour and F. Dyson, Nucl. Phys. B **480**, 37 (1996) [hep-ph/9606486]; T. Damour and F. Dyson, Nucl. Phys. B **480**, 37 (1996); S. Blatt et al., Phys. Rev. Lett. **100**, 140801 (2008); J. D. Barrow and

*Leandros Perivolaropoulos*

D. J. Shaw, Phys. Rev. D **78**, 067304 (2008) [arXiv:0806.4317 [hep-ph]]; J. Magueijo, J. D. Barrow and H. B. Sandvik, Phys. Lett. B **549**, 284 (2002) [astro-ph/0202374].

[51] A. Mariano and L. Perivolaropoulos, Phys. Rev. D **87**, no. 4, 043511 (2013) [arXiv:1211.5915 [astro-ph.CO]].



# Can we push the fundamental Planck scale above $10^{19}$ GeV?

Dejan Stojkovic\*

HEPCOS, Department of Physics, SUNY at Buffalo, Buffalo, NY 14260-1500

## Abstract

The value of the quantum gravity scale is  $M_{\text{Pl}} = 10^{19}$  GeV. However, this is inherently a three-dimensional quantity. We know that we can bring this scale all the way down to TeV if we introduce extra dimensions with large volume. This will solve the hierarchy problem by destroying the desert between the electroweak and gravity scales, but will also introduce a host of new problems since some things (e.g. proton stability, neutrino masses etc) have their natural habitat in this desert. In contrast, we can also solve the hierarchy problem by reducing the number of dimensions at high energies. If the fundamental theory (which does not have to be gravity as we understand it today) is lower dimensional, then the fundamental energy scale might be much greater than  $10^{19}$  GeV. Then, some experimental and observational limits (e.g. on Lorentz invariance violation) which are coming close to or even exceeding the scale of  $10^{19}$  GeV can be evaded. In addition, scattering of particles at transplanckian energies will not produce mini-black holes which could prevent us from probing arbitrarily short distances, and thus avoid "the end of short distance physics".

The scale at which quantum effects in gravity become important is known as the Planck scale. In 3D, there is a unique expression with dimensions of mass (energy) that involves all the known fundamental constants

$$M_{\text{Pl}}^{3D} = \sqrt{\frac{\hbar c}{G_{3D}}} \quad (1)$$

If we substitute the measured values for  $c$ ,  $\hbar$  and  $G_{3D}$ , we get the numerical value of  $M_{\text{Pl}}^{3D} = 10^{19}$  GeV. However, this is inherently a three-dimensional value. In theories where the number of dimensions is not three, the numerical values of  $M_{\text{Pl}}$  maybe quite different. In the context of large extra dimensions [1, 2] (see also [3, 4]), we learned that  $M_{\text{Pl}}$  could be as low as 1 TeV if gravity can propagate in more than three spatial dimensions. To make the model realistic and not in obvious contradiction with experiments, the authors of proposed that all the standard model particles are confined on a  $(3 + 1)$ -dimensional subspace (a brane) of a higher-dimensional manifold, while gravitons, being geometrical degrees of freedom, can propagate everywhere. In this framework, fundamentally strong gravity is diluted due to the presence of extra dimensions. An observer located on the brane, observing only the force lines along the brane, does not register the gravitational force lines which propagate through the bulk, so he concludes that gravity is weak (i.e. suppressed by much larger energy scale). Bringing the scale of quantum gravity down to 1 TeV requires having a large enough volume of the extra space. If the number of extra dimensions is three or greater, then we can have large enough volume, and still avoid conflict with table-top gravitational experiments. Among the other things, this setup resolves the standard model hierarchy problem.

Going exactly in the opposite direction, a framework of "vanishing" or "evolving" dimensions was proposed in [5–10], (see also [11–18] for related work). In this framework the dimensionality of the space we live in is not fixed, but actually depends on the length scale we are probing. As the length scale increases, new dimensions open up. At short scales the space is lower dimensional; at the intermediate scales the space is three-dimensional, and at large scales, the space is effectively higher dimensional. This

---

\*E-mail: ds77@buffalo.edu

*Can we push the fundamental Planck scale above  $10^{19}$  GeV?*

setup is free of many problems that plague three-dimensional theories. If the space is lower dimensional in the high energy regime, then there are no ultraviolet divergencies in field theories, it is possible to quantize gravity, and the theory of matter plus gravity is free of divergencies and renormalizable. If the space is higher dimensional at cosmological scales, then some cosmological problems (including the cosmological constant problem) can be attacked from a completely new perspective.

In the context of evolving dimensions, the fundamental energy scale is much more peculiar. For example, in  $2D$ , we would like to find the quantity with dimensions of mass which can be expressed in terms of the constants  $c$ ,  $\hbar$  and  $G$ . Thus we write

$$M = c^{n_1} \hbar^{n_2} G_{2D}^{n_3} \quad (2)$$

Since dimensionally  $c = L/T$ ,  $\hbar = ML^2/T$ , and  $G_{2D} = L^2/(MT^2)$ , the system of equations that we have to solve is

$$\begin{aligned} n_1 + 2n_2 + 2n_3 &= 0 \\ -n_1 - n_2 - 2n_3 &= 0 \\ n_2 - n_3 &= 1 \end{aligned} \quad (3)$$

The solution is  $n_1 = 2$ ,  $n_2 = 0$ , and  $n_3 = -1$ . Thus, in two dimensions, there is no quantity with dimensions of mass that involves all the constants  $c$ ,  $\hbar$  and  $G$ . The only quantity that we can construct in  $2D$  is

$$M_{\text{Pl}}^{2D} = \frac{c^2}{G_{2D}} \quad (4)$$

The absence of  $\hbar$  is notable. This may be perhaps connected with the fact that  $2D$  general relativity has no local propagating degrees (i.e. no gravitons in quantum case). Since  $G_{2D}$ , unlike  $G_{3D}$ , is a number of unknown magnitude, the exact numerical value of  $M_{\text{Pl}}^{2D}$  is also unknown. In principle, the value of  $M_{\text{Pl}}^{2D}$  could be much greater than  $10^{19}$  GeV.

If we formally extend our discussion to one spatial dimension, where  $G_{1D} = L/(MT^2)$  while  $c$  and  $\hbar$  remain the same, the system of equations that we have to solve becomes

$$\begin{aligned} n_1 + 2n_2 + n_3 &= 0 \\ -n_1 - n_2 - 2n_3 &= 0 \\ n_2 - n_3 &= 1 \end{aligned} \quad (5)$$

We find that there is no solution to this system, i.e. there is no quantity with dimensions of mass that involves any combination of  $c$ ,  $\hbar$  and  $G$  (or at least some of them). This is perhaps connected with the fact that  $1D$  general relativity is not a dynamical theory.

If we accept the assumption that a fundamental high energy theory is lower dimensional, and our  $3D$  theories are just low energy approximations, then it appears that general relativity is also an emergent theory that emerges for the first time in  $2D$ , and becomes a fully fledged propagating theory only in  $3D$ . In that case  $M_{\text{Pl}}^{3D} = 10^{19}$  GeV plays no fundamental role. The ultimate theory of space-time has its own fundamental scale, which for all we know could be much lower or much greater than  $10^{19}$  GeV. This would also imply that it does not make much sense to quantize gravity as we know it, especially not in  $3D$ .

If  $M_{\text{Pl}}^{3D} = 10^{19}$  GeV loses its fundamental role, then we have to re-examine many concepts that we are taking for granted. As we mentioned, the scale at which quantum effects become important in gravity does not have to be  $10^{19}$  GeV. There are two options: this scale can be either smaller or greater than  $10^{19}$  GeV. Our experience with quantum gravity energy scale much smaller than  $10^{19}$  GeV is very unpleasant. For example, low scale quantum gravity may introduce unacceptably fast proton decay. Conservation of baryon number is just an accidental global low-energy effective symmetry, and quantum

gravity is not expected to preserve it (as opposed to local gauge symmetries which are dynamically preserved) [19]. The proton life-time for gravitationally induced decay (in  $3D$ ) is

$$\tau_{\text{proton}} \approx m_{\text{proton}}^{-1} \left( \frac{M_{\text{Pl}}}{m_{\text{proton}}} \right)^4. \quad (6)$$

In the context of the large extra dimensions, where  $M_{\text{Pl}} = 1\text{TeV}$ , the proton lifetime is just a tiny fraction of a second, thus requiring elaborate setups to avoid it. In general, to satisfy the current lower limit on the proton lifetime of  $10^{34}$  years, we need  $M_{\text{Pl}} > 10^{16}\text{GeV}$ . Another potentially dangerous quantum gravity induced process comes from neutron-antineutron oscillations. An operator responsible for this process is "UDDUDD" where "U" stands for the up-quark and "D" for the down quark. This is a dimension-nine operator, so in  $3D$  it is suppressed by five powers of  $M_{\text{Pl}}$ , which lifts this process safely above the current experimental limits for  $M_{\text{Pl}} > 10^5\text{GeV}$ .

While there are many other potential dangers of the low scale quantum gravity (e.g. large mixings between leptons, large flavor changing neutral currents, etc.) perhaps the most serious one comes from the limits on the scale at which Lorentz invariance is violated. Near the Planck scale, the space-time metric is expected to fluctuate wildly. Hawking suggested that that we can view these wild fluctuations as virtual black holes which constantly pop in and out of vacuum [20]. Thus, the space-time at these scales may not be smooth, but actually full of bumps. Particles propagating in such a background are just slightly affected by these tiny bumps, but the effect may accumulate for particles that travel long cosmological distances. For example, high energy photons from gamma ray bursts (GRBs) propagating from a distant part of the universe toward us may be affected by these quantum fluctuations, which in turn could modify their dispersion relation. Recent observations established extremely tight limits on such effects limiting the scale at which Lorentz invariance is violated to greater than  $10^{19}\text{GeV}$  for linear (and close to that value for quadratic) energy corrections to the dispersion relations [21].

Many problems that plague low scale quantum gravity indicate that the possibility of having quantum gravity scale higher than  $10^{19}\text{GeV}$  is much more plausible. If that is really the case, then there will be some immediate interesting consequences. For example, the perturbative quantum gravity effects, which are usually suppressed by powers of Planck scale [22] are now much more suppressed than in theories where  $M_{\text{Pl}} = 10^{19}\text{GeV}$ . This could obviously evade the limits where the current experiments and observations are already excluding effects suppressed by  $M_{\text{Pl}} = 10^{19}\text{GeV}$  (e.g. Lorentz invariance violation). It would also be much more difficult to look for the signature of the Planck scale physics in the Cosmic Microwave Background Radiation [23–28]. In an extreme case where  $M_{\text{Pl}} \rightarrow \infty$ , there would effectively be no quantum gravity.

Many consequences of a high scale quantum gravity would be model dependent. For example, in the "vanishing dimensions" scenario where the space-time is just an ordered lattice which is lower dimensional on short scales [5, 6], once we are probing the length scales shorter than the dimensional crossover (say  $\text{TeV}^{-1}$ ), we do not expect our  $3D$  intuition to hold. While in  $3D$  scattering of particles at transplanckian energies inevitably produces Planck-size black holes, which effectively represents "the end of short distance physics", this does not have to be true anymore. Most of the conventional  $2D$  theories of gravity do not contain true singularities, and thus there are no true black holes in  $2D$  (unless we add cosmological constant or radically modify gravity). In  $1D$ , gravity stops being dynamical theory, unless augmented by some extra fields (eg. dilaton gravity). Thus scattering at transplanckian energies does not have to produce a mini-black hole and prevents us from probing arbitrarily short distances. In addition, a large  $3D$  black hole, approaching the end of its evolution by emitting Hawking quanta, inevitably reaches lower dimensional regime where it stops being a true black hole. This scenario might effectively circumvent the information loss paradox.

In conclusions, the purpose of this note is to point out that the scale of quantum gravity, or rather the scale of fundamental physics of space-time (which does not have to be gravity as we understand it today), could be greater than  $10^{19}\text{GeV}$ . One of the concrete realizations of this possibility is the framework

of “vanishing” or “evolving” dimensions where the number of dimensions depends on the energy scale that we are probing. If the fundamental theory is lower dimensional, and observed  $3D$  gravity is just a low energy effective theory, then the fundamental scale might be larger than  $10^{19}$  GeV. There are many interesting consequences of this proposal. Some experimental and observational limits which in recent years came close to, and in some cases even exceeded the scale of  $10^{19}$  GeV can be obviously evaded. Since there are no true singularities in generic lower dimensional space-times, scattering of particles at the center of mass energies higher than the fundamental energy scale will not yield black holes. This implies that we can in principle probe arbitrary short distances, which was not possible in  $3D$ . Absence of true singularities may also have important implications for the information loss paradox. Finally, having the fundamental scale which is much higher than  $10^{19}$  GeV implies that our calculations concerning early universe must be revisited.

### Acknowledgement

This work was also partially supported by the US National Science Foundation, under Grant No. PHY-1066278.

### References

- [1] N. Arkani-Hamed, S. Dimopoulos and G. R. Dvali, Phys. Lett. B **429**, 263 (1998)
- [2] L. Randall and R. Sundrum, Phys. Rev. Lett. **83**, 4690 (1999)
- [3] G. D. Starkman, D. Stojkovic and M. Trodden, Phys. Rev. Lett. **87**, 231303 (2001) [hep-th/0106143].
- [4] G. D. Starkman, D. Stojkovic and M. Trodden, Phys. Rev. D **63**, 103511 (2001) [hep-th/0012226].
- [5] L. Anchordoqui, D. C. Dai, M. Fairbairn, G. Landsberg and D. Stojkovic, Mod. Phys. Lett. A **27**, 1250021 (2012) [arXiv:1003.5914 [hep-ph]].
- [6] L. A. Anchordoqui, D. C. Dai, H. Goldberg, G. Landsberg, G. Shaughnessy, D. Stojkovic and T. J. Weiler, Phys. Rev. D **83**, 114046 (2011) [arXiv:1012.1870 [hep-ph]].
- [7] D. Stojkovic, arXiv:1304.6444 [hep-th].
- [8] J. R. Mureika and D. Stojkovic, Phys. Rev. Lett. **106**, 101101 (2011) [arXiv:1102.3434 [gr-qc]]; Phys. Rev. Lett. **107**, 169002 (2011) [arXiv:1109.3506 [gr-qc]].
- [9] G. Landsberg, PoS ICHEP **2010**, 399 (2010).
- [10] X. Calmet and G. Landsberg, chapter 7 in A.J. Bauer and D.G.Eiffel editors, Black Holes: Evolution, Theory and Thermodynamics Nova Publishers, New York, 2012 [arXiv:1008.3390 [hep-ph]].
- [11] R. Loll, Nucl. Phys. Proc. Suppl. **94**, 96–107 (2001); J. Ambjorn, J. Jurkiewicz, R. Loll, Phys. Rev. **D72**, 064014 (2005); J. Ambjorn, J. Jurkiewicz, R. Loll, “Title: Quantum Gravity, or The Art of Building Spacetime,” in *Approaches to Quantum Gravity*, ed. D. Oriti, Cambridge University Press (2006)
- [12] L. Modesto and P. Nicolini, Phys. Rev. D **81**, 104040 (2010) [arxiv:0912.0220 [hep-th]].
- [13] S. Carlip, R. A. Mosna and J. P. M. Pitelli, Phys. Rev. Lett. **107**, 021303 (2011) [arXiv:1103.5993 [gr-qc]].
- [14] R. B. Mann and J. R. Mureika, Phys. Lett. B **703**, 167 (2011) [arXiv:1105.5925 [hep-th]].
- [15] J. F. Nieves, Int. J. Mod. Phys. A **26**, 5387 (2011) [arXiv:1105.2546 [hep-ph]].
- [16] J. R. Mureika and P. Nicolini, Phys. Rev. D **84**, 044020 (2011) [arXiv:1104.4120 [gr-qc]].
- [17] O. C. Stoica, arXiv:1301.2231 [gr-qc].
- [18] L. Gonzalez-Mestres, arXiv:1009.1853 [astro-ph.HE].
- [19] D. Stojkovic, F. C. Adams and G. D. Starkman, Int. J. Mod. Phys. D **14**, 2293 (2005) [gr-qc/0604072].

- [20] S. W. Hawking, *Phys. Rev. D* **53**, 3099 (1996) [hep-th/9510029].
- [21] V. Vasileiou, A. Jacholkowska, F. Piron, J. Bolmont, C. Couturier, J. Granot, F. W. Stecker and J. Cohen-Tanugi *et al.*, *Phys. Rev. D* **87**, 122001 (2013) [arXiv:1305.3463 [astro-ph.HE]].
- [22] D. Stojkovic, arXiv:1305.6960 [gr-qc].
- [23] J. Martin and R. H. Brandenberger, “The trans-Planckian problem of inflationary cosmology,” *Phys. Rev. D* **63**, 123501 (2001) [arXiv:hep-th/0005209].
- [24] R. H. Brandenberger and J. Martin, “On signatures of short distance physics in the cosmic microwave background,” *Int. J. Mod. Phys. A* **17**, 3663 (2002) [arXiv:hep-th/0202142].
- [25] C. P. Burgess, J. M. Cline, F. Lemieux and R. Holman, “Are inflationary predictions sensitive to very high energy physics?,” *JHEP* **0302**, 048 (2003) [arXiv:hep-th/0210233].
- [26] R. Easther, B. R. Greene, W. H. Kinney and G. Shiu, “Inflation as a probe of short distance physics,” *Phys. Rev. D* **64**, 103502 (2001) [arXiv:hep-th/0104102].
- [27] R. Easther, W. H. Kinney and H. Peiris, “Observing trans-Planckian signatures in the cosmic microwave background,” *JCAP* **0505**, 009 (2005) [arXiv:astro-ph/0412613].
- [28] R. Easther, W. H. Kinney and H. Peiris, “Boundary effective field theory and trans-Planckian perturbations: Astrophysical implications,” *JCAP* **0508**, 001 (2005) [arXiv:astro-ph/0505426].



# REM - the Shape of Potentials for $f(R)$ Theories in Cosmology and Tachyons

Dumitru N. Vulcanov<sup>a,\*</sup>, Goran S. Djordjevic<sup>b,c,†</sup> and Ciprian A. Sporea<sup>a,‡</sup>

<sup>a</sup> West University of Timisoara, Faculty of Physics, B-dul V. Parvan no. 4, 300223, Timisoara, Romania

<sup>b</sup> University of Nis, Faculty of Science and Mathematics, Visegradska 33, Nis, Serbia

<sup>c</sup> Theory Group, Physics Department, CERN, CH-1211, Geneva 23, Switzerland

## Abstract

We investigated the reverse engineering method (REM) for constructing the potential of the scalar field in cosmological theories based on metric  $f(R)$  gravity and Friedman Robertson Walker (FRW) metric. Then transposing the new field and Friedman equations in an algebraic computing special library (in Maple + GrTensorII platform) we graphically investigate the shape of the potentials in terms of the scalar field in at least two type of cosmology with exponential and linear scale factor expansion. Some perspectives and conclusions relating these results with tachyonic cosmology theories are noticed.

## 1 Introduction

The reverse engineering method (REM) was proposed [1] in order to reconstruct the shape of the scalar field potentials, including tachyon-like, in cosmology starting with a certain time behavior of the scale factor. Recently we studied REM in cosmologies with minimally and non-minimally coupled scalar field [2] for Friedmann-Robertson-Walker metrics. We extended our study for higher order metric theories of gravity (generically called  $f(R)$  theories [3–6]).

This time we are mostly focused on a lagrangian of the theory having the form  $L = R + \alpha R^2 + L_\phi$ , where  $R$  is the Ricci scalar and  $L_\phi$  represents the lagrangian of the scalar field (minimally coupled with gravity). The field equations (modified Friedmann equations in FRW metric) will contain second order derivatives of the scale factor. It is hard to find analytical solutions for this type of field equations and thus a numerical investigation is necessary. For this reason we developed a series of Maple+GrTensorII programs, organized in a special library, using the symbolic computation and graphical facilities for processing REM in several cases: exponential, linear or sinusoidal expansion of the Universe. The shape of the potential as a function of the scalar field is graphically investigated in order to establish a convenient theory producing the respective time evolution of the universe.

We also present the classical behavior of several tachyon-like scalar-field potentials [1] which are still good candidates for describing a realistic scale factor of the Universe, in particular for describing inflation, with accent on its early phase on archimedean and nonarchimedean spaces. This approach applied in [7] on classical and quantum dynamics for a tachyonic field with exponential potential, here is briefly extended applied on a model with  $V(T) \sim \cosh^{-1}(T)$ . Possibility for its generalization and quantization is pointed out in Section 4.

## 2 Scalar field cosmology in metric $f(R)$ gravity

We are dealing with cosmologies based on Friedman-Robertson-Walker (FRW) metric

$$ds^2 = c^2 dt^2 - a(t)^2 \left[ \frac{dr^2}{1 - kr^2} + r^2 (d\theta^2 + \sin^2\theta d\varphi^2) \right] \quad (1)$$

---

\*E-mail: vulcan@physics.uvt.ro

†E-mail: gorandj@junis.ni.ac.rs

‡E-mail: sporea\_89@yahoo.com

where  $a(t)$  is the scale factor and  $k = -1, 0, 1$  for open, flat or closed cosmologies. The dynamics of the system with a scalar field minimally coupled with metric  $f(R)$  gravity is described by the following action [4,6]

$$\mathcal{S} = \int d^4x \sqrt{-g} \left\{ \frac{1}{2} \frac{M_P^2}{8\pi} f(R) + \frac{1}{2} \nabla_\mu \phi \nabla^\mu \phi - V(\phi) \right\} + \int d^4x \mathcal{L}_M(g_{\mu\nu}, \psi_M) \quad (2)$$

where  $f(R)$  is in principle an arbitrary function of the Ricci scalar  $R$ ,  $V(\phi)$  is the potential of the scalar field and  $\mathcal{L}_M$  represents the Lagrange density for regular matter (dust, radiation, etc).

As in the Starobinsky model [5] (known to be an excellent model of chaotic inflation) we choose for  $f(R)$  the following expression

$$f(R) = R + \alpha R^2 \quad (3)$$

where we consider  $\alpha$  to be a real constant (inversely proportional with the rest mass of the scalar particle in the Starobinsky model).

Varying the action  $\mathcal{S}$  with respect to the metric  $g^{\mu\nu}$  we get the new field equations

$$\begin{aligned} (1 + 2\alpha R) R_{\alpha\beta} - \frac{1}{2} (R + \alpha R^2) g_{\alpha\beta} - 2\alpha g^{\mu\nu} (\nabla_\alpha \nabla_\beta - g_{\alpha\beta} g^{\sigma\tau} \nabla_\sigma \nabla_\tau) R_{\mu\nu} = \\ = -\phi_{,\alpha} \phi_{,\beta} + g_{\alpha\beta} \left( \frac{1}{2} g^{\mu\nu} \phi_{,\mu} \phi_{,\nu} - V(\phi) \right) \end{aligned} \quad (4)$$

### 3 Algebraic computing, "Cosmo" library and some graphical results

As reported previously [1] we composed a new library (called generically "Cosmo") for use in cosmology embedded in Maple+GrTensorII algebraic computing platform (see at <http://grtensor.org>). GrTensorII is a free library (developed by a community of users) which incorporates a Riemannian geometry in a Maple symbolic computation environment. The Cosmo library defines the main cosmological functions and operators (Hubble constant/function, deceleration, scale factor etc.) producing the main Friedman equations from Einstein eqs. in FRW metric. This time for our purposes we cannot use the predefined (in GrTensorII) Einstein equations, thus we have to define new tensor components for the field equations above mentioned by introducing a sequence of GrTensorII commands as

`> grdef('Ec{a b} := (1+2*alpha*Ricciscalar)*R{a b} - (1/2)*g{a b}*(Ricciscalar + alpha*Ricciscalar^2) - s{,a}*s{,b} + (1/2)*g{a b}*((1/2)*g{^i ^j}*s{,i}*s{,j} - V)');`

where  $s$  represents the scalar field and  $Ec\{a b\}$  is a tensorial object having as components the main field equations here replacing the Einstein equations.

Fortunately we still can use the Riemannian environment defined by GrTensorII (Riemann and Ricci tensors, Christoffel symbols for covariant derivatives, the Ricci scalar - called *Ricciscalar* in the above command line, etc.). Finally after loading the FRW metric (using `qload GrTensorII` command) and a sequence of `gralter`, `simplify` and `subs` commands we obtain the new Friedmann equations as

$$V(\phi) = 3\dot{H}(t) + 6H(t)^2 + 3\frac{k}{a(t)^2} + h_1(k, \alpha, \dot{H}, \ddot{H}..) \quad (5)$$

$$\dot{\phi}^2 = -2\dot{H}(t)^2 + 2\frac{k}{a(t)^2} + h_2(k, \alpha, \dot{H}, \ddot{H}..) \quad (6)$$

where  $H(t) = \dot{a}(t)/a(t)$  is the Hubble function. We arranged the equations to resemble the form of eqs. (12)-(13) in [1] and we collected in  $h_1$  and  $h_2$  the terms containing higher order time derivatives of  $H(t)$ .

Thus treating analytically these equations as we done in REM for previous cases mentioned above is almost impossible so we analyzed them graphically, using the numerical and graphic facilities of Maple. Actually the aim of REM is to recover the shape of the potential in term of the scalar field (eliminating the time from the above equations).

To illustrate our graphical results obtained after processing the Cosmo library, we concentrate on some examples (mainly the exponential and the linear expansion of the universe) taken from Table no. 1 of [1]. For the exponential case, when we have

$$a(t) = a_0 e^{\omega t}, \tag{7}$$

$\omega$  being a real constant, we obtained the results presented in Figure 1.

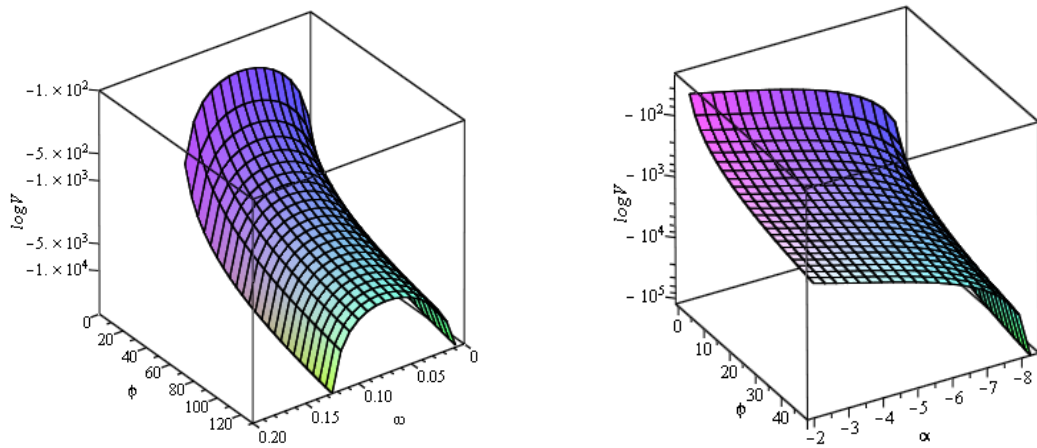


Fig. 1:  $V(\phi)$  in terms of different  $\omega$  at  $k = 0$  (left panel) and of different  $\alpha$  at  $k = 1$  and  $\omega = 0.1$  (right panel)

Similar results were obtained in the case of a linear expansion. For the sake of completeness we analyses also several cases for the time behavior of the potential which also can offer valuable information on the interaction theory governing the universe. Figure no. 2 below illustrates some of these results for the two cases we processed, the exponential and the linear one.

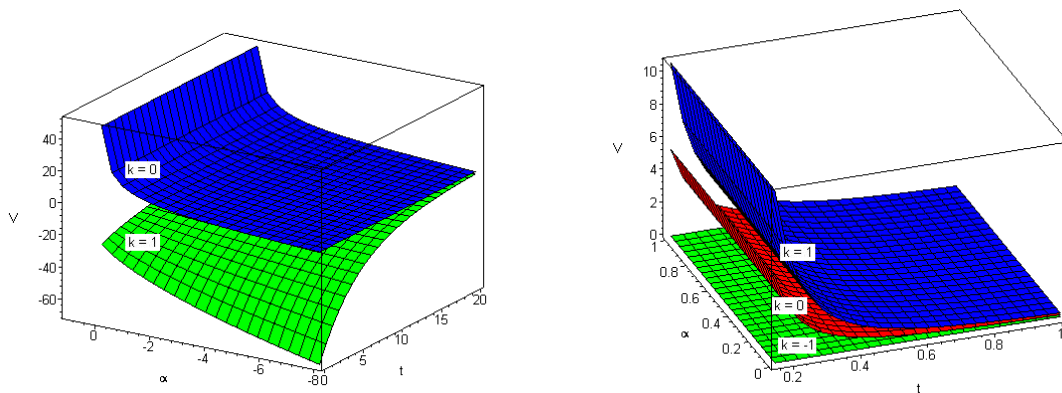


Fig. 2: Time behavior of  $V$  in terms of different  $\alpha$  at  $k = 0, 1, -1$  in the exponential case (left panel) and the linear case (right panel)

#### 4 Concluding remarks and the connection with tachyonic cosmological theories

Our investigations proved that the REM is feasible even in non-Einsteinian gravity cosmologies when no analytical solution of the REM is possible to obtain. Actually the graphical solution we applied and processed can show the shape of the potential of the scalar field providing good information for building an interaction theory in non-standard cosmologies.

Besides several possible approaches to include tachyonic potentials in cosmology, first of all in its inflationary phase, we will notice here an approach triggered by Sen's conjecture on tachyonic matter in context of D-brane dynamics [8]. In short, he proposed the following lagrangian

$$L_{tach} = L_{tach}(V, \partial_\mu T) = -V(T) \sqrt{1 + g^{\mu\nu} \partial_\mu T \partial_\nu T} \quad (8)$$

For a spatially homogenous (tachyon) field  $T(t)$ , a simplified lagrangian and the corresponding equation of motion are respectively

$$L_{tach} = L_{tach}(T(t), \dot{T}(t)) = -V(T) \sqrt{1 - \dot{T}^2} \quad (9)$$

$$\ddot{T}(t) - \frac{1}{V(T)} \frac{dV}{dT} \dot{T}^2(t) + \frac{1}{V(T)} \frac{dV}{dT} = 0 \quad (10)$$

There are numerous interesting potentials that can be incorporated in  $L_\phi$ , either motivated by string theory or by its solvability in context of inflation theory and "Friedmanology". For instance

$$V_1(T) = e^{-\alpha T} \quad V_2(T) = \frac{V_m}{\cosh(\beta T)} \quad (11)$$

One gets, up to some unimportant constants, equations of motion for these potentials

$$\ddot{T}(t) + \alpha \dot{T}^2(t) - \alpha = 0 \quad (12)$$

$$\ddot{T}(t) + \beta \tanh(\beta T) \dot{T}^2(t) = \beta \tanh(\beta T) \quad (13)$$

However, this form of lagrangian (action), as well equation of motion, is highly nonlinear and quite unsuitable for analytic solutions of Friedman equations, and in particular for quantization of any particular potential, i.e. model. However, as it was shown in [7] in case of exponential potential it is possible to find a locally equivalent lagrangian in the standard form producing the same equation of motion. In case of the later of of above mentioned potentials it can be shown [9] that

$$L_1(Y_1, \dot{Y}_1) = \frac{1}{2} \dot{Y}_1^2(t) + \frac{\alpha^2}{2} Y_1^2(t) \quad (14)$$

$$L_2 = \frac{1}{2} \cosh^2(\beta T) (1 + \dot{T}^2(t)) = \frac{1}{2} \dot{Y}_2^2(t) + \frac{\beta^2}{2} Y_2^2(t) + \frac{1}{2} \quad (15)$$

where

$$T \rightarrow Y_1 = \alpha^{-1} e^{\alpha T} \quad T(t) \rightarrow Y_2(t) = \beta^{-1} \sinh(\beta T(t)) \quad (16)$$

A generalization of this approach for a wide class of tachyonic potentials and quantization of the corresponding models with quadratic lagrangians via path integral technique will be presented elsewhere [9]. These results, as well as our REM approach to  $f(R)$  theories and (non)minimally coupled tachyonic fields with gravity [2] are a good point for testing string-theory motivated potentials and scale factor obtained from this approach, in least complicated solvable models and shape of potentials obtained from rather realistic models using REM methods [10].

### Acknowledgements

This work was supported by ICTP - SEENET-MTP project PRJ-09 Cosmology and Strings. One of the authors (D.N.V.) expresses his gratitude to the organizers of the BW2013 Workshop, Vrnjackja Banja, Serbia, where a part of this work was considered. G.S.Dj would like to thank to CERN-TH, for kind hospitality and support, where the final part of the paper was worked out, and to acknowledge support of the Serbian Ministry for Education, Science and Technological Development under project No 176021.

### References

- [1] D.N. Vulcanov, Cent. Eur. J. Phys., 6, No.1, (2008), p.84
- [2] D.N. Vulcanov, G.S. Djordjevic, Rom. Journ. of Phys., 57, No. 5-6 (2012), p. 1011
- [3] M.B. Mijic, M.S. Morris, Wai-Mo Suen, Phys.Rev. D, 34, No. 10, (1986) , p. 2934
- [4] A. De Felice, S.Tsujikawa, arXiv: 1002.4928v2 [gr-qc]
- [5] A.A. Starobinsky, Phys. Lett. B, 91 (1), 99-102 (1980).
- [6] T.P. Sotiriou, V. Faraoni, Rev. Mod. Phys., 82, 451-497 (2010); arXiv:0805.1726 [gr-qc]
- [7] D. D. Dimitrijevic, G. S. Djordjevic and Lj. Nestic, Fort. der Phys., 56, No. 4-5, p. 412
- [8] A. Sen, JHEP 0204, (2002) 048
- [9] D.D. Dimitrijevic, G.S. Djordjevic and M. Miliosevic, *On classicalization and quantization of tachyon-like matter (non)archimedean spaces*, to appear in Rom. Rep. of Phys.
- [10] D.D. Dimitrijevic, G.S. Djordjevic, M. Miliosevic, C.A. Sporea and D.N. Vulcanov, *On analytical and numerical DBI cosmologies*, work in progress.



# Fermi Large Area Telescope as a dark matter search tool

Gabrijela Zaharijas<sup>a,\*</sup>, Aldo Morselli<sup>b</sup> and Eric Nuss<sup>c</sup>  
(on behalf of the Fermi-LAT collaboration)

<sup>a</sup> The Abdus Salam International Centre for Theoretical Physics and INFN, Trieste, Italy

<sup>b</sup> INFN Roma Tor Vergata

<sup>c</sup> Laboratoire Univers et Particules de Montpellier, Université, Montpellier 2, Montpellier

## Abstract

Since its launch five years ago, the Large Area Telescope, onboard of the Fermi Gamma-ray Space Telescope, has detected the largest amount of gamma rays in the 20 MeV -  $\geq$  300 GeV energy range (nicely covering electro weak scale) with good angular resolution and good rejection power of more numerous charged cosmic rays. These impressive performance allows to attempt to learn about New Physics with astronomical and astro-particle data. We will present the latest results on these searches.

## 1 Introduction

The Large Area Telescope (LAT), one of two instruments onboard the Fermi Observatory, [1], is a pair conversion telescope for photons above 20 MeV up to a few hundreds of GeV. The field of view is  $\sim 2.4$  sr and the LAT observes the entire sky every  $\sim 3$  hours (2 orbits). The operation of the instrument through the first five years of the mission was smooth: the LAT has been collecting science data for more than 99% of the time spent outside the South Atlantic Anomaly.

Its data are made public and distributed to the Community through the Fermi Science Support Center (FSSC) <sup>1</sup> and have been used widely.

In what follows we will present some of the most important results of the Fermi LAT mission, focusing on those related to searches for signatures of Dark Matter (DM) annihilations in our and neighboring Galaxies.

## 2 The Second Fermi-LAT catalog

The high-energy gamma-ray sky is dominated by diffuse emission: more than 70% of the photons detected by the LAT are produced in interactions of the Galactic cosmic rays with interstellar medium and radiation fields. As a consequence the disk of our Milky Way Galaxy shines brightly in the Fermi sky. An additional diffuse component with an almost-isotropic distribution presents another significant fraction of the LAT photons. Due to its isotropic distribution it is thought to be of extragalactic in origin. The rest consists of various different types of point-like or extended sources: extragalactic ones as Active Galactic Nuclei (AGN) and normal star forming galaxies, as well as Galactic sources as pulsars and their relativistic wind nebulae, globular clusters, binary systems, shock-waves remaining from supernova explosions and nearby solar-system bodies like the Sun and the Moon.

The Second Fermi-LAT catalog (2FGL) [2] is the deepest catalog ever produced in the energy band between 100 MeV and 100 GeV, containing more than 1800 sources. Most of the sources are of extragalactic origin, blazars being the most numerous kind, with more than 800 detected ones. Among Galactic sources, LAT identified 117 gamma ray pulsars [3] and discovered millisecond gamma ray pulsars, being therefore dubbed the 'pulsar machine'. In addition to firmly identified sources, based either on periodic variability or on spatial morphology or on correlated variability, 576 (i.e. 31% of

---

\*E-mail: gzaharij@ictp.it

<sup>1</sup>The FSSC is available at <http://fermi.gsfc.nasa.gov/ssc>

the total number of entries in the catalog) are still unassociated with known astrophysical objects. In addition, the first catalog of high energy sources has recently been published [4] and the first catalog of Super Nova Remnants (SNRs) is in preparation [5].

### **3 Indirect Dark Matter searches**

One of the major open issues in our understanding of the Universe is the nature of an extremely-weakly interacting form of matter, the dark matter. The evidence for its existence is supported by a wide range of observations including large scale structures, the cosmic microwave background and the isotopic abundances resulting from the primordial nucleosynthesis, all of them being sensitive to its gravitational interaction. Due to the universal nature of gravity a different kind of probe is needed to pinpoint its particle physics properties. Complementary to direct searches being carried out in underground facilities and at accelerators, the indirect search for DM is one of the main of goals of Fermi Science. The indirect searches look for signatures of Weakly Interactive Massive Particle (WIMP) annihilation or decay in the surplus of its final products: stable standard model particles as gamma-rays, electrons and positrons, antiprotons. Among many other ground-based and space-borne instruments, the LAT plays a prominent role in this search through a variety of distinct search targets: gamma-ray lines, Galactic and isotropic diffuse gamma-ray emission, dwarf satellites, Cosmic Ray (CR) electrons and positrons.

#### **3.1 Galactic center**

The center of our Galaxy is expected to be the strongest source of  $\gamma$ -rays from DM annihilation, due to its coincidence with the cusped part of the DM halo density profile [6], [7], [8].

The diffuse gamma-ray backgrounds and discrete sources, as we know them today, can account for the large majority of the detected gamma-ray emission from the Galactic Center. Nevertheless in a preliminary analysis of the data, taken during the first 11 months of the Fermi satellite, a residual emission not accounted for by the above models was found [9], [10]. Improved modeling of the Galactic diffuse emission (for example, by taking advantage of advanced statistical analysis tools to scan over many parameters of the diffuse emission, along the lines of work presented in [11, 13]), as well as the potential contribution from other astrophysical sources (for instance unresolved point sources) should provide a more robust description of the data. Analyses are underway to investigate these possibilities. At the same time the community has responded actively to this issue, with many papers discussing properties and nature of such residual emission, e.g. [14, 15]. It should be noted that based only on gamma ray signatures in the Galactic Center it might be impossible to distinguish between dark matter signal and that of the unresolved population of pulsars. In such case DM detection can be claimed only if its signatures are confirmed by some other probe and/or in a different target.

#### **3.2 Galactic halo**

In order to minimize uncertainties connected with the region of the Galactic Center, analysis in [11] considered a region of interest consisting of two off-plane rectangles ( $5^{\circ} \leq |b| \leq 15^{\circ}$  and  $|l| \leq 80^{\circ}$ ) and searched for continuum emission from dark matter annihilation or decay in the smooth Galactic dark matter halo. They considered two approaches: a more conservative one in which limits were set on DM models assuming that all gamma ray emission in that region might come from dark matter (i.e. no astrophysical signal is modeled and subtracted). In a second, arguably more realistic approach, dark matter source and astrophysical emission were fit simultaneously to the data, marginalizing over several relevant parameters of the astrophysical emission. As no robust signal of DM emission is found, further conservative choices were made in a process of setting the DM limits.

These limits are particularly strong on leptonic DM channels, which are hard to constrain in most other probes (notably in the analysis of the dwarf Galaxies, described below). This analysis strongly

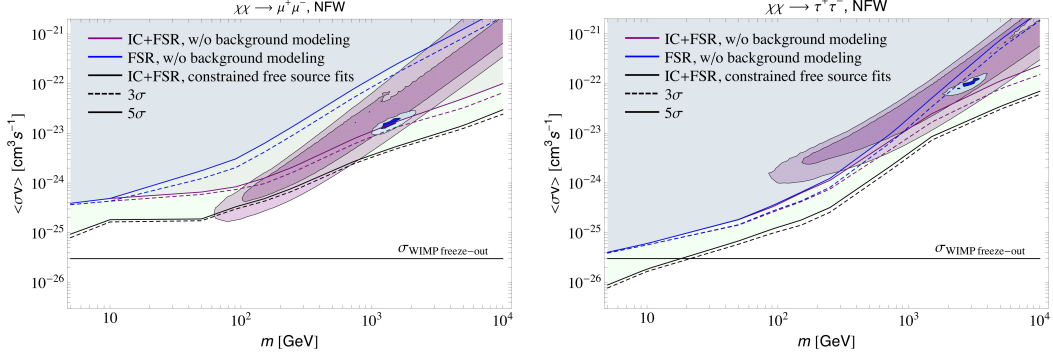


**Fig. 1:** Upper limits on WIMP annihilation cross sections in the Milky Way halo, for the muon (*left*) and tau (*right*) annihilation channels, as derived in [11].

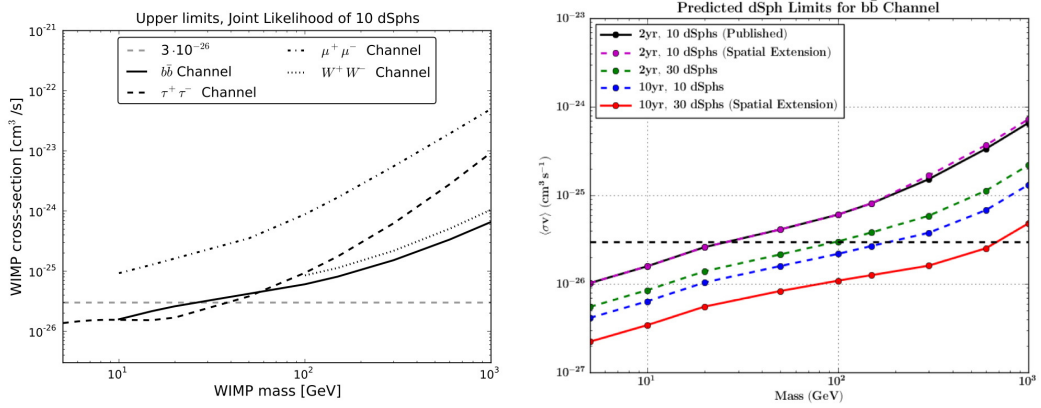


**Fig. 2:** *Left:* 95% C.L. upper limits on WIMP annihilation cross sections for different channels, from [21]. *Right:* Predicted 95% C.L. upper limits on WIMP annihilation cross sections in 10 years for  $b\bar{b}$  channel, from [22].

challenges DM interpretation [12] of the positron rise, observed by PAMELA [16], Fermi LAT [17, 18] and most recently AMS-02 [19] (see figure 1).

### 3.3 Dwarf galaxies

Dwarf spheroidal (dSphs) satellites of the Milky Way are old system with small amount of interstellar gas and with a very large mass-to-luminosity ratio (i.e. systems which are largely DM dominated). Detection of gamma rays from dwarf Galaxies is therefore considered to be one of the "smoking guns" of dark matter detection. The LAT so far detected no significant emission from these objects and the upper limits on the  $\gamma$ -ray flux were used to put stringent constraints on the parameter space of well motivated WIMP models [21].

A combined likelihood analysis of the 10 most promising dwarf galaxies, based on 24 months of data was presented in [21]. The main advantages of the combined likelihood are that the background analysis can be individually optimized for location of each dwarf galaxy, while the combined limits are more robust under individual background fluctuations and under uncertainties related to the estimated dark matter content, when compared to the limits from each individual dwarf galaxy. The derived 95% C.L. upper limits on WIMP annihilation cross sections for different channels are shown in figure 2 (left). The most generic cross section ( $\sim 3 \cdot 10^{-26} \text{cm}^3 \text{s}^{-1}$  for a purely s-wave cross section) is plotted as a reference. These results are obtained for NFW profiles [20] but for cored dark matter profile the J-factors for most of the dSphs would either increase or not change much so these results includes J-factor

uncertainties [21].

With the present data we are able to rule out large parts of the parameter space, in particular thermally produced WIMPS with mass of few tens of GeV.

Future improvements (apart from increased amount of data) will include an improved event selection with a larger effective area and photon energy range, and the inclusion of more satellite galaxies. In figure 2 (right) are shown the predicted upper limits in the hypothesis of 10 years of data instead of 2; 30 dSphs instead of ten (supposing that the new optical surveys, such as Dark Energy Survey (DES) and PanSTARSS will find new dSph due to their larger coverage of the sky) and due to the inclusion of the spatial extension of dSphs in the analysis (source extension increases the signal region at high energy  $E \geq 10 \text{ GeV}$ ,  $M \geq 200 \text{ GeV}$ ) as calculated in [22].

Other complementary limits derived with the Fermi LAT collaboration include the search for DM signatures in Galaxy clusters [23], possible anisotropies generated by the DM halo substructures [24], the search for Dark Matter Satellites [25] and a search for high-energy cosmic-ray electrons from the Sun [26].

### 3.4 Gamma-ray lines

A gamma-ray spectral line at the WIMP mass could be produced in annihilations or decays of DM particles to two photons (via loop processes, as direct coupling to photons is usually considered forbidden for standard *dark* matter candidates<sup>2</sup>). It could be observed as a particular feature in the astrophysical source spectrum [8]. Such an observation would be another “smoking gun” for WIMP DM as it is difficult to explain such feature by usual astrophysical processes, specially if it is observed over several directions in the sky. A presence of a feature due to annihilation into  $\gamma Z$  in addition would be even more convincing. No significant evidence of gamma-ray line(s) has been found in the first two years of data from 7 to 200 GeV [27] (see also [28]).

In early 2012, the claim of an indication of line emission in Fermi-LAT data [29, 30] has drawn considerable attention. Using an analysis technique similar to [28], but doubling the amount of data as well as optimizing the region of interest for signal over square-root of background, [29] found a (trial corrected)  $3.2 \sigma$  significant excess at a mass of  $\sim 130 \text{ GeV}$  that, if interpreted as a signal would amount to a cross-section of about  $\langle \sigma v \rangle \sim 10^{-27} \text{ cm}^3 \text{ s}^{-1}$ .

The signal is found to be concentrated on the Galactic Centre with a spatial distribution consistent with an Einasto profile [31]. This is marginally compatible with the upper limit presented in [27].

The follow up analysis of the Fermi LAT team uses 4 year data and has improved over the two year paper in three important aspects: i) the search was performed in five regions of interest optimized for DM search under five different assumptions on the morphology of the DM signal, ii) new improved data set (pass 7 reprocessed, [32]) was used, as it corrects for loss in calorimeter light yield due to radiation damage during the four years of the Fermi mission and iii) point spread function (PDF) was improved by adding a second dimension to the previously used triple Gaussian PDF model (such procedure is shown to increase the sensitivity to a line detection by 15%). In that analysis [33, 34] no globally significant lines have been found and new limits to this DM annihilation channel were set (see figure 3). In a close inspection of the 130 GeV feature it was found that indeed there exist a 133 GeV signal at  $4.5\sigma$  local significance, when a ‘1D’ PSF and old data sets were used (consistently with what [29, 30] have found). However, the significance drops to  $3.3\sigma$  (local, or  $\leq 2\sigma$  global significance once trials factors are taken into account). In addition, a weaker signal is found at the same energy in the control sample (in the Earth limb), which might point to a systematics effect present in this data set. In order to examine this possibility weekly observations of the Limb are scheduled, and a better understanding of a nature of the excess in the control sample should be available soon.

<sup>2</sup>However, there are several models which can generate the  $\gamma$ -ray line from tree level. For instance, some composite Dark Matter models or magnetic dipole interaction have the photon production directly.

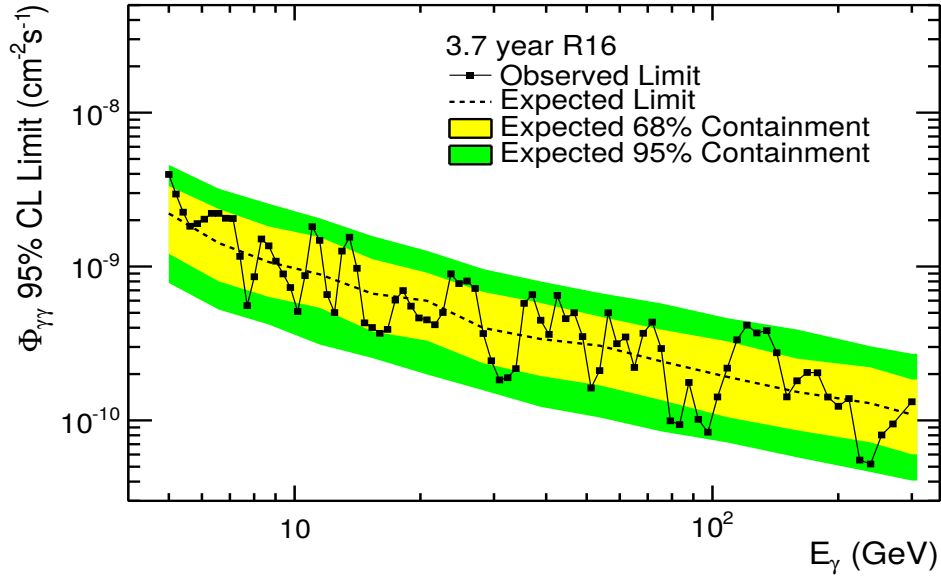


**Fig. 3:** Dark matter annihilation 95% CL cross section upper limits into  $\gamma\gamma$  for the Einasto profile for a circular region of interest (ROI) with a radius  $R_{GC} = 16^\circ$  centered on the GC with  $|b| < 5^\circ$  and  $|l| > 6^\circ$  masked, [34].

A new version of the event-level reconstruction and analysis framework (called Pass 8 , [35]) is being prepared for release within the Fermi LAT collaboration. With this new analysis software we should increase the efficiency of the instrument at high energy and have a data set based on independent event analysis thus gaining a better control of the systematic effects. Also, a new observational strategy exposing favorably the region of the Galactic Center has recently been recommended<sup>3</sup> and could start already towards the end of this year.

#### 4 Conclusions

The Fermi LAT turned five years in orbit on June, 2013, and it is living up to its expectations in terms of richness of scientific results delivered to the community. The mission is planned to continue at least four more years with many remaining opportunities for discoveries, both astrophysics-related and some hopefully in the fundamental sector.

#### Acknowledgments

The Fermi LAT Collaboration acknowledges support from a number of agencies and institutes for both development and the operation of the LAT as well as scientific data analysis. These include NASA and DOE in the United States, CEA/Irfu and IN2P3/CNRS in France, ASI and INFN in Italy, MEXT, KEK, and JAXA in Japan, and the K. A. Wallenberg Foundation, the Swedish Research Council and the National Space Board in Sweden. Additional support from INAF in Italy and CNES in France for science analysis during the operations phase is also gratefully acknowledged.

#### References

- [1] W.B.Atwood *et al.* [Fermi Coll.], *ApJ* **697** (2009) 1071-1102 [arXiv:0902.1089]
- [2] A. Abdo *et al.* [Fermi Coll.], *ApJS* **199** (2012) 31 [arXiv:1108.1435]

<sup>3</sup>See [http://fermi.gsfc.nasa.gov/ssc/proposals/alt\\_obs/obs\\_modes.html](http://fermi.gsfc.nasa.gov/ssc/proposals/alt_obs/obs_modes.html) for more info.

- [3] A. Abdo *et al.* [The Fermi-LAT Collaboration], *Astrophysical Journal Supplement* 208, **17** (2013) [arXiv:1305.4385 [astro-ph.HE]].
- [4] M.Ackermann, *et al.*, [Fermi-LAT Collaboration], *Astrophysical Journal Supplement* 2013, 209, 34, arXiv:1306.6772 [astro-ph.IM]
- [5] F. de Palma *et al.* [ for the Fermi LAT Collaboration], arXiv:1304.1395 [astro-ph.HE].
- [6] A. Morselli *et al.*, *Nucl.Phys.* **113B** (2002) 213
- [7] A.Cesarini, F.Fucito, A.Lionetto, A.Morselli, P. Ullio, *Astropart. Phys.* **21** (2004) 267 [astro-ph/0305075]
- [8] E. Baltz *et al.*, *JCAP* **07** (2008) 013 [arXiv:0806.2911]
- [9] V. Vitale and A. Morselli for the Fermi/LAT Collaboration, 2009 Fermi Symposium [arXiv:0912.3828]
- [10] A. Morselli, B.Cañadas, V.Vitale, *Il Nuovo Cimento* **34 C**, N. 3 (2011) [arXiv:1012.2292]
- [11] M.Ackermann *et al.* [Fermi Coll.], *ApJ* **761** (2012) 91 [arXiv:1205.6474]
- [12] D. Grasso, S. Profumo, A. W. Strong, L. Baldini, R. Bellazzini, E. D. Bloom, J. Bregeon, G. di Bernardo, D. Gaggero, N. Giglietto, T. Kamae, L. Latronico, F. Longo, M. N. Mazziotta, A. A. Moiseev, A. Morselli, J. F. Ormes, M. Pesce-Rollins, M. Pohl, M. Razzano, C. Sgro, G. Spandre and T. E. Stephens, *Astroparticle Physics* **32** (2009) 140 [arXiv:0905.0636]
- [13] R. Trotta, G. Johannesson, I. V. Moskalenko, T. A. Porter, R. R. de Austri and A. W. Strong, *Astrophys. J.* **729**, 106 (2011) [arXiv:1011.0037 [astro-ph.HE]].
- [14] D. Hooper and T. Linden, *Phys. Rev. D* **84**, 123005 (2011) [arXiv:1110.0006 [astro-ph.HE]].
- [15] K. N. Abazajian and M. Kaplinghat, *Phys. Rev. D* **86**, 083511 (2012) [arXiv:1207.6047 [astro-ph.HE]].
- [16] O.Adriani. *et al.* [PAMELA Coll.], *Phys. Rev. Lett.* **106** ( 2011) 201101
- [17] A.A.Abdo *et al.* [Fermi Coll.], *PRL* **102** (2009) 181101 [arXiv:0905.0025]
- [18] M.Ackermann *et al.* [Fermi Coll.], *Phys. Rev. D* **82** (2010) 092004 [arXiv:1008.3999]
- [19] M. Aguilar *et al.* [AMS Collaboration], *Phys. Rev. Lett.* **110**, no. 14, 141102 (2013).
- [20] J.Navarro, J.Frenk, S.White *Astrophys. J.* **462** (1996) 563 [arXiv:astro-ph/9508025]
- [21] M.Ackermann *et al.* [Fermi Coll.], *Phys. Rev. Lett.* **107** (2011) 241302 [arXiv:1108.3546]
- [22] R. C. Cotta, A. Drlica-Wagner, S. Murgia, E. D. Bloom, J. L. Hewett and T. G. Rizzo, *JCAP* **1204**, 016 (2012) [arXiv:1111.2604 [hep-ph]].
- [23] M.Ackermann, *et al.* [The Fermi-LAT Collaboration], arXiv:1308.5654 [astro-ph.HE].
- [24] M. Ackermann *et al.* [Fermi Coll.], *Phys. Rev. D* **85** (2012) 083007 [arXiv:1202.2856]
- [25] M. Ackermann *et al.* [Fermi Coll.], *ApJ* **747** (2012) 121 [arXiv:1201.2691]
- [26] M. Ajello *et al.* [Fermi Coll.], *Phys. Rev. D* **84** (2011) 032007 [arXiv:1107.4272]
- [27] M. Ackermann *et al.* [Fermi Coll.], *Physical Review D* **86** (2012) 022002 [arXiv:1205.2739]
- [28] A. Abdo *et al.* [Fermi Coll.], *Phys. Rev. Lett.* **104** (2010) 091302 [arXiv:1001.4836]
- [29] C. Weniger, *JCAP* **1208** (2012) 007 [arXiv:1204.2797 [hep-ph]].
- [30] M. Su and D. P. Finkbeiner, arXiv:1206.1616 [astro-ph.HE].
- [31] T. Bringmann and C. Weniger, *Dark Universe* 1 (2012) 194-217 [arXiv:1208.5481]
- [32] J. Bregeon *et al.* [ M. Wood Fermi-LAT Collaboration], arXiv:1304.5456 [astro-ph.HE].
- [33] E. Bloom *et al.* [On Behalf of the Fermi-LAT Collaboration], arXiv:1303.2733 [astro-ph.HE].
- [34] M. Ackermann *et al.* [Fermi-LAT Collaboration], *Physical Review D* 88, 082002 (2013) arXiv:1305.5597 [astro-ph.HE].
- [35] W. Atwood *et al.* [Fermi-LAT Collaboration], arXiv:1303.3514 [astro-ph.IM].

## Summary Reports



# AdS braneworld with Backreaction

Neven Bilić<sup>a, c, \*</sup> and Gary B. Tupper<sup>b, d, †</sup>

<sup>a</sup> Rudjer Bošković Institute, 10002 Zagreb, Croatia

<sup>b</sup> Centre for Theoretical and Mathematical Physics, Department of physics, University of Cape Town, Rondebosch 7701, South Africa

<sup>c</sup> Departamento de Física, Universidade Federal de Juiz de Fora, 36036-330, Juiz de Fora, MG, Brazil

<sup>d</sup> Associate Member, National Institute for Theoretical Physics

## Abstract

We review the tachyon model derived from the dynamics of a 3-brane moving in the AdS<sub>5</sub> bulk. The bulk geometry is based on the Randall–Sundrum II model extended to include the radion. The effective tachyon Lagrangian is modified due to the back-reaction of the brane on the bulk geometry.

In the Randall–Sundrum model (RS II) [1] the bulk metric is AdS<sub>5</sub>/Z<sub>2</sub> with the observer brane at  $y = 0$  and a negative tension brane at the AdS horizon ( $y = \infty$ ). However, the naive AdS<sub>5</sub> geometry is distorted by a scalar mode, the radion, related to the interbrane distance. One arrives at the 5-dimensional line element [2]

$$ds_{(5)}^2 = \left( \phi + e^{-2ky} \right) g_{\mu\nu}(x) dx^\mu dx^\nu - \left( \frac{e^{-2ky}}{\phi + e^{-2ky}} \right)^2 dy^2, \quad (1)$$

where the field  $\phi = \phi(x)$  represents the radion. Integrating the 5-dim bulk action over the fifth coordinate from  $y = 0$  to  $y = \infty$  and imposing the RS II fine tuning condition

$$\sigma_0 = -\sigma_\infty = \frac{6k}{K_{(5)}} \equiv \sigma_{\text{RS}} \quad (2)$$

one obtains the effective 4-dim action on observer's brane [2]

$$S_{\text{bulk}} = \int d^4x \sqrt{-g} \left( -\frac{R}{2K} + \frac{1}{2} g^{\mu\nu} \Phi_{,\mu} \Phi_{,\nu} \right). \quad (3)$$

Here we have introduced the 4-dim gravitational constant  $K = K_{(5)}k$  and the  $\phi(x)$  substitute

$$\Phi(x) = \sqrt{\frac{6}{K}} \sinh^{-1} \sqrt{\phi(x)} \quad (4)$$

is the canonically normalized radion.

Next we consider a 3-brane moving in the 5-dimensional bulk with the geometry (1). The brane may be parameterized by  $X^M = (x^\mu, Y(x))$ . The 5-th coordinate  $Y$  is treated as a dynamical field. By making use of the induced metric

$$g_{\mu\nu}^{\text{ind}} = g_{(5)MN} X_{,\mu}^M X_{,\nu}^N \quad (5)$$

we find the brane action in the form

$$S_{\text{brane}} = -\sigma \int d^4x \sqrt{-g} (e^{-2kY} + \phi)^2 \left( 1 - \frac{(e^{-2kY})^2}{(e^{-2kY} + \phi)^3} g^{\mu\nu} Y_{,\mu} Y_{,\nu} \right)^{1/2}. \quad (6)$$

---

\*E-mail: bilic@irb.hr

†E-mail: gary.tupper@uct.ac.za

Changing  $Y$  to a tachyon field  $\theta = e^{kY}/k$ , we obtain the total effective Lagrangian

$$\mathcal{L} = \frac{1}{2}g^{\mu\nu}\Phi_{,\mu}\Phi_{,\nu} - \frac{\sigma}{k^4} \frac{(1 + k^2\theta^2\phi)^2}{\theta^4} \sqrt{1 - g^{\mu\nu}\theta_{,\mu}\theta_{,\nu}(1 + k^2\theta^2\phi)^{-3}}. \quad (7)$$

If the radion were absent we would have an undistorted AdS<sub>5</sub> geometry and the above Lagrangian would describe a pure tachyon condensate with inverse quartic potential [3].

The total energy momentum tensor may be expressed in terms of two ideal fluids. As usual we identify the pressure with the Lagrangian (7) from which we derive the energy density as the Hamiltonian. We then derive Hamilton's equations and examine the model assuming a homogeneous isotropic evolution. We take  $\sigma = \sigma_{RS}/3 = 2k^2/K$  and solve numerically Hamilton's equations starting from  $t = 0$  with appropriately chosen initial conditions. We find that the radion field  $\phi$  undergoes damped oscillations with the amplitude decreasing as  $1/t$ . Unlike the pressure of a pure tachyon with inverse quartic potential, the modified pressure does not vanish as the tachyon rolls near minimum. The effective equation of state obtained by averaging over large scales describes a warm dark matter [4, 5].

We have found the effective tachyon Lagrangian modified by the interaction with the radion in an AdS-5 geometry distorted by the back-reaction. As a consequence of the back-reaction, the tachion fluid behaves as a kind of warm dark matter in contrast to pressureless pure tachyon matter

## References

- [1] L. Randal and R. Sundrum, Phys. Rev. Lett. **83**, 4690 (1999).
- [2] J.E. Kim, G.B. Tupper, and R.D. Viollier, Phys. Lett. B **593**, 209 (2004).
- [3] A. Sen, JHEP 0207, 065 (2002)
- [4] N. Bilic and G. B. Tupper, arXiv:1302.0955 [hep-th].
- [5] N. Bilic and G. B. Tupper, Cent. Eur. J. Phys., (2013), DOI: 10.2478/s11534-013-0325-y, arXiv:1309.6588 [hep-th].